HEAT RELEASE AND THE COMBUSTION BEHAVIOUR OF UPHOLSTERED FURNITURE

A thesis

submitted in partial fulfilment

of the requirements for the degree

of

Doctor of Philosophy

in the

University of Canterbury

by

P. A. Enright

University of Canterbury

1999

TABLE OF CONTENTS

ACKNOWLEDGEMENTS

This work is dedicated to my wife Dr Kira Michalova, who has made many personal and career sacrifices so that this thesis can be undertaken. Co-dedication goes to our baby daughter, Galina Michaela, whose recent arrival has provided the impetus to finish. – *Mockrat dekuju.*

A debt of gratitude is owed to my supervisor Dr Charley Fleischmann, who gave me enough rein to explore and encouraged occasional diversions. I am thankful for Charley's enthusiasm, particularly in the laboratory. Thanks also to Professor Andy Buchanan who is largely responsible for the existence of the fire engineering programme.

Many thanks to the financial supporters of both the research and researcher. To the New Zealand Public Good Science Fund, New Zealand Fire Service Commission, NFPA Memorial Educational Fund and the Royal Society of New Zealand. This category also includes my part-time employers, FPEC Consulting Fire Engineers, Alan Reay Consultants and the Department of Civil Engineering.

Thanks to all the university general staff who assisted with the research. Especially, Catherine Price, Denise Forbes, Frank Greenslade, Michael Weaver, Geoff Hill, Peter Coursey, Brandon Hutcheson. Thanks to all the library staff, especially Pat Roddick.

Thanks to fellow students. My officemates Jason Clement and Ee Yii. To the past intakes of Masters' students. Especially, Neil Gravestock from the Class of 1998 and all of the Class of 1999 – a particularly colourful group. Thanks also to supportive friends. Tania Daly and Jason Roberts. Julie and Adrian Paterson and the rest of the adventurous guys, Simon Crampton, Cor Vink and James Ross.

Finally, thanks to Kira's and my families. In New Zealand thanks to Josie, Paddy, Vicky, Rex, Wade, Jodi, Stephanie, David and Jessie. In the Czech Republic thanks to Kyra, Vaclav, Vera and Dina.

Tony Enright

June 1999

ABSTRACT

This work forms the first phase of a continuing initiative aimed at reducing fire deaths in residential dwellings in New Zealand (NZ).

Loss of life in residential buildings dominates NZ annual fire death statistics. Few items within these buildings have the potential to bring about untenable conditions as swiftly as upholstered furniture. It is a major goal of safety research – and this work in particular – to better assess the hazard of furniture fires. Especially, in respect to our ability to predict this hazard.

The heat release rate of a burning item is acknowledged as the most important property in fire hazard analysis. As a starting point, this work includes a critical review of reaction to fire calorimetric techniques. These techniques are the basis of heat release rate measurement.

The technique of oxygen consumption calorimetry is subjected to a comprehensive uncertainty analysis. This includes a detailed example of the application of this analysis to a common Standard Test Method. A less favoured calorimetry technique based on thermochemistry is redeveloped. Its usefulness as a calibration tool in respect to oxygen consumption calorimetry is explored. This is helpful as the thermochemistry technique is independent of oxygen concentration measurement, which in turn is the crucial parameter in oxygen consumption calorimetry.

The combustion behaviour of dozens of small-scale furniture composites and 13 full-scale furniture items are tested using the above principles. The experimental programme used the newly commissioned cone and furniture calorimeters. The characterisation of these apparatuses appear in this work.

The experimental results are used to validate the applicability of widely published European furniture fire models, to NZ items. This study shows that these existing techniques, while comprehensive, do not predict with goodness the combustion behaviour of NZ furniture. However, the NZ data set is small and the direction of future initiatives are detailed.

CHAPTER 1: INTRODUCTION

1.1 Objectives

A primary objective of this work, is to determine the applicability of contemporary fire models to exemplary New Zealand (NZ) furniture. This 'modelling' objective is specifically directed towards the ability to predict full-scale combustion behaviour of upholstered furniture (CBUF) from small-scale tests and experiments. The benefit of a good, applicable model is that the hazard of unwanted fires in domestic and residential buildings can be predicted relatively economically and easily, from small-scale material testing. Such hazard analysis, is a first step in hazard mitigation.

In order to examine the applicability and goodness of the modelling, a second objective is pursued. That is, the examination and critique of the theory of contemporary and novel calorimetry, i.e. heat release rate (HRR) measurement. This is largely theoretical work and precedes the modelling.

Fundamental to the experimental work – necessary in the modelling – is the third objective. That is, an examination and critique of the propagation of uncertainty in heat release rate measurement. As with the HRR work, this precedes the modelling. It is unusual but important to understand the limitations of experimental results.

These three objectives; modelling, calorimetry and uncertainty, form the backbone of this work.

1.2 Impetus

Following the trend of many other developed countries, loss of life in domestic and residential buildings continue to dominate New Zealand's (NZ) annual fire death statistics. Few items within these buildings have the potential to bring about untenable conditions as swiftly as upholstered furniture.

Therefore, it is a major goal of safety research in general – and this work in particular – to better assess the hazard of furniture fires. Especially, in respect to the ability to predict the hazard.

This work is the first phase of a significant and ongoing University of Canterbury (UC) research initiative in this direction. It is intended that this work forms the foundation upon which the continuing research is built.

1.3 Previous work in this field

Of the various publications referenced throughout this work, most are directly related to this field. Some of these are cornerstone to this work. Either, in terms of a particular piece of work, or a particular researcher who has published prolifically. The cornerstone publications include Thornton (1917)[1], Huggett (1980)[2], Parker (1982)[4] and Sundstrom (Ed.) (1995)[26]. The eminent researchers include Babrauskas[14],[21],[22],[24],[28],[33],[34] and Janssens[3],[5],[15].

1.4 Direction of this work

Before developing good predictive furniture fire models, much groundwork needs covering. This is the role of a large proportion of this work. In it, contemporary experimental calorimetry techniques are reviewed. Analytical derivations of calculation techniques are scrutinised and refined. Complete laboratory facilities were to be built parallel to this research, this work includes details of the characterisation of the UC Cone and Furniture calorimeters.

The latter part of this dissertation reaches the topic of furniture fire modelling. However, it is the focus of the main body of this work to dwell on the philosophy and details of the methodology. This is important foundation work.

The form of the foundation work manifests first as an analytical interest in contemporary oxygen consumption and thermochemistry techniques. Second, as a critique and uncertainty analyses of the calculation techniques. Third as characterisation of the UC Cone and Furniture calorimeter. Fourth, as an examination of the applicability of existing comprehensive furniture fire models to NZ furniture.

This work provides a sound platform for the continuation of the initiative to reduce furniture fires in NZ residential and domestic buildings.

1.5 Layout of this work

This dissertation is presented in three parts. PART A: 'Calorimetric techniques', PART B: 'Uncertainty analysis of calorimetric techniques' and PART C: 'Instrumentation and validation of furniture fire modelling'.

PART A: 'Calorimetric techniques' consists of three chapters. CHAPTER 2: 'Heat release rate measurement, oxygen consumption technique', CHAPTER 3: 'Heat release rate measurement, thermochemistry technique', CHAPTER 4: 'Measurement of mass flow rate of the exhaust gases'. This Part is the background to the experimental methodology and is largely covering existing work – except that the derivation of thermochemistry equations in this format is original work.

PART B: 'Uncertainty analysis of calorimetric techniques' consists of one large chapter. CHAPTER 5: 'Propagation of uncertainty of heat release rate measurement'. Within this are two examples 'Example 1: An uncertainty analysis of the HRR calculation of the ISO5660-1 and ASTM1354 Cone Calorimeter standard test methods' and 'Example 2: An alternative calculation of the cone calorimeter calibration constant'. This Part is wholly original and largely represents the analytical contribution of this work.

PART C: 'Instrumentation and validation of furniture fire modelling' consists of two chapters. CHAPTER 6: 'Instrumentation' and CHAPTER 7: 'CBUF Model I and II applied to exemplary NZ furniture'. This Part is the beginning of the furniture fire hazard analysis and represents the experimental portion of the dissertation. Details of the commissioning calibrations and instrument characterisation are given. Dozens of Cone Calorimeter and 13 Furniture Calorimeter fire tests were undertaken to strict protocols. The results are applied in this work to existing and comprehensive European predictive models to validate the applicability of the models to NZ furniture. Part C does not necessarily begin where Part B finished. The propagation of uncertainty work developed in Part B is applied to the HRR. However, the same methodology is not applied within the highly empirical CBUF Models where high uncertainties within the regression analysis outweigh the value of such an exercise.

CHAPTER 2: HEAT RELEASE RATE MEASUREMENT, OXYGEN CONSUMPTION TECHNIQUE

2.1 Introduction

The principle of oxygen consumption is based on Thornton's rule. Thornton[1] discovered the fact that for a large number of organic liquid and gas fires, a more or less constant amount of heat is released per unit mass of oxygen consumed during complete combustion. Huggett[2] established that this principle also applied to organic solids. He measured the constant as 13.1 $MJ.kg^{-1}$ of oxygen consumed, on average. Huggett reported that calculations using this figure yield values generally accurate to within ±5%.

2.2 Calculation of heat release rate

Using Thornton's rule, as expanded by Huggett, it was realised that the heat release rate can be calculated as being linearly proportional to the amount of oxygen consumed. The proportionality constant, Huggett's constant, $\Delta h_c / r_0$ is 13.1 $MJ.kg^{-1}$. The amount of oxygen consumed being the difference between the oxygen concentration in the ambient air entering the apparatus and the oxygen concentration in the exhaust gases extracted from the system. This is described by Equation 1.

Equation 1
$$\dot{q} = \frac{\Delta h_c}{r_0}(\dot{m}^o_{O_2} - \dot{m}_{O_2})$$

For a detailed description of the background to the calculation of the heat release rate refer to Janssens and Parker[3].

2.3 General equations of HRR

Following are the derivations of equations used in the calculation of the heat release rate. These equations were first derived by Parker[4] and then again by Janssens[5]. They are included here as background. They also form the basis of comparison to the thermochemistry technique derivations of CHAPTER 3: 'Heat release rate measurement, thermochemistry technique'.

In a simplified but equivalent form, these equation also appear in the Standard Test Methods for the Cone Calorimeter[6] and Furniture Calorimeter[7]. Therefore, their use is widespread in fire tests and experiments.

The major assumptions follow. For unknown fuel composition, the amount of energy released by complete combustion per unit mass of O_2 is constant at 13.1 MJ/kg. Gases are assumed to behave ideally. Incoming air consists of O_2, CO_2, H_2O and N_2. All inerts not taking part in the combustion reaction are lumped into the nitrogen. Where O_2, CO_2 and CO are measured, this is done on a dry basis.

Several configurations of gas analysers are considered. The simplest, Configuration 1, assumes only an oxygen analyser is present in the gas sampling train. Configurations 2 to 4 incorporate CO_2, CO and H_2O analysers respectively. These configurations are illustrated in the Standard Test Methods described by Reference [6] and Reference [7].

2.3.1 Configuration 1: O_2 Gas Analysis

This is the simplest, cheapest and least accurate of the various analysis configurations. A sample of exhaust gases is drawn from the duct. Of the species present, the mole fraction of O_2 is measured and the N_2 is calculated. But, prior to this CO_2 is removed by a chemical agent and H_2O is removed by a desiccant. Note that only O_2 and N_2 enter the analyser and in a dry air state. It is assumed combustion is complete and that CO is not produced in significant concentrations. It is assumed that oxides of nitrogen are similarly not produced in significant concentrations.

The oxygen depletion factor ϕ, is defined as the fraction of incoming air that is fully depleted of it's oxygen during the combustion process. This is described by Equation 2.

Equation 2

$$\phi = \frac{\dot{m}^o_{O_2} - \dot{m}_{O_2}}{\dot{m}^o_{O_2}}$$

Convert the mass terms in Equation 2 to measured concentrations (mole fractions). Working backwards, consider the mole fraction of oxygen in dry ambient air as measured by the

oxygen analyser. This is described by Equation 3. Similarly during an experiment the mole fraction of oxygen in the dry exhaust is described by Equation 4.

Equation 3

$$x^{o}_{O_2} = \frac{\frac{\dot{m}^{o}_{O_2}}{M_{O_2}}}{\frac{\dot{m}^{o}_{O_2}}{M_{O_2}} + \frac{\dot{m}^{o}_{N_2}}{M_{N_2}}}$$

Equation 4

$$x^{a}_{O_2} = \frac{\frac{\dot{m}_{O_2}}{M_{O_2}}}{\frac{\dot{m}_{O_2}}{M_{O_2}} + \frac{\dot{m}_{N_2}}{M_{N_2}}}$$

Rearranging Equation 3 to get an expression in terms of the mass flow rate, first gives Equation 5. Equation 5 then simplifies, via intermediate steps not included here, to Equation 6. Similarly, Equation 4 rearranges to Equation 7.

Equation 5

$$x^{o}_{O_2} = \frac{\frac{\dot{m}^{o}_{O_2}}{M_{O_2}}}{\frac{\dot{m}^{o}_{O_2}}{M_{O_2}}\left(1 + \frac{\dot{m}^{o}_{N_2}}{M_{N_2}}\frac{M_{O_2}}{\dot{m}^{o}_{O_2}}\right)}$$

Equation 6

$$\dot{m}^{o}_{O_2} = \dot{m}^{o}_{N_2}\frac{M_{O_2}}{M_{N_2}}\frac{1}{\left(\frac{1}{x^{o}_{O_2}} - 1\right)}$$

Equation 7

$$\dot{m}_{O_2} = \dot{m}_{N_2}\frac{M_{O_2}}{M_{N_2}}\frac{1}{\left(\frac{1}{x^{a}_{O_2}} - 1\right)}$$

Subtracting Equation 7 from Equation 6 and dividing by Equation 6 gives Equation 8

Equation 8

$$\phi = \frac{\dot{m}^o_{N_2} \frac{M_{O_2}}{M_{N_2}} \frac{1}{\left(\frac{1}{x^o_{O_2}} - 1\right)} - \dot{m}_{N_2} \frac{M_{O_2}}{M_{N_2}} \frac{1}{\left(\frac{1}{x^a_{O_2}} - 1\right)}}{\dot{m}^o_{N_2} \frac{M_{O_2}}{M_{N_2}} \frac{1}{\left(\frac{1}{x^o_{O_2}} - 1\right)}}$$

We know the mass flow rate of N_2 is conserved, $\dot{m}^o_{N_2} = \dot{m}_{N_2}$, so all the mass and molecular weight terms cancel and Equation 8 simplifies, via intermediate steps not included here, to Equation 9. Equation 9 is the expression of the oxygen depletion factor in terms of measured values.

Equation 9

$$\phi = \frac{\left(x^o_{O_2} - x^a_{O_2}\right)}{x^o_{O_2}\left(1 - x^a_{O_2}\right)}$$

The emphasis in oxygen consumption calorimetry is quantification of the mass of oxygen consumed, i.e. $(\dot{m}^o_{O_2} - \dot{m}_{O_2})$. This is described in the parenthesis in Equation 1. The mass of oxygen consumed also appears as the numerator of the first description of the oxygen depletion factor in Equation 2. Equation 2 is rearranged and substituted into Equation 1 to give Equation 10.

Equation 10

$$\dot{q} = \frac{\Delta h_c}{r_0} \dot{m}^o_{O_2} \phi$$

Where the oxygen mass term in Equation 10 is redefined in terms of measured variables by Equation 11 and Equation 12.

Equation 11

$$\frac{\dot{m}^o_{O_2}}{M_{O_2}} = x^o_{O_2}\left(1 - x^o_{CO_2} - x^o_{H_2O}\right)\frac{\dot{m}_a}{M_a}$$

Equation 12

$$\dot{m}^o_{O_2} = x^o_{O_2}\left(1 - x^o_{CO_2} - x^o_{H_2O}\right)\frac{M_{O_2}}{M_a}\dot{m}_a$$

Except that the mass flow rate of incoming air $\dot{m}_a$, in Equation 12 is not a measured variable. This must be related to the mass flow rate of the exhaust gases, $\dot{m}_e$ via the following steps.

The number of moles of species' in the exhaust at any instant in time is the sum of the number of moles of incoming air not depleted of O_2, plus the product of the number of moles of incoming air depleted of O_2 multiplied by some expansion factor due to the combustion chemistry. This is described by Equation 13.

Equation 13 $$n_e = \left(n_{air\_not\_O_2\_depleted}\right) + \left(n_{air\_O_2\_depleted}\right)\alpha$$

The combustion expansion factor, α is expressed as a function of the stoichiometric expansion factor β, by Equation 14.

Equation 14 $$\alpha = 1 + x_{O_2}^{o}\left(\beta - 1\right)$$

The stoichiometric expansion factor β is defined as the ratio number of moles of products (CO_2 and H_2O) to the number of moles of oxygen consumed in a stoichiometric equation. The value of β is a function of the C to H to O ratio of the fuel. A minimum value is β=1 for pure carbon and β=2 for pure hydrogen. Unless the fuel composition is known an average value for $\beta = 1.5$ corresponding to α=1.105 is used. This is also the correct expansion factor for methane and PMMA.

Therefore, Equation 13 can be rewritten in terms of the oxygen depletion factor and expansion factor. This is described in mole terms by Equation 15 and mass terms by Equation 16 and then Equation 17 (assuming $M_e \approx M_a$). Rearranging Equation 17 for $\dot{m}_a$ gives us Equation 18.

Equation 15 $$n_e = (1 - \phi).n_a + \alpha.\phi.n_a$$

Equation 16 $$\frac{\dot{m}_e}{M_e} = (1 - \phi)\frac{\dot{m}_a}{M_a} + \alpha.\phi.\frac{\dot{m}_a}{M_a}$$

Equation 17 $$\dot{m}_e = (1-\phi)\dot{m}_a + \alpha.\phi.\dot{m}_a$$

Equation 18 $$\dot{m}_a = \frac{\dot{m}_e}{1+\phi.(\alpha-1)}$$

Equation 18 is substituted into Equation 12 to give Equation 19. Equation 19 describes the mass flow rate of oxygen in the incoming air. Equation 19 is then substituted into Equation 10 to give Equation 20. Equation 20 brings the analysis back to the HRR. Within Equation 20 constant terms are grouped at the front of the expression and like terms grouped together.

Equation 19 $$\dot{m}^o_{O_2} = x^o_{O_2}\left(1 - x^o_{CO_2} - x^o_{H_2O}\right)\frac{M_{O_2}}{M_a}\frac{\dot{m}_e}{1+\phi.(\alpha-1)}$$

Equation 20 $$\dot{q} = \frac{\Delta h_c}{r_0}\cdot\frac{M_{O_2}}{M_a}\cdot\frac{\phi}{1+\phi(\alpha-1)}\cdot x^o_{O_2}\left(1 - x^o_{CO_2} - x^o_{H_2O}\right)\cdot\dot{m}_e$$

Equation 20 is the final expression for HRR calculation for Configuration 1. The oxygen depletion factor ϕ is described by Equation 9.

2.3.2 Configuration 2: O_2 and CO_2 Gas Analysis

A CO_2 analyser joins the O_2 analyser in the sampling train for this configuration and CO_2 is no longer chemically removed. It is assumed combustion is complete and that CO is not produced in significant concentrations. It is assumed that oxides of nitrogen are similarly not produced in significant concentrations.

The methodology is the same as Configuration 1. Equation 20 is used as the general equation for HRR except that the oxygen depletion factor in Equation 9 changes to reflect the CO_2 concentrations present in the sampling train. This algebraic adjustment involves Equation 21 superseding Equation 3 and Equation 22 superseding Equation 4.

Equation 21 $$x^o_{O_2} = \frac{\frac{\dot{m}^o_{O_2}}{M_{O_2}}}{\frac{\dot{m}^o_{O_2}}{M_{O_2}} + \frac{\dot{m}^o_{CO_2}}{M_{CO_2}} + \frac{\dot{m}^o_{N_2}}{M_{N_2}}}$$

Equation 22

$$x_{O_2}^{a} = \frac{\dfrac{\dot{m}_{O_2}}{M_{O_2}}}{\dfrac{\dot{m}_{O_2}}{M_{O_2}} + \dfrac{\dot{m}_{CO_2}^{o}}{M_{CO_2}} + \dfrac{\dot{m}_{CO_2}^{g}}{M_{CO_2}} + \dfrac{\dot{m}_{N_2}}{M_{N_2}}}$$

Equation 21 and Equation 22 are rearranged about $\dot{m}_{O_2}^{o}$ and $\dot{m}_{O_2}$ and making use of the relationship $\dot{m}_{N_2}^{o} = \dot{m}_{N_2}$ Equation 23 is derived. Equation 23 is the expression of the oxygen depletion factor in terms of measured values.

Equation 23

$$\phi = \frac{x_{O_2}^{o}\left(1 - x_{CO_2}^{a}\right) - x_{O_2}^{a}\left(1 - x_{CO_2}^{o}\right)}{x_{O_2}^{o}\left(1 - x_{O_2}^{a} - x_{CO_2}^{a}\right)}$$

2.3.3 Configuration 3: O_2 , CO_2 and CO Gas Analysis

A CO analyser joins the O_2, and CO_2 analysers in the sampling train for this configuration. CO is no longer assumed insignificant. Therefore, it need not be assumed combustion is complete as is the case for ventilation limited combustion. It is nevertheless still assumed that oxides of nitrogen are similarly not produced in significant concentrations.

The oxygen depletion factor in Configuration 3 changes from earlier configurations to reflect the CO concentrations present in the sampling train. As ambient conditions do not vary (no ambient CO) Equation 21 from Configuration 2 is valid for Configuration 3 but Equation 24 supersedes Equation 22. Therefore, the final expression of the oxygen depletion factor is given by Equation 25.

Equation 24

$$x_{O_2}^{a} = \frac{\dfrac{\dot{m}_{O_2}}{M_{O_2}}}{\dfrac{\dot{m}_{O_2}}{M_{O_2}} + \dfrac{\dot{m}_{CO_2}^{o}}{M_{CO_2}} + \dfrac{\dot{m}_{CO_2}^{g}}{M_{CO_2}} + \dfrac{\dot{m}_{CO}^{g}}{M_{CO_2}} + \dfrac{\dot{m}_{N_2}}{M_{N_2}}}$$

Equation 25

$$\phi = \frac{x_{O_2}^{o}\left(1 - x_{CO_2}^{a} - x_{CO}^{a}\right) - x_{O_2}^{a}\left(1 - x_{CO_2}^{o}\right)}{x_{O_2}^{o}\left(1 - x_{O_2}^{a} - x_{CO_2}^{a} - x_{CO}^{a}\right)}$$

There are also changes in the general equation for HRR. Previously, for both Configuration 1 and 2, Equation 20 has held. However, if significant concentrations of CO are produced the universal "Huggett's" constant must be corrected to allow for incomplete combustion. Janssens derives the correction in Reference [5] and it is not repeated here but appears in Equation 26. Equation 26 is the general equation for HRR calculation for Configuration 3. Note that Equation 20 (the general equation for HRR calculation in Configurations 1 and 2) is recognisable within Equation 26. As x_{CO}^{a} becomes zero the expression in the square parentheses goes to $\Delta h_c / r_0 \cdot \phi$.

Equation 26
$$\dot{q} = \left[\frac{\Delta h_c}{r_0}\phi - \left(\frac{\Delta h_c}{r_0}\bigg|_{\substack{CO \\ \rightarrow CO_2}} - \frac{\Delta h_c}{r_0} \right) \frac{1-\phi}{2} \frac{x_{CO}^{a}}{x_{O_2}^{a}} \right] \frac{M_{O_2}}{M_a} \frac{x_{O_2}^{o}\left(1 - x_{CO_2}^{o} - x_{H_2O}^{o}\right) \cdot \dot{m}_e}{1 + \phi(\alpha - 1)}$$

2.3.4 Configuration 4: O_2, CO_2, CO and H_2O Gas Analysis

A H_2O analyser joins the O_2, CO_2 and CO analysers in the sampling train for this configuration. As with Configuration 3, it need not be assumed combustion is complete as is the case for ventilation limited combustion. It is nevertheless still assumed that oxides of nitrogen are similarly not produced in significant concentrations.

The oxygen depletion factor in Configuration 4 remains the same as that of the previous configurations. This is because the water vapour analyser is on a separate heated sample line than the O_2, CO_2 and CO analysers. Therefore, the O_2, CO_2 and CO concentrations are measured on a dry basis and hence ϕ retains the form of Equation 25.

One significant improvement of this Configuration is that a mass balance of the products in the exhaust system can be completed. This means the assumptions relating $\dot{m}_a$ to $\dot{m}_e$ (via Equation 18) need not be made as $\dot{m}_a$ can be calculated directly from the measured $\dot{m}_e$ via measured species concentrations without the assumed combustion expansion factor. Accuracy is improved significantly by not having to assume the combustion expansion factor as this is fuel dependent and generally unknown in fire tests and experiments.

As a first step in deriving the new relationship between $\dot{m}_a$ and $\dot{m}_e$ consider Equation 27 to Equation 30.

Equation 27 $$\frac{\dot{m}_{O_2}}{M_{O_2}} = \left(1 - x_{H_2O}\right) x^a_{O_2} \frac{\dot{m}_e}{M_e}$$

Equation 28 $$\frac{\dot{m}_{CO_2}}{M_{CO_2}} = \left(1 - x_{H_2O}\right) x^a_{CO_2} \frac{\dot{m}_e}{M_e}$$

Equation 29 $$\frac{\dot{m}_{CO}}{M_{CO}} = \left(1 - x_{H_2O}\right) x^a_{CO} \frac{\dot{m}_e}{M_e}$$

Equation 30 $$\frac{\dot{m}_{H_2O}}{M_{H_2O}} = x_{H_2O} \frac{\dot{m}_e}{M_e}$$

Equation 27 to Equation 30 are definitions for the number of moles of the species O_2, CO_2, CO and H_2O in the exhaust gases. The theoretical mole fraction of N_2, x_{N_2} in the exhaust gases is described by extending this analogy. This is described in Equation 31. Note that the variable x_{N_2} is not measured.

Equation 31 $$\frac{\dot{m}_{N_2}}{M_{N_2}} = x_{N_2} \frac{\dot{m}_e}{M_e}$$

Also, x_{N_2} is unity less the sum of the other mole fractions as described by Equation 32. Equation 32 is described in terms of the measured concentrations in Equation 33 which simplifies to Equation 34.

Equation 32 $$x_{N_2} = 1 - x_{O_2} - x_{CO_2} - x_{CO} - x_{H_2O}$$

Equation 33 $$x_{N_2} = 1 - \left(1 - x_{H_2O}\right) x^a_{O_2} - \left(1 - x_{H_2O}\right) x^a_{CO_2} - \left(1 - x_{H_2O}\right) x^a_{CO} - x_{H_2O}$$

Equation 34 $$x_{N_2} = \left(1 - x_{H_2O}\right) \cdot \left(1 - x^a_{O_2} - x^a_{CO_2} - x^a_{CO}\right)$$

Substituting Equation 34 into Equation 31 gives Equation 35.

Equation 35
$$\frac{\dot{m}_{N_2}}{M_{N_2}} = \left(1 - x_{H_2O}\right) \cdot \left(1 - x^a_{O_2} - x^a_{CO_2} - x^a_{CO}\right) \frac{\dot{m}_e}{M_e}$$

Consider the number of moles of N_2 in the ambient state as described by Equation 36 and compare this to the exhaust state as described by Equation 35. These two Equations are equal and the number of moles of ambient air as a function of the exhaust gases is obtained by solving as described by Equation 37.

Equation 36
$$\frac{\dot{m}_{N_2}}{M_{N_2}} = \left(1 - x^o_{H_2O}\right) \cdot \left(1 - x^o_{O_2} - x^o_{CO_2}\right) \frac{\dot{m}_a}{M_a}$$

Equation 37
$$\frac{\dot{m}_a}{M_a} = \frac{\left(1 - x_{H_2O}\right) \cdot \left(1 - x^a_{O_2} - x^a_{CO_2} - x^a_{CO}\right)}{\left(1 - x^o_{H_2O}\right) \cdot \left(1 - x^o_{O_2} - x^o_{CO_2}\right)} \frac{\dot{m}_e}{M_e}$$

Equation 37 is an improvement of the description of the $\dot{m}_a$ to $\dot{m}_e$ relationship used in the other Configurations. Equation 37 is further refined by specifically calculating M_e rather than assuming $M_e \approx M_a$.

Substituting Equation 27 to Equation 30 and Equation 35 into Equation 38 gives Equation 39.

Equation 38
$$\dot{m}_e = \dot{m}_{N_2} + \dot{m}_{O_2} + \dot{m}_{CO_2} + \dot{m}_{CO} + \dot{m}_{H_2O}$$

Equation 39
$$\dot{m}_e = \begin{bmatrix} M_{N_2}\left(1 - x_{H_2O}\right) \cdot \left(1 - x^a_{O_2} - x^a_{CO_2} - x^a_{CO}\right) \\ + \left(1 - x_{H_2O}\right)\left(M_{O_2} x^a_{O_2} + M_{CO_2} x^a_{CO_2} + M_{CO} x^a_{CO}\right) \\ + M_{H_2O} x_{H_2O} \end{bmatrix} \frac{\dot{m}_e}{M_e}$$

Equation 39 is then rearranged for M_e with $\dot{m}_e$ cancelling and values for molecular weights inputted giving Equation 40.

Where: $M_{N_2} = 28.02$ (g.mol^{-1})

$$M_{O_2} = 32.00 \ \text{(g.mol}^{-1}\text{)}$$

$$M_{CO_2} = 44.01 \ \text{(g.mol}^{-1}\text{)}$$

$$M_{CO} = 28.01 \ \text{(g.mol}^{-1}\text{)}$$

$$M_{H_2O} = 18.02 \ \text{(g.mol}^{-1}\text{)}$$

Equation 40

$$M_e = 28\left(1 - x_{H_2O}\right)\left(1 - x^a_{O_2} - x^a_{CO_2} - x^a_{CO}\right) + \left(1 - x_{H_2O}\right)\left(32x^a_{O_2} + 44x^a_{CO_2} + 28x^a_{CO}\right) + 18x_{H_2O}$$

Equation 40 simplifies via the steps in Equation 41 and Equation 42 and becomes Equation 43.

Equation 41

$$M_e = \left(1 - x_{H_2O}\right) \cdot \left(28 + 4x^a_{O_2} + 16x^a_{CO_2}\right) + 18x_{H_2O}$$

Equation 42

$$M_e = 28 - 10 + \left(4x^a_{O_2} + 16x^a_{CO_2} + 10\right) - x_{H_2O}\left(4x^a_{O_2} + 16x^a_{CO_2} + 10\right)$$

Equation 43

$$M_e = 18 + 4\left(1 - x_{H_2O}\right)\left(x^a_{O_2} + 4x^a_{CO_2} + 2.5\right)$$

Therefore, the relationship between $\dot{m}_a$ and $\dot{m}_e$ is calculated via Equation 37. With $\dot{m}_e$ measured experimentally. M_e is calculated from measured species concentrations via Equation 43.

Consider now Equation 26. This is the general equation for HRR in Configuration 3. For Configuration 4 regress this equation by back substituting $\dot{m}_a$ (now that $\dot{m}_a$ can be calculated directly the combustion expansion assumption is no longer necessary). The HRR is described by Equation 44.

Equation 44

$$\dot{q} = \left[\frac{\Delta h_c}{r_0}\phi - \left(\frac{\Delta h_c}{r_0}\bigg|_{\substack{CO \\ \rightarrow CO_2}} - \frac{\Delta h_c}{r_0}\right)\frac{1-\phi}{2}\frac{x^a_{CO}}{x^a_{O_2}}\right]\frac{M_{O_2}}{M_a} \cdot \dot{m}_a \cdot x^o_{O_2}\left(1 - x^o_{CO_2} - x^o_{H_2O}\right)$$

Equation 44 is the general equation for HRR in Configuration 4 with ϕ described by Equation 25 and the relationship m_a / M_a by Equation 37. Within Equation 37, $\dot{m}_e$ is measured experimentally. M_e is calculated from measured species concentrations via Equation 43.

2.4 Mass flow rate

The mass flow rate calculation $\dot{m}_e$ is apparatus dependant. In the case of the Cone Calorimeter the calculation is taken from measurements of temperature and differential pressure across an orifice of known dimensions and properties. In the case of the furniture calorimeter it is taken from measurements of the temperature, differential pressure at a bi-directional probe, duct dimensions and duct velocity profile. The mass flow rates of the respective apparatus are the subject of CHAPTER 4: 'Measurement of mass flow rate of the exhaust gases'. Additional mass flow rate information is detailed in CHAPTER 6: 'Instrumentation'.

2.5 Calculation of ambient water vapour concentration

For Configurations 1,2 and 3 there is no H_2O analyser. The ambient water vapour concentration of incoming air must be calculated.

Gibbs' Phase Rule specifies the number of independent properties which must be specified in order to fix the state. Ambient moist air is a single phase, two component mixture. Therefore, Gibbs' rule requires three independent properties to fix the ambient moist air state. Atmospheric pressure and dry-bulb temperature provide two properties which are easily measured with a high degree of certainty. Because of this pairing, most generally used for the third property is either the relative humidity or thermodynamic wet bulb temperature. Intuitively, we prefer to measure the relative humidity as alternatively, calculations of the moist air state from wet bulb temperatures require the sum of the difference of dry and wet bulb temperatures. This leads to a small difference in two numerical similar properties which leads to an increase in uncertainty.

So given the atmospheric pressure, dry-bulb temperature and relative humidity the mole fraction of water vapour present in the ambient air is calculated from Equation 45.

Equation 45

$$x^o_{H_2O} = \frac{RH}{100} \cdot \frac{P_s(T_a)}{P_a}$$

$P_s(T_a)$ is the saturation pressure of water vapour at T_a and can be obtained from standard tables of thermodynamic properties of fluids.

Alternatively, Janssens[5] presents Equation 46. This is a curve-fit having the functional form of a solution to the Clasius-Clapeyron equation. It is valid for the range $0^o C \le T_a \le 50^o C$ which covers the range of ambient temperatures anticipated.

Equation 46 $$\ln[P_S(T_a)] = 23.2 - \frac{3816}{T_a - 46}$$

Rearranging Equation 46 for $P_s(T_a)$ and substituting into Equation 45 gives Equation 47. Equation 47 is the calculation of the ambient water vapour concentration.

Equation 47 $$x^o_{H_2O} = 1.19 \times 10^8 \frac{RH}{P_a} e^{\left(\frac{-3816}{T-46}\right)}$$

2.6 Calculation of molecular weight of incoming air

The molecular weight of the incoming ambient air M_a is calculated from the molecular weight of dry air, M_{dry} the molecular weight of the water vapour M_{H_2O} and the ambient water vapour concentration, $x^o_{H_2O}$. This relationship is described by Equation 48.

Equation 48 $$M_a = M_{dry}\left(1 - x^o_{H_2O}\right) + M_{H_2O} x^o_{H_2O}$$

Where: $M_{dry} = 28.96$ (g.mol^{-1})

$M_{H_2O} = 18.02$ (g.mol^{-1})

CHAPTER 3: HEAT RELEASE RATE MEASUREMENT, THERMOCHEMISTRY TECHNIQUE

3.1 Introduction

Prior to the development of the oxygen consumption technique[2] some HRR measurements in fire tests and experiments were made via a thermochemistry technique. This technique is based on CO_2 and CO production. Unfortunately, whereas the oxygen consumption technique incorporates on Thornton's Rule[1] to account for unknown fuel composition, the thermochemistry technique is not based on any such universal constant. Following the development of oxygen consumption calorimetry and stable oxygen analysers, the thermochemistry technique became practically obsolete[3].

While not being preferred, in some instances this technique provides a useful tool. For example if the composition of fuel is known as is the case during calibrations the thermochemistry technique has advantages. One is that the CO_2 analyser measures concentrations over a greater part of its range (say from 0 to 3% over a 0-5% range) than the O_2 analyser (say from 21% to 19% over a 0-25% range). Another advantage is that it is not (significantly) necessary to relate the mass flow rate of the exhaust to the incoming air, as oxygen consumption is not of concern.

Using thermochemistry, this chapter develops the theory of HRR measurement from stoichiometry. It then presents general equations for various common gas analyser configurations.

3.2 Calculation of heat release rate

Thermochemistry (Chang[8]) and the first law of thermodynamics provide an explanation of the change from chemical energy to thermal energy during a process such as combustion. The basis is therefore provided for calculating this energy change.

There is an associated change in energy in the formation of a chemical compound from its elements. This is termed the 'enthalpy of formation' of that particular product. It is sometimes also called the heat of formation. Associated terms are the 'enthalpy of reaction' and 'enthalpy of combustion'. The enthalpy of reaction is the magnitude of the total energy change, when several elements or compounds are reacting with each other to form products.

If the reactants include a fuel and oxidant then the enthalpy of reaction is redefined as the enthalpy of combustion. The enthalpy of combustion is another name for the heat release.

The heat release can be calculated from the enthalpy of formations of the reactants and products. Assuming the conservation of energy implied by the first law of thermodynamics, there are two further laws that serve as tools in heat release calculations. These are Hess' law and the Lavoisier-Laplace law.

Hess' law, also known as Hess' law of summation, allows the initial and final stages of a chemical process to be considered independent of any intermediate stages. The Lavoisier-Laplace law states that the thermal energy required to decompose an element into its compounds, is the same magnitude but opposite sign as the energy evolved when the compound is formed form its elements. We can therefore say that the heat release is the difference of the enthalpy's of formation of the products and reactants. Independent of the complex intermediate steps.

The HRR is described by Equation 49. The number of moles of the products are multiplied by their respective enthalpy's of formation. From this the enthalpy of formation of the fuel is subtracted. Note the enthalpy of formation of the reactant O_2 is zero (kJ.kmol^{-1}) as it remains in its datum phase. The sum per unit time interval is the heat release. The history of the time intervals is the HRR. The HRR appears as a negative in Equation 49 as the heat of formation terms are negative for exothermic reactions.

Equation 49

$$-\dot{q} = \sum_{\text{products}=i} \left[\left(\Delta H_f^o \right)_i \cdot \dot{n}_i \right] - \sum_{\text{reactants}=j} \left[\left(\Delta H_f^o \right)_j \cdot \dot{n}_j \right]$$

For known compositions of reactants and products the heat of the formation is obtained from tabulated data. For unknown or complex reactants or products, it is not a simple task to directly calculate the heat release rate using this technique.

3.3 General equations of HRR

Following are general equations for HRR using the thermochemistry technique. In the following cases the oxygen term is not used. This is to provide a method independent of the

oxygen analyser. Configuration 1, a sole oxygen analyser, is not considered as the equations are being derived independent of the oxygen term.

3.3.1 Configuration 2, O_2 and CO_2 analyser

Assume; complete combustion, all gasses behave in an ideal manner and incoming air consists of only N_2, O_2, CO_2 and H_2O. Consider then, from stoichiometry Equation 50.

Equation 50
$$C_a H_b O_c + \left(a + \frac{b}{4} - \frac{c}{2}\right) O_2 \rightarrow aCO_2 + \frac{b}{2} H_2O$$

Expand Equation 49 to include the products of CO_2 and H_2O. This is described by Equation 51.

Equation 51
$$-\dot{q} = \left(\Delta H_f^o\right)_{CO_2} \dot{n}_{CO_2}^g + \left(\Delta H_f^o\right)_{H_2O} \dot{n}_{H_2O}^g - \left(\Delta H_f^o\right)_{fuel} \dot{n}_{fuel}^l$$

From stoichiometry as described in Equation 50, the fuel mole loss and H_2O produced can be related to the number of moles of CO_2 generated (and subsequently measured). These relationships are described in Equation 52 and Equation 53.

Equation 52
$$\dot{n}_{fuel}^l = \frac{1}{a} \dot{n}_{CO_2}^g$$

Equation 53
$$\dot{n}_{H_2O}^g = \frac{b}{2a} \dot{n}_{CO_2}^g$$

Substituting Equation 52 and Equation 53 into Equation 51 and rearranging for $\dot{n}_{CO_2}^g$, gives Equation 54. Equation 54 describes the heat release rate in terms of the enthalpy of formation of the products and reactants, the fuel dependent mole ratio and the transient variable mole production rate of CO_2.

Equation 54
$$-\dot{q} = \left(\left(\Delta H_f^o\right)_{CO_2} + \frac{b}{2a} \cdot \left(\Delta H_f^o\right)_{H_2O} - \frac{1}{a} \left(\Delta H_f^o\right)_{fuel} \right) \cdot \dot{n}_{CO_2}^g$$

The mole flow rate term in Equation 54 needs to be redefined in terms of the measured CO_2 concentration. There are several subtleties involved in this process.

Firstly, the measured variable is in mole fractions not moles. The relationship between moles and mole fractions is described in Equation 55. Secondly, the mole fraction being measured is not solely that generated. It also includes an ambient component (constant at 300 ppm in dry ambient air). Thirdly, the mole fraction being measured has had the water vapour component removed, both ambient water and generated. Allowances for the ambient CO_2 and H_2O and generated H_2O are included in Equation 56. The generated water vapour term in Equation 56 is substituted by Equation 53 to give Equation 57. Finally, Equation 57 is rearranged around the generated CO_2 term to give Equation 58.

Equation 55 $$\dot{n}^g_{CO_2} = x^g_{CO_2} \cdot \frac{\dot{m}_e}{M_e}$$

Equation 56 $$x^g_{CO_2} = \left(1 - x^g_{H_2O} - x^o_{H_2O}\right) \cdot x^a_{CO_2} - x^o_{CO_2}$$

Equation 57 $$x^g_{CO_2} = x^a_{CO_2}\left(1 - \frac{b}{2a} x^g_{CO_2} - x^o_{H_2O}\right) - x^o_{CO_2}$$

Equation 58 $$x^g_{CO_2} = \frac{x^a_{CO_2}\left(1 - x^o_{H_2O}\right) - x^o_{CO_2}}{1 + \frac{b}{2a} x^a_{CO_2}}$$

Equation 58 is the expression of the mole fraction of generated CO_2 in the exhaust gases as a function of the CO_2 analyser measurement, the H to C ratio of the fuel and ambient concentrations of H_2O and CO_2 in the incoming air. Equation 55 and Equation 58 can be substituted into Equation 54 to give the equation for heat release rate described by Equation 59.

Equation 59 $$-\dot{q} = \left(\left(\Delta H^o_f\right)_{CO_2} + \frac{b}{2a} \cdot \left(\Delta H^o_f\right)_{H_2O} - \frac{1}{a}\left(\Delta H^o_f\right)_{fuel}\right) \cdot \left(\frac{x^a_{CO_2}\left(1 - x^o_{H_2O}\right) - x^o_{CO_2}}{1 + \frac{b}{2a} x^a_{CO_2}}\right) \cdot \frac{\dot{m}_e}{M_e}$$

Values of enthalpy of formation for the species of products in Equation 59 can be obtained from tabulated data at 25 ^{o}C from Drysdale[9].

Where: $\left(\Delta H_f^o\right)_{CO_2} = -393.5 \quad (\text{kJ.mol}^{-1})$

$\left(\Delta H_f^o\right)_{H_2O} = -241.8 \quad (\text{kJ.mol}^{-1})$

However, the fuel composition must also be known for Equation 59 to be solved.

3.3.2 Configuration 3, O_2, CO_2 and CO analyser

The following derivation follows the same general methodology as Configuration 2 in Section 3.3.1. Assume that all gasses behave in an ideal manner, that incoming air consists of only N_2, O_2, CO_2 and H_2O. Consider the stoichiometric Equation 60.

Equation 60 $$C_a H_b O_c + \left(a + \frac{b}{4} - \frac{c}{2}\right) O_2 \rightarrow n_{CO_2} CO_2 + n_{CO} CO + \frac{b}{2} H_2O$$

Expand Equation 49 to include the products of CO_2, CO and H_2O. This is described by Equation 61.

Equation 61 $$-\dot{q} = \left(\Delta H_f^o\right)_{CO_2} \dot{n}_{CO_2}^g + \left(\Delta H_f^o\right)_{CO} \dot{n}_{CO}^g + \left(\Delta H_f^o\right)_{H_2O} \dot{n}_{H_2O}^g - \left(\Delta H_f^o\right)_{fuel} \dot{n}_{fuel}^l$$

From stoichiometry as described in Equation 60,the fuel mass loss and H_2O produced can be related to the number of moles of CO_2 generated (and subsequently measured). These relationships are described in Equation 62 and Equation 63.

Equation 62 $$\dot{n}_{fuel}^l = \frac{1}{a}\left(\dot{n}_{CO_2}^g + \dot{n}_{CO}^g\right)$$

Equation 63 $$\dot{n}_{H_2O}^g = \frac{b}{2a}\left(\dot{n}_{CO_2}^g + \dot{n}_{CO}^g\right)$$

Substituting Equation 62 and Equation 63 into Equation 61 and rearranging for $\dot{n}^{g}_{CO_2}$, gives Equation 64. Equation 64 describes the heat release rate in terms of the enthalpy of formation of the products and reactants, fuel dependent mole ratios and the transient variable mole production rates of CO_2 and CO. Equation 64 simplifies to Equation 65.

Equation 64

$$-\dot{q} = \left(\Delta H^{o}_{f}\right)_{CO_2}\dot{n}^{g}_{CO_2} + \left(\Delta H^{o}_{f}\right)_{CO}\dot{n}^{g}_{CO} + \left(\Delta H^{o}_{f}\right)_{H_2O}\left[\frac{b}{2a}\left(\dot{n}^{g}_{CO_2} + \dot{n}^{g}_{CO}\right)\right] - \left(\Delta H^{o}_{f}\right)_{fuel}\left[\frac{1}{a}\left(\dot{n}^{g}_{CO_2} + \dot{n}^{g}_{CO}\right)\right]$$

Equation 65

$$-\dot{q} = \left\{\left[\left(\Delta H^{o}_{f}\right)_{CO_2} + \frac{b}{2a}\left(\Delta H^{o}_{f}\right)_{H_2O} - \frac{1}{a}\left(\Delta H^{o}_{f}\right)_{fuel}\right]\dot{n}^{g}_{CO_2} + \left[\left(\Delta H^{o}_{f}\right)_{CO} + \frac{b}{2a}\left(\Delta H^{o}_{f}\right)_{H_2O} - \frac{1}{a}\left(\Delta H^{o}_{f}\right)_{fuel}\right]\dot{n}^{g}_{CO}\right\}$$

The mole flow rate terms need to be redefined in terms of measured CO_2 and CO concentrations. This is described by Equation 66 to Equation 68.

Equation 66

$$\dot{n}^{g}_{CO_2} = x^{g}_{CO_2} \cdot \frac{\dot{m}_e}{M_e}$$

Equation 67

$$\dot{n}^{g}_{CO} = x^{g}_{CO} \cdot \frac{\dot{m}_e}{M_e}$$

Equation 68

$$-\dot{q} = \left\{\left[\left(\Delta H^{o}_{f}\right)_{CO_2} + \frac{b}{2a}\left(\Delta H^{o}_{f}\right)_{H_2O} - \frac{1}{a}\left(\Delta H^{o}_{f}\right)_{fuel}\right]x^{g}_{CO_2} + \left[\left(\Delta H^{o}_{f}\right)_{CO} + \frac{b}{2a}\left(\Delta H^{o}_{f}\right)_{H_2O} - \frac{1}{a}\left(\Delta H^{o}_{f}\right)_{fuel}\right]x^{g}_{CO}\right\} \cdot \frac{\dot{m}_e}{M_e}$$

As with Equation 54 in Configuration 2, Equation 68 must also be reconciled to allow for the ambient CO_2 and H_2O concentrations in the exhaust gases and the removal of water vapour. These relationships are described in Equation 69 and Equation 70.

Equation 69

$$x^{g}_{CO_2} = \left(1 - x^{g}_{H_2O} - x^{o}_{H_2O}\right) \cdot x^{a}_{CO_2} - x^{o}_{CO_2}$$

Equation 70 $$x_{CO}^{g} = \left(1 - x_{H_2O}^{g} - x_{H_2O}^{o}\right) \cdot x_{CO}^{a}$$

Equation 69 and Equation 70 are rearranged as Equation 71 and Equation 72 (respectively) to describe the water vapour term as a function of CO_2 and CO generated.

Equation 71 $$x_{CO_2}^{g} = \left(1 - \frac{b}{2a}\left(x_{CO_2}^{g} + x_{CO}^{g}\right) - x_{H_2O}^{o}\right) \cdot x_{CO_2}^{a} - x_{CO_2}^{o}$$

Equation 72 $$x_{CO}^{g} = \left(1 - \frac{b}{2a}\left(x_{CO_2}^{g} + x_{CO}^{g}\right) - x_{H_2O}^{o}\right) \cdot x_{CO}^{a}$$

Rearrange Equation 71 and Equation 72 about $x_{CO_2}^{g}$ and x_{CO}^{g} to get Equation 73 and Equation 74. This latest step, from Equation 71 to Equation 73 and Equation 72 to Equation 74 involves many intermediate steps which, for brevity are not repeated here.

Equation 73 $$x_{CO_2}^{g} = \frac{x_{CO_2}^{a}\left(1 - x_{H_2O}^{o}\right) - x_{CO_2}^{o} + \frac{b}{2a} x_{CO_2}^{o} x_{CO}^{a}}{1 + \frac{b}{2a}\left(x_{CO_2}^{a} + x_{CO}^{a}\right)}$$

Equation 74 $$x_{CO}^{g} = \frac{x_{CO}^{a}\left(1 - x_{H_2O}^{o}\right) + \frac{b}{2a} x_{CO_2}^{o} x_{CO}^{a}}{1 + \frac{b}{2a}\left(x_{CO_2}^{a} + x_{CO}^{a}\right)}$$

Equation 73 and Equation 74 are expressions of the mole fraction of generated CO_2 and CO in the exhaust gases as a function of the CO_2 and CO analyser measurements, the H to C ratio of the fuel and ambient concentrations of H_2O and CO_2 in the incoming air. Note the similar form to Equation 58 in Configuration 2. Equation 73 and Equation 74 are substituted into Equation 68 to give Equation 75. This is the general equation for heat release rate.

Equation 75

$$-\dot{q} = \left\{ \left[\left(\Delta H_f^o\right)_{CO_2} + \frac{b}{2a}\left(\Delta H_f^o\right)_{H_2O} - \frac{1}{a}\left(\Delta H_f^o\right)_{fuel} \right] \left[\frac{x_{CO_2}^a\left(1 - x_{H_2O}^o\right) - x_{CO_2}^o + \frac{b}{2a} x_{CO_2}^o x_{CO}^a}{1 + \frac{b}{2a}\left(x_{CO_2}^a + x_{CO}^a\right)} \right] \right.$$
$$\left. + \left[\left(\Delta H_f^o\right)_{CO} + \frac{b}{2a}\left(\Delta H_f^o\right)_{H_2O} - \frac{1}{a}\left(\Delta H_f^o\right)_{fuel} \right] \left[\frac{x_{CO}^a\left(1 - x_{H_2O}^o\right) + \frac{b}{2a} x_{CO_2}^o x_{CO}^a}{1 + \frac{b}{2a}\left(x_{CO_2}^a + x_{CO}^a\right)} \right] \right\} \cdot \frac{\dot{m}_e}{M_e}$$

Values of enthalpy of formation for the species of products in Equation 75 can be obtained from tabulated data at 25 ^oC from Reference [9].

Where:
$$\left(\Delta H_f^o\right)_{CO_2} = -393.5 \quad (\text{kJ.mol}^{-1})$$
$$\left(\Delta H_f^o\right)_{CO} = -110.5 \quad (\text{kJ.mol}^{-1})$$
$$\left(\Delta H_f^o\right)_{H_2O} = -241.8 \quad (\text{kJ.mol}^{-1})$$

However, the fuel composition must also be known for Equation 75 to be solved.

3.3.3 Configuration 4, O_2, CO_2, CO and H_2O analyser

The following derivation follows the same general methodology as Configuration 3 in Section 3.3.2. Assume all gasses behave in an ideal manner. Assume incoming air consists of only N_2, O_2, CO_2 and H_2O. The first steps are the same as previously except that as H_2O is now being measured. Note that CO_2 and CO are still measured dry. Equation 64 becomes Equation 76 and this rearranges to becomes Equation 77.

Equation 76 $$-\dot{q} = \left(\Delta H_f^o\right)_{CO_2}\dot{n}_{CO_2}^g + \left(\Delta H_f^o\right)_{CO}\dot{n}_{CO}^g + \left(\Delta H_f^o\right)_{H_2O}\dot{n}_{H_2O}^g - \left(\Delta H_f^o\right)_{fuel}\left[\frac{1}{a}\left(\dot{n}_{CO_2}^g + \dot{n}_{CO}^g\right)\right]$$

Equation 77
$$-\dot{q} = \left\{ \left[\left(\Delta H_f^o\right)_{CO_2} - \frac{1}{a}\left(\Delta H_f^o\right)_{fuel} \right] \dot{n}_{CO_2}^g + \left[\left(\Delta H_f^o\right)_{CO} - \frac{1}{a}\left(\Delta H_f^o\right)_{fuel} \right] \dot{n}_{CO}^g \right.$$
$$\left. + \left(\Delta H_f^o\right)_{H_2O}\dot{n}_{H_2O}^g \right\}$$

The mole flow rate terms need to be redefined in terms of measured CO_2, CO and H_2O concentrations. This is described by Equation 78 to Equation 81.

Equation 78 $$\dot{n}^g_{CO_2} = x^g_{CO_2} \cdot \frac{\dot{m}_e}{M_e}$$

Equation 79 $$\dot{n}^g_{CO} = x^g_{CO} \cdot \frac{\dot{m}_e}{M_e}$$

Equation 80 $$\dot{n}^g_{H_2O} = x^g_{H_2O} \cdot \frac{\dot{m}_e}{M_e}$$

Equation 81
$$-\dot{q} = \left\{ \left[\left(\Delta H^o_f\right)_{CO_2} - \frac{1}{a}\left(\Delta H^o_f\right)_{fuel} \right] x^g_{CO_2} + \left[\left(\Delta H^o_f\right)_{CO} - \frac{1}{a}\left(\Delta H^o_f\right)_{fuel} \right] x^g_{CO} + \left(\Delta H^o_f\right)_{H_2O} x^g_{H_2O} \right\} \cdot \frac{\dot{m}_e}{M_e}$$

As with Equation 54 in Configuration 2 and Equation 68 in Configuration 3 Equation 81 must also be reconciled to allow for the ambient CO_2 and H_2O concentrations in the exhaust gases and the removal of water vapour from the CO_2 and CO measurement. These relationships are described in Equation 82 to Equation 84.

Equation 82 $$x^g_{CO_2} = \left(1 - x^g_{H_2O} - x^o_{H_2O}\right) \cdot x^a_{CO_2} - x^o_{CO_2}$$

Equation 83 $$x^g_{CO} = \left(1 - x^g_{H_2O} - x^o_{H_2O}\right) \cdot x^a_{CO}$$

Equation 84 $$x^g_{H_2O} = x^a_{H_2O} - x^o_{H_2O}$$

Substitute Equation 84 into Equation 82 and Equation 83 to get Equation 85 and Equation 86.

Equation 85 $$x^g_{CO_2} = \left(1 - x^a_{H_2O}\right) \cdot x^a_{CO_2} - x^o_{CO_2}$$

Equation 86 $$x^g_{CO} = \left(1 - x^a_{H_2O}\right) \cdot x^a_{CO}$$

Substitute Equation 84, Equation 85 and Equation 86 into Equation 82 to give Equation 87. This is the general equation for heat release rate.

Equation 87

$$-\dot{q} = \left\{ \left[\left(\Delta H_f^o\right)_{CO_2} - \frac{1}{a}\left(\Delta H_f^o\right)_{fuel} \right] \left[\left(1 - x_{H_2O}^a\right) \cdot x_{CO_2}^a - x_{CO_2}^o \right] \right.$$
$$+ \left[\left(\Delta H_f^o\right)_{CO} - \frac{1}{a}\left(\Delta H_f^o\right)_{fuel} \right] \left(1 - x_{H_2O}^a\right) \cdot x_{CO}^a$$
$$\left. + \left(\Delta H_f^o\right)_{H_2O} \left(x_{H_2O}^a - x_{H_2O}^o\right) \right\} \cdot \frac{\dot{m}_e}{M_e}$$

Values of enthalpy of formation for the species of products in Equation 87 can be obtained from tabulated data at 25 ^{o}C from Reference [9].

Where:

$$\left(\Delta H_f^o\right)_{CO_2} = -393.5 \quad (\text{kJ.mol}^{-1})$$
$$\left(\Delta H_f^o\right)_{CO} = -110.5 \quad (\text{kJ.mol}^{-1})$$
$$\left(\Delta H_f^o\right)_{H_2O} = -241.8 \quad (\text{kJ.mol}^{-1})$$

However, the fuel composition must also be known for Equation 87 to be solved.

3.4 Mass flow rate and molecular weight of exhaust gases

The mass flow rate calculation $\dot{m}_e$ is apparatus dependant. In the case of the Cone Calorimeter the calculation is taken from measurements of temperature and differential pressure across an orifice of known dimensions and properties. In the case of the furniture calorimeter it is taken from measurements of the temperature, differential pressure at a bidirectional probe duct dimensions and duct velocity profile. The mass flow rates of the respective apparatus are the subject of CHAPTER 4: ‘Measurement of mass flow rate of the exhaust gases’. Additional mass flow rate information is detailed in CHAPTER 6: ‘Instrumentation’.

The molecular mass of the exhaust gasses M_e is assumed approximately equal with the molecular mass of dry incoming ambient air at $M_e \approx M_{a\_(dry)} = 0.02896$ kg.mol^{-1}. This

assumption is discussed in more detail in Example 2 of CHAPTER 5: 'Propagation of uncertainty of heat release rate measurement'. The Example is a comparison of the Configuration 2 general equations based on thermochemistry to the standardised equations based on the principal of oxygen consumption. It is noted in the Example that the $M_e \approx M_{a\_(dry)}$ assumption is common to the oxygen consumption technique.

3.5 Relationship between gas concentrations in the incoming air and exhaust gases

Within the general equations for HRR expressed by Equation 59, Equation 75 and Equation 87, the input values of $x^o_{CO_2}$ and $x^o_{H_2O}$ are properties of the incoming air $\left(x^o_{CO_2}\right)_a$ and $\left(x^o_{H_2O}\right)_a$ rather than the exhaust gas $\left(x^o_{CO_2}\right)_e$ and $\left(x^o_{H_2O}\right)_e$. This assumes that $\left(x^o_{CO_2}\right)_a \approx \left(x^o_{CO_2}\right)_e$ and $\left(x^o_{H_2O}\right)_a \approx \left(x^o_{H_2O}\right)_a$. This assumption is justified on the following basis.

The mole fractions of these species vary between the incoming air and exhaust gases due to the combustion process. However, the number of moles of each remain the same. Consider Equation 88 and Equation 89.

Equation 88 $$n^o_{CO_2} = \left(x^o_{CO_2}\right)_a n_a = \left(x^o_{CO_2}\right)_e n_e$$

Equation 89 $$n^o_{H_2O} = \left(x^o_{H_2O}\right)_a n_a = \left(x^o_{H_2O}\right)_e n_e$$

Considering generic species i, Equation 90 follows from Equation 89.

Equation 90 $$\left(x^o_i\right)_e = \left(x^o_i\right)_a \frac{n_a}{n_e}$$

From stoichiometry we can describe n_a and n_e as Equation 91 and Equation 92.

Equation 91 $$n_a = n^o_{N_2} + n^o_{O_2} + n^o_{CO_2} + n^o_{H_2O}$$

Equation 92 $$n_e = n^o_{N_2} + \left(n^o_{O_2} - n^{cons}_{O_2}\right) + \left(n^g_{CO_2} + n^o_{CO_2}\right) + \left(n^g_{H_2O} + n^o_{H_2O}\right)$$

Rearranging Equation 92 gives Equation 93 which simplifies to Equation 94.

Equation 93 $$n_e = \left(n^o_{N_2} + n^o_{O_2} + n^o_{CO_2} + n^o_{H_2O}\right) + \left(n^g_{CO_2} + n^g_{H_2O} - n^{cons}_{O_2}\right)$$

Equation 94 $$n_a = n_e - \left(n^g_{CO_2} + n^g_{H_2O} - n^{cons}_{O_2}\right)$$

From stoichiometry we can redefine the species terms in Equation 94 by their relationship to CO_2 generated. This gives Equation 95 which simplifies first to Equation 96 and then to Equation 97.

Equation 95 $$n_a = n_e - \left(\frac{a}{a} n^g_{CO_2} + \frac{b}{2a} n^g_{CO_2} - \left(\frac{a}{a} + \frac{b}{4a} - \frac{c}{2a}\right) n^g_{CO_2}\right)$$

Equation 96 $$n_a = n_e - \left(\frac{a}{a} + \frac{b}{2a} - \left(\frac{a}{a} + \frac{b}{4a} - \frac{c}{2a}\right)\right) n^g_{CO_2}$$

Equation 97 $$n_a = n_e - \left(\frac{b+2c}{4a}\right) n^g_{CO_2}$$

Equation 97 can be substituted into Equation 90 to give Equation 98 which in turn simplifies to Equation 99 and Equation 100.

Equation 98 $$\left(x^o_i\right)_e = \left(x^o_i\right)_a \frac{\left[n_e - \left(\frac{b+2c}{4a}\right) n^g_{CO_2}\right]}{n_e}$$

Equation 99 $$\left(x^o_i\right)_e = \left(x^o_i\right)_a \left[1 - \left(\frac{b+2c}{4a}\right) \frac{n^g_{CO_2}}{n_e}\right]$$

Equation 100 $$\left(x^o_i\right)_e = \left(x^o_i\right)_a \left[1 - \left(\frac{b+2c}{4a}\right) x^g_{CO_2}\right]$$

Consider the coefficient $(b+2c)/4a$. This has a maximum value of 1.50 for fuels such as methyl alcohol (CH_2O) and formic acid (CH_2O_2). Therefore, the maximum difference in the incoming and exhaust terms is described by Equation 101.

Equation 101 $$\left(x_i^o\right)_e = \left(x_i^o\right)_a \left[1 - 1.5 x_{CO_2}^g\right]$$

Typically the mole fraction of CO_2 generated in free burning test and experiments is ≈1% by volume. Therefore, for the worst case fuel at the peak HRR (when the most CO_2 is generated), $\left(x_i^o\right)_e$ is a minimum with respect to $\left(x_i^o\right)_a$ as described by

Equation 102 $$\left(x_i^o\right)_{e,\min} \approx 0.985 \cdot \left(x_i^o\right)_a$$

As the circumstances required for Equation 102 to hold are unusual it is justifiable to assume Equation 103 and Equation 104.

Equation 103 $$\left(x_{CO_2}^o\right)_e \approx \left(x_{CO_2}^o\right)_a$$

Equation 104 $$\left(x_{H_2O}^o\right)_e \approx \left(x_{H_2O}^o\right)_a$$

Further to Equation 103, it is generally assumed the dry ambient CO_2 concentration is 300 ppm. Therefore, the actual (wet) ambient concentration is described by Equation 105.

Equation 105 $$x_{CO_2}^o = \frac{300}{10^6}\left(1 - x_{H_2O}^o\right)$$

In conclusion, the water vapour concentration (mole fraction) in the exhaust gases may be assumed to be the same as that calculated from ambient incoming air. Similarly, the ambient CO_2 concentration can be assumed to also have the same value.

CHAPTER 4: MEASUREMENT OF MASS FLOW RATE OF THE EXHAUST GASES

4.1 Introduction

Common to both Cone and Furniture Calorimeter measurements (and other calorimetry applications), is the requirement to measure the total mass flow rate of products, $\dot{m}_e$ in the exhaust duct.

The $\dot{m}_e$ term is present in all of the general equations for HRR for each configuration described in CHAPTER 2: 'Heat release rate measurement, oxygen consumption technique' and CHAPTER 3: 'Heat release rate measurement, thermochemistry technique'. An understanding of the experimental technique for measuring $\dot{m}_e$ in both the small-scale and full-scale is needed prior to moving on to the following Chapters.

The mass flow rate is the product of the volumetric flow rate and gas density. Measurements of velocity profile are sought to calculate the volumetric flow rates. Then assuming ideal gas behaviour the gas density is calculated from a temperature measurement.

There are two primary velocity measurement methods. Measuring the pressure drop across an orifice plate (from which the centre line velocity can be calculated) or measuring the centreline differential pressure with a bi-directional probe (from which the centre line velocity can be calculated). The first method is used for small scale tests and experiments on the Cone Calorimeter. The second method is used for full-scale scale tests and experiments on the Furniture Calorimeter.

4.2 Orifice plate method (small-scale)

The volumetric flow rate is calculated via measurements of pressure drop across an orifice plate by applying Bernoulli's equation. The centreline velocity (or any velocity at the cross-sectional point the differential pressure is measured) is described by Equation 106 where Δp is the (centreline) differential pressure and ρ_e is the density of the exhaust gases.

Equation 106 $$v = \sqrt{\frac{2\Delta p}{\rho_e}}$$

Assuming ideal gas behaviour, Equation 106 may be further developed by relating the density of the exhaust gases to temperature (a measured variable). Refer to Equation 107, where ρ_{ref} and T_{ref} are corresponding reference temperatures and densities of air. Typical values are 1.29 kg/m^{-3} at 273 K. Equation 107 is substituted into Equation 106 to give Equation 108.

Equation 107 $$\rho_e \approx \frac{\rho_{ref} T_{ref}}{T_e}$$

Equation 108 $$v = \sqrt{2\rho_{ref} T_{ref}} \sqrt{\frac{\Delta p}{T_e}}$$

The mass flow rate $\dot{m}_e$ is related to the velocity v as a function of the cross-sectional area and density as described by Equation 109.

Equation 109 $$\dot{m}_e = C\sqrt{\frac{\Delta p}{T_e}}$$

The constant *C* is derived experimentally from the methane HRR calibration. Its value includes the constants from Equation 108. The value of the constant C is actually a function of the fluid properties and constants as per Equation 110.

Equation 110 $$C = C'MA_0\sqrt{2g_c T_{ref}\rho_{ref}}$$

The flow coefficient is $C'M$, (the orifice plate coefficient is C' , the overall coefficient $C'M$), the flow area A_0 and the root of the product of a reference temperature T_{ref} , density ρ_{ref} and a gravitational constant g_c (value of 1.0 kg.m.N^{-1}.s^{-2}). A more detailed discussion of flow measurement can be found in Holman[10].

4.3 Centreline velocity method (full-scale)

4.3.1 Mass flow rate

The full-scale method for measuring the mass flow rate of exhaust gases $\dot{m}_e$, is to place a velocity measuring device along the centreline of the duct. Assuming fully developed flow, the shape factor k_c (the ratio of average velocity $\bar{v}$ to centreline velocity v_c) remains constant over the length of the duct. The shape factor k_c is given by Equation 111.

Equation 111 $$k_c = \frac{\bar{v}}{v_c}$$

By measuring the centreline velocity and having an experimentally predetermined shape factor (see later section) the average velocity can be calculated. This is given by Equation 112. The volumetric flow rate $\dot{V}$ in $m^3 \cdot s^{-1}$ is then expressed as Equation 113 where A is the cross sectional area of the duct in m^2.

Equation 112 $$\bar{v} = k_c v_c$$

Equation 113 $$\dot{V} = A k_c v_c$$

As with the small-scale experiments, the volumetric flow rate is related to the exhaust mass flow rate $\dot{m}_e$ from velocity calculations via Bernoulli's equation. The centreline velocity (or any velocity at the cross-sectional point the differential pressure is measured) is described by Equation 106 where Δp is the (centreline) differential pressure and ρ_e is the density of the exhaust gases. Setting v to v_c by measuring differential pressure at the centreline and substituting Equation 106 into Equation 113 gives Equation 114. Multiplying both sides of Equation 114 by the density of the exhaust gases converts the volumetric flow rate to a mass flow rate. This is described by Equation 115.

Equation 114 $$\dot{V} = A k_c \sqrt{\frac{2\Delta p}{\rho_e}}$$

Equation 115 $$\dot{m}_e = A k_c \sqrt{2 \rho_e \Delta p}$$

Also similarly to the small-scale method, assumed ideal gas behaviour relates the density of the exhaust gases to the temperature (of the exhaust gases). This described by Equation 116 which simplifies to Equation 117.

Equation 116 $$\dot{m}_e = Ak_c\sqrt{2\rho_{ref}T_{ref}}\sqrt{\frac{\Delta p}{T_e}}$$

Equation 117 $$\dot{m}_e = 26.55Ak_c\sqrt{\frac{\Delta p}{T_e}}$$

The differential pressure Δp term in Equation 117 is measured by a bi-directional probe. This probe is described by McCaffrey and Heskestad[11] as suitable for use in elevated temperatures and sooty conditions. Further advantages are that it is robust, relatively simple to construct and use and has angular insensitivity to within about ±50°. It has an overall reported accuracy of ±5% under full-scale fire experimental conditions.

An apparatus dependant correction has to be made to the mass flow rate calculation in Equation 117. This correction is a function of the Reynolds number with respect to the flow around the probe. Note, the Reynolds number characteristic dimension is the inside diameter of the probe. Including the correction Equation 117 becomes Equation 118.

Equation 118 $$\dot{m}_e = 26.55\frac{Ak_c}{f(\mathrm{Re})}\sqrt{\frac{\Delta p}{T_e}}$$

It has been found that for $40 < \mathrm{Re} < 3800$ then Equation 119 applies. Alternatively, if $\mathrm{Re} > 3800$ (--) Equation 120 applies as $f(\mathrm{Re})$ becomes asymptotic. The correction has been derived from comparisons in ambient air with values from a pitot-static tube of 1.00.

Equation 119 $$f(\mathrm{Re}) = \begin{pmatrix} 1.533 - 1.366\times10^{-3}\,\mathrm{Re} + 1.688\times10^{-6}\,\mathrm{Re}^2 - 9.706\times10^{-11}\,\mathrm{Re}^3 \\ + 2.555\times10^{-13}\,\mathrm{Re}^4 - 2.484\times10^{-17}\,\mathrm{Re}^5 \end{pmatrix}$$

Equation 120 $$f(\mathrm{Re}) = 1.08$$

It has been found experimentally that with bi-directional probes of 16 mm diameter even at very low velocities, Re exceeds 3800, further simplifying Equation 118 to Equation 121.

Equation 121 $$\dot{m}_e = 26.55 \frac{A k_c}{1.08} \sqrt{\frac{\Delta p}{T_e}}$$

Given a predetermined velocity shape factor Equation 121 is the general equation for the mass flow rate of the exhaust gases in terms of a centreline differential pressure measurement and an adjacent temperature measurement.

4.3.2 Determination of the UC Furniture Calorimeter velocity shape factor

For the UC Furniture calorimeter the velocity shape factor was determined simplistically. The result (of $k_c = 0.99$) is more fully detailed in Chapter [6]: 'Instrumentation'.

The velocity profile was specifically measured at 50 mm increments across the 580 mm diameter duct in the horizontal plane. The factor being the integral of the profile divided by the duct diameter. Unfortunately, a vertical profile was not able to be obtained due to lack of access. Several profiles were undertaken at varying conditions of extract rate and exhaust gas temperature. The profile was found to be consistent over the varying conditions.

More detailed methods of determining the velocity shape factor are available. The following section discusses one of these methods, the log-linear method.

4.3.3 The log-linear method for determining the velocity shape factor

Rather than taking incremental velocity measurements uniformly across the duct diameter as was the case in the UC Furniture Calorimeter velocity shape factor determination, this method advocates more selective locations.

This method is based on the assumption that the velocity distribution of non-fully developed flow can be represented by (the log-linear) Equation 122, where D is the duct diameter, $v(y)$ is the velocity at point y, along the diameter and C_1, C_2, and C_3 are numerical constants.

Equation 122 $$v(y) = C_1 + C_2 \log\left(\frac{y}{D}\right) + C_3\left(\frac{y}{D}\right)$$

Assuming Equation 122 holds, and it has been found to do so by Ross and Robertson[12] then the ideal positions at which representative mean local velocities would occur can be determined from Table 1. Table 1 is reproduced from Ower and Pankhurst[13].

NO. OF AREAS (N)	NO. OF MEAS. POINTS (2N)	LOCATION OF MEASURING POINTS ALONG DIAMETER (Y/D)
2	4	0.043, 0.290, 0.710, 0.957
3	6	0.032, 0.135, 0.321, 0.679, 0.865, 0.968
4	8	0.021, 0.117, 0.184, 0.345, 0.655, 0.816, 0.883, 0.979
5	10	0.019, 0.076, 0.153, 0.217, 0.361, 0.639, 0.783, 0.847, 0.924, 0.981

Table 1: Positions of Mean Local Velocities. (Ower and Pankhurst[13]).

The overall mean velocity $\bar{v}$ used in determining the velocity shape factor k_c is then calculated as the average of the measured local mean velocities. This is described by Equation 123, for N elements of area.

Equation 123 $$\bar{v} = \frac{\sum_{i=1}^{N}\left\{\left(\frac{2\Delta p}{\rho_e}\right)^{\frac{1}{2}}\right\}}{2N}$$

Substituting Equation 123 back into the velocity shape factor expression of Equation 111 gives Equation 124. This simplifies to Equation 125.

Equation 124 $$k_c = \frac{\bar{v}}{v_c} = \frac{\sum_{i=1}^{2N}\left\{\left(\frac{2(\Delta p)}{\rho_e}\right)^{\frac{1}{2}}\right\}}{2N\left(\frac{2(\Delta p)}{\rho_e}\right)^{\frac{1}{2}}}$$

Equation 125

$$k_c = \frac{\sum_{i=1}^{2N} (\Delta p)^{\frac{1}{2}}}{2N(\Delta p)^{\frac{1}{2}}}$$

The velocity shape factor can be determined using Equation 125 from differential pressure measurements from the y/D locations of Table 1.

CHAPTER 5: PROPAGATION OF UNCERTAINTY OF HEAT RELEASE RATE MEASUREMENT

5.1 Introduction

The heat release rate (HRR) of a material when subject to fire, is widely considered the single most important variable in fire hazard assessment (Babrauskas and Peacock[14]). It is of primary interest to both the fire researcher and engineering practitioner. Experimental techniques and Standard Test Methods have been developed to indirectly measure the HRR. The most accepted of these, are based on oxygen consumption calorimetry (Huggett[2], Janssens[15]). Examples of Standard Test Methods are; ISO5660-1[6] and ASTM1354[16] for the cone calorimeter, NT FIRE 032[7] for the furniture calorimeter and the ISO9705[17] for room fire tests of surface products.

The cone, furniture and room calorimeter Standard Test Methods calculate the HRR from several measurements. Measurement theory dictates that each measured value has an associated uncertainty. When these values are used in a mathematical function, there is a corresponding propagation of uncertainty associated with that function.

Ku[18] reports that there are two kinds of 'orthodox' uncertainties associated with these measurements and the functional relationship. Random and systematic. A random uncertainty is defined by Ku as "…derived by a statistical analysis of repeated measurement" - such as the oxygen analyser short term noise and drift calibration. A systematic uncertainty is estimated as a "…credible bound to an error that is likely to affect all the measurement in the same manner" – such as the effective heat of combustion term in tests of the same fuel.

This chapter focuses on the propagation of random and systematic uncertainties through the heat release rate calculation for the cone and furniture calorimeters. Four different gas analyser configurations are considered. From a sole O_2 analyser to a configuration including O_2, CO_2, CO and H_2O analysers.

The types of uncertainty investigated in this chapter and the following uncertainty examples are necessarily limited to random uncertainties associated with measuring instruments and systematic uncertainties associated with major simplifying assumptions.

The random uncertainty of an instrument measurement is investigated in so far as the instrument can be relied upon to be giving a true reading. An analogy is a ruler with single millimetre gradations. We would assume a measurement to be within half of the smallest gradation. In this chapter examples of our 'ruler' might be the oxygen analyser, thermocouple or pressure transducer. Secondly, the systematic uncertainties associated with - in particular - empirical constants used in the calculation have uncertainties associated with them. An example is the ratio of the assumed effective net heat of combustion to stoichiometric oxygen/fuel mass ratio.

Whilst this Chapter considers two sources of uncertainty, i.e. instrument and assumption uncertainties, it does not investigate two other sources, i.e. random uncertainties associated with fuel properties or random or systematic errors associated with sample preparation and test operation. In respect to these latter two unconsidered sources of uncertainty Ku's work[18] recommends that a factor of safety of two may be applied, or that instead of the root mean square (RMS) being taken the component uncertainty terms are added directly. These recommendations are not adopted in this work nor pursued further. Rather they are mentioned as a source for further investigation.

To a limited degree, these random uncertainties associated with the fuel and operation may be found in the characterisation of the precision the cone calorimeter appended to the Standard Test Methods[6],[16]. This reported precision in the Standard Test Methods results in repeatability and reproducibility bounds, determined from a rigorous statistical analysis of a round robin series of a limited number of test samples involving a limited number of testing laboratories.

However, the precision reported in the Standard Test Method may only be considered an experimentally determined 'end point'. It is only of value for certain key test properties. It doesn't account for systematic errors in the calculation or test procedures because the fuels have known values of effective heat of combustion. Its validity is limited to the materials tested in the participating testing laboratories.

In contrast to this 'end point' , this chapter is an analytically quantifying 'beginning point'. It is complimentary to established precision procedures.

This chapter does not develop the instrument dependent component uncertainties as these will vary from apparatus to apparatus. However, these are included in – for the University of Canterbury (UC) Cone Calorimeter – in the following examples.

5.2 Propagation of uncertainty

The result of a measurement is only an approximation of the value of the specific property, subject to the measurement (Baird[19]). In many cases, such as in the HRR, a direct measurement is not possible. Instead, a value is calculated from other measurements through a functional relationship. The partial derivatives of this function can be used to calculate uncertainty and provide a powerful general analytical method.

If we have a function $z = f(x, y)$ there is an absolute uncertainty δz, and a relative uncertainty $\delta z/z$. In order to calculate δz we must first consider the total differential dz.

Equation 126 $$dz = \left(\frac{\partial f}{\partial x}\right)dx + \left(\frac{\partial f}{\partial y}\right)dy$$

Treating Equation 126 as a finite difference δz, in terms of the component uncertainties δx and δy. Where the partial derivatives $\partial f/\partial x$ and $\partial f/\partial y$ are evaluated for the values x_0 and y_0 for which δz is the required uncertainty.

As an aside, the partial derivatives $\partial f/\partial x$ and $\partial f/\partial y$ are often referred to as sensitivity coefficients. This is because the uncertainty is sensitive to the product of the partial derivative and the component uncertainty. If all the component measurements are of a system are of a similar magnitude of order, the sensitivity coefficients can be compared directly to gauge sensitivity. Unfortunately this is not the case in HRR measurement where for example, the species concentration measurements are several magnitudes of order different than the ratio of the assumed effective heat of combustion to stoichiometric ratio. Analytical work, effectively normalising the sensitivity coefficients with respect to the component measured would be useful future research. Returning to Equation 127.

Equation 127 $$\delta z = \left(\frac{\partial f}{\partial x}\right)\delta x + \left(\frac{\partial f}{\partial y}\right)\delta y$$

If probabilistic based values are not used for the component uncertainties ∂x and ∂y, Equation 127 is concerned with outer limits of uncertainty for the measured values. This may represent an unrealistically pessimistic approach. If this is the case and the random variable associated with the uncertainty is assumed to have a rectangular distribution we adopted the value of the RMS of the component uncertainties as described in Equation 128.

Equation 128

$$\delta z = \left(\left[\left(\frac{\partial f}{\partial x} \right) \delta x \right]^2 + \left[\left(\frac{\partial f}{\partial y} \right) \right]^2 \delta y \right)^{\frac{1}{2}}$$

Equation 128 is an expression of the RMS absolute uncertainty of function *z*. It is expressed in the units of the value. Typically, it is the relative uncertainty that is of interest. The relative uncertainty is the absolute uncertainty divided by the calculated value. It is useful to express the uncertainty as a percentage of the value. The relative uncertainty of function *z* is described by Equation 129.

Equation 129

$$\frac{\delta z}{z} = \frac{\left(\left[\left(\frac{\partial f}{\partial x} \right) \delta x \right] + \left[\left(\frac{\partial f}{\partial y} \right) \delta y \right] \right)^{\frac{1}{2}}}{f(x, y)}$$

5.3 General equations for HRR measurement by the oxygen consumption technique

The derivations of the general equations for HRR referred to in the following sections, may be found in CHAPTER 3: ‘Heat release rate measurement, thermochemistry technique’ and CHAPTER 4: ‘Measurement of mass flow rate of the exhaust gases’.

General equations of uncertainty are presented for the four typical gas analysis configurations. The partial derivatives (sensitivity coefficients) within the general equations of uncertainty are derived. However, assumption and instrument dependent component uncertainties are not included in this chapter. This is on the basis that this chapter is generally applicable, not specifically applicable. Specific component uncertainties relating to the University of Canterbury (UC) Cone Calorimeter are included in the following examples.

5.3.1 Configuration 1: O_2 Gas Analysis

In Configuration 1, the general equation for HRR is described by Equation 20 with the oxygen depletion factor ϕ as Equation 9 and the mass flow rate Equation 109 in the small-scale and Equation 121 in the full-scale.

The ratio M_{O_2}/M_a may be assumed to have the value 1.10 which is correct for dry air. For now make the simplifying assumption that the uncertainty of M_{O_2}/M_a, is negligible $\delta\left(M_{O_2}/M_a\right)=0$. Although, $\delta\left(M_{O_2}/M_a\right)$ is in fact a function of ambient water vapour concentration, $x^o_{H_2O}$. This point is analysed and discussed in greater detail in the following examples.

The ambient concentrations of oxygen and carbon dioxide, $x^o_{O_2}$ and $x^o_{CO_2}$, may be assumed to have the values 0.2095 and 0.0003 in dry air. The uncertainty associated with these values $\delta x^o_{O_2}$ and $\delta x^o_{CO_2}$ may be assumed negligible. Even were this not the case, the experimental baseline measurements also used to determine these values have a decreasing uncertainty tending towards zero with the very large number of measurements taken during the baseline measurements. This is to say, confidence increases with the number of measurements.

The assumption of a fixed value for $x^o_{O_2}$ is very important, as it allow variable independence to be assumed between ϕ and $x^o_{O_2}$ as ϕ conceals $x^a_{O_2}$ terms.

The ambient water vapour concentration $x^o_{H_2O}$ is determined from Equation 47 from measurements of ambient temperature T_a, atmospheric pressure P_a, and relative humidity *RH*. The simplifying assumption is made that the uncertainty associated with this value $\delta x^o_{H_2O}$ is negligible. Although, there is less basis to do this than with $\delta x^o_{O_2}$ and $\delta x^o_{CO_2}$. This assumption is also explored more fully in the following applications.

Given these simplifying assumptions the HRR in Equation 20 may be rewritten as Equation 130. With $x^o_{O_2}$, $x^o_{CO_2}$ and $x^o_{H_2O}$ as predetermined constants of negligible uncertainty ($\delta x^o_{O_2}$,

$\delta x^o_{CO_2}$ and $\delta x^o_{H_2O}$ are zero). If $x^o_{O_2}$, $x^o_{CO_2}$ and $x^o_{H_2O}$ are predetermined constants of negligible uncertainty $x^o_{O_2}\left(1 - x^o_{CO_2} - x^o_{H_2O}\right)$ can therefore be assumed to also be a predetermined constant of negligible uncertainty.

Equation 130
$$\dot{q} = 1.10 \cdot \left(\frac{\Delta h_c}{r_0}\right) \cdot \left[\frac{\phi}{1+\phi(\alpha-1)}\right] \cdot x^o_{O_2}\left(1 - x^o_{CO_2} - x^o_{H_2O}\right) \cdot \dot{m}_e$$

Where ϕ and α expand to Equation 131 and Equation 132 respectively and $\dot{m}_e$ to Equation 133 in the small-scale and Equation 134 in the full-scale.

Equation 131
$$\phi = \frac{\left(x^o_{O_2} - x^a_{O_2}\right)}{x^o_{O_2}\left(1 - x^a_{O_2}\right)}$$

Equation 132
$$\alpha = 1 + x^o_{O_2}\left(\beta - 1\right)$$

Equation 133
$$\dot{m}_e = C\sqrt{\frac{\Delta p}{T_e}}$$

Equation 134
$$\dot{m}_e = 24.58 \cdot A \cdot k_c\sqrt{\frac{\Delta p}{T_e}}$$

For the purposes of the uncertainty analysis it is useful to substitute the expanded ϕ, α and $\dot{m}_e$ terms of into Equation 130. However, allowance needs be made between small-scale and full-scale mass flow rates of Equation 133 and Equation 134. As the terms left of the square root in Equation 134 are constants, Equation 133 and Equation 134 may be rewritten as Equation 135.

Equation 135
$$\dot{m}_e = C_x\sqrt{\frac{\Delta p}{T_e}}$$

Where x=1 in the small-scale and x=2 in the full-scale as per Equation 136 and Equation 137.

Equation 136 $$C_1 = C'MA_0\sqrt{2 \cdot T_{ref}\rho_{ref}}$$

Equation 137 $$C_2 = \frac{k_c}{f(\mathrm{Re})}A\sqrt{2 \cdot T_{ref}\rho_{ref}}$$

Expanding for ϕ, α and $\dot{m}_e$ (in both the small and full scale).

Equation 138 $$\dot{q} = 1.10 \cdot \left(\frac{\Delta h_c}{r_0}\right) \cdot \left[\frac{\frac{\left(x_{O_2}^o - x_{O_2}^a\right)}{x_{O_2}^o\left(1 - x_{O_2}^a\right)}}{1 + \frac{\left(x_{O_2}^o - x_{O_2}^a\right)}{x_{O_2}^o\left(1 - x_{O_2}^a\right)}x_{O_2}^o(\beta - 1)}\right] \cdot x_{O_2}^o\left(1 - x_{CO_2}^o - x_{H_2O}^o\right) \cdot C_x\sqrt{\frac{\Delta p}{T_e}}$$

Equation 139 $$\dot{q} = 1.10 \cdot \left(\frac{\Delta h_c}{r_0}\right) \cdot \left[\frac{x_{O_2}^o - x_{O_2}^a}{\beta\left(x_{O_2}^o - x_{O_2}^a\right) - x_{O_2}^o + 1}\right] \cdot \left(1 - x_{CO_2}^o - x_{H_2O}^o\right) \cdot C_x\sqrt{\frac{\Delta p}{T_e}}$$

The general uncertainty expression Equation 128 applied to Equation 139 is Equation 140.

Equation 140

$$\delta\dot{q} = \left\{\left(\frac{\partial\dot{q}}{\partial\frac{\Delta h_c}{r_0}}\delta\frac{\Delta h_c}{r_0}\right)^2 + \left(\frac{\partial\dot{q}}{\partial x_{O_2}^a}\delta x_{O_2}^a\right)^2 + \left(\frac{\partial\dot{q}}{\partial\beta}\delta\beta\right)^2 + \left(\frac{\partial\dot{q}}{\partial C_x}\delta C_x\right)^2 + \left(\frac{\partial\dot{q}}{\partial\Delta p}\delta\Delta p\right)^2 + \left(\frac{\partial\dot{q}}{\partial T_e}\delta T_e\right)^2\right\}^{\frac{1}{2}}$$

The partial derivatives follow. These are sometimes referred to as the sensitivity coefficients. As the product of these coefficients and an individual component's uncertainty gives the individual component's contribution to the overall uncertainty.

The partial derivatives must be independent for an analysis to be mathematically valid. Previous work published on uncertainty analysis of HRR measurements in full-scale room fires (Yeager[20]) lumped the variables into three basic groups. These groups are a heat of combustion term, a gas analysis term and a volumetric flow rate term. In this grouping the gas

analysis term and volumetric flow rate term both contain an oxygen depletion factor. Therefore, the terms are not independent of each other.

(i) Effective heat of combustion term, $\Delta h_c / r_0$:

Equation 141 $$\frac{\partial \dot{q}}{\partial \frac{\Delta h_c}{r_0}} = 1.10 \cdot \left[\frac{x_{O_2}^o - x_{O_2}^a}{\beta\left(x_{O_2}^o - x_{O_2}^a\right) - x_{O_2}^o + 1} \right] \cdot \left(1 - x_{CO_2}^o - x_{H_2O}^o\right) \cdot C_x \sqrt{\frac{\Delta p}{T_e}}$$

(ii) Oxygen measurement, $x_{O_2}^a$:

Equation 142 $$\frac{\partial \dot{q}}{\partial x_{O_2}^a} = -1.10 \cdot \left(\frac{\Delta h_c}{r_0} \right) \cdot \left[\frac{1 - x_{O_2}^o}{\left(\beta\left(x_{O_2}^o - x_{O_2}^a\right) - x_{O_2}^o + 1\right)^2} \right] \cdot \left(1 - x_{CO_2}^o - x_{H_2O}^o\right) \cdot C_x \sqrt{\frac{\Delta p}{T_e}}$$

(iii) Stoichiometric expansion factor, β :

Equation 143 $$\frac{\partial \dot{q}}{\partial \beta} = -1.10 \cdot \left(\frac{\Delta h_c}{r_0} \right) \cdot \left[\frac{x_{O_2}^o - x_{O_2}^a}{\beta\left(x_{O_2}^o - x_{O_2}^a\right) - x_{O_2}^o + 1} \right]^2 \cdot \left(1 - x_{CO_2}^o - x_{H_2O}^o\right) \cdot C_x \sqrt{\frac{\Delta p}{T_e}}$$

(iv) Mass flow rate coefficient, C_x :

Equation 144 $$\frac{\partial \dot{q}}{\partial C_x} = 1.10 \cdot \left(\frac{\Delta h_c}{r_0} \right) \cdot \left[\frac{x_{O_2}^o - x_{O_2}^a}{\beta\left(x_{O_2}^o - x_{O_2}^a\right) - x_{O_2}^o + 1} \right] \cdot \left(1 - x_{CO_2}^o - x_{H_2O}^o\right) \cdot \sqrt{\frac{\Delta p}{T_e}}$$

(v) Differential pressure, Δp :

Equation 145 $$\frac{\partial \dot{q}}{\partial \Delta p} = \frac{1.10}{2} \cdot \left(\frac{\Delta h_c}{r_0} \right) \cdot \left[\frac{x_{O_2}^o - x_{O_2}^a}{\beta\left(x_{O_2}^o - x_{O_2}^a\right) - x_{O_2}^o + 1} \right] \cdot \left(1 - x_{CO_2}^o - x_{H_2O}^o\right) \cdot C_x \sqrt{\frac{1}{\Delta p T_e}}$$

(vi) Exhaust temperature, T_e :

Equation 146 $$\frac{\partial \dot{q}}{\partial T_e} = -\frac{1.10}{2} \cdot \left(\frac{\Delta h_c}{r_0} \right) \cdot \left[\frac{x_{O_2}^o - x_{O_2}^a}{\beta\left(x_{O_2}^o - x_{O_2}^a\right) - x_{O_2}^o + 1} \right] \cdot \left(1 - x_{CO_2}^o - x_{H_2O}^o\right) \cdot C_x \sqrt{\frac{\Delta p}{T_e^3}}$$

5.3.2 Configuration 2: O_2 and CO_2 Gas Analysis

In Configuration 2, the general equation for HRR is again described by Equation 20 but with the oxygen depletion factor ϕ as Equation 23.

Substituting Equation 23, Equation 132 and Equation 135 into Equation 20 gives Equation 147. This simplifies to Equation 148.

Equation 147
$$\dot{q} = 1.10\left(\frac{\Delta h_c}{r_0}\right)\left[\frac{\left(\frac{x_{O_2}^o\left(1-x_{CO_2}^a\right)-x_{O_2}^a\left(1-x_{CO_2}^o\right)}{x_{O_2}^o\left(1-x_{O_2}^a-x_{CO_2}^a\right)}\right)\cdot x_{O_2}^o\left(1-x_{CO_2}^o-x_{H_2O}^o\right)}{1+\frac{x_{O_2}^o\left(1-x_{CO_2}^a\right)-x_{O_2}^a\left(1-x_{CO_2}^o\right)}{x_{O_2}^o\left(1-x_{O_2}^a-x_{CO_2}^a\right)}x_{O_2}^o\left(\beta-1\right)}\right]C_x\sqrt{\frac{\Delta p}{T_e}}$$

Equation 148
$$\dot{q} = 1.10\left(\frac{\Delta h_c}{r_0}\right)\left[\frac{\left[x_{O_2}^o\left(1-x_{CO_2}^a\right)-x_{O_2}^a\left(1-x_{CO_2}^o\right)\right]\cdot\left(1-x_{CO_2}^o-x_{H_2O}^o\right)}{\left(1-x_{O_2}^o\left(1-\beta\right)\right)\left(1-x_{CO_2}^a\right)-x_{O_2}^a x_{CO_2}^o\left(1-\beta\right)-\beta x_{O_2}^a}\right]C_x\sqrt{\frac{\Delta p}{T_e}}$$

The general equation for uncertainty is given by Equation 149.

Equation 149
$$\delta\dot{q} = \left\{\left(\frac{\partial\dot{q}}{\partial\frac{\Delta h_c}{r_0}}\delta\frac{\Delta h_c}{r_0}\right)^2+\left(\frac{\partial\dot{q}}{\partial x_{O_2}^a}\delta x_{O_2}^a\right)^2+\left(\frac{\partial\dot{q}}{\partial x_{CO_2}^a}\delta x_{CO_2}^a\right)^2+\left(\frac{\partial\dot{q}}{\partial\beta}\delta\beta\right)^2+\left(\frac{\partial\dot{q}}{\partial C_x}\delta C_x\right)^2+\left(\frac{\partial\dot{q}}{\partial\Delta p}\delta\Delta p\right)^2+\left(\frac{\partial\dot{q}}{\partial T_e}\delta T_e\right)^2\right\}^{\frac{1}{2}}$$

The partial derivatives follow:

(i) Effective heat of combustion term, $\Delta h_c/r_0$:

Equation 150
$$\frac{\partial\dot{q}}{\partial\frac{\Delta h_c}{r_0}} = 1.10\left[\frac{\left[x_{O_2}^o\left(1-x_{CO_2}^a\right)-x_{O_2}^a\left(1-x_{CO_2}^o\right)\right]\cdot\left(1-x_{CO_2}^o-x_{H_2O}^o\right)}{\left(1-x_{O_2}^o\left(1-\beta\right)\right)\left(1-x_{CO_2}^a\right)-x_{O_2}^a x_{CO_2}^o\left(1-\beta\right)-\beta x_{O_2}^a}\right]C_x\sqrt{\frac{\Delta p}{T_e}}$$

(ii) Oxygen measurement, $x^a_{O_2}$:

Equation 151 $$\frac{\partial \dot{q}}{\partial x^a_{O_2}} = 1.10 \frac{\Delta h_c}{r_0} \left[\frac{\left(1 - x^a_{CO_2}\right)\left(1 - x^o_{O_2} - x^o_{H_2O}\right) \cdot \left(1 - x^o_{CO_2} - x^o_{H_2O}\right)}{\left[\left[1 - x^o_{O_2}(1-\beta)\right]\left(1 - x^a_{CO_2}\right) - x^a_{O_2} x^o_{CO_2}(1-\beta) - \beta x^a_{O_2}\right]^2} \right] C_x \sqrt{\frac{\Delta p}{T_e}}$$

(iii) Carbon dioxide measurement, $x^a_{CO_2}$:

Equation 152 $$\frac{\partial \dot{q}}{\partial x^a_{CO_2}} = {}^{-}1.10 \left(\frac{\Delta h_c}{r_0} \right) \left[\frac{x^a_{O_2}\left(1 - x^o_{O_2} - x^o_{H_2O}\right)\left(1 - x^o_{CO_2} - x^o_{H_2O}\right)}{\left[\left[1 - x^o_{O_2}(1-\beta)\right]\left(1 - x^a_{CO_2}\right) - x^a_{O_2} x^o_{CO_2}(1-\beta) - \beta x^a_{O_2}\right]^2} \right] C_x \sqrt{\frac{\Delta p}{T_e}}$$

(iv) Stoichiometric expansion factor

Equation 153 $$\frac{\partial \dot{q}}{\partial \beta} = {}^{-}1.10 \left(\frac{\Delta h_c}{r_0} \right) \left[\frac{\left[x^o_{O_2}\left(1 - x^a_{CO_2}\right) - x^a_{O_2}\left(1 - x^o_{CO_2}\right)\right]^2 \cdot \left(1 - x^o_{CO_2} - x^o_{H_2O}\right)}{\left[\left[1 - x^o_{O_2}(1-\beta)\right]\left(1 - x^a_{CO_2}\right) - x^a_{O_2} x^o_{CO_2}(1-\beta) - \beta x^a_{O_2}\right]^2} \right] C_x \sqrt{\frac{\Delta p}{T_e}}$$

(v) Mass flow rate coefficient, C_x :

Equation 154 $$\frac{\partial \dot{q}}{\partial C_x} = 1.10 \left(\frac{\Delta h_c}{r_0} \right) \left[\frac{\left[x^o_{O_2}\left(1 - x^a_{CO_2}\right) - x^a_{O_2}\left(1 - x^o_{CO_2}\right)\right] \cdot \left(1 - x^o_{CO_2} - x^o_{H_2O}\right)}{\left[1 - x^o_{O_2}(1-\beta)\right]\left(1 - x^a_{CO_2}\right) - x^a_{O_2} x^o_{CO_2}(1-\beta) - \beta x^a_{O_2}} \right] \sqrt{\frac{\Delta p}{T_e}}$$

(vi) Differential pressure, Δp :

Equation 155 $$\frac{\partial \dot{q}}{\partial \Delta p} = \frac{1.10}{2} \left(\frac{\Delta h_c}{r_0} \right) \left[\frac{\left[x^o_{O_2}\left(1 - x^a_{CO_2}\right) - x^a_{O_2}\left(1 - x^o_{CO_2}\right)\right] \cdot \left(1 - x^o_{CO_2} - x^o_{H_2O}\right)}{\left[1 - x^o_{O_2}(1-\beta)\right]\left(1 - x^a_{CO_2}\right) - x^a_{O_2} x^o_{CO_2}(1-\beta) - \beta x^a_{O_2}} \right] C_x \sqrt{\frac{1}{\Delta p T_e}}$$

(vi) Exhaust temperature, T_e :

Equation 156 $$\frac{\partial \dot{q}}{\partial T_e} = \frac{{}^{-}1.10}{2} \left(\frac{\Delta h_c}{r_0} \right) \left[\frac{\left[x^o_{O_2}\left(1 - x^a_{CO_2}\right) - x^a_{O_2}\left(1 - x^o_{CO_2}\right)\right] \cdot \left(1 - x^o_{CO_2} - x^o_{H_2O}\right)}{\left[1 - x^o_{O_2}(1-\beta)\right]\left(1 - x^a_{CO_2}\right) - x^a_{O_2} x^o_{CO_2}(1-\beta) - \beta x^a_{O_2}} \right] C_x \sqrt{\frac{\Delta p}{T_e^3}}$$

5.3.3 Configuration 3: O_2, CO_2 and CO Gas Analysis

In Configuration 3, the general equation for HRR is described by Equation 26 with the oxygen depletion factor ϕ as Equation 25.

Substituting Equation 25, Equation 132 and Equation 135 into Equation 26 gives Equation 157. This assumes a constant 'catalytic' value of $\Delta h_c / r_0 \big|_{\substack{CO \\ \rightarrow CO_2}} = 17{,}600$ ($MJ \cdot kg^{-1}$ of O_2) with negligible uncertainty. Equation 157 simplifies to Equation 158.

Equation 157

$$\dot{q} = \left[\frac{\Delta h_c}{r_0} \phi - \left(\frac{\Delta h_c}{r_0} \bigg|_{\substack{CO \\ \rightarrow CO_2}} - \frac{\Delta h_c}{r_0} \right) \frac{1-\phi}{2} \frac{x_{CO}^a}{x_{O_2}^a} \right] \frac{M_{O_2}}{M_a} \frac{x_{O_2}^o \left(1 - x_{CO_2}^o - x_{H_2O}^o\right) \cdot \dot{m}_e}{1 + \phi(\alpha - 1)}$$

Equation 158

$$\dot{q} = \frac{\left(\frac{\Delta h_c}{r_0} \right) \left[x_{O_2}^o \left(1 - x_{CO_2}^a - x_{CO}^a\right) - x_{O_2}^a \left(1 - x_{CO_2}^o\right) \right] - \left(\frac{\Delta h_c}{r_0} \bigg|_{\substack{CO \\ \rightarrow CO_2}} - \frac{\Delta h_c}{r_0} \right) \frac{x_{CO}^a}{2} \left(1 - x_{O_2}^o - x_{CO_2}^o\right)}{\left[x_{O_2}^o \left(1 - x_{CO_2}^a - x_{CO}^a\right) - x_{O_2}^a \left(1 - x_{CO_2}^o\right) \right] \left[x_{O_2}^o (\beta - 1) + 1 \right] + x_{O_2}^o \left(1 - x_{O_2}^o - x_{CO_2}^o\right)}$$
$$\times 1.10 \cdot x_{O_2}^o \left(1 - x_{CO_2}^o - x_{H_2O}^o\right) \cdot C_x \sqrt{\frac{\Delta p}{T_e}}$$

The general equation for uncertainty is given as Equation 159.

Equation 159

$$\delta \dot{q} = \left\{ \left(\frac{\partial \dot{q}}{\partial \frac{\Delta h_c}{r_0}} \delta \frac{\Delta h_c}{r_0} \right)^2 + \left(\frac{\partial \dot{q}}{\partial x_{O_2}^a} \delta x_{O_2}^a \right)^2 + \left(\frac{\partial \dot{q}}{\partial x_{CO_2}^a} \delta x_{CO_2}^a \right)^2 + \left(\frac{\partial \dot{q}}{\partial x_{CO}^a} \delta x_{CO}^a \right)^2 \right.$$
$$\left. + \left(\frac{\partial \dot{q}}{\partial \beta} \delta \beta \right)^2 + \left(\frac{\partial \dot{q}}{\partial C_x} \delta C_x \right)^2 + \left(\frac{\partial \dot{q}}{\partial \Delta p} \delta \Delta p \right)^2 + \left(\frac{\partial \dot{q}}{\partial T_e} \delta T_e \right)^2 \right\}^{\frac{1}{2}}$$

The partial derivatives follow. They are, in most cases too lengthy to present in expanded form, so they are rewritten as differential equations where $\dot{q}$ is derived from Equation 158.

(i) Effective heat of combustion term, $\Delta h_c / r_0$:

Equation 160 $$\frac{\partial \dot{q}}{\partial \dfrac{\Delta h_c}{r_0}} = \frac{1}{\left(\dfrac{\Delta h_c}{r_0}\right)} \cdot \dot{q}$$

(ii) Oxygen measurement, $x^a_{O_2}$:

Equation 161 $$\frac{\partial \dot{q}}{\partial x^a_{O_2}} = \frac{\begin{pmatrix} -\dot{q}\left[\left(-1+x^o_{CO_2}\right)\left[x^o_{O_2}(\beta-1)+1\right]+\left(1-x^o_{O_2}-x^o_{CO_2}\right)\right] \\ -1.10\left(\dfrac{\Delta h_c}{r_0}\right)\left(1-x^o_{CO_2}\right)\left(1-x^o_{CO_2}-x^o_{H_2O}\right)\cdot C_x\sqrt{\dfrac{\Delta p}{T_e}} \end{pmatrix}}{\left[x^o_{O_2}\left(1-x^a_{CO_2}-x^a_{CO}\right)-x^a_{O_2}\left(1-x^o_{CO_2}\right)\right]\left[x^o_{O_2}(\beta-1)+1\right]+x^o_{O_2}\left(1-x^o_{O_2}-x^o_{CO_2}\right)}$$

(iii) Carbon dioxide measurement, $x^a_{CO_2}$:

Equation 162 $$\frac{\partial \dot{q}}{\partial x^a_{CO_2}} = \frac{\dot{q}\cdot x^o_{O_2}\left[x^o_{O_2}(\beta-1)+1\right]-1.10\left(\dfrac{\Delta h_c}{r_0}\right)\left(x^o_{O_2}\right)^2\left(1-x^o_{CO_2}-x^o_{H_2O}\right)\cdot C_x\sqrt{\dfrac{\Delta p}{T_e}}}{\left[x^o_{O_2}\left(1-x^a_{CO_2}-x^a_{CO}\right)-x^a_{O_2}\left(1-x^o_{CO_2}\right)\right]\left[x^o_{O_2}(\beta-1)+1\right]+x^o_{O_2}\left(1-x^o_{O_2}-x^o_{CO_2}\right)}$$

(iv) Carbon monoxide measurement, x^a_{CO}:

Equation 163

$$\frac{\partial \dot{q}}{\partial x^a_{CO}} = \frac{\dot{q}}{x^a_{CO}} + \frac{\dot{q}\cdot x^o_{O_2}\left[x^o_{O_2}(\beta-1)+1\right]+\begin{pmatrix} \dfrac{1.10}{x^a_{CO}}\dfrac{\Delta h_c}{r_0}\left[x^a_{O_2}\left(1-x^o_{CO_2}\right)-x^o_{O_2}\left(1-x^a_{CO_2}\right)\right] \\ \times x^o_{O_2}\left(1-x^o_{CO_2}-x^o_{H_2O}\right)C_x\sqrt{\dfrac{\Delta p}{T_e}} \end{pmatrix}}{\left[x^o_{O_2}\left(1-x^a_{CO_2}-x^a_{CO}\right)-x^a_{O_2}\left(1-x^o_{CO_2}\right)\right]\left[x^o_{O_2}(\beta-1)+1\right]+x^o_{O_2}\left(1-x^o_{O_2}-x^o_{CO_2}\right)}$$

(v) Stoichiometric expansion factor, β:

Equation 164 $$\frac{\partial \dot{q}}{\partial \beta} = \frac{x^o_{O_2}\left[x^o_{O_2}\left(1-x^a_{CO_2}-x^a_{CO}\right)-x^a_{O_2}\left(1-x^o_{CO_2}\right)\right]}{\left[x^o_{O_2}\left(1-x^a_{CO_2}-x^a_{CO}\right)-x^a_{O_2}\left(1-x^o_{CO_2}\right)\right]\left[x^o_{O_2}(\beta-1)+1\right]+x^o_{O_2}\left(1-x^o_{O_2}-x^o_{CO_2}\right)}\cdot\dot{q}$$

(vi) Mass flow rate coefficient, C_x:

Equation 165 $$\frac{\partial \dot{q}}{\partial C_x} = \frac{1}{C_x}\cdot\dot{q}$$

(vii) Differential pressure, Δp :

Equation 166 $$\frac{\partial \dot{q}}{\partial \Delta p} = \frac{1}{2\Delta p} \cdot \dot{q}$$

(viii) Exhaust temperature, T_e :

Equation 167 $$\frac{\partial \dot{q}}{\partial T_e} = -\frac{1}{2T_e} \cdot \dot{q}$$

5.3.4 Configuration 4: O_2, CO_2, CO and H_2O Gas Analysis

In Configuration 4, the general equation for HRR is described by Equation 44 with the oxygen depletion factor ϕ as Equation 25. The oxygen depletion factor is the same as Configuration 3 as the water vapour sampling is via a separate heated sample line. Within Equation 44, the ratio of mass of incoming air to molecular weight of air m_a / M_a (i.e. the number of moles of ambient air) is given by Equation 37 with the molecular weight of the exhaust gases M_e being Equation 43.

The general equation is derived by substituting Equation 25, Equation 37 and Equation 43 into Equation 44, with the mass flow rate defined by Equation 135. The expansion factor Equation 132 is no longer needed.

However, if differentiated in the expanded form the partial derivatives become too lengthy to document easily. Therefore, in Configuration 4 as opposed to the earlier Configurations the terms for HRR, oxygen depletion factor, molecular weight of the exhaust gases and the mass flow rate of the exhaust gases are differentiated separately.

The general equation for uncertainty is given as Equation 168. Note now that all four species are measured the expansion factor assumption need not be made and therefore the expansion factor term is superseded (i.e. no β in the equations). Note that the measured mole fraction of water vapour in the heated sample line is the proper concentration. Therefore, it is not denoted with the “a” superscript.

Equation 168

$$\delta\dot{q} = \left\{ \left(\frac{\partial \dot{q}}{\partial \dfrac{\Delta h_c}{r_0}} \delta \frac{\Delta h_c}{r_0} \right)^2 + \left(\frac{\partial \dot{q}}{\partial x^a_{O_2}} \delta x^a_{O_2} \right)^2 + \left(\frac{\partial \dot{q}}{\partial x^a_{CO_2}} \delta x^a_{CO_2} \right)^2 + \left(\frac{\partial \dot{q}}{\partial x^a_{CO}} \delta x^a_{CO} \right)^2 + \left(\frac{\partial \dot{q}}{\partial x_{H_2O}} \delta x_{H_2O} \right)^2 + \left(\frac{\partial \dot{q}}{\partial C_x} \delta C_x \right)^2 + \left(\frac{\partial \dot{q}}{\partial \Delta p} \delta \Delta p \right)^2 + \left(\frac{\partial \dot{q}}{\partial T_e} \delta T_e \right)^2 \right\}^{\frac{1}{2}}$$

The partial derivatives follow. They are, in most cases too lengthy to present in expanded form.

(i) Effective heat of combustion term, $\Delta h_c / r_0$:

Equation 169

$$\frac{\partial \dot{q}}{\partial \dfrac{\Delta h_h}{r_0}} = M_{O_2} \left[\phi - \frac{1-\phi}{2} \frac{x^a_{CO}}{x^a_{O_2}} \right] \frac{\dot{m}_a}{M_a} \cdot x^o_{O_2} \left(1 - x^o_{CO_2} - x^o_{H_2O} \right)$$

(ii) Oxygen measurement, $x^a_{O_2}$:

Equation 170

$$\frac{\partial \dot{q}}{\partial x^a_{O_2}} = M_{O_2} \left[\left[\frac{\Delta h_c}{r_0} + \frac{1}{2} \left(\frac{\Delta h_c}{r_0}\bigg|_{\substack{CO \\ \to CO_2}} - \frac{\Delta h_c}{r_0} \right) \frac{\partial \phi}{\partial x^a_{O_2}} + \left(\frac{\Delta h_c}{r_0}\bigg|_{\substack{CO \\ \to CO_2}} - \frac{\Delta h_c}{r_0} \right) \frac{1-\phi}{2} \frac{x^a_{CO}}{{x^a_{O_2}}^2} \frac{\dot{m}_a}{M_a} \right] + \left[\frac{\Delta h_c}{r_0} \phi - \frac{1}{2} \left(\frac{\Delta h_c}{r_0}\bigg|_{\substack{CO \\ \to CO_2}} - \frac{\Delta h_c}{r_0} \right) (1-\phi) \frac{x^a_{CO}}{x^a_{O_2}} \right] \left(\frac{\partial \dfrac{\dot{m}_a}{M_a}}{\partial x^a_{O_2}} \right) \right] x^o_{O_2} \left(1 - x^o_{CO_2} - x^o_{H_2O} \right)$$

Equation 171

$$\frac{\partial \phi}{\partial x^a_{O_2}} = \frac{x^o_{O_2} \left(1 - x^a_{CO_2} - x^a_{CO} \right) - x^a_{O_2} \left(1 - x^o_{CO_2} \right)}{x^o_{O_2} \left(1 - x^a_{O_2} - x^a_{CO_2} - x^a_{CO} \right)^2} - \frac{\left(1 - x^o_{CO_2} \right)}{x^o_{O_2} \left(1 - x^a_{O_2} - x^a_{CO_2} - x^a_{CO} \right)}$$

Equation 172

$$\frac{\partial \dfrac{\dot{m}_a}{M_a}}{\partial x^a_{O_2}} = \frac{-\left(1 - x_{H_2O} \right) \dfrac{\dot{m}_e}{M_e}}{\left(1 - x^o_{H_2O} \right) \cdot \left(1 - x^o_{O_2} - x^o_{CO_2} \right)} - \frac{\left(1 - x_{H_2O} \right) \cdot \left(1 - x^a_{O_2} - x^a_{CO_2} - x^a_{CO} \right) \dfrac{\dot{m}_e}{M_e^2}}{\left(1 - x^o_{H_2O} \right) \cdot \left(1 - x^o_{O_2} - x^o_{CO_2} \right)} \frac{\partial M_e}{\partial x^a_{O_2}}$$

Equation 173

$$\frac{\partial M_e}{\partial x^a_{O_2}} = 4 \left(1 - x_{H_2O} \right)$$

(iii) Carbon dioxide measurement, $x^a_{CO_2}$:

$$\frac{\partial \dot{q}}{\partial x^a_{CO_2}} = M_{O_2}\left[\left(\left(\frac{\Delta h_c}{r_0}+\frac{1}{2}\left(\frac{\Delta h_c}{r_0}\Big|_{\substack{CO\\ \rightarrow CO_2}}-\frac{\Delta h_c}{r_0}\right)\frac{x^a_{CO}}{x^a_{O_2}}\right)\left(\frac{\partial \phi}{\partial x^a_{CO_2}}\right)\right)\frac{\dot{m}_a}{M_a}\right.$$

Equation 174

$$\left.+\left(E\phi-\left(\frac{\Delta h_c}{r_0}\Big|_{\substack{CO\\ \rightarrow CO_2}}-\frac{\Delta h_c}{r_0}\right)\left(\frac{1-\phi}{2}\right)\frac{x^a_{CO}}{x^a_{O_2}}\right)\frac{\partial \frac{\dot{m}_a}{M_a}}{\partial x^a_{CO_2}}\right]x^o_{O_2}\left(1-x^o_{CO_2}-x^o_{H_2O}\right)$$

Equation 175 $$\frac{\partial \phi}{\partial x^a_{CO_2}} = \frac{x^o_{O_2}\left(1-x^a_{CO_2}-x^a_{CO}\right)-x^a_{O_2}\left(1-x^o_{CO_2}\right)}{x^o_{O_2}\left(1-x^a_{O_2}-x^a_{CO_2}-x^a_{CO}\right)^2}-\frac{1}{x^o_{O_2}\left(1-x^a_{O_2}-x^a_{CO_2}-x^a_{CO}\right)}$$

Equation 176 $$\frac{\partial \frac{\dot{m}_a}{M_a}}{\partial x^a_{CO_2}} = \frac{-\left(1-x_{H_2O}\right)\frac{\dot{m}_e}{M_e}}{\left(1-x^o_{H_2O}\right)\cdot\left(1-x^o_{O_2}-x^o_{CO_2}\right)}-\frac{\left(1-x_{H_2O}\right)\cdot\left(1-x^a_{O_2}-x^a_{CO_2}-x^a_{CO}\right)\frac{\dot{m}_e}{M_e^2}}{\left(1-x^o_{H_2O}\right)\cdot\left(1-x^o_{O_2}-x^o_{CO_2}\right)}\frac{\partial M_e}{\partial x^a_{CO_2}}$$

Equation 177 $$\frac{\partial M_e}{\partial x^a_{CO_2}} = 16\left(1-x_{H_2O}\right)$$

(iv) Carbon monoxide measurement, x^a_{CO}:

Equation 178

$$\frac{\partial \dot{q}}{\partial x^a_{CO}} = M_{O_2}\left[\left(\left(\left(\frac{\Delta h_c}{r_0}+\frac{1}{2}\left(\frac{\Delta h_c}{r_0}\Big|_{\substack{CO\\ \rightarrow CO_2}}-\frac{\Delta h_c}{r_0}\right)\frac{x^a_{CO}}{x^a_{O_2}}\right)\left(\frac{\partial \phi}{\partial x^a_{CO}}\right)-\left(\frac{\Delta h_c}{r_0}\Big|_{\substack{CO\\ \rightarrow CO_2}}-\frac{\Delta h_c}{r_0}\right)\left(\frac{1-\phi}{2}\right)\frac{1}{x^a_{O_2}}\right)\frac{\dot{m}_a}{M_a}\right.$$

$$\left.+\left(E\phi-\left(\frac{\Delta h_c}{r_0}\Big|_{\substack{CO\\ \rightarrow CO_2}}-\frac{\Delta h_c}{r_0}\right)\left(\frac{1-\phi}{2}\right)\frac{x^a_{CO}}{x^a_{O_2}}\right)\frac{\partial \frac{\dot{m}_a}{M_a}}{\partial x^a_{CO}}\right]x^o_{O_2}\left(1-x^o_{CO_2}-x^o_{H_2O}\right)$$

Equation 179 $$\frac{\partial \phi}{\partial x^a_{CO}} = \frac{x^o_{O_2}\left(1-x^a_{CO_2}-x^a_{CO}\right)-x^a_{O_2}\left(1-x^o_{CO_2}\right)}{x^o_{O_2}\left(1-x^a_{O_2}-x^a_{CO_2}-x^a_{CO}\right)^2}-\frac{1}{x^o_{O_2}\left(1-x^a_{O_2}-x^a_{CO_2}-x^a_{CO}\right)}$$

Equation 180 $$\frac{\partial \frac{\dot{m}_a}{M_a}}{\partial x^a_{CO}} = \frac{-\left(1-x_{H_2O}\right)\frac{\dot{m}_e}{M_e}}{\left(1-x^o_{H_2O}\right)\cdot\left(1-x^o_{O_2}-x^o_{CO_2}\right)}$$

(v) Water vapour measurement, $x^a_{H_2O}$:

Equation 181 $$\frac{\partial \dot{q}}{\partial x_{H_2O}} = M_{O_2}\left[\frac{\Delta h_c}{r_0}\phi - \left(\frac{\Delta h_c}{r_0}\bigg|_{\substack{CO\\ \rightarrow CO_2}} - \frac{\Delta h_c}{r_0}\right)\frac{1-\phi}{2}\frac{x^a_{CO}}{x^a_{O_2}}\right]\left(\frac{\partial \frac{\dot{m}_a}{M_a}}{\partial x_{H_2O}}\right)x^o_{O_2}\left(1-x^o_{CO_2}-x^o_{H_2O}\right)$$

Equation 182 $$\frac{\partial \frac{\dot{m}_a}{M_a}}{\partial x^a_{H_2O}} = \frac{-\left(1-x^a_{O_2}-x^a_{CO_2}-x^a_{CO}\right)\frac{\dot{m}_e}{M_e}}{\left(1-x^o_{H_2O}\right)\left(1-x^o_{O_2}-x^o_{CO_2}\right)} - \frac{\left(1-x_{H_2O}\right)\left(1-x^a_{O_2}-x^a_{CO_2}-x^a_{CO}\right)\frac{\dot{m}_e}{M_e^2}}{\left(1-x^o_{H_2O}\right)\left(1-x^o_{O_2}-x^o_{CO_2}\right)}\frac{\partial M_e}{\partial x^a_{H_2O}}$$

Equation 183 $$\frac{\partial M_e}{\partial x_{H_2O}} = -4\left(x_{O_2}+4x_{CO_2}+2.5\right)$$

(vi) Mass flow rate coefficient, C_x:

Equation 184 $$\frac{\partial \dot{q}}{\partial C_x} = \frac{1}{C_x}\cdot\dot{q}$$

(vii) Differential pressure, Δp:

Equation 185 $$\frac{\partial \dot{q}}{\partial \Delta p} = \frac{1}{2\Delta p}\cdot\dot{q}$$

(viii) Exhaust temperature, T_e:

Equation 186 $$\frac{\partial \dot{q}}{\partial T_e} = -\frac{1}{2T_e}\cdot\dot{q}$$

A detailed example, including component uncertainties is follows.

5.4 Applications

5.4.1 Example 1: An uncertainty analysis of the HRR calculation of the ISO5660-1 and ASTM1354 Cone Calorimeter standard test methods

This example focuses on the uncertainty associated with the heat release rate calculation for the cone calorimeter, Configuration 1. The component uncertainties of the simplifying assumptions and experimental measurements are quantified in order to assess the overall uncertainty of heat release rate calculation. Random uncertainties associated with the sample and operator errors are not included. An example is presented which shows how the individual component uncertainties propagate through calculation. It is clear that the greatest proportion of the uncertainties are attributed to the assumed combustion expansion factor, assumed effective heat of combustion and the measured oxygen concentration. Having examined the component uncertainties, several strategies for reducing overall uncertainty are proposed.

An uncertainty analysis of heat release rate calculation involves the determination of the variation in calculated heat release rate, from the collective variation of the component physical measurements forming the model variables.

The Standard Test Method expression, for the calculation of heat release rate for the cone calorimeter is given below as Equation 187. This is recognised from Equation 20 developed in CHAPTER 2: 'Heat release rate measurement, oxygen consumption technique'.

Note that the notation from the standard is varied slightly to be consistent with the notation in the earlier chapters (which themselves required wider variability to illustrate the intermediate steps of the derivations). The ISO5660-1 calculation method is mathematically identical to that in ASTM 1354. We refer to the ISO5660-1 standard test method, but note that the analysis applies equally to ASTM 1354.

Equation 187

$$\dot{q} = \left(\frac{\Delta h_c}{r_0} \right) (1.10) C \sqrt{\frac{\Delta p}{T_e}} \left(\frac{x_{O_2}^o - x_{O_2}^a}{1.105 - 1.5 x_{O_2}^a} \right)$$

Where $x_{O_2}^o$ the initial (ambient) value of oxygen analyser reading is the dry-air oxygen concentration, this is 0.2095.

Equation 187 assumes only an oxygen analyser is present in the gas analysis. An informative annex to the standard includes more sophisticated equations for additional gas analysers. Such as CO_2, CO and H_2O (vapour). This discussion does not include these additional analysers. Qualitatively, we can say that additional analysers should improve accuracy by reducing the uncertainty of assumptions. However, they also add to the uncertainty by adding more instrument uncertainty.

Equation 187 is a simplification of the general equations developed by Parker [4] and elaborated by Janssens [5]. Consider this simplification, Equation 187 beside the more detailed 'general' equation for this gas analysis configuration, Equation 188.

Equation 188

$$\dot{q} = \left(\frac{\Delta h_c}{r_0} \right) \left(\frac{M_{O_2}}{M_a} \right) \left(1 - x^o_{H_2O}\right) C \sqrt{\frac{\Delta p}{T_e}} \left(\frac{x^o_{O_2} \phi}{1 + \phi(\alpha - 1)} \right)$$

Again, Equation 188 is recognised from Equation 20 developed in CHAPTER 2: 'Heat release rate measurement, oxygen consumption technique'.

It can be seen that Equation 187 is a simplification of Equation 188 in three major ways:

- 1.10 is assumed as the ratio of the molecular weight of oxygen to air
- the term involving the mole fraction of water vapour is assumed at unity
- the term describing oxygen depletion is simplified and a value of β=1.5 assumed for the stoichiometric expansion factor

Upon closer inspection, the two simplifications are related. This is because a value of 1.10 for the ratio of molecular weights is assuming dry air, while the actual value is dependent on the moist ambient air state. Therefore, both simplifications are a function of the mole fraction of water vapour. The mole fraction of water vapour in ambient air is determined from three independent moist air properties. The recommended combination is; dry-bulb temperature, atmospheric pressure and relative humidity. Atmospheric pressure is assumed constant at 101,325 Pa.

The third simplification, relating to the mole fraction of oxygen consumed is an algebraic manipulation and is mathematically equivalent. This is a minor mathematical arrangement, not really a simplifying assumption. However, the expansion factor uncertainty needs to be incorporated into the analysis and so it is included to complete the discussion.

Additionally, the role of the calibration constant for oxygen consumption analysis, *C* requires some further consideration.

Consider the first and second simplifications to quantify any error introduced.

Equation 189

$$\frac{M_{O_2}}{M_{dry}} = \frac{0.03200}{0.02896} \approx 1.10$$

Where M_{dry} is the molecular weight of dry air. But:

Equation 190

$$\frac{M_{O_2}}{M_{dry}} \neq \frac{M_{O_2}}{M_a}$$

It is more correct to express the ratio as:

Equation 191

$$\frac{M_{O_2}}{M_a} = \frac{M_{O_2}}{\left(1 - x^o_{H_2O}\right)M_{dry} + x^o_{H_2O} M_{H_2O}}$$

Where M_{H_2O} is the molecular weight of water vapour. We can therefore quantify the error introduced by the first and second simplifying assumptions and treat it as an additional source of uncertainty. It is the variation of the product of Equation 192 below from the assumed constant of 1.10.

Equation 192

$$\frac{\left(1 - x^o_{H_2O}\right)M_{O_2}}{M_a} = \frac{\left(1 - x^o_{H_2O}\right)M_{O_2}}{\left(1 - x^o_{H_2O}\right)M_{dry} + x^o_{H_2O} M_{H_2O}}$$

Assume that atmospheric pressure is 101,325 Pa. (Note the *outdoor* standard deviation of monthly data averaged over 10 years in Christchurch, NZ is 406 Pa.) Figure 1 considers the combinations of dry-bulb temperature and relative humidity specified by the standard test method and reports the inherent error. It can be seen that the water vapour assumptions in the simplification of the general HRR equation introduce noteworthy errors for combinations of high temperature and high relative humidity. It is simple to calculate the ambient water vapour $x^o_{H_2O}$ from dry-bulb temperature, relative humidity and atmospheric pressure measurements. These measurements individually have a high accuracy allowing for an accurate calculation of $x^o_{H_2O}$.

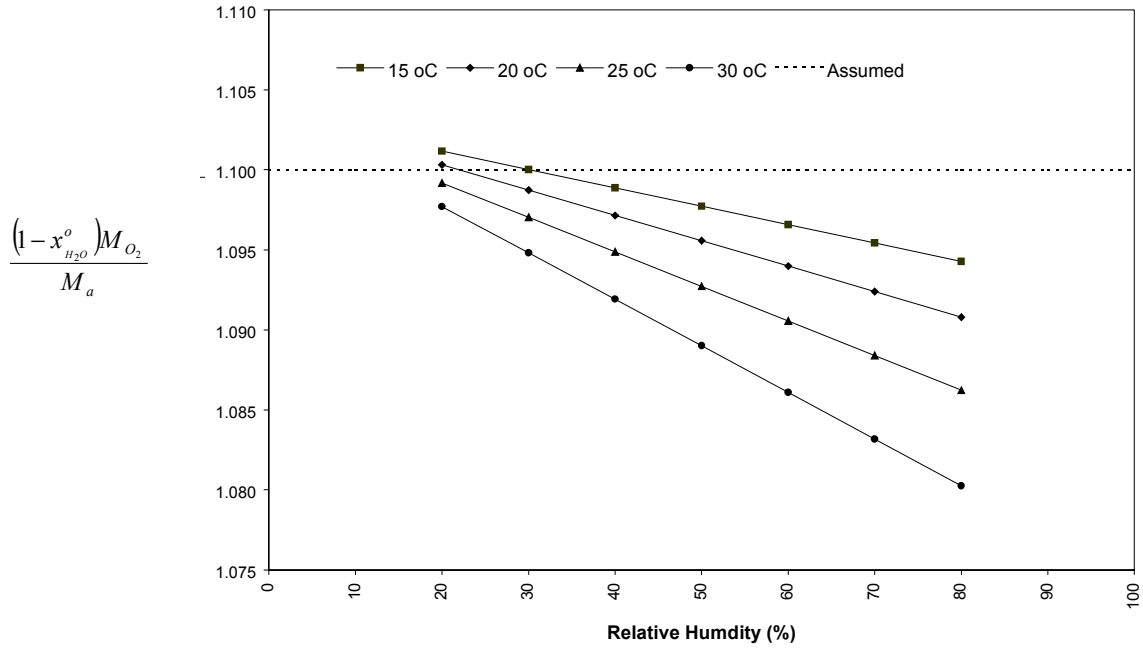

Figure 1: Influence of water vapour on the assumed ratio of molecular weight of oxygen to dry air. Deviation from the assumed constant value of 1.10 is clearly demonstrated.

Note that in almost all of the cases the error is making the calculation over-estimate the HRR. Therefore, the error is conservative, if undesirable. Further mitigating the error is that the same error is encountered in the daily methane calibration. This has the effect of 'hiding' the error in the calculated *C* value.

Janssens [5] has shown that for temperature ranges of 10 ^oC (283 K) to 50 ^oC (323 K), Equation 193 can be used to calculate the mole fraction of water vapour.

Equation 193 $$x_{H_2O}^{o} = 1.19 \cdot 10^{8} \frac{RH}{P_a} e^{\left(\frac{-3816}{T-46}\right)}$$

Where *RH* is the relative humidity, *T* temperature and P_a atmospheric pressure. The equation is based on a curve-fit that has the functional form of a solution to the Clasius-Clapeyron equation. It is described in more detail by Janssens [5].

The relationship of Equation 193 would allow the inclusion of the ambient water vapour in the calculation of the HRR, Equation 187. However, the ambient water vapour calculation also has uncertainty associated with ambient; temperature, pressure and relative humidity measurements. In the HRR calculation it is recommended to use the measured ambient temperature and relative humidity to correct the error if applicable.

The denominator of Equation 187 is an expansion correction to account for the difference in flow rate between the incoming air and exhaust gases. This accounts for the increased ratio of the number of moles of combustion products to the number of moles of oxygen depleted. If the simplification is expanded, Equation 187 becomes Equation 194.

Equation 194 $$\dot{q} = \left(\frac{\Delta h_c}{r_0}\right)(1.10)C\sqrt{\frac{\Delta p}{T_e}}\left(\frac{x_{O_2}^{o} - x_{O_2}^{a}}{\left[1 + (\beta - 1)x_{O_2}^{o}\right] - \beta x_{O_2}^{a}}\right)$$

Where β is a stoichiometric factor described by Babrauskas[21] as the ratio of the number of moles of products to moles of oxygen consumed. The value of this factor is dependent on the C to H to O ratio of the fuel It varies from β=1.0 for pure carbon to β=2.0 for pure hydrogen. Equation 187 assumes $x_{O_2}^{o}$ = 0.2095 and β=1.5 (correct for Methane and PMMA).

Consider the constant *C* in the mass flow rate of exhaust gases term.

Equation 195 $$\dot{m}_e = C\sqrt{\frac{\Delta P}{T_e}}$$

Where, $\dot{m}_e$ is the mass flow rate of the exhaust gases. The ISO5660-1 definition of C is the 'calibration constant for oxygen consumption analysis' or the calibration constant. The value of C is derived experimentally from the methane HRR calibration. The value of the constant C is actually a function of the fluid properties and constants.

Equation 196 $$C = C'MA_o\sqrt{2g_cT_{ref}\rho_{ref}}$$

Where the flow coefficient is $C'M$, the orifice plate coefficient is C', the overall coefficient $C'M$, the flow area A_o and the root of the product of a reference temperature T_{ref}, density ρ_{ref} and a gravitational constant g_c (value of 1.0 kg·m/N·s^2). A more detailed discussion of flow measurement can be found in Reference [10].

It is desirable to independently determine C, because other variable influences may be attributed to C. For example, the methane mass flow controller and moisture content of ambient air may cause errors that are 'hidden' in the uncertainty δC.

One approach is empirical. For the dimensional criteria stipulated in ISO5660-1 and the Reynolds number variation, the value of C could be calculated, rather than being determined from methane calibration tests. One difficulty is that the flow is not fully developed at the orifice plate having had only three diameter lengths from the exhaust fan. Additionally, there are issues associated with orifice soot coating and edge erosion which may appear with time and seasoning.

Given some idea of a baseline C, perhaps supplied by the manufacturer, it would be more meaningful to compare daily variation from the baseline, with possibly a gradual drift due to the aforementioned effects, rather than each variation itself.

Alternatively, if CO_2 is being measured, C can be determined by oxygen to carbon dioxide mole balance for a known gas such as methane. This is discussed in detail with results demonstrated in Babrauskas[22].

Due to the 'hidden' influences mentioned above, the actual uncertainty δC is not the same as the daily calibration constant variation. The actual uncertainty δC is most strongly influenced by the flow coefficient $C'M$. A typical value of the uncertainty of the flow coefficient on its

own, for an orifice plate made to standard is approximately 0.5% over the normal working range (Hayward[23]).

The typical calibration constant variation of up to 5% from day to day is a function of the overall 'system' uncertainty of the measurements for a given HRR. If analysed correctly, and especially at lower HRR values (say 1.0 to 3.0 kW), the calibration constant variation is a very useful indication of the combined instrument accuracy.

Reconsider Equation 194 for Configuration 1. This includes the combustion expansion effect due to the fuel dependant stoichiometric factor β, and an assumed value of 0.2095 for $x_{O_2}^o$. This assumes that the uncertainty of $x_{O_2}^o$ is negligible.

Equation 197 $$\dot{q} = f\left(\frac{\Delta h_c}{r_0}, C, \Delta p, T_e, x_{O_2}^a, \beta\right) = \left(\frac{\Delta h_c}{r_0}\right)(1.10)C\sqrt{\frac{\Delta p}{T_e}}\left(\frac{x_{O_2}^o - x_{O_2}^a}{\left[1+(\beta-1)x_{O_2}^o\right]-\beta x_{O_2}^a}\right)$$

The general expression for absolute uncertainty of HRR from this functional relationship is described by Equation 198.

Equation 198

$$\delta\dot{q} = \left\{\left(\frac{\partial\dot{q}}{\partial\left(\frac{\Delta h_c}{r_O}\right)}\delta\left(\frac{\Delta h_c}{r_O}\right)\right)^2 + \left(\frac{\partial\dot{q}}{\partial C}\delta C\right)^2 + \left(\frac{\partial\dot{q}}{\partial(\Delta p)}\delta(\Delta p)\right)^2 + \left(\frac{\partial\dot{q}}{\partial T_e}\delta T_e\right)^2 + \left(\frac{\partial\dot{q}}{\partial x_{O_2}^a}\delta x_{O_2}^a\right)^2 + \left(\frac{\partial\dot{q}}{\partial\beta}\delta\beta\right)^2\right\}^{\frac{1}{2}}$$

The partial derivatives follow as Equation 199 to Equation 204. These are sometimes referred to as the sensitivity coefficients. As the product of these coefficients and an individual component's uncertainty gives the individual component's contribution to the overall uncertainty.

Equation 199

$$\frac{\partial \dot{q}}{\partial\left(\frac{\Delta h_c}{r_O}\right)} = (1.10)C\sqrt{\frac{\Delta p}{T_e}}\left(\frac{0.2095 - x_{O_2}^a}{[1+0.2095(\beta-1)]-\beta x_{O_2}^a}\right)$$

Equation 200

$$\frac{\partial \dot{q}}{\partial C} = \left(\frac{\Delta h_c}{r_O}\right)(1.10)\sqrt{\frac{\Delta p}{T_e}}\left(\frac{0.2095 - x_{O_2}^a}{[1+0.2095(\beta-1)]-\beta x_{O_2}^a}\right)$$

Equation 201

$$\frac{\partial \dot{q}}{\partial(\Delta p)} = \frac{1}{2}\left(\frac{\Delta h_c}{r_O}\right)(1.10)C\sqrt{\frac{1}{\Delta p T_e}}\left(\frac{0.2095 - x_{O_2}^a}{[1+0.2095(\beta-1)]-\beta x_{O_2}^a}\right)$$

Equation 202

$$\frac{\partial \dot{q}}{\partial T_e} = -\frac{1}{2}\left(\frac{\Delta h_c}{r_O}\right)(1.10)C\sqrt{\frac{\Delta p}{T_e^3}}\left(\frac{0.2095 - x_{O_2}^a}{[1+0.2095(\beta-1)]-\beta x_{O_2}^a}\right)$$

Equation 203

$$\frac{\partial \dot{q}}{\partial x_{O_2}^a} = -\left(\frac{\Delta h_c}{r_O}\right)(1.10)C\sqrt{\frac{\Delta p}{T_e}}\left(\frac{0.7905}{\left([1+0.2095(\beta-1)]-\beta x_{O_2}^a\right)^2}\right)$$

Equation 204

$$\frac{\partial \dot{q}}{\partial \beta} = -\left(\frac{\Delta h_c}{r_O}\right)(1.10)C\sqrt{\frac{\Delta p}{T_e}}\left(\frac{\left(0.2095 - x_{O_2}^a\right)^2}{\left([1+0.2095(\beta-1)]-\beta x_{O_2}^a\right)^2}\right)$$

The partial differential equations must be independent for an analysis to be mathematically valid. Previous work published on uncertainty analysis of HRR measurements in full-scale room fires [20] lumped the variables into three basic groups. These groups are a heat of combustion term, a gas analysis term and a volumetric flow rate term. In this grouping the gas analysis term and volumetric flow rate term both contain an oxygen depletion factor. Therefore, the terms are not independent of each other.

We acknowledge there is a very minor temperature dependence in the *C* term, seemingly indicating some non-independence of the partial derivatives chosen here. This is due to thermal expansion effects on the orifice plate, changing the flow coefficient and orifice area, and hence *C*. However, this is a minor effect and considered insignificant.

To illustrate the calculation of uncertainty using Equation 198 to Equation 204, consider the following example using data from cone calorimeter tests at the University of Canterbury. The sample tested was an upholstered furniture composite, therefore the fuel composition and

hence combustion expansion effect due to the fuel dependant stoichiometric factor β is unknown. Similarly, the value of the heat of combustion term is unknown. Values for these are recommended in ISO5660-1.

Temperature is measured with a type K Chromel-Alumel thermocouple, differential pressure across the orifice is measured with a differential pressure transducer and oxygen concentration is measured with a paramagnetic oxygen analyser. Each sensor was connected through a multiplexor to an A to D card inside the PC. Each channel was scanned at 10 Hz and the average of 10 scans was recorded each second.

The component uncertainties are taken from manufacturer's specification in the cases of the temperature and differential pressures (random uncertainties). It is conservative to use manufacturers specifications. Less conservative values could be experimentally determined. However, the overall contribution of the temperature and differential pressure measurements border on insignificance. The sensitivity coefficients are small in value and the values appear inside a square root. The component uncertainty of the oxygen analyser (also a random uncertainty) is assumed to be ±100 ppm. This is the maximum uncertainty acceptable by the standard test method. Another, more detailed value could be gained from the results of the commissioning calibrations via the short-term (30 minute) noise and drift. The assumed effective heat of combustion term (a quasi-systematic uncertainty) may vary ±5% from its value of 13100 kJ·kg^{-1} (±655 kJ·kg^{-1}). As discussed in the earlier section the assumed β value of 1.5 may vary by ±0.5.

Assumed:	$\frac{\Delta h_c}{r_o} = 13100$ (kJ/kg)	$\delta\frac{\Delta h_c}{r_o} = 655$ (kJ/kg)
	$\beta = 1.5$ (--)	$\delta\beta = 0.5$ (--)
Calculated:	$C = 0.0404$ (--)	$\delta C = 0.0004$ (--)
Measured:	$T_e =$ variable (K)	$\delta T_e = 2.2$ (K)
	$\Delta p =$ variable (Pa)	$\delta\Delta p = 0.8$ (Pa)
	$x_{O_2}^a =$ variable (--) by volume	$\delta x_{O_2}^a = 0.0001$ (--) by volume

Figure 2 demonstrates the HRR ± its absolute uncertainty (kW) on the primary y-axis and relative uncertainty (%) on the secondary y-axis, both as functions of time on the x-axis. This demonstrates that at low HRR the uncertainty is very high. The reasons for this are observed

in greater detail in Figure 3 where the components of relative uncertainty are separated and highlighted.

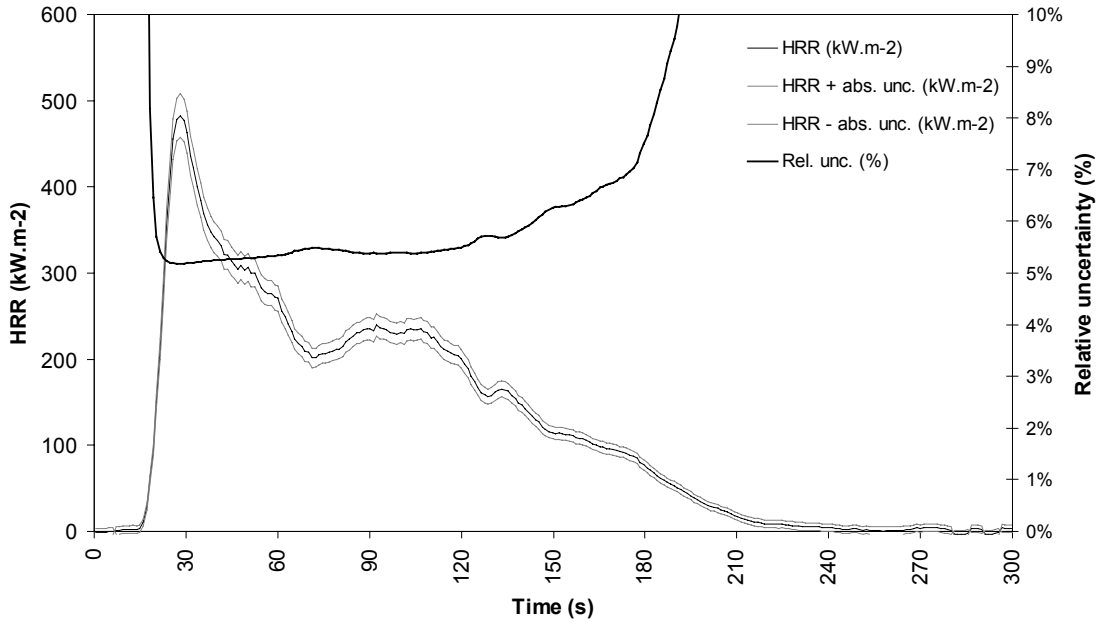

Figure 2: Heat release rate ± absolute uncertainty and relative uncertainty histories taken from cone calorimeter results from an upholstered furniture composite sample.

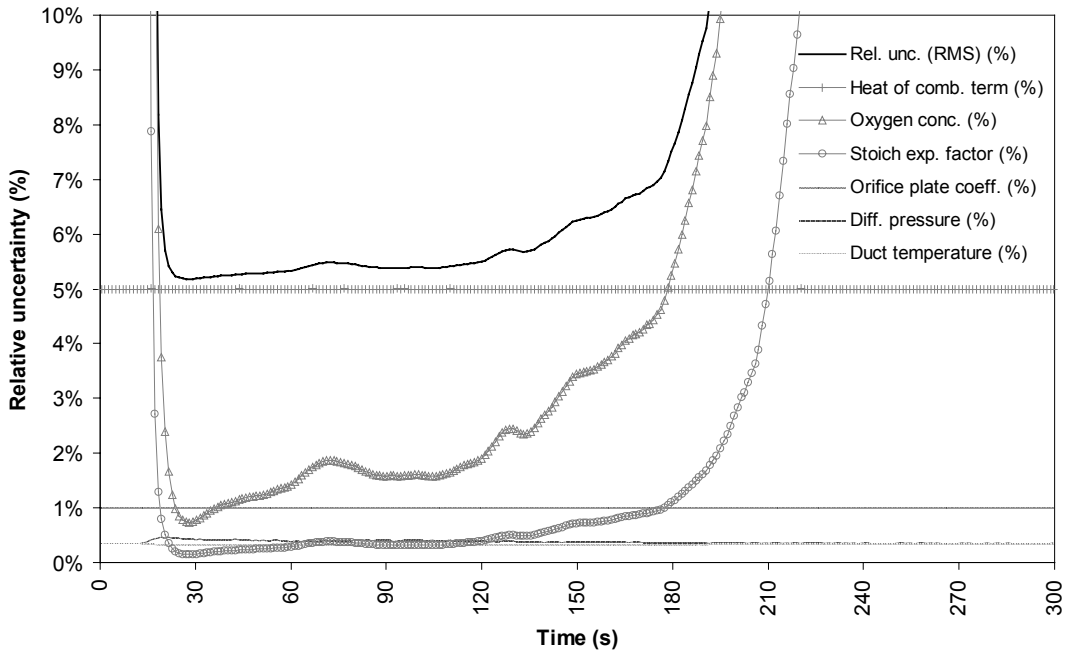

Figure 3: Component uncertainty histories for the stoichiometric expansion factor, heat of combustion , oxygen concentration, orifice flow meter, differential pressure and temperature compared with total (RMS) relative uncertainty from an upholstered furniture composite sample.

Note that in Figure 3 the total relative uncertainty is the root mean squares of the individual components. With the exception of the oxygen concentration measurement and stoichiometric expansion factor, most uncertainty terms remain reasonably constant throughout the test duration.

The example demonstrates that the combustion expansion assumption, the assumption of an effective heat of combustion term and the instrument uncertainty of the oxygen concentration measurement (the latter two pronounced at low HRR levels), contribute significantly to the relative uncertainty of the HRR calculation.

With respect to the expansion factor this uncertainty can be reduced if the composition of the fuel is known, or if additional analysers (CO, CO_2 and H_2O) are used to measure the species. For the assumed effective heat of combustion term, again, this uncertainty can be reduced if the composition of the fuel is known. In respect to oxygen analyser uncertainty at low HRR, using a suppressed zero measuring range or otherwise measuring the oxygen difference directly may reduce this uncertainty. Both of these techniques avoid measuring a small difference across a relatively large scale as is currently done. Typically for a HRR of 5 kW the oxygen concentration depletion is only about 1.0 to 1.5% yet it is measured across a 0-25% scale. However, further research is necessary quantify what improvements may be made in this area.

It is concluded that the types of uncertainties investigated in this example are instrument and assumption orientated. Random errors associated with the sample and operator errors are not included. The uncertainty of an instrument measurement is investigated in so far as the instrument can be relied upon to be giving a true reading. Assumed physical properties used as constants also have uncertainties associated with them. The following conclusions are drawn in order of importance.

An uncertainty analysis of the HRR calculation is not computationally onerous. The partial derivatives are reasonably simple and such a calculation should be incorporated in the cone calorimeter standards and software.

The uncertainty of the calculation is very strongly coupled to any assumed effective heat of combustion term. This uncertainty can be reduced if the composition of the fuel is known. Or

to a lesser degree if additional gases are measured such as H_2O, CO_2 and CO. It is also coupled to any assumed combustion expansion at lower HRR values. This uncertainty can be reduced if the composition of the fuel is known, or if additional analysers (CO, CO_2 and H_2O) are used to measure the species. If the fuel composition is unknown any uncertainty analysis needs to include due allowance for the combustion expansion as it is significant. It is also coupled to the oxygen analyser uncertainty if the analyser is allowed to vary up to its proprietary uncertainty (beyond the +/- 100 ppm by volume specified in the standard). This is not surprising, because the measurement range is a relatively small difference with an increasing uncertainty. Such a disproportional uncertainty contribution of the oxygen analyser may not be necessary. Further research is necessary to quantify the reduction in the oxygen component of the overall uncertainty by using a suppressed zero measuring range or otherwise measuring the oxygen difference directly.

The ISO5660-1 equation for calculating HRR assumes water vapour in the ambient air is insignificant for the given temperature and relative humidity criteria. This simplification introduces an error around 1.0 % to 2.0 % for combinations of high temperature and high relative humidity. Note that in all cases the error is over-estimating the HRR. Mitigating the error is that the same error is encountered in the daily methane calibration. This has the effect of 'hiding' the error in the calculated *C* value. However, this error can be eliminated by substituting the right hand side of Equation 192 instead of the constant 1.10, in Equation 187.

Efforts should be made to determine the flow meter orifice plate coefficient for each calorimeter and from that the 'actual' mass flow rate constant assumed to be the calibration constant. The daily variation of the calibration constant value should be checked against this value. The present calibration constant methodology 'hides' experimental errors not necessarily associated with the variables in the HRR general equation. This may be hindered by the lack of a developed flow between the fan and orifice flow meter and by orifice plate soot coating and edge erosion over time.

5.4.2 Example 2: An alternative calculation of the cone calorimeter calibration constant

Full-scale fire tests and experiments measuring HRR are conducted in several laboratories world-wide, including the University of Canterbury. However, these are cumbersome and expensive. Due to economy of scale and convenience, there is more widespread interest in

small-scale measurement of the HRR per unit area. With emphasis on predicting full-scale behaviour from small-scale results.

The dominant small-scale HRR measuring apparatus is the cone calorimeter (Babrauskas[24]). Standardised cone calorimeter test methods are available. Most notably ISO5660-1[6] and ASTM1354[16]. Within this example, as with the previous example, any mention of the standard test method refers to ISO5660-1 but applies equally to ASTM1354.

Analysis (Enright and Fleischmann[25]) has shown that the uncertainty of HRR calculation from standardised cone calorimeter tests is sensitive to the oxygen concentration measurement. However, if the oxygen analyser performance is to specification as per the standard test method, that is to an accuracy of ±50 ppm, then the overall relative uncertainty is within the bounds normally expected. Say, ≤10% above 50 $kW.m^{-2}$. Unfortunately, if for any reason the oxygen analyser is not performing to specification, then the uncertainty of the HRR calculation increases significantly.

The mechanism within the standard test method for detecting intolerable inaccuracies is the daily methane calibration. Refer to paragraph 12.1 of ISO5660-1. This states, in part:

> *"**12.1 Calibration constant for oxygen consumption analysis***
>
> *The methane calibration shall be performed daily to check for the proper operation of the instrument and to compensate for minor changes in determining of mass flow. (A calibration more than 5% different from the previous one is not normal and suggests instrument malfunction)."*

As stated, the calibration constant *C* serves two purposes. Firstly, as a check of proper operation of the instrument. Secondly, as a variable in the calculation of HRR to compensate for minor changes in determining mass flow. For example, daily changes may be due to variations in the ambient water vapour concentration, assumed constant by the standard test method and 'lumped' into *C*.

When a CO_2 analyser is included in the gas sampling system, a second method of calculation of the *C* value is possible. Assuming the CO production negligible (valid for high purity methane supplied through burner) thermochemistry can be used to calculate *C*. This technique is derived from stoichiometry and is independent of the oxygen concentration. The

objective of this example is to derive this alternative method and compare the results with standard test method.

The alternative is an independent and equally accurate method for calculating *C* and therefore the HRR. However, because the alternative calculation of *C* does not involve the oxygen term, the standard test method must be retained as a check of the proper operation of the instrument, as the operating principle is of oxygen consumption. A comparison of the daily values and variation of the standard test method and alternative methods is a valuable commentary on the performance of the oxygen analyser.

For a more detailed description of the oxygen consumption technique, refer to CHAPTER 2: 'Heat release rate measurement, oxygen consumption technique'. This is the conventional means of HRR measurement in fire tests and experiments is. For the general equations, refer to the standard test method[6], Section [12] 'Calculations' and specifically Annex F 'Calculation of heat release with additional gas analysis'. Assume, O_2, CO_2 and CO concentrations are being measured. Later discussion will show the CO concentration measurement is redundant in the calibration. The HRR is determined by Equation [F.5] of the standard test method. This is reproduced in this example as Equation 205. Similarly, the oxygen depletion factor is determined by Equation [F.6] (Equation 206). The mass flow rate in the exhaust duct by Equation [F.4] (Equation 207). And the ambient oxygen concentration by Equation [F.7] (Equation 208).

As with the previous example, the notation in this example varies from the standard test method's notation. This is to allow a greater number of descriptive combinations required in the later discussion of the thermochemistry technique. They are introduced so that notation is consistent throughout this chapter and with the rest of this thesis.

Equation 205
$$\dot{q} = 1.10\left[\frac{\Delta h_c}{r_0}\right] x_{O_2}\left[\frac{\phi - 0.172(1-\phi)x^a_{CO}/x^a_{O_2}}{(1-\phi)+1.105\phi}\right]\cdot \dot{m}_e$$

Equation 206
$$\phi = \frac{x^o_{O_2}\left(1 - x^a_{CO_2} - x^a_{CO}\right) - x^a_{O_2}\left(1 - x^o_{CO_2}\right)}{x^o_{O_2}\left(1 - x^a_{CO_2} - x^a_{CO} - x^a_{O_2}\right)}$$

Equation 207
$$\dot{m}_e = C\sqrt{\frac{\Delta p}{T_e}}$$

Equation 208 $$x_{O_2} = x_{O_2}^{o}\left(1 - x_{H_2O}^{o}\right)$$

The CO produced in a free burning cone calorimeter test, and particularly in the high-purity methane daily calibration, is assumed to be of insignificant concentration to affect the HRR calculation. Therefore, ignoring CO concentrations as negligible Equation 205 simplifies to Equation 209. Note Equation 208 is substituted into Equation 205 and also appears in Equation 209. The oxygen depletion factor simplifies to Equation 210.

Equation 209 $$\dot{q} = 1.10\left[\frac{\Delta h_c}{r_0}\right] \cdot \left[\frac{\phi \cdot x_{O_2}^{o}\left(1 - x_{H_2O}^{o}\right)}{1 + \phi(1.105 - 1)}\right] \cdot \dot{m}_e$$

Equation 210 $$\phi = \frac{x_{O_2}^{o}\left(1 - x_{CO_2}^{a}\right) - x_{O_2}^{a}\left(1 - x_{CO_2}^{o}\right)}{x_{O_2}^{o}\left(1 - x_{O_2}^{a} - x_{CO_2}^{a}\right)}$$

There is the notable simplifying assumption regarding the ambient moist air state implied by the standard test method's equations. This is discussed in depth in the previous example.

The affect of the varying ambient moist air state on the accuracy of the HRR is noteworthy but minor. (Up to 1% relative error.) It is mitigated within the standard test method by restrictions on operational temperature and relative humidity. It is not allowed for in this example.

For the purposes of this example, we use the standard test method's equations as modified by the explicit simplifications. The HRR is described by Equation 209, the oxygen depletion factor by Equation 210 and the mass flow rate by Equation 207. Substitute Equation 207 into Equation 209 and substitute the value for the net heat release of methane per unit mass of oxygen consumed of 12540 ($kJ.kg^{-1}$) into Equation 209. This gives Equation 211, the overall HRR. Rearranging Equation 211 to solve for the calibration constant *C*, and substituting in a value of 5 kW for the HRR gives Equation 212.

Equation 211 $$\dot{q} = 13.794 \times 10^{3} \cdot \left[\frac{\phi \cdot x_{O_2}^{o}\left(1 - x_{H_2O}^{o}\right)}{1 + \phi(\alpha - 1)}\right] \cdot C\sqrt{\frac{\Delta p}{T_e}}$$

Equation 212
$$C = 3.625\times10^{-4}\cdot\left[\frac{1+\phi(\alpha-1)}{\phi\cdot x_{O_2}^{o}\left(1-x_{H_2O}^{o}\right)}\right]\cdot\sqrt{\frac{T_e}{\Delta p}}$$

For a more detailed description of the thermochemistry technique, refer to CHAPTER 3: 'Heat release rate measurement, thermochemistry technique'. Prior to the development of the oxygen consumption technique some HRR measurements in fire tests and experiments were made via this technique. This technique is based on CO_2 and CO production. Unfortunately, whereas the oxygen consumption technique incorporates on Thornton's Rule[1] to account for unknown fuel composition, the thermochemistry technique is not based on any such universal constant. Following the development of oxygen consumption calorimetry and stable oxygen analysers, the thermochemistry technique become practically obsolete (Janssens and Parker[3]).

Consider Equation 213, the stoichiometric equation for complete combustion of an idealised fuel in oxygen.

Equation 213
$$C_aH_bO_c+\left(a+\frac{b}{4}-\frac{c}{2}\right)O_2\rightarrow aCO_2+\frac{b}{2}H_2O$$

From Equation 213, the HRR is described by Equation 214. The number of moles of the products are multiplied by their respective enthalpy's of formation. From this the enthalpy of formation of the fuel is subtracted. Note the enthalpy of formation of the reactant O_2 is 0.00 ($kJ.kmol^{-1}$) as it remains in its datum phase. The sum per unit time interval is the heat release. The history of the time intervals is the HRR. The HRR appears as a negative Equation 214 as the heat of formation terms are negative for exothermic reactions. For known compositions of reactants and products the heat of the formation is obtained from tabulated data. For unknown or complex reactants or products, it is not a simple task to directly calculate the heat release rate using this technique.

The number of moles of H_2O generated is described in terms of the number of moles of CO_2 produced (or generated) by Equation 215. Similarly, the number of moles of fuel consumed is described in terms of the number of moles of CO_2 generated in and Equation 216. Substituting Equation 215 and Equation 216 into Equation 214 gives Equation 217.

Equation 214 $$-\dot{q} = \left(\Delta H_f^o\right)_{CO_2} \dot{n}_{CO_2}^g + \left(\Delta H_f^o\right)_{H_2O} \dot{n}_{H_2O}^g - \left(\Delta H_f^o\right)_{fuel} \dot{n}_{fuel}^l$$

Equation 215 $$\dot{n}_{fuel}^l = \frac{1}{a} \dot{n}_{CO_2}^g$$

Equation 216 $$\dot{n}_{H_2O}^g = \frac{b}{2a} \dot{n}_{CO_2}^g$$

Equation 217 $$-\dot{q} = \left(\left(\Delta H_f^o\right)_{CO_2} + \frac{b}{2a} \cdot \left(\Delta H_f^o\right)_{H_2O} - \frac{1}{a} \left(\Delta H_f^o\right)_{fuel} \right) \cdot \dot{n}_{CO_2}^g$$

Equation 217 describes the heat release rate in terms of the number of moles of CO_2 produced. The number of moles produced is obtained by describing Equation 217 in terms of the concentration of CO_2 measured. The first step is described in Equation 218.

Equation 218 $$\dot{n}_{CO_2}^g = x_{CO_2}^g \cdot \frac{\dot{m}_e}{M_e}$$

However, the value must be corrected for ambient CO_2, ambient H_2O and generated H_2O. This steps is described by Equation 219 then described again in terms of the CO_2 generated by Equation 220 before being rearranged and simplified to Equation 221.

Equation 219 $$x_{CO_2}^g = \left(1 - x_{H_2O}^g - x_{H_2O}^o\right) \cdot x_{CO_2}^a - x_{CO_2}^o$$

Equation 220 $$x_{CO_2}^g = x_{CO_2}^a \left(1 - \frac{b}{2a} x_{CO_2}^g - x_{H_2O}^o \right) - x_{CO_2}^o$$

Equation 221 $$x_{CO_2}^g = \frac{x_{CO_2}^a \left(1 - x_{H_2O}^o\right) - x_{CO_2}^o}{1 + \frac{b}{2a} x_{CO_2}^a}$$

Equation 221 is substituted into Equation 218 and then the result substituted into Equation 217 to obtain Equation 222. Equation 222 is the general equation for heat release rate.

Equation 222 $$-\dot{q} = \left(\left(\Delta H_f^o\right)_{CO_2} + \frac{b}{2a} \cdot \left(\Delta H_f^o\right)_{H_2O} - \frac{1}{a}\left(\Delta H_f^o\right)_{fuel} \right) \cdot \left(\frac{x_{CO_2}^a \left(1 - x_{H_2O}^o\right) - x_{CO_2}^o}{1 + \frac{b}{2a} x_{CO_2}^a} \right) \cdot \frac{\dot{m}_e}{M_e}$$

It is noted that the values of $x_{CO_2}^o$ and $x_{H_2O}^o$ are respectively assumed and calculated properties of the incoming air, $\left(x_{CO_2}^o\right)_a$ and $\left(x_{H_2O}^o\right)_a$ rather than the exhaust gas which would be more correct, $\left(x_{CO_2}^o\right)_e$ and $\left(x_{H_2O}^o\right)_e$. The relationships are derived in CHAPTER 3: 'Heat release rate measurement, thermochemistry technique' and appears as Equation 223 and Equation 224.

Equation 223 $$\left(\mathrm{x}_{\mathrm{CO_2}}^{\mathrm{o}}\right)_{\mathrm{e}} = \left(\mathrm{x}_{\mathrm{CO_2}}^{\mathrm{o}}\right)_{\mathrm{a}} \cdot \left[1 - \left(\frac{\mathrm{b} + 2\mathrm{c}}{4\mathrm{a}}\right)\mathrm{x}_{\mathrm{CO_2}}^{\mathrm{g}}\right]$$

Equation 224 $$\left(\mathrm{x}_{\mathrm{H_2O}}^{\mathrm{o}}\right)_{\mathrm{e}} = \left(\mathrm{x}_{\mathrm{H_2O}}^{\mathrm{o}}\right)_{\mathrm{a}} \cdot \left[1 - \left(\frac{\mathrm{b} + 2\mathrm{c}}{4\mathrm{a}}\right)\mathrm{x}_{\mathrm{CO_2}}^{\mathrm{g}}\right]$$

In practical terms, and especially in a methane calibration test, the differences are negligible. Usually, during the 5 kW calibration $\left(\mathrm{x}_{\mathrm{CO_2}}^{\mathrm{g}}\right)_{\max} \approx 1.0\%$ and for methane $(\mathrm{b} + 2\mathrm{c})/4\mathrm{a} = 1$. The differences are a maximum of 1.0 % at peak HRR. Assume Equation 225 and Equation 226.

Equation 225 $$\left(\mathrm{x}_{\mathrm{CO_2}}^{\mathrm{o}}\right)_{\mathrm{e}} \approx \left(\mathrm{x}_{\mathrm{CO_2}}^{\mathrm{o}}\right)_{\mathrm{a}}$$

Equation 226 $$\left(\mathrm{x}_{\mathrm{H_2O}}^{\mathrm{o}}\right)_{\mathrm{e}} \approx \left(\mathrm{x}_{\mathrm{H_2O}}^{\mathrm{o}}\right)_{\mathrm{a}}$$

Therefore, it is appropriate to use Equation 222 to calculate the HRR with values of $x_{CO_2}^o$ and $x_{H_2O}^o$ from the incoming ambient air.

For complete combustion of methane in air (oxygen), the stoichiometric Equation 213 simplifies to Equation 227. Substituting mole values of Equation 227 into Equation 222 along with tabulated data for heats of formation at 25 ^{o}C from Drysdale[9] gives Equation 228

Equation 227 $$CH_4 + 2O_2 \rightarrow CO_2 + 2H_2O$$

Where; $a = 1,\ b = 4,\ c = 0$

$\left(\Delta H_f^o\right)_{CO_2} = -393.5 \quad (\text{kJ.mol}^{-1})$

$\left(\Delta H_f^o\right)_{H_2O} = -241.8 \quad (\text{kJ.mol}^{-1})$

$\left(\Delta H_f^o\right)_{CH_4} = -74.9 \quad (\text{kJ.mol}^{-1})$

Equation 228
$$\dot{q} = 802.3 \cdot \left[\frac{x^a_{CO_2}\left(1 - x^o_{H_2O}\right) - x^o_{CO_2}}{\left(1 + 2x^a_{CO_2}\right)} \right] \cdot \frac{\dot{m}_e}{M_e}$$

Equation 229
$$M_e \approx M_{a(\text{dry})} = 0.02896 \ (\text{kg.mol}^{-1})$$

Within Equation 228 is the expression of the ratio of mass flow rate to molecular mass of the exhaust gases rather than incoming air. The latter is the case with the oxygen consumption technique. This is a significant advantage of the thermochemistry technique as the analysis need not allow for the expansion due to combustion as it is not concerned with predicting how much oxygen would be there if no combustion were taking place. Therefore, the thermochemistry technique need not incorporate the oxygen depletion factor ϕ and combustion expansion factor α, both sources of significant uncertainty. As described in Equation 229, the molecular mass of the exhaust gasses is assumed approximately equal with the molecular mass of dry ambient air. Equation 207 and Equation 229 are substituted into Equation 228 to obtain Equation 230. This is the general equation for HRR for the methane calibration. For a 5 kW methane calibration, Equation 230 is rearranged for the daily calibration constant *C*. This is described by Equation 231.

Equation 230
$$\dot{q} = 27.70 \times 10^3 \cdot \left[\frac{x^a_{CO_2}\left(1 - x^o_{H_2O}\right) - x^o_{CO_2}}{\left(1 + 2x^a_{CO_2}\right)} \right] \cdot C\sqrt{\frac{\Delta p}{T_e}}$$

Equation 231
$$C = 1.805 \times 10^{-4} \cdot \left[\frac{\left(1 + 2x^a_{CO_2}\right)}{x^a_{CO_2}\left(1 - x^o_{H_2O}\right) - x^o_{CO_2}} \right] \cdot \sqrt{\frac{T_e}{\Delta p}}$$

Introduce subscripts “O” and “T” to Equation 231 and Equation 212 to distinguish between the two techniques where O refers to the oxygen consumption technique and T refers to the thermochemistry technique. Also substitute ϕ Equation 210 into Equation 212.

Equation 232 $$C_O = 3.625\times10^{-4}\cdot\left[\frac{1+\left(\frac{x_{O_2}^o\left(1-x_{CO_2}^a\right)-x_{O_2}^a\left(1-x_{CO_2}^o\right)}{x_{O_2}^o\left(1-x_{O_2}^a-x_{CO_2}^a\right)}\right)(\alpha-1)}{\left(\frac{x_{O_2}^o\left(1-x_{CO_2}^a\right)-x_{O_2}^a\left(1-x_{CO_2}^o\right)}{\left(1-x_{O_2}^a-x_{CO_2}^a\right)}\right)\cdot\left(1-x_{H_2O}^o\right)}\right]\cdot\sqrt{\frac{T_e}{\Delta p}}$$

Equation 233 $$C_T = 1.805\times10^{-4}\cdot\left[\frac{\left(1+2x_{CO_2}^a\right)}{x_{CO_2}^a\left(1-x_{H_2O}^o\right)-x_{CO_2}^o}\right]\cdot\sqrt{\frac{T_e}{\Delta p}}$$

The following four examples (illustrated in Figure 4 to Figure 7) are taken from methane calibrations undertaken on the University of Canterbury Cone Calorimeter. The calibration constant values are averaged and summarised in Table 2. The first three calibrations are representative of ‘real’ cone calorimeter tests. The fourth is a ‘contrived’ calibration where the oxygen analyser is deliberately spanned incorrectly. These results verify the hypothesis that the thermochemistry technique is independent of the O_2 reading. It also identifies a problem with the O_2 analyser (in this case not being spanned properly) as C_O errs while C_T is correct.

CALIBRATION #	DATE	C_O	C_T
1	12 Nov. 1998	0.0420	0.0420
2	13 Nov. 1998	0.0421	0.0419
3	03 Dec. 1998	0.0424	0.0422
4	07 Jan. 1999	0.0332	0.0416

Table 2: Examples of CH_4 calibrations

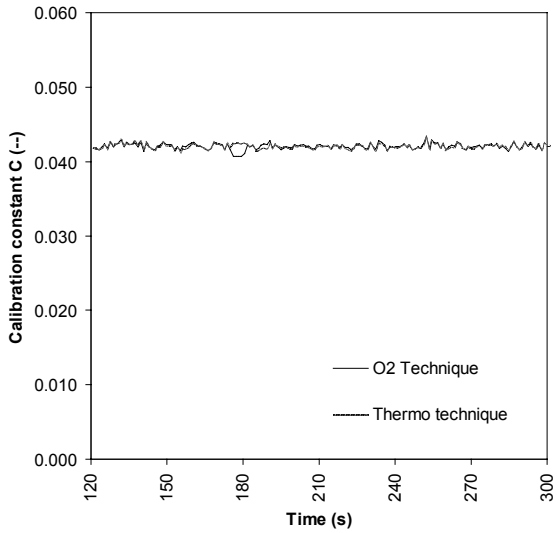

Figure 4: CH_4 Calibration, 12 Nov. 1998

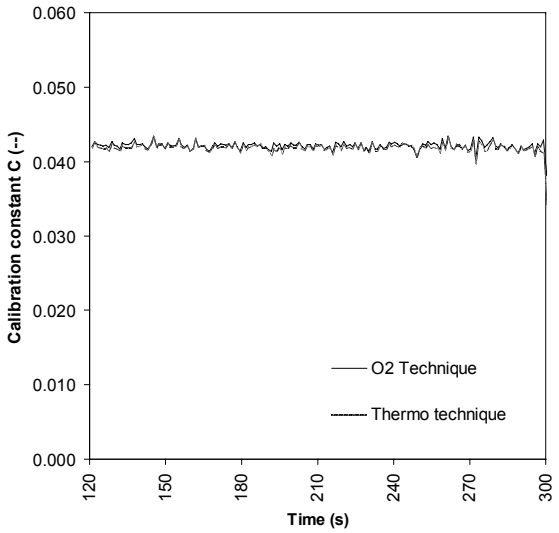

Figure 5: CH_4 Calibration, 13 Nov. 1998

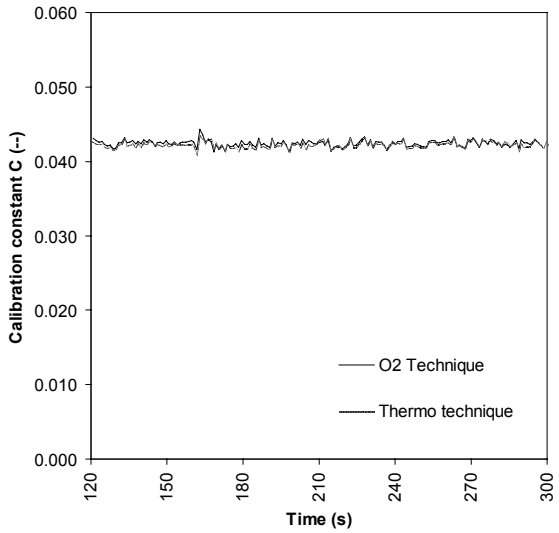

Figure 6: CH_4 Calibration, 03 Dec. 1998

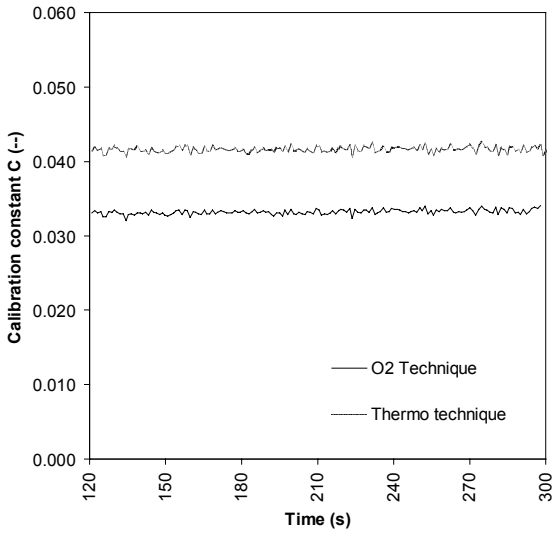

Figure 7: CH_4 Calibration, 07 Jan. 1999

This example derives the uncertainty equations for the two methods in order to further quantify the comparison. Several simplifying assumptions are made. These are consistent between the two techniques so that even if the assumptions are unconservative the techniques remain comparable.

In the case of the oxygen consumption technique the fuel is identified. Therefore, assume insignificant uncertainty in the ratio of net heat of combustion to stoichiometric ratio $\Delta h_c / r_0$, and also insignificant uncertainty in the value of the combustion expansion factor, α. In the case of the thermochemistry technique the fuel is identified. Therefore, assume insignificant

uncertainty in the values of enthalpy of formation of the reactants and products, $\left(\Delta H_f^o\right)_i$. In both cases assume insignificant uncertainty in the assumption that the molecular mass of the exhaust gases is approximately equal to the molecular mass of dry ambient air, $M_e \approx M_a \approx M_{a(dry)}$. Also, in both cases assume there is negligible uncertainty in the calculation of the actual ambient mole fraction of water vapour, $x_{H_2O}^o$. And in the values of the measured (dry) mole fraction of ambient O_2 and CO_2. That is $x_{O_2}^o$ has the value 20.95% by volume and $x_{CO_2}^o$ 300 ppm by volume. Therefore, in the case of the oxygen consumption technique assume uncertainty in the measurement of the temperature at the orifice flow meter T_e, the differential pressure at the orifice flow meter Δp, and the measured (dry) mole fraction species O_2 and CO_2. In the case of the thermochemistry technique also assume uncertainty in the measurement of the temperature at the orifice flow meter T_e, the differential pressure at the orifice flow meter Δp, but the measured (dry) mole fraction species of CO_2 only.

Equation 234 and Equation 235 are the general equation for determining the absolute uncertainty of the oxygen consumption and thermochemistry techniques with respect to the temperature, pressure and species concentrations.

Equation 234 $$\delta C_O = \left[\left(\frac{\partial C_O}{\partial x_{O_2}^a} \cdot \delta x_{O_2}^a \right)^2 + \left(\frac{\partial C_O}{\partial x_{CO_2}^a} \cdot \delta x_{CO_2}^a \right)^2 + \left(\frac{\partial C_O}{\partial T_e} \cdot \delta T_e \right)^2 + \left(\frac{\partial C_O}{\partial \Delta p} \cdot \delta \Delta p \right)^2 \right]^{\frac{1}{2}}$$

Equation 235 $$\delta C_T = \left[\left(\frac{\partial C_T}{\partial x_{CO_2}^a} \cdot \delta x_{CO_2}^a \right)^2 + \left(\frac{\partial C_T}{\partial T_e} \cdot \delta T_e \right)^2 + \left(\frac{\partial C_T}{\partial \Delta p} \cdot \delta \Delta p \right)^2 \right]^{\frac{1}{2}}$$

For the oxygen consumption technique, Equation 236 to Equation 239 describes the partial derivatives. These are also termed sensitivity coefficients.

Equation 236 $$\frac{\partial C_O}{\partial \Delta p} = \frac{-1}{2\Delta p} \cdot C_O$$

Equation 237

$$\frac{\partial C_O}{\partial T_e} = \frac{1}{2T_e} \cdot C_O$$

Equation 238

$$\frac{\partial \mathrm{C_O}}{\partial \mathrm{x}^{\mathrm{a}}_{\mathrm{CO_2}}} = 3.625\times10^{-4} \cdot \left[\frac{\mathrm{x}^{\mathrm{a}}_{\mathrm{O_2}} \left(1 - \mathrm{x}^{\mathrm{o}}_{\mathrm{O_2}} - \mathrm{x}^{\mathrm{o}}_{\mathrm{CO_2}}\right)}{\left(\mathrm{x}^{\mathrm{o}}_{\mathrm{O_2}} \left(1 - \mathrm{x}^{\mathrm{a}}_{\mathrm{CO_2}}\right) - \mathrm{x}^{\mathrm{a}}_{\mathrm{O_2}} \left(1 - \mathrm{x}^{\mathrm{o}}_{\mathrm{CO_2}}\right)\right)^2 \left(1 - \mathrm{x}^{\mathrm{o}}_{\mathrm{H_2O}}\right)} \right] \cdot \sqrt{\frac{\mathrm{T_e}}{\Delta \mathrm{p}}}$$

Equation 239

$$\frac{\partial \mathrm{C_O}}{\partial \mathrm{x}^{\mathrm{a}}_{\mathrm{CO_2}}} = 3.625\times10^{-4} \cdot \left[\frac{\left(1 - \mathrm{x}^{\mathrm{a}}_{\mathrm{CO_2}}\right)\left(1 - \mathrm{x}^{\mathrm{o}}_{\mathrm{O_2}} - \mathrm{x}^{\mathrm{o}}_{\mathrm{CO_2}}\right)}{\left(\mathrm{x}^{\mathrm{o}}_{\mathrm{O_2}} \left(1 - \mathrm{x}^{\mathrm{a}}_{\mathrm{CO_2}}\right) - \mathrm{x}^{\mathrm{a}}_{\mathrm{O_2}} \left(1 - \mathrm{x}^{\mathrm{o}}_{\mathrm{CO_2}}\right)\right)^2 \left(1 - \mathrm{x}^{\mathrm{o}}_{\mathrm{H_2O}}\right)} \right] \cdot \sqrt{\frac{\mathrm{T_e}}{\Delta \mathrm{p}}}$$

For the thermochemistry technique, Equation 240 to Equation 242 describes the partial derivatives.

Equation 240

$$\frac{\partial C_T}{\partial \Delta p} = \frac{1}{2\Delta p} \cdot C_T$$

Equation 241

$$\frac{\partial C_T}{\partial T_e} = \frac{1}{2T_e} \cdot C_T$$

Equation 242

$$\frac{\partial C_T}{\partial x^a_{CO_2}} = 1.805\times10^{-4} \cdot \frac{-\left(2x^o_{CO_2} + \left(1 - x^o_{H_2O}\right)\right)}{\left(x^a_{CO_2}\left(1 - x^o_{H_2O}\right) - x^o_{CO_2}\right)^2} \cdot \sqrt{\frac{T_e}{\Delta p}}$$

And for both techniques (except for α whih is only used in the oxygen consumption technique:

α = 1.105 (--)

$\delta\alpha$ = 0 (--) assumed

Δp = time dependent variable (Pa)

$\delta\Delta p$ = 0.8 (Pa) from manufacturers data

T_e = time dependent variable (K)

δT_e = 2.2 (K) from manufacturers data

$x^a_{O_2}$ = time dependent variable (--)

$\delta x^a_{O_2}$ = 48 ppm (--) determined experimentally

$x^o_{O_2}$ = 0.2095 (--)

$\delta x^o_{O_2}$ = 0 (--) assumed

$x^a_{CO_2}$ = time dependent variable (--)

$\delta x^a_{CO_2}$ = 27 ppm (--) determined experimentally

$x^o_{CO_2}$ = 300 ppm (--)

$\delta x^o_{CO_2}$ = 0 (--) assumed

$x^o_{H_2O}$ = calculated (--)

$\delta x^o_{H_2O}$ = 0 (--) assumed

Values for $\delta x_{O_2}^a$ and $\delta x_{CO_2}^a$ are determined from commissioning calibrations where 30 minute noise and drift calibrations are undertaken. The results of these commissioning tests are demonstrated detailed in CHAPTER 6: 'Instrumentation'.

The uncertainty equations Equation 234 and Equation 235 are solved using the above equations and data from Calibration #1. The mean relative uncertainty (instrument dependent) of the calibration constant calculation using the oxygen consumption technique is determined as less than 1% of the result (0.60%). Similarly, using the thermochemistry technique it is also less than 1% (0.58%). The uncertainty of the calculation using the thermochemistry technique is less than the oxygen consumption technique, but not significantly.

In terms of applications of this concept, the marginally lower uncertainty and simplicity of Equation 233 makes the alternative method ideal for incorporation into data reduction software as a means of checking/troubleshooting problems in the daily calibration of the cone calorimeter. When the daily calibration constant is outside the accept bounds, there are two possible causes: the oxygen measurement or the mass flow calculation. The problem can be quickly diagnosed when the alternative calibration constant is calculated. If the alternative calibration constant is outside the acceptable bounds and the alternative method is within acceptable bounds than the problem can most likely be found in the oxygen measurement. Conversely, if both the Standard and alternative methods are outside the acceptable bounds, then the problem is most likely to be in the mass flow calculation and is either the differential pressure or the temperature measurement.

It is concluded that the thermochemistry technique used is a valid technique for calculating the calibration constant used in the cone calorimeter. This alternative method is independent of the oxygen concentration and has been shown to have a marginally lower uncertainty compared to the Standard method. Although, the Standard method remains the preferred technique for calculating the calibration constant as it is based on the operating principle of the apparatus and includes an oxygen measurement term. The simplicity of the final equation for the alternative method makes it easy to incorporate into software used on the cone calorimeter and can be used as a means of checking/troubleshooting the system.

CHAPTER 6: INSTRUMENTATION

6.1 Introduction

This Chapter is a prelude to the furniture fire modelling experimental work descried more fully in CHAPTER 7: 'CBUF Model I and II applied to exemplary NZ furniture (NZ-CBUF)'. CBUF is an acronym for the Combustion Behaviour of Upholstered Furniture (CBUF). NZ-CBUF denotes the models applied to exemplary NZ furniture. The current Chapter is devoted to the characterisation of the instrumentation used in the experimental work of the following Chapter.

The experimental portion of the NZ-CBUF initiative involves fire tests on the cone calorimeter (small-scale) and furniture calorimeters (full-scale). The University of Canterbury (UC) Cone Calorimeter complies with the Standard Test Method[6] as amended by Appendix A6 of the CBUF Final Report[26] "Cone Calorimeter testing". The test protocol, specimen preparation, special testing instructions and reporting were all performed according to the strict specification of the CBUF Protocol. Similarly, the UC Furniture Calorimeter complies with the Standard Test Method[7] as amended by Appendix A7 of the CBUF Final Report "Furniture Calorimeter test protocol". Again, the test protocol, specimen preparation, special testing instructions and reporting are all followed as per the Appendix A7. Within the NZ-CBUF programme, the option of measuring smoke density and reporting light obstructing smoke in the cone and furniture calorimeters, was not undertaken.

6.2 Characterisation of the UC Cone Calorimeter

The bench-scale experiments within the NZ-CBUF initiative, involve fire tests undertaken on the UC Cone Calorimeter. This apparatus complies with the standard test method[6] as amended by Appendix A6 of the CBUF Final Report[26]. In addition the supplementary requirements and recommendations of the draft standard test method[27] are followed. Note that the draft standard test method is complimentary to the current and expands upon it in great detail. It is not contradictory to the current, or if any contradictions occur, they have not been introduced to the NZ-CBUF study. The test protocol, specimen preparation, special testing instructions and reporting are all performed according to the strict specification of the CBUF Protocol. While the full protocol is not repeated here, sections of emphasis are, for fuller information refer to the Final Report[26].

6.2.1 Test principles

The ISO 5660.1 standard test method assesses the contribution of a furniture item to the rate of evolution of heat during its involvement in fire. These properties are determined on small representative specimens of the item.

A small scale specimen consisting of composite upholstered furniture materials is placed on a load cell. The load cell is located under a small extraction hood and duct system designed to transport the combustion gases. Probes for gas sampling and instrumentation for the measurement of volumetric flow rate (temperature at, and pressure across an orifice) are located in the exhaust duct leading from the hood. The specimen is subject to a predetermined external irradiance of 35 $kW.m^{-2}$. It is ignited with an electric spark. During the test concentrations of oxygen, carbon dioxide and carbon monoxide are measured in the exhaust duct. Mass loss rate of the burning specimen is also measured by means of the mass scale.

From these measurements the HRR is calculated using the principle of oxygen consumption calorimetry (Huggett[2]). In addition, the mass loss rate, effective heat of combustion and gas species production are also measured. These values together with visual recordings constitute the results from the test.

6.2.2 Test set-up

The general requirements for the test set-up are well specified in ISO 5660.1 and CBUF test protocol. While it is not the purpose of this document to repeated those specifications verbatim, key characteristic's of the UC Cone Calorimeter set-up are discussed.

A 12 mm thick Kaowool blanket is used underneath the specimens. For more details refer to paragraph A6:1.3.2.1 of the CBUF Final Report.

As water vapour concentrations are not measured, a drying agent is used. Drierite indicating 4 mesh is selected as an alternative to the more common drying agent silica gel. This is on the basis that silica gel has recently been found to adversely effect CO_2 readings (Babrauskas and Thureson[28]). As an aside, 8 mesh the next finer size than 4 mesh, would have been more preferable. It is less coarse, while still porous enough to allow the gas sample to flow uninhibited. Refer also to paragraph A6:1.3.2.2 of the CBUF Final Report.

A specimen shield is used to start the test. In the closed position it completely covers the opening in the heater base plate. It is able to be opened within 0.5 s. The adequacy of the shield is checked by closing it for 10 s while the heater element output is 35 kW.m^{-2} irradiance. The irradiance deviation upon opening the shield is 0.25 kW.m^{-2}, the maximum allowed is 1.0 kW.m^{-2}. The 90% FSD response of the radiation shielding is < 3 seconds, the maximum allowed is 10 seconds. The results of this check are demonstrated in Figure 8. Refer also to paragraph A6:1.3.2.4 of the CBUF Final Report.

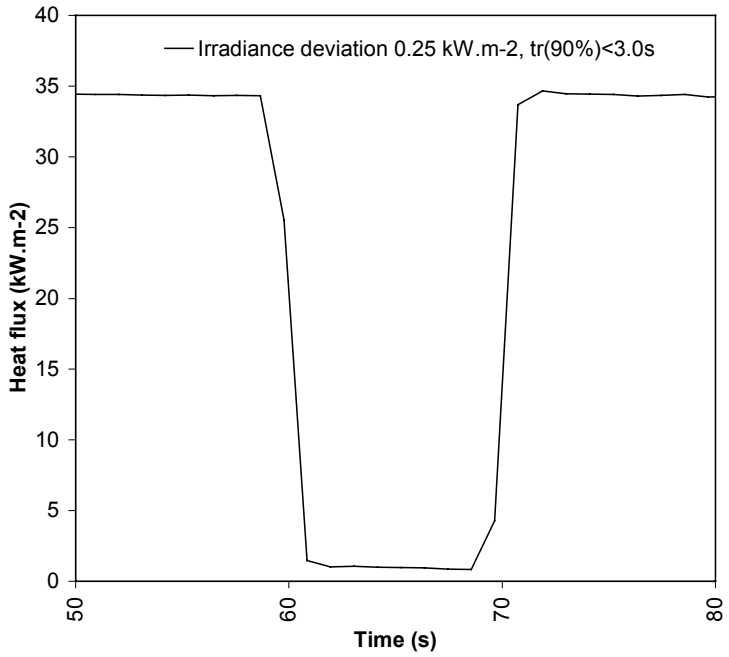

Figure 8: Response of the working heat flux meter to the specimen shield being closed at t=60 s and opened at t=70 s.

6.2.3 Test procedure

The test procedure is as per the standard test method, Section 11 'Test procedure' and is amended by the CBUF Final Report. It is not reproduced in full here. However, key features are discussed.

All completed specimens in their foil cups were placed in a conditioning room for a minimum 24 hour period at 23 ± 2 C and 50 ± 5 % *RH*..

All cone calorimeter tests were conducted at an irradiance level of 35 kW.m^{-2}. All specimens were tested in the horizontal orientation. At least three specimens were tested. If any

specimen's $\dot{q}''_{180}$, the three-minute (from ignition) average heat release rate varied by more than 10% from the mean value, then three more specimen were tested.

In all cone calorimeter tests the spark igniter was removed after 4 s of sustained ignition. In no time did any specimen flame out early.
A two minute baseline was run before each cone calorimeter test. At 1:50 minutes of recorded data, still in baseline, the shield was manually closed and the specimen placed on the load cell. At 2:00 minutes of recorded baseline data the shield was withdrawn exposing the sample to the radiation source and simultaneously setting off the spark igniter. Post test, during data analysis time zero was set at 2:00 minutes of recorded data.

6.2.4 Commissioning calibrations

The UC Cone Calorimeter was commissioned prior to the NZ-CBUF tests. Commissioning calibrations were undertaken in accordance with the specifications of the draft standard test method. The results are presented in the following sections.

Refer to paragraph 10.1.1 of the draft standard test method 'Irradiance control system response characteristics'. With an irradiance level of 50 $kW.m^{-2}$ and an exhaust flow rate of 0.024 $m^3.s^{-1}$ a 6 mm thick specimen of black PMMA is tested in accordance with the procedure of the standard test method section 11 'Test procedure'. Refer to paragraph 6.4 of the draft standard test method for quantification of the objectives. The irradiance control system is required to maintain the average temperature at the pre-set level to within ± 10 ^oC. The calibrated temperature held to within ± 2 ^oC. Figure 9 demonstrates this results.

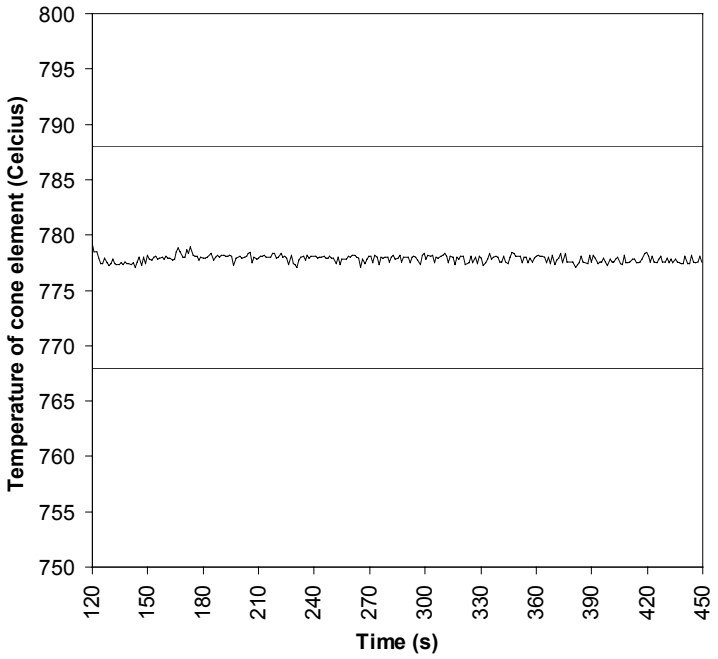

Figure 9: Irradiance (heater element temperature) control during a PMMA test – the HRR history is described by Figure 10. The ±10 C bands are maximum bounds of variation.

As a further check the average HRR over the first three minutes from ignition is required to be 590 ± 30 kW.m^2. The calibrated average HRR is 587 kW.m^2. Figure 10 demonstrates the HRR time history.

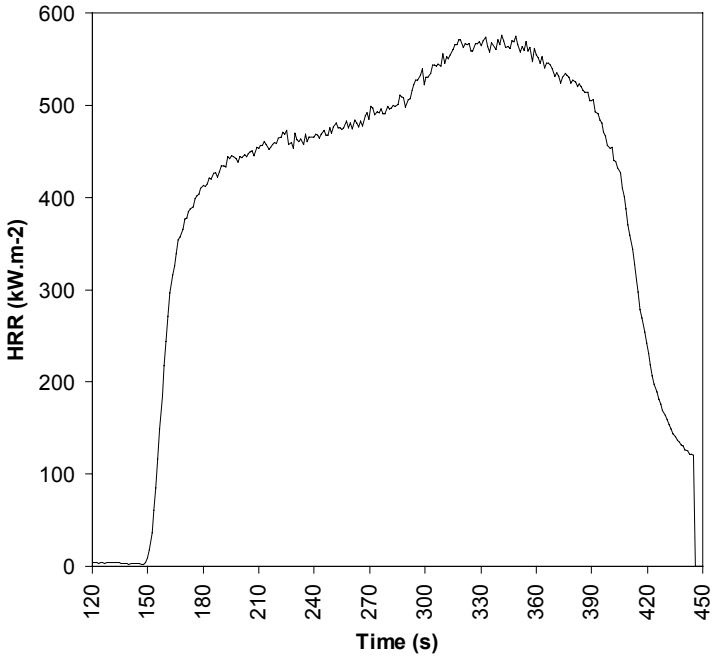

Figure 10: HRR history during the PMMA calibration of irradiance control – heater element temperature control. See Figure 9 for performance of heater element temperature.

Refer to paragraphs 10.1.2 of the draft standard test method ‘Weighing device response time’. The response time is checked by replacing and removing 250 g weights. The response time is defined as the 10-90% FSD deflection and is required by paragraph 6.5 of the draft standard test method to be 1-4 seconds. The calibrated response time is determined to be less than 3 seconds. Figure 11 demonstrates this result.

Refer to paragraphs 10.1.3 of the draft standard test method ‘Weighing device output drift’. The drift is checked by adding a 250 g weight with an irradiance stabilised at 50 $kW.m^2$, an exhaust flow rate of 0.024 $m^3.s^{-1}$ and recording 30 minutes of data. The drift is the difference between the initial and final mass and is required by paragraph 6.5 of the draft standard test method to be no more than ± 0.5 g. The calibrated output drift is 1.7 g, exceeding the limit. However, given that the NZ-CBUF cone calorimeter test results are terminated after only 5.0 minutes, the 30 minute drift of 1.7 g is assumed acceptable as the drift is approximately linear. Figure 12 demonstrates this result. Note the 5.0 minute drift is 0.3 g.

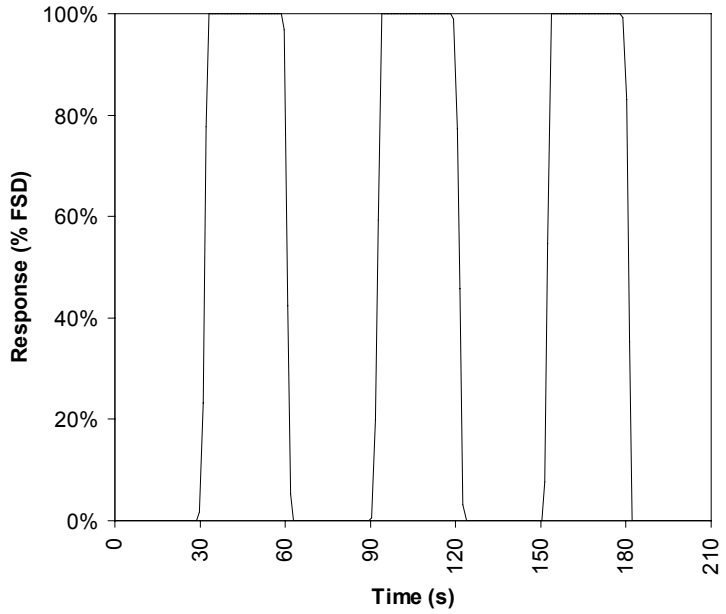

Figure 11: Weighing device response time to a 250 g load being applied and removed at 10 s intervals.

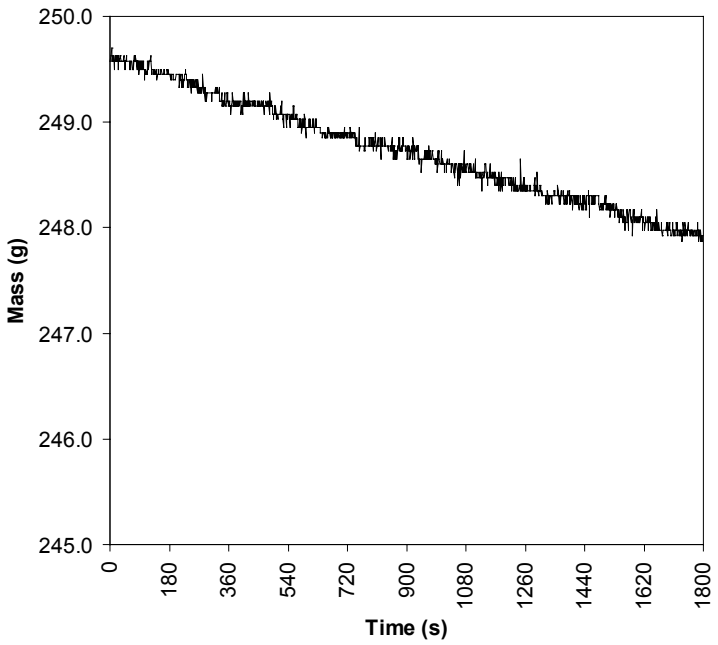

Figure 12: Weighing device output drift over 30 minutes with a load of 250 g applied and an incident heat flux of 50 kW.m^{-2}. The exhaust fan is on for this calibration.

6.2.5 Less frequent calibrations

In addition to daily operating calibrations the draft standard test method specifies certain less frequent checks to be made of the system.

The operating or 'working' heat flux meter is checked against a reference meter at irradiance levels of 10, 25, 35, 50, 65, 70 and 100 kW.m^{-2}. In this instance two reference meters are used. The readings are required to agree within ± 2% of each other. If a gauge is noted to be consistently high or low, the calibration factor may be changed. Against reference meter #1 the working meter is within ± 2% and assumed acceptable. It is interesting to note that reference meter #2 is consistently and slightly 'low' against the other two meter suggesting that the calibration factor supplied may be low. Figure 13 demonstrates this result. Refer also to paragraph 10.3.1 of the draft standard test method.

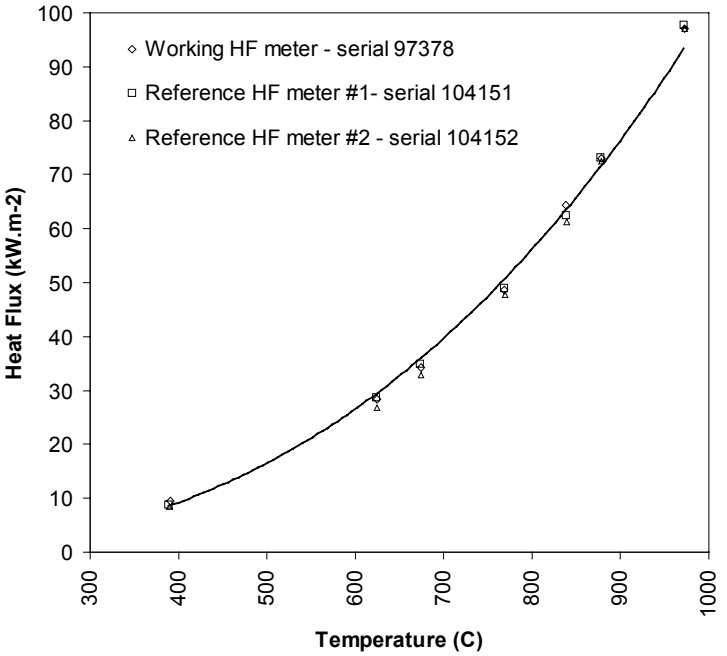

Figure 13: Calibration of the working heat flux meter and the two reference meters. Note that the second reference meter is consistently low, suggesting the calibration constant may need to be adjusted.

The overall HRR measuring apparatus is tested by flowing known mass flow rates corresponding to 1, 3 and 5 kW ± 10%. The calibration constant is calculated for each HRR and compared. An acceptable maximum deviation of 5% is specified. The system is calibrated to 5 kW, at the lower HRR of 1 and 3 kW the system demonstrates a slight positive bias. The measured means are 1.03 and 3.07 kW with a standard deviation of 0.01 and 0.03 kW, or 1% in both cases. Good linearity at the lower HRR calibration of 1 and 3 kW indicates the system is running with very good accuracy, this is discussed in greater detail in Enright and Fleischmann[25]. Figure 14 demonstrates this result. Refer also to paragraph 10.3.2 of the draft standard test method.

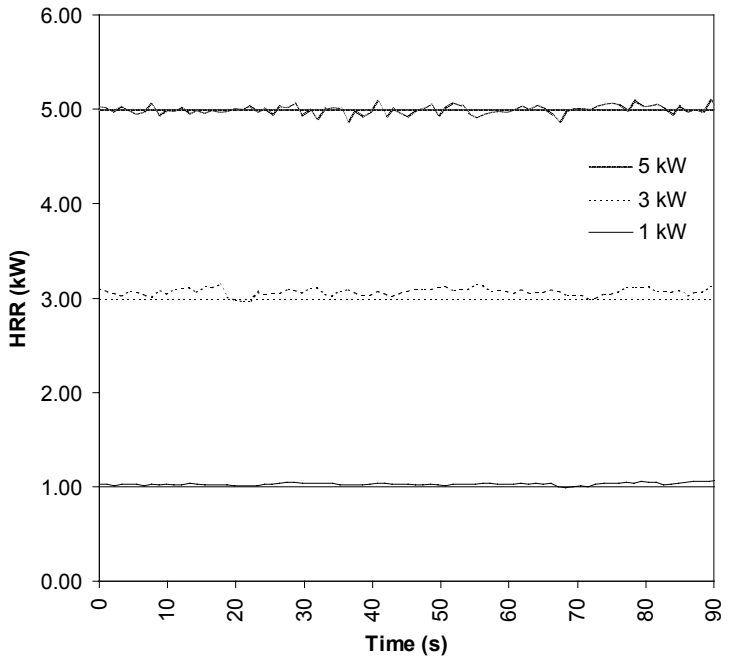

Figure 14: Linearity of HRR. The calibration constant C is calculated from the 5 kW test and then used to calculate 1 and 3 kW calibrations. The agreement is good.

6.3 Characterisation of the UC Furniture Calorimeter

The full-scale experiments of the NZ-CBUF initiative, involve fire tests undertaken on the UC Furniture Calorimeter. This apparatus complies with the standard[7] as amended by Appendix A7 of the CBUF Final Report[26]. The test protocol, specimen preparation, special testing instructions and reporting are all performed according to the strict specification of the CBUF Protocol. While the full protocol is not repeated here, sections of emphasis are, for fuller information refer to the Final Report[26].

6.3.1 Test principles

This standard test method is used for the evaluation of fire behaviour of an item of upholstered furniture in the full-scale under free burning conditions.

A full-scale item of upholstered furniture is placed on a weighing platform. The platform is located under an extraction hood specially designed to transport the combustion gases. There should be virtually no obstructions to the air supply to the test set-up. Probes for gas sampling and instrumentation for the measurement of volumetric flow rate are located in the exhaust duct leading from the hood. The specimen is ignited with a square ring gas burner. During the

test concentrations of carbon monoxide, carbon dioxide and oxygen and volume flow rate are measured in the exhaust duct. Mass loss rate of the burning sample is measured by means of a weight measuring device.

From these measurements the HRR is calculated using the principle of oxygen consumption calorimetry (Huggett[2]). In addition, the mass loss rate, effective heat of combustion and gas species production are also measured. These values together with visual recordings constitute the results from the test.

A Photograph of an item on the UC Furniture Calorimeter during a test is shown in Figure 15. The Photograph is taken 3 minutes after ignition and the HRR is peaking at ~2.25 MW.

Figure 15: UC Furniture Calorimeter during NZ-CBUF test. A two-seat furniture item at a peak HRR of ~2250 kW, approximately 180s from ignition

6.3.2 Test set-up

The general requirements for the test set-up are well specified in the standard and protocol. While it is not the purpose of this document to repeat those specifications verbatim, key characteristics of the UC Furniture Calorimeter set-up are discussed. Of particular interest are the variations of the UC Furniture Calorimeter from the standard.

The environment around the sample is required to be a draught free area with no more than two enclosing walls. An enclosing wall is defined as a wall closer than 2.0 m from the outer edge of the smoke hood. The UC environment is in a draught free area but has three enclosing walls. From the outer edge of the hood, the North wall is 1.3 m, the South 1.0 m, the East 0.8 m and the West 2.8 m. Mitigating this, the East and South walls have corrugated profile sheet metal fixed to 50 mm battens. Make-up air is naturally drawn by the fire source and partially directed behind these sheets. This cools these enclosing walls and minimises radiative feed-back to the fire source. For fuller details refer to paragraph A7:3.1 of the CBUF Final Report.

The weighing platform is a slab placed on top of a mass scale. It is used to continuously measure the mass loss of the burning sample. The UC weighing platform consists of a 2.4 m by 1.2 m slab upon a mass scale metered by a Metler-Toledo unit. The slab is 12 mm thick calcium silicate board of density of approximately 850 kg/m^3. It has a 100 mm high edge border to prevent debris from falling from the platform and also to prevent molten foam from falling to the floor. There are 100 mm wide strips of 12 mm thick calcium silicate board placed between the underside of the slab and the mass scale. This is to inhibit over-heating of the scale by direct conduction from the slab. These strips are evenly distributed to avoid eccentric loading of the scale by the slab. Dimensionally, the distance to the lower edge of the hood from the top of the slab is 2380 mm. This is greater than the specified 1750-2000 mm. Between the floor and the top of the slab the distance is 600 mm. This is within the 500 ± 200 mm limits. Refer also to paragraphs A7:2.3 and A7:3.2 of the CBUF Final Report and paragraph 6 of NT FIRE 32.

Dimensionally, the specifications of the smoke collection hood and exhaust system are detailed in great depth and are not repeated here except to say that the UC hood complies. In terms of capacity, the exhaust is required to achieve at least 3.5 m^3/s at normal pressure and at a temperature of 25 C. The UC exhaust exceeds 4.0 m^3/s in these conditions. Refer to paragraph A7:2.4 of the CBUF Final Report, paragraph 7 of NT FIRE 032, and Annex A of NT FIRE 032.

Of importance is the calculation of duct mass flow rate is the velocity profile factor, k_c. The factor's relevance is discussed in the following section. It is determined experimentally by taking readings across the horizontal width of the duct at the sampling point. Unfortunately, vertical readings are not physically possible. The profile is demonstrated in Figure 16.

This profile is far from being the smooth curve expected for quasi-laminar flow. However, the profile was checked at different flow rates and temperatures and found not to differ significantly. Refer also to the Section [4.3.2] 'Determination of the UC Furniture Calorimeter velocity shape factor'.

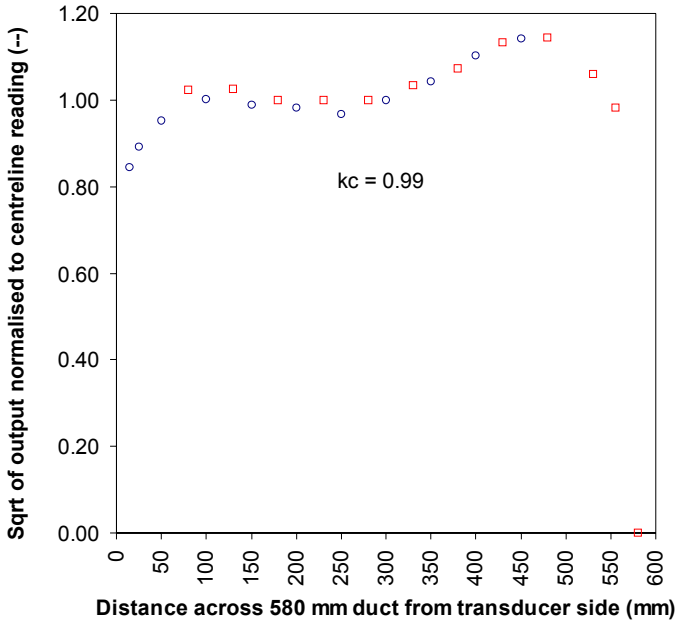

Figure 16: Normalised duct velocity profile at the sampling point across a horizontal plane

The specified ignition source is a square-ring burner developed in the California TB 133[29] furniture test. The specified gas supply is 95% propane at 30 kW. Refer also to paragraph A7:2.5 of the CBUF Final Report.

Instead of Propane, a 50-50 mix of Propane/Butane is used. This is known locally as Liquefied Petroleum Gas (LPG). The ignition burner fuel supply is metered and controlled via a MKS Mass-Flo® controller Type 1559A with a range of 0-100 standard litres per minute of (SLPM) of N_2. The power-supply, readout and set-point controller for the 1559A is a multiple channel MKS Type 247C.

The N_2 equivalent flow rate was calculated as follows. Consider Equation 243.

Equation 243: $$\dot{q} = \dot{m}_{LPG} \cdot \Delta H_c$$

Where,

$\dot{q}$ = heat release rate of ignition burner ≈ 30 kW

$\dot{m}_{LPG}$ = mass flow rate of LPG, to be determined (kg·s^{-1})

Δh_c = net heat of combustion per unit mass of fuel (Tewarson[30] LPG ≈ 45.7 kJ·g)

Rearranging Equation 243 about the mass flow term, substituting in values for heat release rate and net heat of combustion and changing mass flow rate units to g·min^{-1} from g·s^{-1}:

Equation 244: $\dot{m}_{LPG}$ = 39.4 (g·min^{-1})

Convert the mass flow rate in Equation 244 to a molar flow rate based on the molecular weight of LPG (51 g). Assume LPG is an ideal gas and then by applying Avogardo's law, that states at standard temperature and pressure (STP), one mole of an ideal gas occupies a fixed volume, of value 22.14 L. We can calculate the STP volume flow rate of LPG required for a mass flow rate equivalent to 30 kW.

Equation 245: $\dot{V}_{LPG}$ = 17.1 SLPM (LPG)

Where,

$\dot{V}_{LPG}$ = volume flow rate of LPG (SLPM)

Finally, we convert the value in Equation 245 to equivalent of N_2 flow, which is in the units of the mass flow controller. From data from the manual of the MKS 1559 controller, a mass flow conversion factor of 0.31 mat be interpolated from the data for butane and propane. Dividing this into Equation 245:

Equation 246: $\dot{V}_{LPG}$ = 55.2 SLPM (N_2)

The mass flow controller set-point is then fixed at the value in Equation 246 for the ignition burner.

In addition to the instrumentation specified in the standard, a thermocouple tree was located in the fire plume and three heat flux gauges were installed adjacent to the fire plume.

6.3.3 Commissioning calibrations

The following sections consider the compliance of the key components of the UC Furniture Calorimeter with respect to specified accuracy.

The load cell, is required to measure the specimen mass with an accuracy of at least ± 150 g up to at least 90 kg of specimen mass. Refer also to paragraph 6.3 NT FIRE 032.
The UC Furniture Calorimeter weighing platform has an accuracy of ± 50 g and weighing capacity up to 300 kg.

The volume flow rate in the exhaust duct is required to be measured with an accuracy of at least ± 5%. Refer also to paragraph 8.1 NT FIRE 032. Unfortunately, the mass/volume flow rate apparatus is not a proprietary item with accuracy published by the manufacturer, so to approximate the accuracy we have to consider the component accuracy's and make a statement of the overall performance.

Consider Equation 247. This is the equation used for calculating mass flow rate at the sampling point from temperature and pressure measurements.

Equation 247

$$\dot{m}_e = \sqrt{\left(2 \cdot T_{ref}\,\rho_{ref}\right)} \times \left(\frac{\pi \cdot D^2}{4}\right) \times \left(\frac{k_c}{f(\mathrm{Re})}\right) \times \sqrt{\frac{\Delta p}{T_e}}$$

Where,

$\dot{m}_e$ = mass flow rate in the exhaust duct ($kg \cdot s^{-1}$)

T_{ref} = ref. temperature of air, assume 273 (K)

ρ_{ref} = ref. density of air corresponding to reference temperature, assume 1.29 ($kg \cdot m^{-3}$)

D = exhaust duct diameter (m)

k_c = velocity profile shape factor (--)

$f(\mathrm{Re})$ = Reynolds number correction, assume 1.08 if Re > 3800 (--)

Δp = differential pressure across the probe (Pa)

T_e = Exhaust gas temperature at the probe (K)

The sum of the inaccuracies (or the uncertainty) of all variables and constants barring k_c, and Δp, may be assumed at say ± 1% relative uncertainty. This is discussed in detail in CHAPTER 5: 'Propagation of uncertainty of heat release rate measurement'. The most uncertain measurement is that of the differential pressure, Δp. This is measured by the bi-directional probe (McCaffrey and Heskestad[11]). It is reported to have an relative uncertainty of ± 10%. It's contribution to relative uncertainty is therefore half this as it is inside a square root, say ± 5%. We can assume the uncertainty of the shape factor, k_c, is ± 2%. The root-mean-square (RMS) of these three contributions; the differential pressure and the shape factor is 5.5% relative uncertainty. This is the assumed accuracy of the volume flow rate and slightly exceeds the specified accuracy of 5%.

If we consider the test-daily 300 kW calibrations, we will note that they have within 5% agreement between (i) the predicted fuel mass loss calculated from the oxygen consumption which includes the mass-volume flow rate in the exhaust duct, and (ii) the measured fuel mass loss. This generally implies that the mass-volume flow rate apparatus is also accurate within 5% or the HRR calculation and therefore predicted mass loss would be out of the 5% accuracy envelope.

The precision of the overall system is checked by changing the volume flow rate of the extract system in a stepwise manner with for steps from 2.0 m^3/s to 4.0 m^3/s. Refer to paragraph 9.0 NT FIRE 032, 'Calibration' and specifically 9.5 relating to precision. The heat output is held steady at ~250-350 kW. The acceptable drift, in HRR comparing 60 second time averaged values at each step is specified as being not more than 10% of the heat output from the burner.

After the burner output was allowed to stabilised at maximum flow rate, the extract rate is incrementally lowered in four approximately equal increments. The lowering instead of raising is due to the idiosyncrasies of our extract system controller. The resulting drift is 56 kW or 14 % of the heat output. Figure 17 demonstrates this result. The 'result' of this test of precision would be improved on the UC Furniture Calorimeter if the actual flow of LPG were regulated and metered as it may be that the gas flow may have drifted too over the test period.

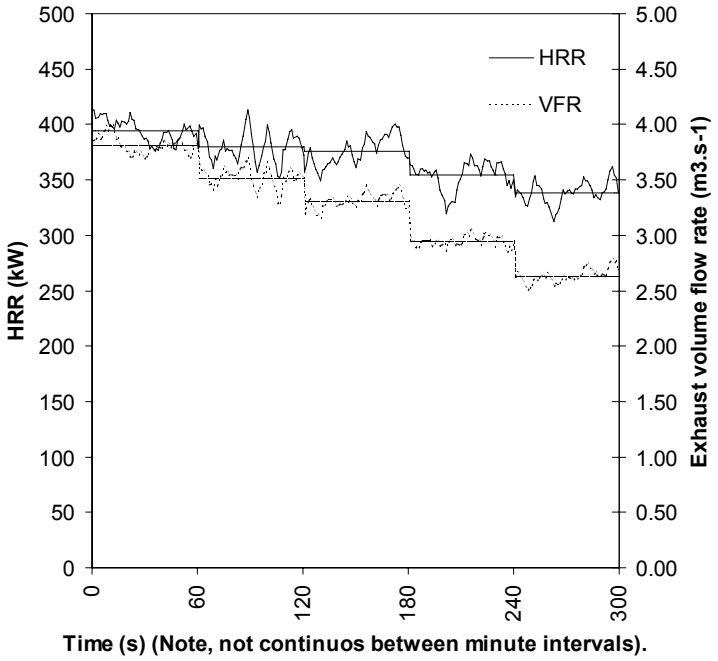

Figure 17: System precision demonstrated by varying the extract rate in a stepwise manner for a relatively constant HRR ~300-350 kW.

6.3.4 Operating calibrations and test procedure

The specimens were conditioned for a minimum two weeks (actually in excess of three months) at 23 ± 2 C and 50 ± 5 % *RH*. All packing material was removed prior to conditioning. Refer also to paragraph A7:5.1 of the CBUF Final Report and paragraph 10 of NT FIRE 032.

Refer to paragraph 10.2.2 'Operating calibrations' of the cone calorimeter ISO standard test method for instructions regarding zeroing and spanning of the oxygen analyser. The CO_2 and CO analysers are zeroed spanned in a similar manner but spanned with special gas mixes representing about 80% of the selected measuring range.

More detailed however than the 5 kW cone calorimeter HRR calibration, is the description of the 300 kW HRR calibration of the furniture calorimeter. Here also, a departure is taken from the standard method outlined in paragraph 9 of NT FIRE 032.

At the beginning of each test day, a calibration is run. The fuel consists of a supply of 50-50 Butane-Propane (LPG) introduced through a burner under the hood, with all instruments

recording. The LPG supply is delivered through permanent pipe-work from a bottle bank in a nearby dangerous goods store. The gas supply flow is controlled via a series of stop valves, needle valve and regulators but is not metered accurately (other than a rotometer that is installed for approximate flow metering). Each calibration is run at approximately 300 kW for 10 minutes.

Following the test, total heat release is calculated from the HRR history using the oxygen consumption principle. From this, the total mass of LPG consumed is calculated by dividing the total heat released by the effective heat of combustion of LPG. This is then compared to the actual mass loss of the LPG supply obtained by weighing the bottles before and after the calibration. If the values of actual mass consumed and predicted mass consumed are within 5% of each other, then the UC Furniture Calorimeter is considered adequately calibrated.

During commissioning of the UC Furniture Calorimeter, many of these calibrations were run with varying duct flow rates, varying fuel delivery flow rate and varying duration of fuel supply.

Paragraph A7:5.2 of the CBUF Final Report and paragraph 11.1 of NT FIRE 032 specify the initial test conditions. Of note here is that NZ-CBUF tests conducted over winter do not fall within the specification of ambient temperature at 20 ± 5 C. Tests are undertaken in temperatures as low as 8 *C*. This is considered acceptable, on the basis that at UC, the moist air state is defined and mole fraction of water vapour in the ambient air calculated for each test rather than assumed. The UC calculation methods therefore specifically allow for ambient moisture variations whereas the standard calculation methods assume within the prescribed temperature range.

The standard recommends the ambient volume flow rate is set to approximately 2.5 m^3/s. However, following commissioning calibrations and experiments with upholstered foam mock-ups, our procedure is to set the flow rate at 4.0 m^3/s.

6.4 Gas Analyser Accuracy

6.4.1 Proprietary gas analysers

The UC Cone and Furniture Calorimeter gas sampling train is shared between the two calorimeters. Therefore, the accuracy of both is considered in this section rather than repeated

in the previous sections characterising each calorimeter. The gas analysing components of the sampling train includes a Servomex 540A paramagnetic oxygen analyser for O_2 and a Siemens ULTRAMAT 6.0 NDIR gas analyser (dual-cell, dual-beam with a flowing reference gas) for CO_2 and CO.

6.4.2 Required accuracy

For the Cone Calorimeter, refer to part-paragraph 6.10 of the ISO standard test method that specifies the required accuracy for the O_2 analyser. *"The analyser shall exhibit a linear response and drift of not more than ± 50 parts per million of oxygen (root mean square value) over a period of 30 min."* Accuracy's for the CO_2 and CO analysers are not specified. It is implicitly assumed that the operating principle inherently leads to more accurate generic analysers.

For the Furniture Calorimeter, refer to part-paragraph 8.2.2 NT FIRE 032. *"The oxygen consumption shall be measured with an accuracy of at least ± 0.01 percent by volume oxygen."* Refer also to part-paragraph 8.2.3 NT FIRE 032. *"The gas species shall be measured with an instrument having an accuracy of at least ± 0.1 percent by volume for carbon dioxide and ± 0.02 percent by volume for carbon monoxide."*

The minimum requirements for the two calorimeters are summarised in Table 3. Where the standards have differing requirements for accuracy, the minimum values govern.

ANALYSER	REQUIRED ACCURACY (PPM)	
	Cone Cal.	Furniture Cal.
Oxygen	50 (short term)	100
Carbon dioxide	unspecified	200
Carbon monoxide	unspecified	1000

Table 3: Gas analyser accuracy required by the test protocols.

6.4.3 Available accuracy

It is reasonable to assume that if the reported accuracy of a proprietary analyser is within the limits specified in the standard, then this satisfies the standard. Unfortunately, while generic NDIR gas analysers (i.e. the CO_2 and CO analysers) comfortably satisfy these limits, this is not the case for generic paramagnetic oxygen analysers. Manufacturers of paramagnetic oxygen analysers typically report an accuracy of ± 0.5-1.0 % of its full scale deflection (FSD).

Across a 0-25% scale, this corresponds to ± 0.125-0.250 %. A magnitude of order greater than the limit of ± 0.01 % required by the standards.

It is generally acknowledged that paramagnetic oxygen analysers will perform better than specified by their manufacturers in the relatively stable environment of a cone or furniture calorimeter. Therefore, the actual accuracy is determined experimentally, under the conditions in which the analyser is normally operated.

The methodology of determining the available accuracy (test of 30 minute noise and drift) follows. It is specified in the draft ISO standard test method for the Cone Calorimeter[27] as a commissioning calibration of the oxygen sampling system. Note the draft standard is only used where it expands upon the current ISO standard test method and never in contradiction to it. The methodology of this commissioning calibration is expanded to include our CO_2 and CO analysers.

The 30 minute noise and drift test is described as follows. Supply the O_2, CO_2 and CO analysers with zero grade N_2. After 60 minutes, in the O_2 analyser, switch to dried ambient air from the exhaust duct with the extract fan running at the normal test rate and with sampling also at the normal flow rate and pressure as during a test. Simultaneously, flow span gas through the CO_2 and CO analyser. The span gas is a special mix of CO_2 and CO in N_2, typically 80% of measuring range selected. Upon reaching equilibrium, adjust the O_2 analyser output to 20.95% ± 0.01% and the CO/CO_2 channels to their respective span concentrations depending on the measuring range chosen. Start recording all analyser outputs at maximum 5 second intervals for a period of 30 minutes. Determine the drift by use of a least squares fitting procedure to fit a straight line through the data points for each respective gas species. The analysis can be undertaken with relative ease on a spreadsheet. For the straight line fitted per species, the absolute value of the difference between the reading at 0 and 30 minutes represents the short-term drift. Determine the noise by computing the root-mean-square deviation around the linear trend line. Record this RMS noise value in terms of ppm by volume concentration for O2, CO_2 and CO. Figure 18 to Figure 21 shows the histories of O_2 concentration using the 0-25% range, O_2 concentration using the zero suppressed 16-21% range with a built-in drift correction, CO_2 concentration and CO.

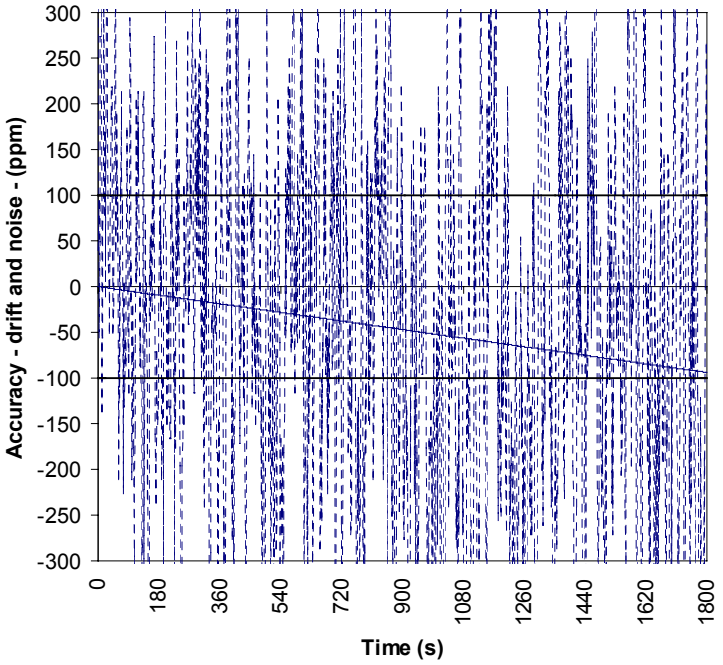

Figure 18: Oxygen analyser noise and drift from the span gas (dry air) over 30 minutes.

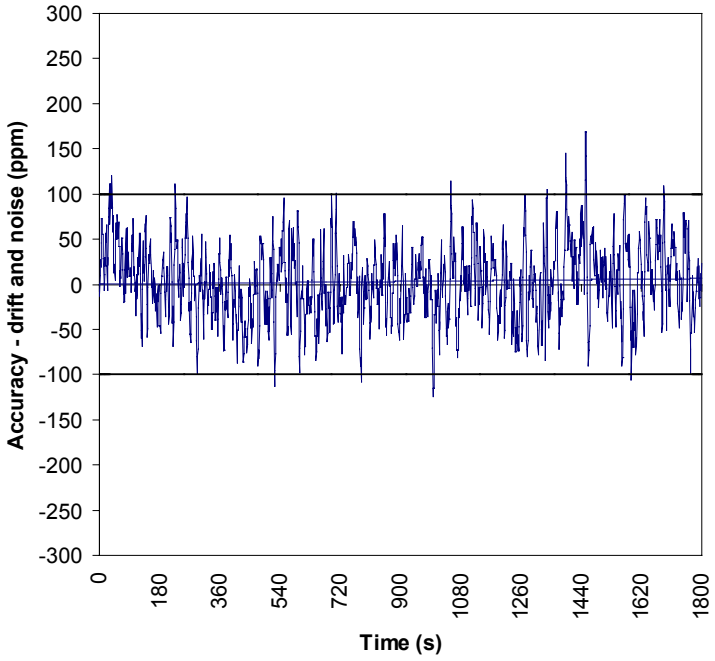

Figure 19: Oxygen analyser noise and drift with zero suppression and drift corrected

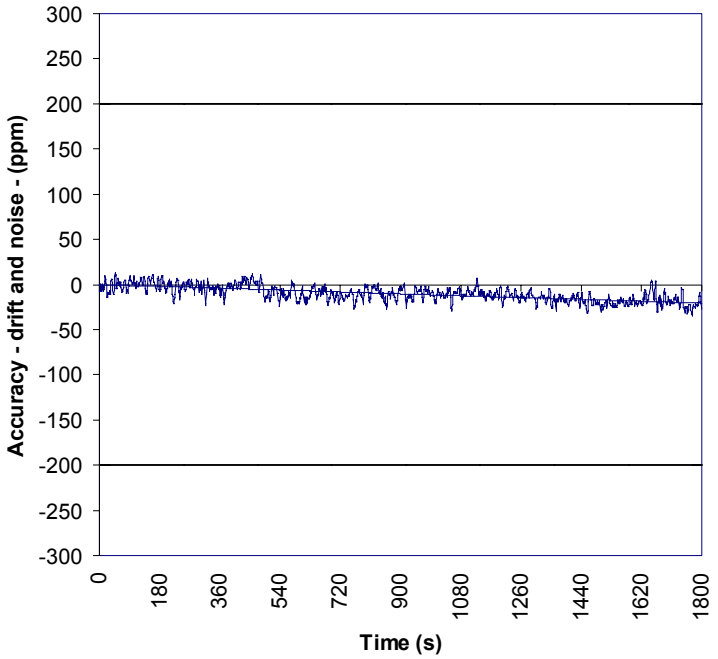

Figure 20: CO_2 analyser noise and drift from the span gas over a 30 min. period.

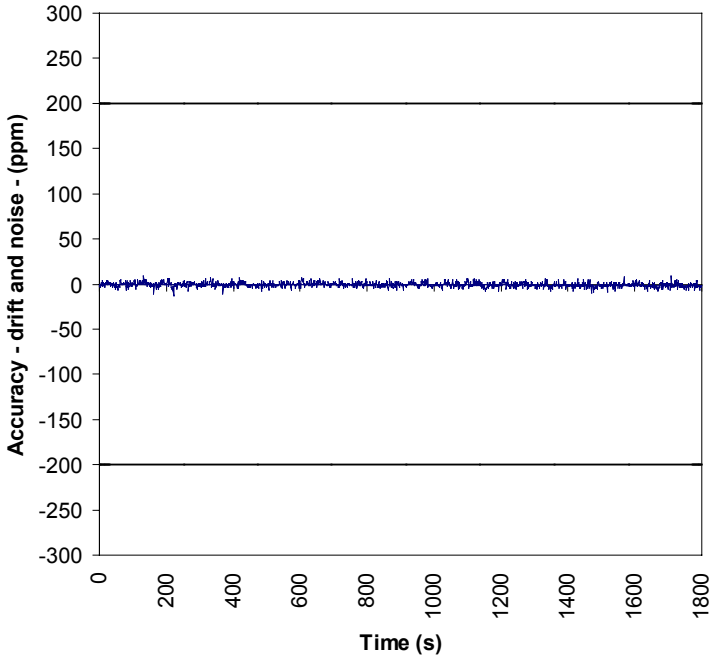

Figure 21: CO analyser noise and drift from the span gas over a 30 min. period.

Table 4 summarises the results of the short-term noise and drift tests. It is observed that measurements taken from the O_2 analyser across the 0-25% range are not accurate enough. This is not surprising given that our data acquisition system operates with a 12 bit card (i.e. 1 bit of data is ≈ 61 ppm across the 0-25% range). Fortunately however, measurements from the zero suppressed range are five times more accurate (i.e. 1 bit of data is ≈ 12 ppm across the

16-21% range).. The CO/CO_2 analyser is within the acceptable accuracy limits without need for modification.

ANALYSER	REQUIRED ACCURACY (PPM)		AVAILABLE ACCURACY (PPM)
	Cone Cal.	Furniture Cal.	
Oxygen 0-25%	50	100	308
Oxygen 16-21%	50	100	48
Carbon dioxide	unspecified	1000	27
Carbon monoxide	unspecified	200	4

Table 4: Gas analyser accuracy required and available

6.5 Time delays and response times

6.5.1 Introduction

The calculated HRR is a function of time-dependant measured values. There are time delays between each property being produced and its value being measured. These time delays are not equal for the different properties of interest such as temperature, pressure and species concentration. Therefore, at any time-step recorded on the data acquisition system the properties recorded correspond to different times in respect to the event and relative to each other. As part of the data reduction these differences must be reconciled prior to calculation by offsetting the measurements against each other. The value of the offset is the time delay t_d for any particular measuring instrument.

The time delay is a function of two different types of lags. We term these the transport time lag and response time lag. The transport time lag occurs due to the time taken for the sample to physically reach the measuring instruments. The response time lag is the time taken for an instrument to read and register the measurement and this response is assumed to behave exponentially. In the case of the cone calorimeter the time delay is a function of the sum of the transport time lag and time to 50% response. In the furniture calorimeter the time delay is the sum of the transport time lag and 'just a trace' of response.

While the full value of the response time is not used in the time delay calculation, there are response limits are specified in ISO 5660.1 and NT FIRE 032. The response of the differential pressure probe is assumed instantaneous. The thermocouples response and the response of the

gas analysers are determined experimentally. The response of the gas analysers depends on the characteristics of the individual analyser as well as the sample train. It is specific to the cone and furniture calorimeter, because the filter, sample line and most importantly the sample pump, vary between the two. The remainder of the train is in common.

6.5.2 Time delays – Cone Calorimeter

Firstly, consider the gas analysers. The methodology for determining the time delays is specified as a commissioning calibration for the O_2 analyser and is described in the ISO standard test method. Refer to paragraph 10.2.1 'Preliminary calibrations'. As with the earlier discussion on accuracy, the standard implicitly assumes the delay times are better for the CO_2 and CO analyser than the O_2 analyser. This is expected because the transport delay times are equal for all species as the sample passes the same conditioning set up, and the response of an NDIR analyser is reported by the manufacturer as faster than a paramagnetic oxygen analyser. Nevertheless, the exercise is repeated for the CO_2 analyser, however not the CO analyser because of negligible CO production in the free-burning cone experiment.

The methodology follows. The cone heater is off for this calibration but the exhaust system is running normally and the gas train sampling. A 5 kW methane source flowing through the calibration burner is ignited outside of the hood and the flame is allowed to stabilise. The burner is then introduced quickly under the hood and held in place for three minutes, after which it is removed and the methane flow terminated. The output is recorded on the data acquisition with a two minute baseline prior to the flame introduction and three minute tail following its removal.

The turn-on delay is the time from the exhaust orifice thermocouple reaching 50% of its normalised full scale deflection to the oxygen analyser reaching 50% of its normalised FSD. The turn-off delay is calculated similarly. The delay time t_d, is calculated as the average of three turn-on and turn-off delays. To comply with paragraph 6.8 'Gas sampling apparatus' of the draft ISO standard test method, the transport time delay determined by the above methodology must not exceed 60 s.

The normalised results of the turn-on and turn-off delays is demonstrated in Figure 22 with the turn-on delay highlighted in Figure 23 and the turn-off delay in Figure 24.

There are time delays of 4 seconds and 1 second for the O_2 and CO_2 analysers respectively. These are introduced in the HRR calculations as a time shift between differential pressure measurement and gas concentrations.

Secondly, consider the differential pressure. The time delay of differential pressure measurement in the cone calorimeter is assumed to be negligible relative to the adjacent temperature measuring thermocouple. No offset of differential pressure data is used.

Thirdly and finally, the time delay of exhaust flow temperature measurement in the cone calorimeter is assumed to be zero as this is the reference instrument.

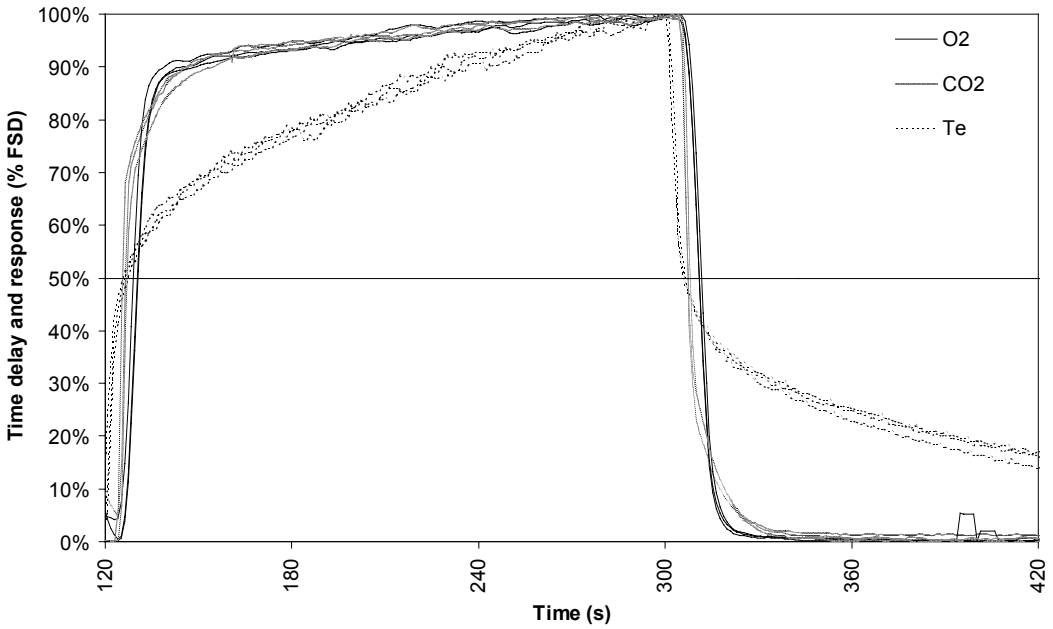

Figure 22: UC Cone Calorimeter - normalised delay and response time to a 5 kW methane fuelled fire.

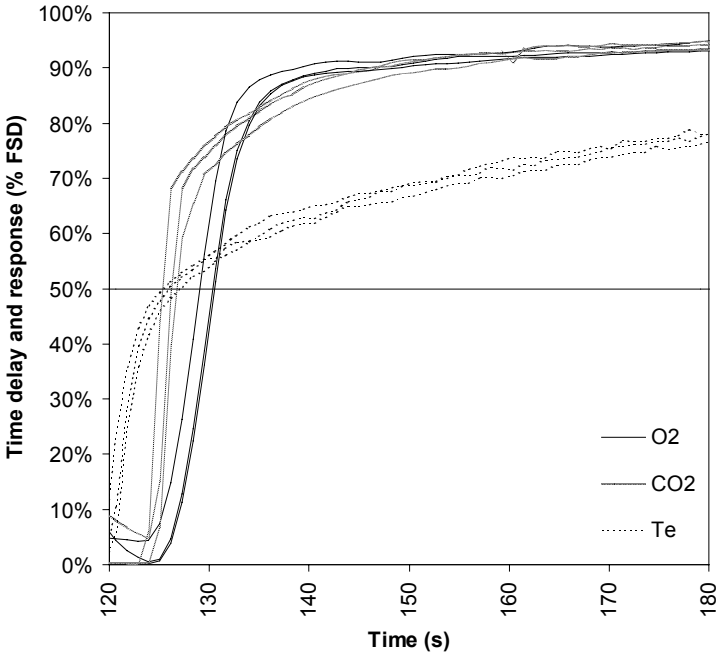

Figure 23: UC Cone turn on delay, expanded extract from Figure 22.

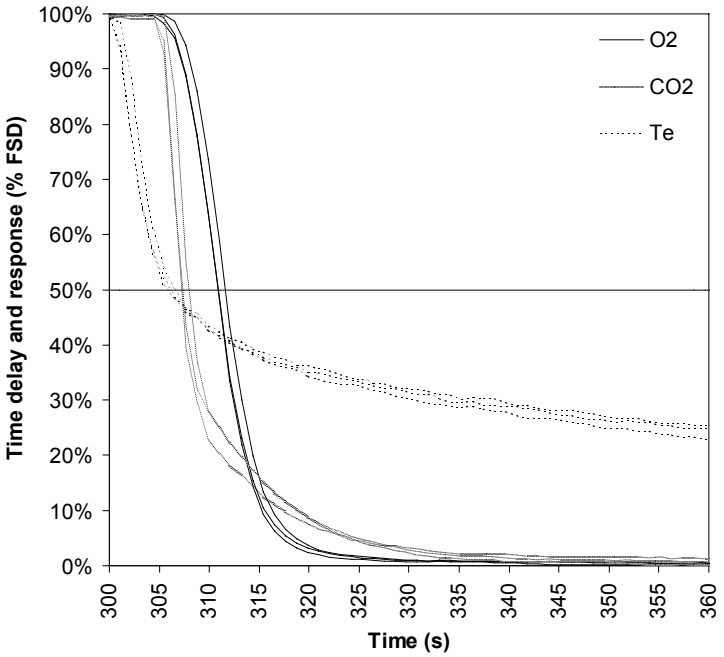

Figure 24: UC Cone turn off delay, expanded extract from Figure 22.

6.5.3 Time delays – Furniture Calorimeter

Firstly, consider the gas analysers. Refer to paragraph 9.0 ‘Calibration’ and specifically section 9.4 of NT Fire 032. The experimentally determined time delay used in data offsets, is

taken as the time from ignition of the 300 kW burner to "…when the instruments start to respond". The specified maximum time delay is 20 seconds.

The methodology follows. It generally follows paragraph 9.0 'Calibration' section 9.4, of NT FIRE 032. It is run similar to the daily 300 kW calibration. The delay times are established by the following test sequence: 0 to 3 minutes of 0 kW, 3 to13 minutes of ~250-300 kW and 13 to 16 minutes of 0 kW. The stepwise changes (i.e. ignition and shut off) are completed within the scan time period of 5 seconds. The time delay is measured from the moment the burner output is changed from 0 to 300 kW to when the analysers start to respond. The maximum acceptable time delay is 20 seconds.

The normalised results of the average of three 300 kW turn on delays is demonstrated in Figure 25. It is observed that the time from ignition to when the instruments begin to respond (i.e. the transport time lag with 'just a trace' of response time) is 6 seconds for both the O_2 and CO_2 analysers. These times satisfy the specified limits of NT FIRE 032. In data offsets the time delay of 6 seconds is introduced in the HRR calculations as a time shift between differential pressure measurement and gas concentrations.

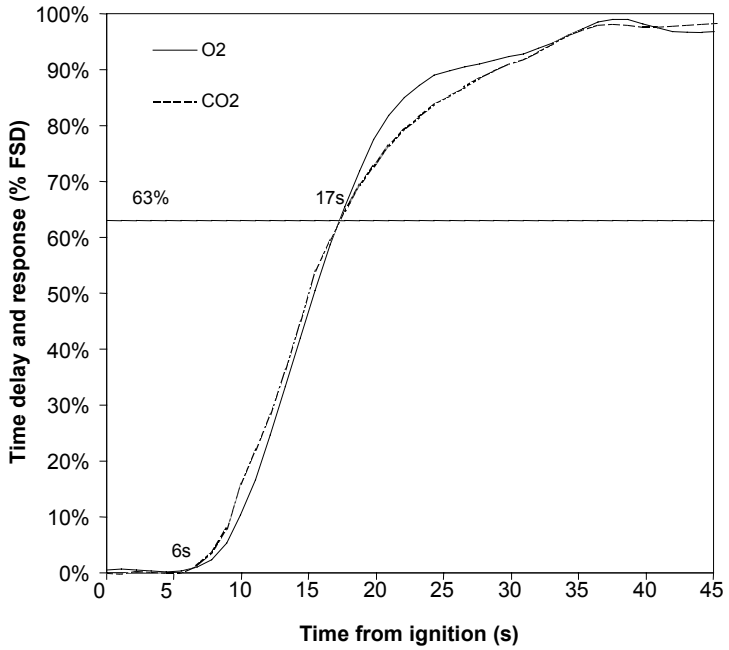

Figure 25: UC Furn. Calor. normalised time delay & response (gas analysers)

Secondly, the time delay of differential pressure measurement in the furniture calorimeter is assumed to be negligible relative to the adjacent temperature measuring thermocouple. No offset of differential pressure data is used.

Thirdly and finally, the time delay of exhaust flow temperature measurement in the furniture calorimeter is assumed to be negligible relative to the adjacent differential pressure measurement. No offset of the temperature data is used. Figure 26 demonstrates that the temperature measuring thermocouple begins to respond almost instantaneously.

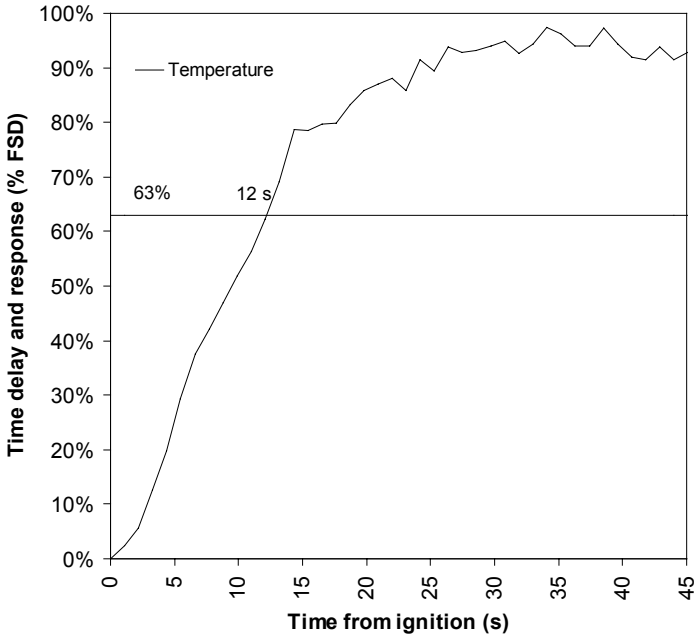

Figure 26: UC Furn. Calor. normalised time delay & response (exhaust temp)

6.5.4 Response times – Cone Calorimeter

Firstly, consider the gas analysers. Refer to paragraph 6.10 ‘Oxygen analyser’ of ISO 5660.1. The value of the 10% to 90% FSD response time is specified as required, less than 12 s.

The results of the response time tests are demonstrated in Figure 22 with the turn-on delay highlighted in Figure 23 and the turn-off delay in Figure 24. Note from the turn-on delay test, Figure 23 there is an inflection point in the oxygen analyser reading at approximately 142 seconds (22 seconds from the introduction of the burner). At this point, about 90% 'ultimate' FSD it can be assumed 100% 'relative' FSD. The resulting 'creep' due to steadily increasing temperatures and therefore flow rates, with compensating steady increases in oxygen

depletion. This phenomena holds only to the turn-on delay and not the turn off. It also indicates the burner is not an ideal test of response. An alternative might be to introduce the zero gas at the sample point within the same expected pressure and flow rate ranges as the sample.

The average of the 'ultimate' 10-90% FSD turn-on delay is 13 s. However, the average of the 'relative' turn-on delay as with the actual turn off delay is 8 seconds. This is the value deemed to be the response time and satisfies the 'less than' 12 second criteria. Note that even if the 'inflection' and 'creep' assumptions are ignored the average response time is satisfactory.

This response time is not used in the data offsets but is nevertheless a check on minimum required system performance. It is curious that the 10-90% response time of less than 12 seconds is greater than the sampling time of 5 s intervals.

Secondly, the response of the bi-directional differential pressure probe and transducer is assumed instantaneous.

Thirdly and finally, the response of the thermocouple adjacent to the differential pressure measurement in the cone calorimeter is implicitly allowed for in the earlier test for delay time and response time of the oxygen analyser.

6.5.5 Response times – Furniture Calorimeter

Firstly, consider the gas analysers. Refer to paragraph 8.2.2 ‘Oxygen analyser’ and 8.2.3 ‘Carbon monoxide and carbon dioxide analyser’ of NT FIRE 032. “The gas sample shall be taken from the end of the sampling line from where the time delay including the time constant of the instrument shall be a maximum 20 seconds.” This should not be confused with the determination of the time delay which is from ignition to when the analyser begins to respond.

The time constant is defined (Verdin[31]) as 63% full-scale response. From Figure 25 the 63% response from ignition is 17 seconds. Therefore, the response from the “…end of the sample line…” is necessarily something less than or equal to 17 seconds and therefore less than the 20 second specified maximum limit.

Secondly, the response of the bi-directional probe and transducer is assumed instantaneous.

Thirdly and finally, Figure 26 demonstrates that the 63% response of the temperature measuring thermocouple is 12 seconds. Significantly, this is almost the same response of the gas analysers less their transport time lags. Therefore, the response of the temperature measurement is comparable to the time shifted gas species measurements.

6.5.6 Effect of volume changes in sampling system

It was observed while experimenting and commissioning with different gas sampling configurations, that the transport and response time lags but especially the response time lag, are adversely affected by changes in volume of the sampling system going from smaller to bigger volumes. In both the UC Calorimeters volume changes occur at the filter, cold-trap, cold-trap separation chamber and desiccant chambers. The time lags increase due to mixing of concentrations in each of these volume spaces. To mitigate against this, the increased volumes have been limited as much as possible in the UC Calorimeters. Experimentally, this is found to improve the response by several seconds for each of the separation and desiccant chambers.

6.5.7 Conditioning data for improved response times

If the response time exceeds the limits specified in ISO 5660.1 or NT FIRE 032, then the data may be conditioned for a faster response. Fortunately, this is not necessary with the UC Cone and Furniture Calorimeters which each exhibit satisfactory response. However, this response may be adversely effected by the introduction of future conditioning units incorporating volume changes or the future introduction of slower instrumentation. Therefore, the methodology of this conditioning is introduced as a reference for future users of the apparatuses. The methodology is described in detail in Croce[32].

A simple experiment is conducted by introducing a step input (plug flow) into the sampling system to which the analysers will respond. Either zero grade N_2 introduced at the sampling point or preferably the 5 kW and 300 kW burners. Assuming the analyser is a linear system the exponential output (analyser response) to the step input (plug flow) is fitted by an exponential function. The linear differential equation describing the response function is determined from back analysis. The function is forced by a constant term to improve response. However, care must be taken to ensure that conditioned data is reconciled with the oxygen analyser required accuracy of ± 50 ppm. Because improving the response via forcing the differential equation also amplifies the noise.

6.5.8 Data reduction summary – Cone Calorimeter

All measuring instruments respond within the time limits specified. However, the following offsets apply to allow for transport time lags.

- The differential pressure probe is assumed to begin to respond at nominal time zero
- The exhaust duct thermocouple is assumed to also respond at time zero and the data is not time shifted
- The O_2 analyser data is time shifted forward with respect to the differential pressure data by 4 seconds
- The CO_2 analyser data is time shifted forward with respect to the differential pressure data by 1 second

6.5.9 Data reduction summary – Furniture Calorimeter

All measuring instruments respond within the time limits specified. The following offsets apply to allow for transport time lags.

- The differential pressure probe is assumed to begin to respond at nominal time zero
- The exhaust duct thermocouple is assumed to also respond at time zero and the data is not time shifted
- The O_2 analyser data is time shifted forward with respect to the differential pressure data by 6 seconds
- The CO_2 analyser data is time shifted forward with respect to the differential pressure data by 6 seconds

6.5.10 Conclusions of time delays and response times

The preceding sections of 6.5 ‘Time delays and response times’ characterise the time delays and response times of the UC Cone and Furniture Calorimeters. They demonstrate the calorimeters comply with the respective Standards and Protocols. Conditioning of the data – other than applying the time delay offsets – is not necessary. However, following future reconfiguring, should any of the instrument response times have exceeded their allowable maximum, the improvements described in 6.5.7 ‘Conditioning data for improved response times’ may be adopted, with the caveat that analyser noise may be amplified.

CHAPTER 7: CBUF MODEL I AND II APPLIED TO EXEMPLARY NZ FURNITURE (NZ-CBUF)

7.1 Introduction

Loss of life in domestic and residential type buildings continue to dominate New Zealand's (NZ) annual fire death statistics. Few items within these buildings have the potential to bring about untenable conditions as swiftly as upholstered furniture. Therefore, it is a major goal of safety research to better assess the hazard of furniture fires. Especially, in respect to the ability to predict the hazard.

Full-scale fire testing of furniture as a hazard predictor is much more costly and unwieldy than bench-scale. One of the objectives of modern reaction to fire research is to improve bench-scale based predictive models of full-scale behaviour.

The first notable predictive model based on the cone calorimeter (the pre-eminent bench scale HRR tool) was developed at the National Institute of Standards and Technology (NIST) formerly named the National Bureau of Standards, in 1985[33]. This model is based on materials and furniture items originating mostly from the 1970s. Since that time, the materials and predictive techniques have changed significantly.

Recent developments were made in the extensive European Commission sponsored study Combustion Behaviour of Upholstered Furniture (CBUF). From this study, three predictive combustion behaviour models are developed and presented in the CBUF Final Report[26].

Model I of CBUF is a factor based model which uses statistical curve fitting on key variables from the cone calorimeter results along with style factors which accounts for differences in the physical shape of the item.

Model II of the CBUF is based on an area convolution technique with expressions of burning area over time determined for furniture types. The expressions empirically include complex flame spread phenomena such as underside burning and pool burning of molten foam. These are phenomena typically not incorporated in a physics-based model. An effective burning area is determined from a number of tests of a chair type and then the Furniture Calorimeter HRR

history is determined using a convolution integral of the Cone Calorimeter HRR history and the burning area curve.

Model III is based on extensions to thermal fire spread theory. It is a physics-based approach and generally follows a thermal fire spread model developed for wall linings and adapted for furniture. The CBUF study applied this model to mattresses. Model III is not considered in this NZ study.

To assess the applicability of the CBUF Model I and Model II to NZ furniture, eight single seat chairs and five two-seat sofa's have been tested in both the cone and furniture calorimeters. Comparisons are made with the CBUF results to determine the fire hazard of NZ furniture relative to its European counterpart. This study is titled NZ-CBUF.

7.2 Experimental procedure and apparatus

The experimental portion of NZ-CBUF involves fire tests on the cone and furniture calorimeters.

The University of Canterbury (UC) Cone Calorimeter complies with the standard[6] as amended by Appendix A6 of the CBUF Final Report[26] "Cone Calorimeter testing". The test protocol, specimen preparation, special testing instructions and reporting are all performed according to the strict specification of the CBUF Protocol.

Similarly, the UC Furniture Calorimeter complies with the standard[7] as amended by Appendix A7 of the CBUF Final Report[26] "Furniture Calorimeter test protocol". Again, the test protocol, specimen preparation, special testing instructions and reporting are all followed as per the Appendix A7.

For complete documentation of the characterisation of the UC Cone and Furniture Calorimeters, refer to CHAPTER 6 'Instrumentation'.

7.3 Furniture items

The terminology "item" or "sample" are used synonymously throughout this chapter to refer to the full-scale generic piece of furniture that the predictions are made. The term "foam" refers to the padding material that in this study was polyurethane manufactured in New

Zealand. The covering material referred to as "fabric" are primarily made from synthetic materials. The items tested in NZ-CBUF consist of eight exemplary chairs and five two-seat sofa's purchased on the open market. They are representative of typical NZ domestic furniture in the low to mid level price range. These are described generally in Table 5. The first five items are of the same manufacture, with only the fabric varying.

	FOAM (MAIN FILLING)		FABRIC (COVER)		INTER-LINER (WRAP)		SEAT
ITEM	CODE	DESCRIPTION	CODE	DESCRIPTION		DESCRIPTION	No.
1	A	Polyether foam pad	1	Polyester and blended fabrics	No	N/A	1
2	A	Polyether foam pad	2	Polyester and blended fabrics	No	N/A	1
3	A	Polyether foam pad	3	Polyester and blended fabrics	No	N/A	1
4	A	Polyether foam pad	4	Nylon pile with polyester backing	No	N/A	1
5	A	Polyether foam pad	5	Polypropylene fibre	No	N/A	1
6	B	Generic PU foam	6	Nylon pile 65/35 polyester-cotton back	No	N/A	1
7	C	Generic PU foam	7	Nylon pile	Yes	Fibre (not specifically FR)	1
8	D	Generic PU foam	8	Polypropylene fibre	Yes	Fibre (not specifically FR)	1
9	A	Polyether foam pad	1	Polyester and blended fabrics	No	N/A	2
10	A	Polyether foam pad	2	Polyester and blended fabrics	No	N/A	2
11	B	Generic PU foam	6	Nylon pile, 65/35 polyester-cotton back	No	N/A	2
12	C	Generic PU foam	7	Nylon pile	Yes	Fibre (not specifically FR)	2
13	D	Generic PU foam	8	Polypropylene fibre	Yes	Fibre (not specifically FR)	2

Table 5: Coding of NZ-CBUF items

Table 5 gives material components for the items investigated in this study. Column 1 is the item number used throughout this chapter. The size, foam, fabric, and inter-liner are given in columns 2 through to 5 respectively. Additional samples of items 1, 6, 7 and 8 were purchased and disassembled to determine the mass of each component and to obtain foam and fabric for the composite samples required for cone calorimeter tests. Additional fabric for items 2-5 was purchased and composite samples prepared using the extra foam from the disassembled item 1.

Figure 27a: (i) LEFT. Item 9 (A2S1), this is also representative of item 1 (A1S1) through to item 5 (A5S1) and item 10 (A2S2), **(ii)** RIGHT. Item 6 (B6S1), this is also representative of item 11 (B6S2).

Figure 27b: (iii) LEFT. Item 7, (C7S1), this is also representative of item 12 (C7S2). **(iv)** RIGHT. Item 8 (D8S1), this is also representative of item 13 (D8S2).

Figure 27 shows items representative of the tested specimens, that were disassembled for mass data and cone calorimeter samples. Item 1 (also 9) (A1S2) is also the two-seat version of specimen A1S1 and is representative also of items 2 to 5 (A2S1-A5S1), with only the fabric varying. The mass of the soft materials and combustibles for item 1 (A1S1) is interpolated from the disassembled item 9 (A1S2). Based on the ratio of fabric densities of items 2-5 and 10, (A2S1-A5S1 and A2S2) the full-scale mass data for these specimens is interpolated and extrapolated. The mass data for items 11,12 and 13 (B6S2, C7S2 and D8S2) is extrapolated from the disassembled items 6, 7 and 8 (B6S1, C7S1 and D8S1).

7.4 Experimental results (HRR histories)

The full cone and furniture calorimeter test reports are not included. The primary property of interest (the HRR) for the varies samples and items are detailed below. More complete details of the full-scale fire tests are included in APPENDIX A: 'Full-scale Test Data'.

7.4.1 Cone calorimeter HRR histories

Within the Final Report[26] there is a sub-model for 'thickness scaling' of the cone calorimeter results. The author of the modelling chapter – Dr V. Babrauskas – was contacted to question whether the thickness scaling subroutine was adopted in Model I predictions. It is his recollection and advice that is not the case. Therefore, the following results are presented without thickness scaling demonstrated. However, the effect of thickness scaling is calculated and examined in the discussion of results.

The following HRR histories are exemplary of the three or more composite samples tested for each specimen.

Uncertainty bounds of the HRR calculation as per CHAPTER 5: 'Propagation of Uncertainty of Heat Release Rate Measurement' are included. These bounds include random uncertainties associated with the instruments and systematic uncertainties associated with the calculation assumptions but exclude random uncertainties associated with the sample (including its preparation) or systematic uncertainties associated with the operator.

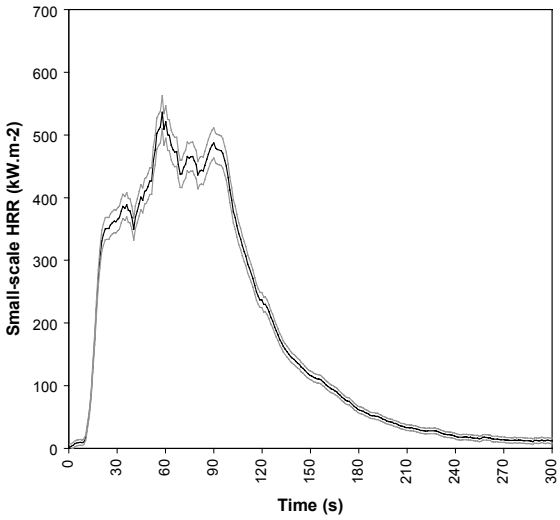

Figure 28: HRR history, sample A1

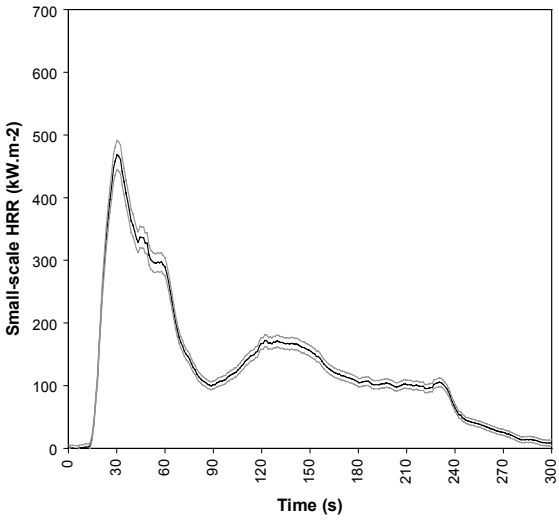

Figure 29: HRR history, sample A2

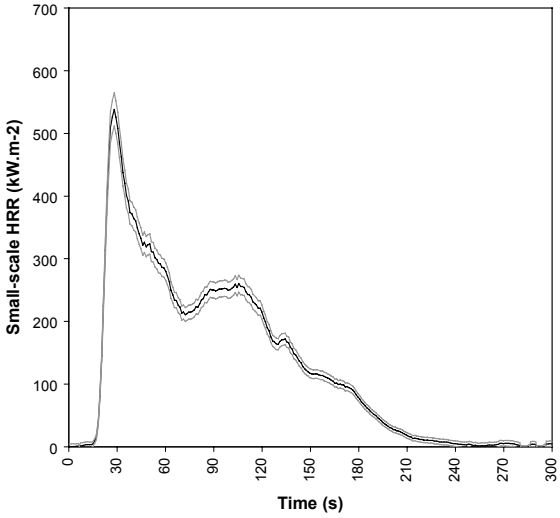

Figure 30: HRR history, sample A3

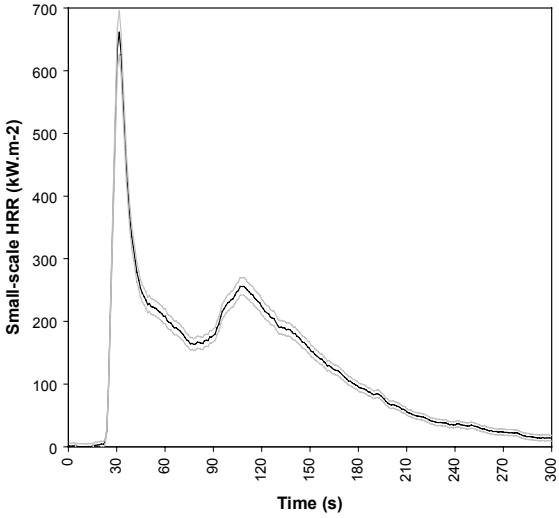

Figure 31: HRR history, sample A4

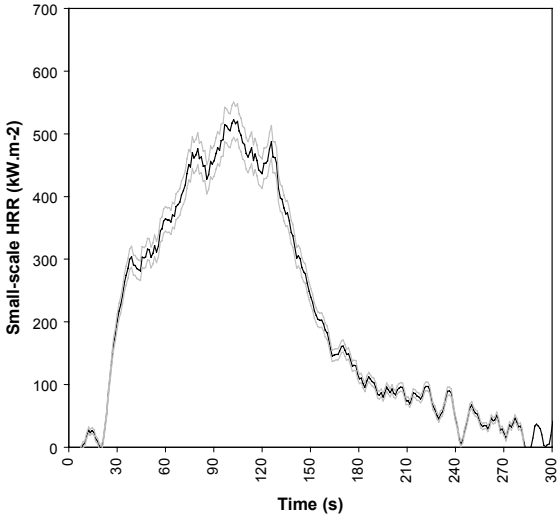

Figure 32: HRR history, sample A5

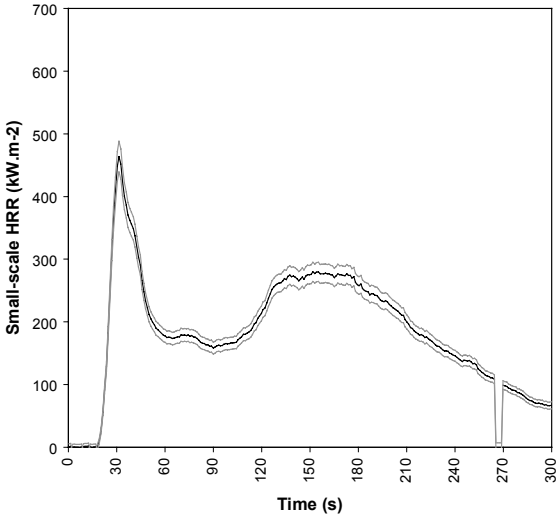

Figure 33: HRR history, sample B6

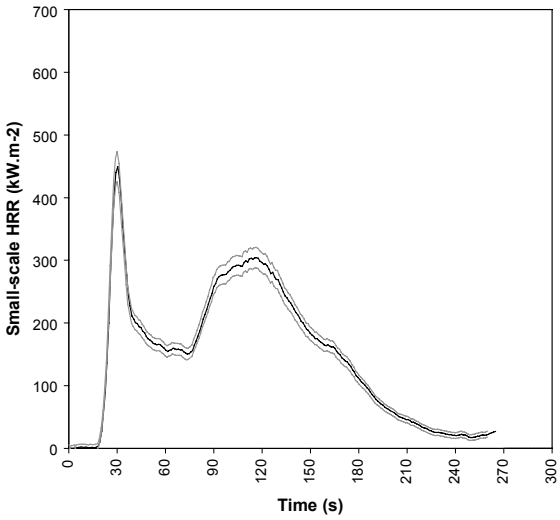

Figure 34: HRR history, sample C7

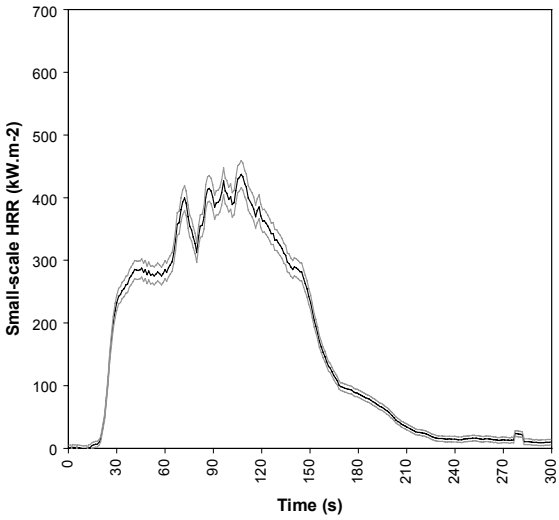

Figure 35: HRR history, sample D8

7.4.2 Furniture calorimeter HRR histories

The following HRR histories are of the full-scale specimen. Uncertainty bounds of the HRR are included and are calculated as per CHAPTER 5: 'Propagation of uncertainty of heat release rate measurement'. These bounds include random uncertainties associated with the instruments and systematic uncertainties associated with the significant calculation assumptions but exclude random uncertainties associated with the specimen or systematic uncertainties associated with the operator.

The following histories are based on a 5 s running average. A 30 s running average is used in the data analysis. Note for item A2S2 and B6S2 the water sprinkler deluge head was activated for short bursts at 180 s from ignition as the test was exceeding the operating range. Although this data is quantitatively invalid it is included for qualitative comparisons.

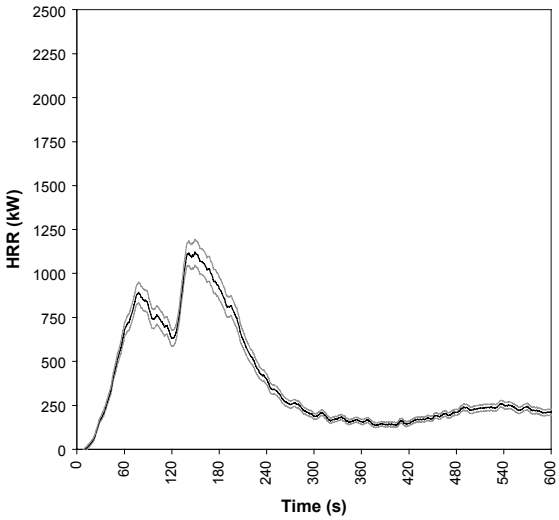

Figure 36: HRR history of item A1S1

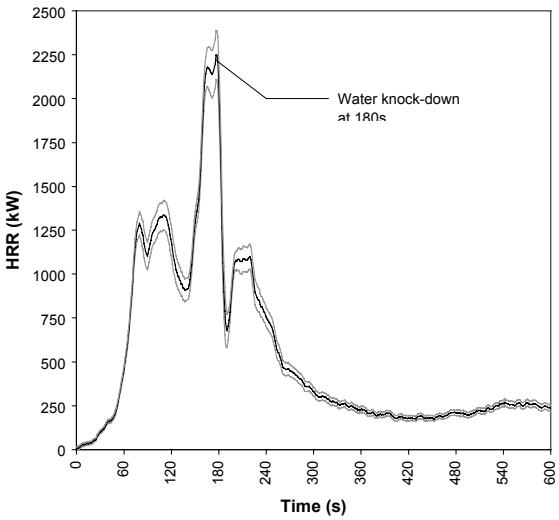

Figure 37: HRR history of item A1S2

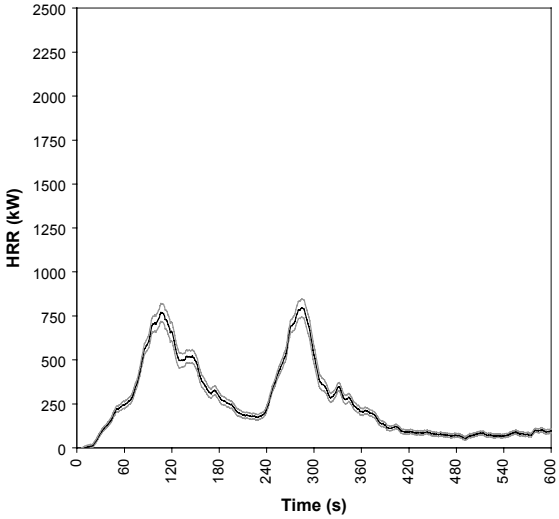

Figure 38: HRR history of item A2S1

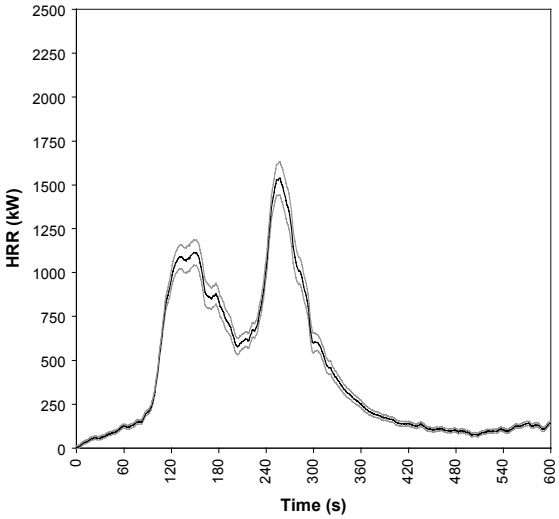

Figure 39: HRR history of item A2S2

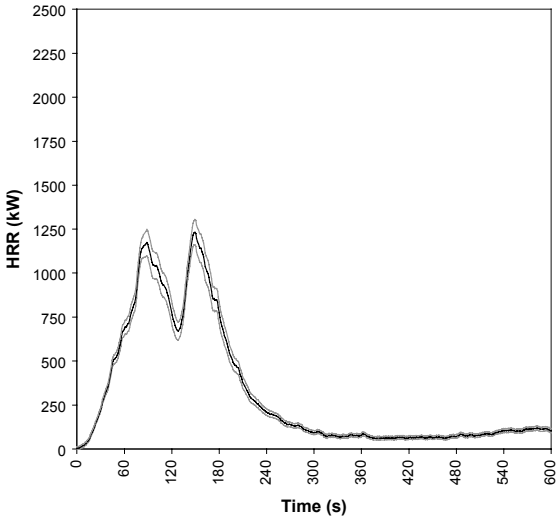

Figure 40: HRR history of item A3S1

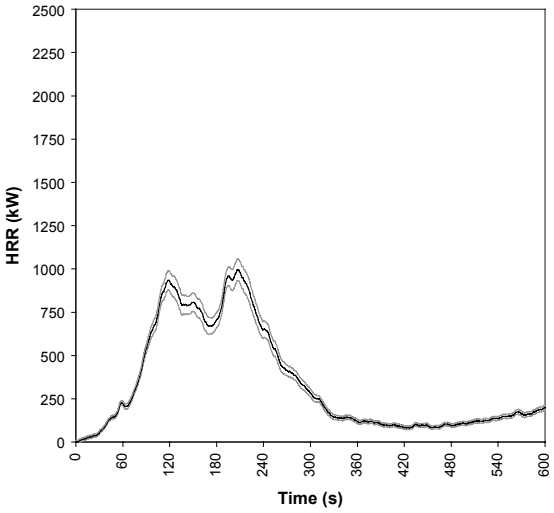

Figure 41: HRR history of item A4S1

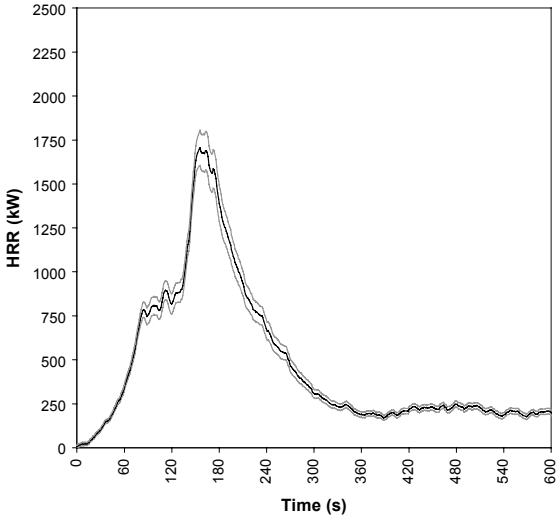

Figure 42: HRR history of item A5S1

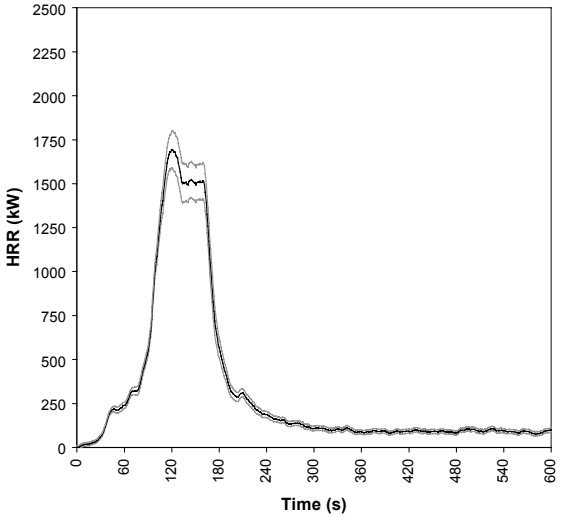

Figure 43: HRR history of item B6S1

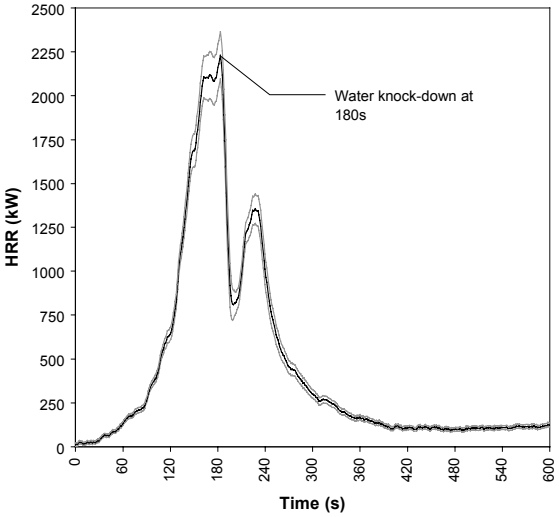

Figure 44: HRR history of item B6S2

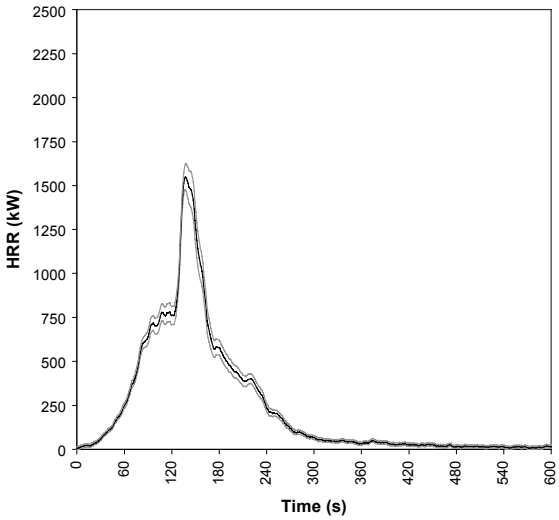

Figure 45: HRR history of item C7S1

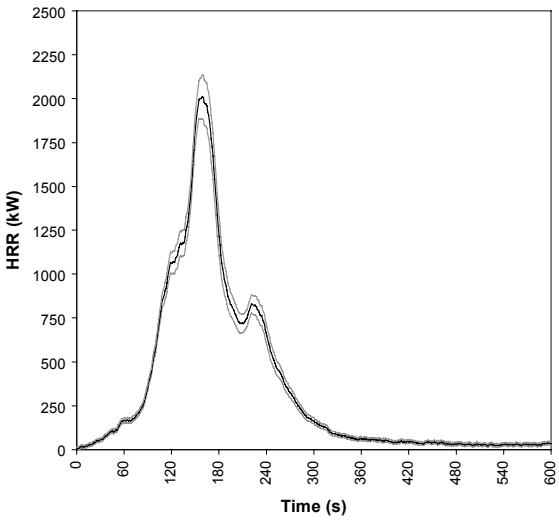

Figure 46: HRR history of item C7S2

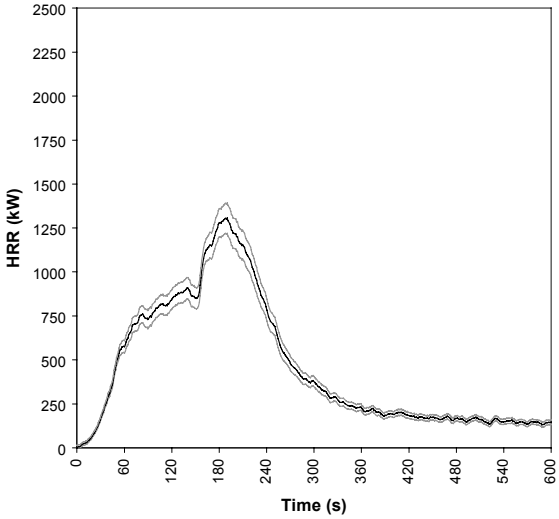

Figure 47: HRR history of item D8S1

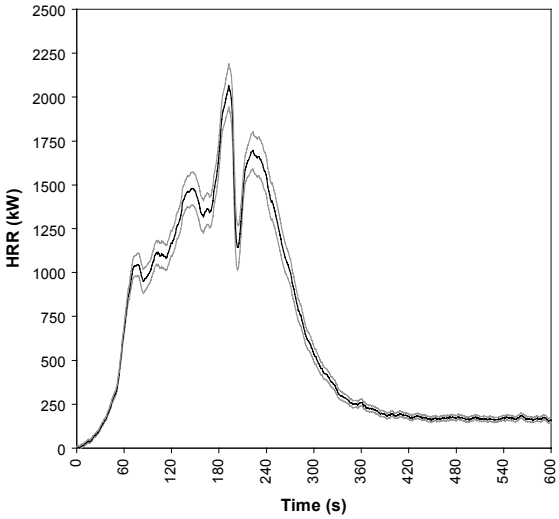

Figure 48: HRR history of item D8S2

7.4.3 Discussion of results of Cone and Furniture Calorimeter test results

This discussion of results is of a general nature independent of whether Model I or Model II is adopted and is therefore included separately.

A pronounced fabric affect is demonstrated in samples A1 to A5 and items A1S1 to A5S1. The following two Figures show the HRR time history from the cone (5 minutes) and furniture calorimeter (10 minutes) for the single armchair series (items 1-5). The time to peak and magnitude of the peak HRR vary considerably. Note that the time scale begins at 0s in the cone and 180 s in the furniture calorimeters. This is because the Cone Calorimeter data has

been corrected for the two minute baseline while the Furniture Calorimeter has not - for its three minute baseline.

During the cone calorimeter tests, the fabric showed a trend to either (i) melt and peel, or (ii) split and remain in place – that is become char forming. The first phenomena is characterised by curves 1 and 5. Here there is typically a large single peak with both fabric and foam contributing to the energy in a similar manner. The second phenomena, characterised by curves 2, 3 and 4 is more complex. Here a single sharp first peak is observed followed by a lower slower 'foam' peak. The first peak is believed to occur once the foam block has melted below the charring fabric. The additional flux previously used in thermal decomposition is then available to assist. The charring fabrics are believed to be due to cotton backing.

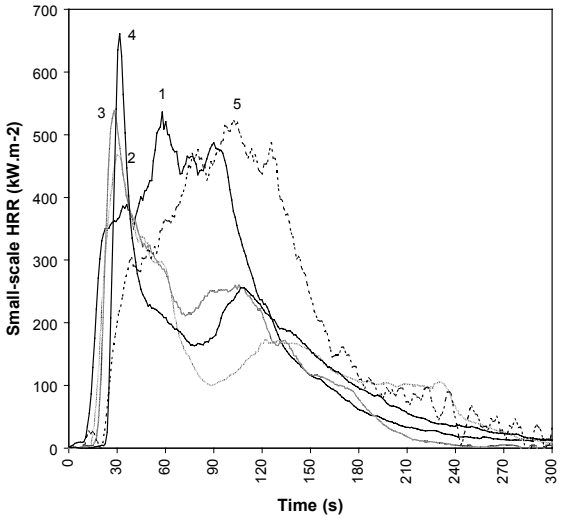

Figure 49: Fabric effects, 1 to 5 (Cone)

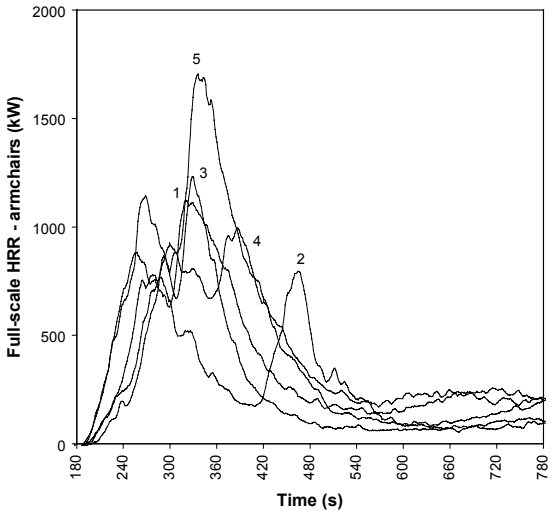

Figure 50: Fabric effects, 1 to 5 (Furn.)

Table 6 compares the results of NZ-CBUF directly with the available CBUF results for the peak heat release rate and total heat release. For this exercise, 'comparative' CBUF furniture items (armchairs) were selected from the photographic record appended to the Final Report[26].

Relative to CBUF items overall, the NZ-CBUF armchairs exhibited significantly higher peak HRR for relatively similar total heat. However, exemplary NZ items do not include combustion modified or high resilience foams or fire resistant fabrics or interliners. In comparison to equivalently composed European items, the peak HRR results were more

comparable, although still generally higher. Unfortunately, data for time to peak HRR for the CBUF items were not reported.

Table 6 indicates exemplary NZ furniture (single armchairs) presents a higher fire hazard than its European counterparts. This is seen in the relatively poor fit of the model to measurements, as the NZ samples are considered 'extreme'. In addition, the exemplary NZ furniture fire will grow to a high peak HRR in a short period of time.

NZ-CBUF				CBUF		
ITEM #	$\dot{Q}_{pk}$ (kW)	Q (MJ)	t_{pk} (s)	Code	$\dot{Q}_{pk}$ (kW)	Q (MJ)
1	1123	378	122	1.04	784	368
2	795	244	261	1.05	742	463
3	1233	299	132	1.06	1158	412
4	995	333	175	1.07	596	314
5	1705	387	131	1.08	1490	498
6	1693	262	92	1.09	552	144
7	1550	150	104	1.10	866	449
8	1306	363	169	1.11	1259	375
				1.12	652	172
$\bar{x}$	**1300**	**302**	**148**	$\bar{x}$	**900**	**355**

Table 6: NZ-CBUF (measured) peak HRR, time to peak HRR and total heat, compared against the CBUF data, for comparatively similar single armchairs

7.5 CBUF Model I

7.5.1 Introduction

The CBUF research programme developed a factor-based model – CBUF Model I – for predicting full scale results for the peak heat release rate, time to peak, total heat release and time to untenable conditions.

The applicability of the CBUF Model I to exemplary New Zealand (NZ) furniture items is examined. Model I, predictions of the full-scale furniture behaviour were made. Comparisons between the full-scale furniture results and the model predictions show that NZ furniture consistently exhibits higher peak heat release rates for similar total heat. Based on these comparisons it is clear that exemplary NZ furniture presents a significantly greater fire hazard than its European counterparts by reaching this higher peak heat release rate in shorter periods

of time. Further research is required to determine what modifications are necessary before this model can be applied to NZ furniture.

7.5.2 Propagation of uncertainty through Model I

An analysis of the propagation of uncertainty in Model I via the method described in CHAPTER 5: 'Propagation of Uncertainty of Heat Release Rate Measurement' is not undertaken. This is on the basis that there are extremely significant systematic uncertainties associated with the highly empirical correlation's – such as the various regression analyses – in Model I. It is suspected that systematic uncertainties will greatly exceed the significance of instrument based random uncertainties. Therefore, any analysis of propagation of the correlation's becomes an insignificant exercise.

7.5.3 CBUF model I predictions

CBUF Model I - described in detail in the Final Report[26] and by Babrauskas et al[34] - is a factor-based method that uses a series of statistically correlated factors to predict the peak HRR, total heat release, time to peak, and time to untenability. The model is an improvement on the earlier (1985) factor-based prediction from NIST. The original model was examined for applicability to the CBUF items. It was found to apply only generally and displayed tendencies to under-predict the more modern and varied European furniture. The study undertook further development and refinement of this model. They tested a series of differing furniture styles constructed from the same 'soft' combustible material combinations (soft being the foam, fabric, and inter-liner). An analysis of the results brought about several refinements from the 1985 NIST model to the CBUF Model I. Notably, the mass of soft combustibles replaced the mass of total combustibles, and the power was raised from 1 to 1.25. The time to ignition in the cone calorimeter test was seen as an important variable and included.

The style factor also required significant change to account for the new European furniture. Incorporated in the calculation of the peak heat release rate, time to peak, and untenability time, the style factor accounts for the physical differences that cannot be resolved by the cone calorimeter test method including the ornate and intricate detail that can be found in some furniture. As seen in Figure 27, items 6 and 7 are obviously more ornate than the rectilinear shape seen in items 1 and 8.

CBUF	STYLE FACTOR A	STYLE FACTOR B	TYPE OF FURNITURE
1	1.0	1.0	Armchair, fully upholstered, average amount of padding
2	1.0	0.8	Sofa, two-seat
3	0.8	0.9	Sofa, three-seat
4	0.9	0.9	Armchair, fully upholstered, high amount of padding

Table 7: Furniture styles used in the CBUF and NZ-CBUF programmes

Table 7 provides the style factors needed in the predictive model. It is reproduced in part from a more comprehensive table appearing in References [26] and [34]. Note that that the NZ-CBUF items testes in this series are single seat armchairs and two-seat sofa's with average to high amounts of padding. Code 3 is included in the table for completeness.

Incorporating these new and old variables, Equation 248 emerged as the first correlating variable for the peak heat release rate. It was found that the partially correlating variable x_1 represented well the general trend with the exception of groupings of high peak HRR (over 1200 kW). Considering only these data points, the second correlating variable x_2 emerged in Equation 249.

Equation 248 $$x_1 = \left(m_{soft}\right)^{1.25} \cdot \left(style\_fac.A\right) \cdot \left(\dot{q}''_{pk} + \dot{q}''_{300}\right)^{0.7} \left(15 + t_{ig}\right)^{-0.7}$$

Equation 249 $$x_2 = 880 + 500 \cdot \left(m_{soft}\right)^{0.7} \left(style\_fac.A\right) \cdot \left(\frac{\Delta h_{c,eff}}{q''}\right)^{1.4}$$

Selection rules are established, that we have termed 'regimes', to determine when to use x_1 and x_2, with x_1 displaying a partial dependence.

Regimes:

{1} If, $\left(x_1 > 115\right)$ or $\left(q'' > 70 \text{ and } x_1 > 40\right)$ or $\left(\text{style} = \{3,4\} \text{ and } x_1 > 70\right)$ then, $\dot{Q}_{peak} = x_2$

{2} If, $x_1 < 56$ then, $\dot{Q}_{peak} = 14.4 \cdot x_1$

{3} Otherwise, $\dot{Q}_{peak} = 600 + 3.77 \cdot x_1$

The total heat release (not surprisingly) is determined from the actual mass of the furniture item and small-scale effective heat of combustion. Differentiation is noted between the 'soft' and total combustible masses. Experimental observation reveals that the affect of a wooden frame is not seen until nearly all of the 'soft' materials are consumed. Equation 250 was found to represent the total heat release:

Equation 250 $$Q = 0.9 m_{soft} \cdot \Delta h_{c,eff} + 2.1 \left(m_{comb,total} - m_{soft} \right)^{1.5}$$

The time to peak is as important as the peak heat release rate in hazard calculations. Equation 251 is developed to predict time to peak HRR from sustained burning (50 kW). It is recognised that often other hazard variables are maximised at or near the time of peak HRR. Note that a different style factor is incorporated into the time to peak calculation.

Equation 251 $$t_{pk} = 30 + 4900 \cdot (style\_fac.B) \cdot (m_{soft})^{0.3} \cdot (\dot{q}''_{pk\#2})^{-0.5} \cdot (\dot{q}''_{trough})^{-0.5} \cdot (t_{pk\#1} + 200)^{0.2}$$

Equation 252 is developed to predict time to untenable conditions in a standard room. Untenability time is defined as the time from 50 kW HRR to 100 C temperature 1.1 to 1.2 m above floor level. Although results for the time to untenable conditions are presented here for comparison with the CBUF results, compartment fire experiments were not part of this research program.

Equation 252 $$t_{UT} = 1.5 \times 10^5 (style\_fac.B)(m_{soft})^{-0.6} (\dot{q}''_{trough})^{-0.8} (\dot{q}''_{pk\#2})^{-0.5} (t_{pk\#1} - 10)^{0.15}$$

7.5.4 Results of Model I

Table 8 summarises the results of the cone calorimeter tests used in the CBUF Model I. Each value represents the average results from at least three specimens of each sample composition. N/A refers to the fact that for sample composites 5 and 8 (A5, D8) a second peak and trough were not clearly discernible from the cone results. Samples 5 and 8 (A5, D8) burned with a strong single peak.

Included in Table 8 are values for the 180s average HRR, $\dot{q}''_{180}$. This is a criteria for self propagation of the full-scale item[26]. Model I is applicable only to propagating fires.

	SAMPLE No.							
PROPERTY, x	1	2	3	4	5	6	7	8
m (g)	30.0	16.2	17.7	19.4	22.7	28.1	21.0	20.4
t_{ig} (s)	9	13	12	20	10	17	15	12
q'' (MJ/m^2)	54.4	36.7	38.3	37.0	61.2	56.1	38.3	48.5
$\dot{q}''_{180}$	288	177	207	188	321	248	193	257
$\dot{q}''_{300}$ (kW/m^2)	186	127	133	132	225	227	152	168
$\dot{q}''_{pk}$ (kW/m^2)	546	429	482	623	543	441	431	424
$\Delta h_{c,eff}$ (MJ/kg)	29.3	21.3	23.6	18.4	29.4	20.2	19.0	24.1
$t_{pk\#1}$ (s)	36	29	27	32	**N/A**	32	29	**N/A**
$\dot{q}''_{trough}$ (kW/m^2)	365	133	231	147	**N/A**	158	153	**N/A**
$\dot{q}''_{pk\#2}$ (kW/m^2)	544	173	264	243	**N/A**	293	292	**N/A**

Table 8: Cone calorimeter data used as input to CBUF Model I predictions, including

Table 9 summarises the non-cone calorimeter data required by CBUF predictive model.

	ITEM No. (Armchair)							
	1 A1S1	2 A2S1	3 A3S1	4 A4S1	5 A5S1	6 B6S1	7 C7S1	8 D8S1
m soft (kg)	5.13	4.80	5.10	5.09	5.23	5.39	5.34	7.13
m comb. Total (kg)	25.00	24.67	24.97	24.96	25.10	21.46	22.10	25.04
style code (--)	{1}	{1}	{1}	{1}	{1}	{4}	{4}	{1}
style_fac.A (--)	1.0	1.0	1.0	1.0	1.0	0.9	0.9	1.0
style_fac.B (--)	1.0	1.0	1.0	1.0	1.0	0.9	0.9	1.0

	ITEM No. (Two seat sofa)				
	9 A1S2	10 A2S2	11 B6S2	12 C7S2	13 D8S2
m soft (kg)	7.65	7.16	8.04	7.96	10.63
m comb. total (kg)	32.38	32.38	28.17	32.96	37.34
Style code (--)	{2}	{2}	{2}	{2}	{2}
Style_fac.A (--)	1	1	1	1	1
Style_fac.B (--)	0.8	0.8	0.8	0.8	0.8

Table 9: Supplementary data (non-cone test) required for CBUF Model I predictions

This data relates mostly to the mass and style of the furniture item. As described earlier, only items 6, 7, 8 and 9 (B6S1, C7S1, D8S1 and A1S2) were disassembled. These items are shown

in Figure 27. The mass of the soft materials and combustibles for item 1 (A1S1) is interpolated from the disassembled item 9 (A1S2). Then based on the ratio of fabric densities of items 2-5 and 10, (A2S1-A5S1 and A2S2) the full-scale mass data for these specimens is calculated. The mass data for items 11,12 and 13 (B6S2, C7S2 and D8S2) is extrapolated from the disassembled items 6, 7 and 8 (B6S1, C7S1 and D8S1).

Table 10 summarises the results of CBUF Model I applied from cone calorimeter results and then compares these values to the ones measured in the furniture calorimeter.

	ITEM No. (Armchair)							
	1 A1S1	2 A2S1	3 A3S1	4 A4S1	5 A5S1	6 B6S1	7 C7S1	8 D8S1
x_1	85	58	68	65	88	62	58	101
$\dot{Q}_{peak}$ Regime {1}	1540	1578	1677	1467	1450	1229	1426	1624
$\dot{Q}_{peak}$ Regime {2}	1217	829	984	940	1263	886	840	1457
$\dot{Q}_{peak}$ Regime {3}	**919**	**817**	**858**	**846**	**931**	**832**	**820**	**982**
$\dot{Q}_{peak}$ Measured	1123	795	1233	995	1705	1693	1550	1306
Q Predicted	321	278	295	270	324	233	235	314
Q Measured	378	244	299	333	387	262	150	363
t_{peak} Predicted	84	183	126	155	**N/A**	131	132	**N/A**
t_{peak} Measured	122	261	132	175	92	104	169	151
t_{UT} Predicted	35	139	68	106	**N/A**	80	80	**N/A**
t_{UT} Measured	**N/A**	**N/A**	**N/A**	**N/A**	**N/A**	**N/A**	**N/A**	**N/A**

	ITEM No. (Two seat sofa)				
	9 A1S2	10 A2S2	11 B6S2	12 C7S2	13 D8S2
x_1	139	95	113	107	167
$\dot{Q}_{peak}$ Regime {1}	**1753**	1804	**1394**	1683	**1863**
$\dot{Q}_{peak}$ Regime {2}	2005	1367	1622	1538	2401
$\dot{Q}_{peak}$ Regime {3}	1125	**958**	1025	**1003**	1229
$\dot{Q}_{peak}$ Measured	2248	1538	2230	2011	2065
Q Predicted	460	403	335	399	521
Q Measured	476	447	338	233	515
t_{peak} Predicted	78	168	131	133	**N/A**
t_{peak} Measured	161	240	138	133	173
t_{UT} Predicted	22	87	56	56	**N/A**
t_{UT} Measured	**N/A**	**N/A**	**N/A**	**N/A**	**N/A**

Table 10: Comparison of predicted and measured results

N/A in the table again refers the fact that a second peak and trough were not clearly discernible from the cone tests of sample composites 5 and 8. The x_1 values are included in the table for later comparisons. All three peak HRR predictive regimes are included for comparison. The regime applied by Model I is in bold type.

The following Figures represent the results of measured peak HRR, total heat and time to peak HRR against predicted values. While the time to untenable conditions in a standard room is also predicted by Model I, it is not experimentally measured in NZ-CBUF.

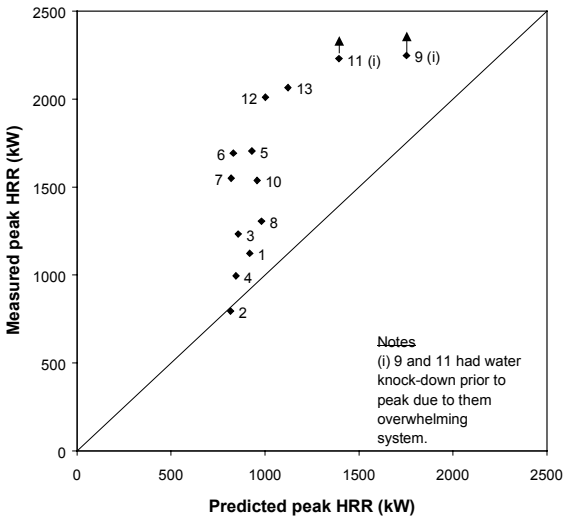

Figure 51: Peak HRR

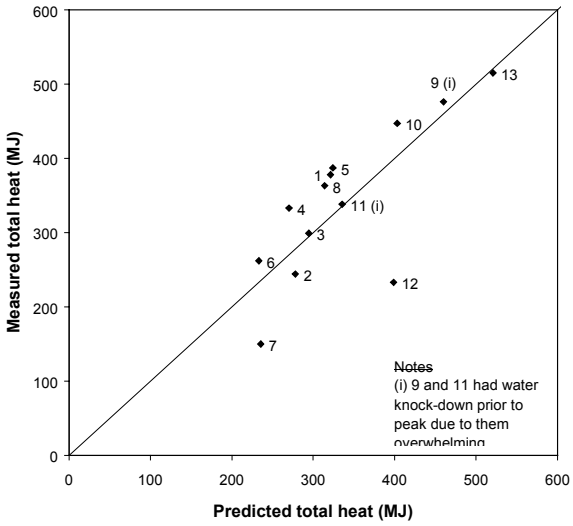

Figure 52: Total heat

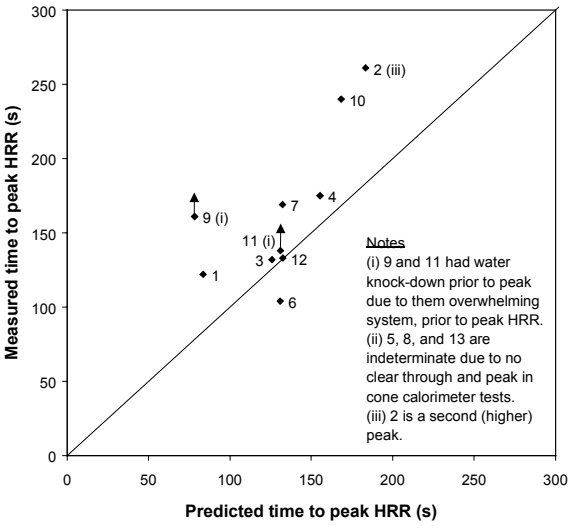

Figure 53: Time to peak HRR

7.5.5 Discussion of results of Model I and its applicability to the NZ items

Unfortunately, the NZ-CBUF sample size is too small to make formal statistical observations – such as a χ^2-Test – with respect to the goodness of the fit of the data to Model I.

The correlation coefficient 'R' (also called the Pearson product-moment correlation coefficient) and the coefficient of determination 'R^2' (also called the percentage of variation explained) are calculated for the sample set.

	CORRELATION 'R'	DETERMINATION 'R^2'
Peak HRR (kW)	57%	32%
Total heat (MJ)	87%	76%
Time to peak (s)	75%	57%
Peak HRR (kW) [modified, c.f. Fig 55]	74%	54%

Table 11: Correlation statistics (Model I)

This data should be used with caution since it is always possible to improve R and R^2 by adding terms to the model without necessarily improving the fit. Additionally, it does not indicate bias such as constant over-prediction or under-prediction.

Qualitatively, we observe that CBUF Model I is not a good predictor of the behaviour of the exemplary NZ furniture tested. The lack of a goodness of fit of the data to the model is especially pronounced in the peak HRR.

An examination of the relationship of the partial correlating variable x_1 to the measured peak HRR provides an insight to the poor results. For single seat items the NZ-CBUF data tends to deny partial dependence.

Assume that there is not the partial dependence applying only regime {2} (that is $\dot{Q}_{peak} = 14.4 \cdot x_1$) for style {1}. Also assume only regime {3} (that is $\dot{Q}_{peak} = x_2$) for style {4}. The following figures illustrate the result of these assumptions. We can see that while the fit may yet not be good, it has improved significantly. Especially, in respect to furniture item 7 (which was style {4} but only $x_1 = 47$). However, of concern is that two items (9 and 11) are

significantly under-predicted by the model. This is considered to be an undesirable result in life safety analysis.

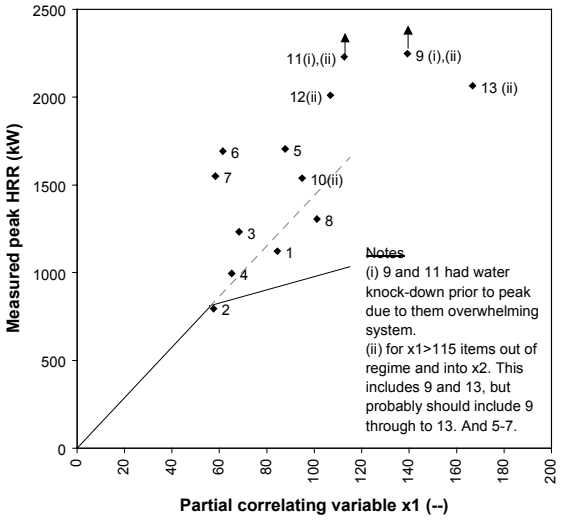

Figure 54: Partial correlating variable x_1

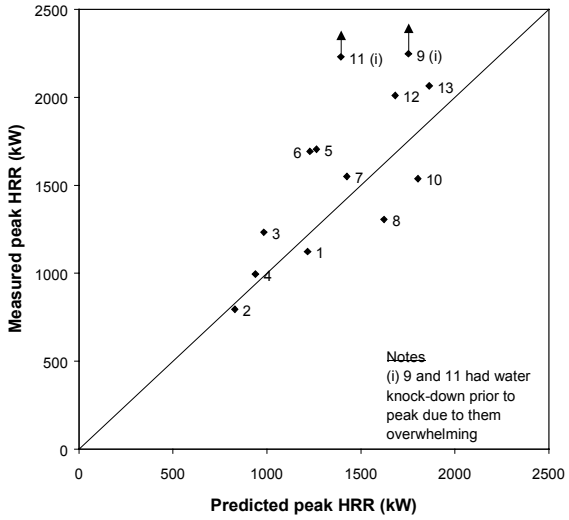

Figure 55: Peak HRR (modified)

The correlating variable x_1 is strongly coupled to the mass of soft combustibles - and the peak HRR prediction is more or less linearly proportional to x_1. The dependence is demonstrated in Figure 54. Many items are clustered in a relatively narrow vertical band - especially items 1 to 5 where only the mass of the fabric varies - yet the cone and furniture calorimeter HRR histories vary greatly. This qualitatively suggests an over dependence on mass of combustibles - where perhaps it would be of greater value to consider the composition of the fabrics.

7.5.6 Thickness scaling and 30 s running averages

Within the Final Report[26] there is a sub-model for 'thickness scaling' of the cone calorimeter results. The author of the modelling chapter – Dr V. Babrauskas – was contacted to question whether the thickness scaling subroutine was adopted in Model I predictions. It is his recollection and advice that is not the case. Therefore, the above results assume no thickness scaling as per the sub-model. Additionally, 5 s running averaging is previously used for the comparisons – not 30 s. The following figures demonstrate the affect of including thickness scaling and 30 s running averages.

The peak HRR prediction is 'artificially' improved, not surprising given that the 30 s averaging significantly lowers peak 'actual' 5 s peaks. In addition, the higher $\dot{q}''_{300}$, q'' and subsequent x_1 lead increased predicted peaks. Often by changing the regime to $\dot{Q} = x_2$. The total energy prediction is significantly worsened – albeit in a conservative manner as the energy is over-predicted. This is also not surprising given that thickness scaling 'artificially' increases $\Delta h_{c,eff}$. The 30 s running averaging does not effect the prediction of total heat. The time to peak HRR prediction is again significantly and 'artificially' worsened – and again in a conservative manner as the time is under predicted. This is also not a surprising due to the affect of the 30 s averaging slowing the response of the measured result.

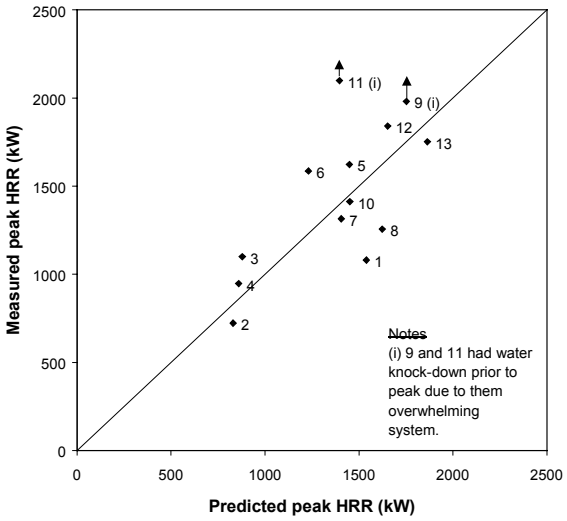

Figure 56: Peak HRR– thickness scaling

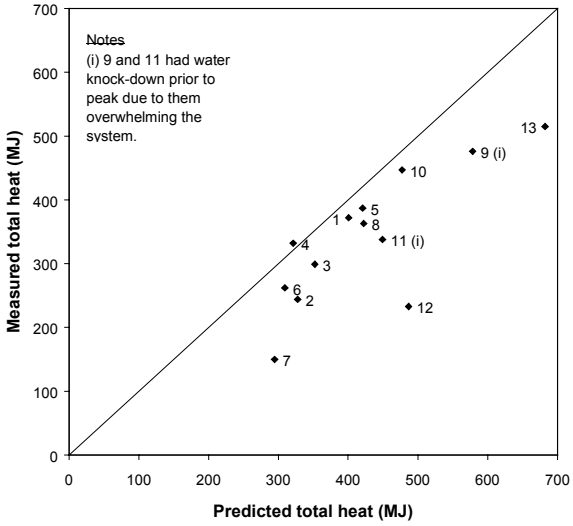

Figure 57: Total heat – thickness scaling

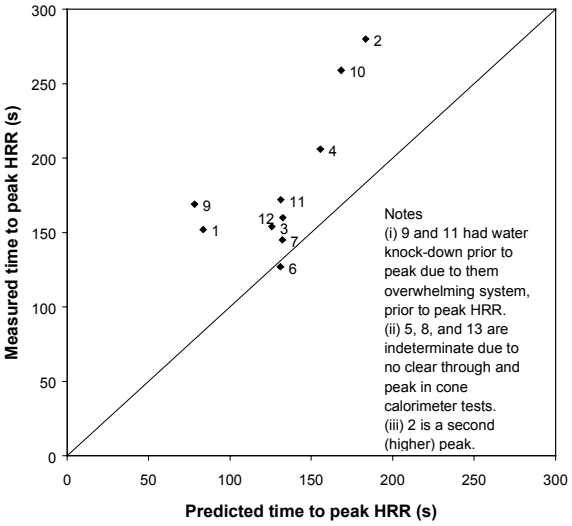

Figure 58: Time to peak HRR – thickness scaling

	CORRELATION 'R'	DETERMINATION 'R^2'
Peak HRR (kW)	67%	45%
Total heat (MJ)	78%	61%
Time to peak (s)	77%	48%

Table 12: Correlation statistics (Model I with thickness scaling)

Comparing the correlation coefficients for peak HRR in Table 12 to Table 11 demonstrates the earlier caution in using this statistic. Clearly, the prediction of peak HRR is improved – in allowing for thickness scaling – whereas the prediction of total heat and time to peak HRR are not improved. Yet a comparison of the 'R' and 'R^2' values demonstrate the opposite.

7.6 CBUF Model II

7.6.1 Introduction

The CBUF research programme developed an area deconvolution based model – CBUF Model II – for predicting full scale HRR time histories from 'representative' furniture calorimeter tests and cone calorimeter data. From this the peak HRR, total HR (up to a certain point) and time to peak HRR are able to be determined from a predicted HRR history.

The applicability of the CBUF Model II to the limited data set of exemplary New Zealand (NZ) furniture items is examined. Full-scale items 1 to 5 (A1S1 to A5S1) are considered as a set and then items 1 to 8 as a second set (i.e. including B6S1, C7S1 and D8S1).

7.6.2 Propagation of uncertainty through Model II

An analysis of the propagation of uncertainty in Model I via the method described in CHAPTER 5: 'Propagation of Uncertainty of Heat Release Rate Measurement' is not undertaken. This is on the basis that there are extremely significant systematic uncertainties associated with the correlation's – such as the effective burning area function – in Model II. It is suspected that systematic uncertainties will greatly exceed the significance of instrument based random uncertainties. Therefore, any analysis of propagation of the correlation's becomes an insignificant exercise.

7.6.3 CBUF model II predictions

Model II is based on an earlier flame spread model by Wickstrom and Goransson[35]. The simple assumption is that during combustion each element of unit area of the full-scale item contributes to the same extent as the corresponding cone calorimeter test. The total contribution is the integral over the all the burning area.

Here a convolution integral is assumed to describe the full-scale behaviour in terms of bench-scale HRR history $\dot{q}''$ and a burning area rate $\dot{A}$.

Equation 253 $$\dot{Q} = \int_0^t \dot{q}''(t-\tau)\dot{A}(\tau)d\tau$$

Due to the complex physics of the problem – described in more detail in the Final Report[26] – it is simplified by assuming an effective burning area rate, determined by working backwards from several 'representative' full scale tests of chairs of a similar geometrical style. Complicating phenomena such as pool and underside burning are therefore partially represented in the 'deconvoluted' burning area rate function.

7.6.4 Results of Model II - Items 1 to 5 only (A1S1-A5S1)

Model II is applied to five single seated armchairs of the same style. In fact each were effectively identical in geometry and construction except that the fabric (cover) varied on each. The cone calorimeter test HRR histories – including thickness scaling – are transformed to the corresponding full-scale furniture calorimeter results via and effective area function for each of the five items. These area functions are non-dimensionalised in time and area. The result, a non-dimensionalised area burning rate history is shown as Figure 59. The form of the mean, non-dimensionalised area burning rate history is described in Table 13.

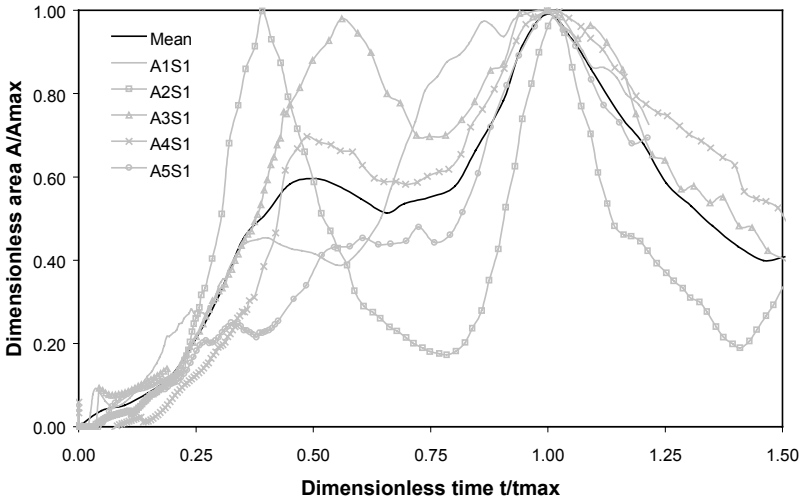

Figure 59: Dimensionless area versus time, items 1-5 (A1S1-A5S1)

t/t_{max}	$a(t/t_{max})/A_{max}$
0.00	0.00
0.10	0.05
0.20	0.12
0.30	0.32
0.40	0.51
0.50	0.60
0.60	0.55
0.70	0.54
0.80	0.58
0.90	0.78
1.00	1.00
1.10	0.86
1.20	0.68
1.30	0.53
1.40	0.43
1.50	0.41

Table 13: Dimensionless area versus time, items 1-5 (A1S1-A5S1)

The mean time to peak, t_{max} from the NZ-CBUF sample set A1S1-A5S1 is 206 s. This compares with the CBUF value of t_{max} = 250 s.

The cone calorimeter data – as is the normal case – is calculated on a 5 s running average. However, due to the high-frequency irregularities near ignition, the first 30 s is calculated on a 30 s running average. This is described in more detail and recommended in Myllymaki and Baroudi[36].

Following determination of the non-dimensionalised area burning rate history and determination of $t_{\max}$, the maximum burning area $A_{\max}$ is correlated as a function of $\dot{q}''_{180}$ and m_{soft}.

Equation 254 $$A_{\max} = k \cdot \dot{q}''^{-0.76}_{180} \cdot m^{0.35}_{soft}$$

CBUF uses the above relationship with a *k* value of 150.2. This relationship is demonstrated in the following figures, the second of which – corresponding to a k value of 201.2 – was adopted for NZ-CBUF items 1 to 5.

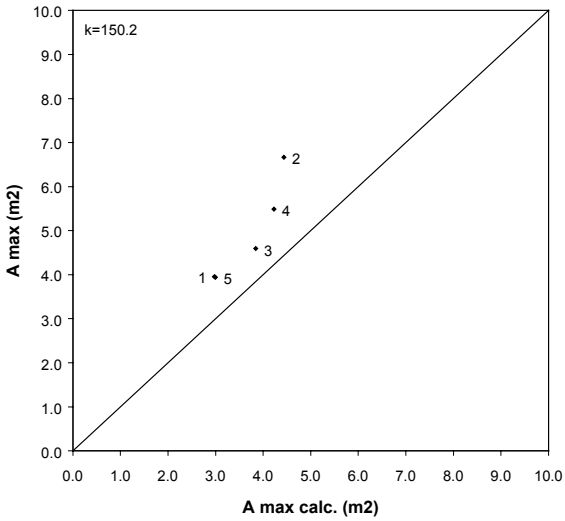

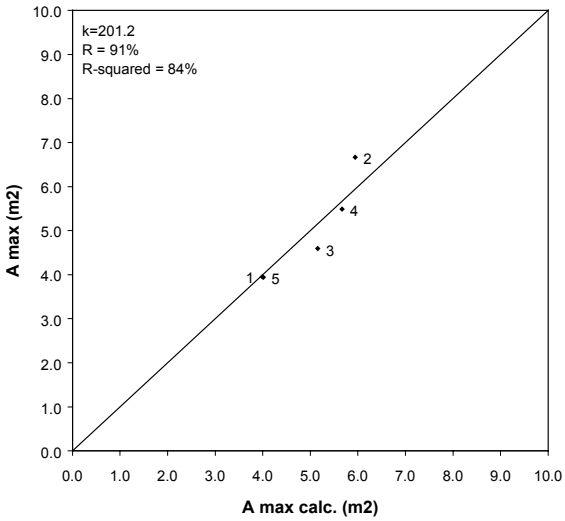

Figure 60: Correlation of $A_{\max}$ with k=150.2 **Figure 61:** Correlation of $A_{\max}$ with k=201.2

The prediction follows as:

Equation 255 $$\dot{Q} = A_{\max} \int_0^t \dot{q}''(t-\tau)\dot{a}\left(\frac{\tau}{t_{\max}}\right)d\tau$$

With $t_{\max}$=206 s, and:

Equation 256 $$A_{\max} = 201.2 \cdot \dot{q}''^{-0.76}_{180} \cdot m^{0.35}_{soft}$$

Following are the predicted and measured HRR histories for items 1 to 5 (A1S1 to A5S1).

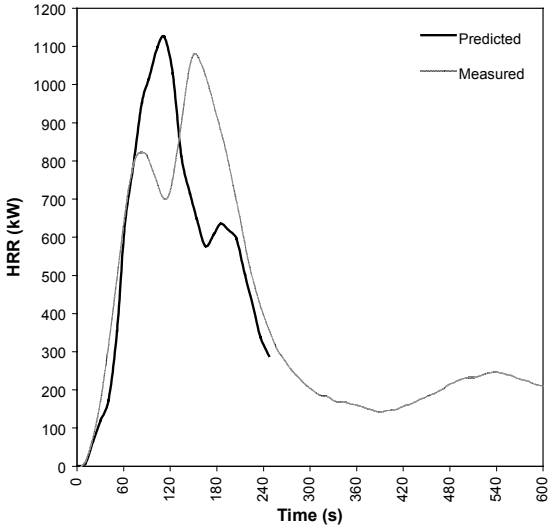

Figure 62: Item 1, A1S1

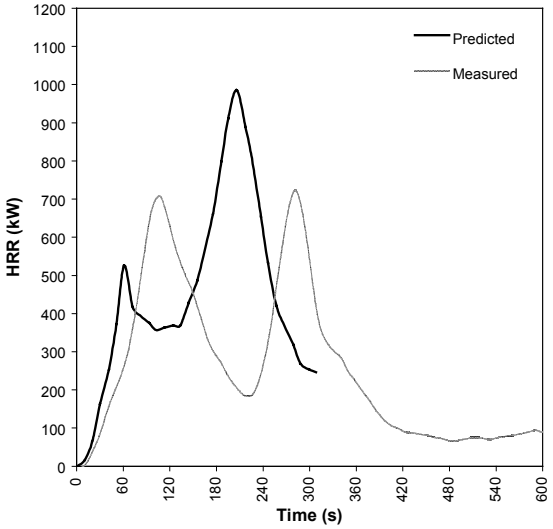

Figure 63: Item 2, A2S1

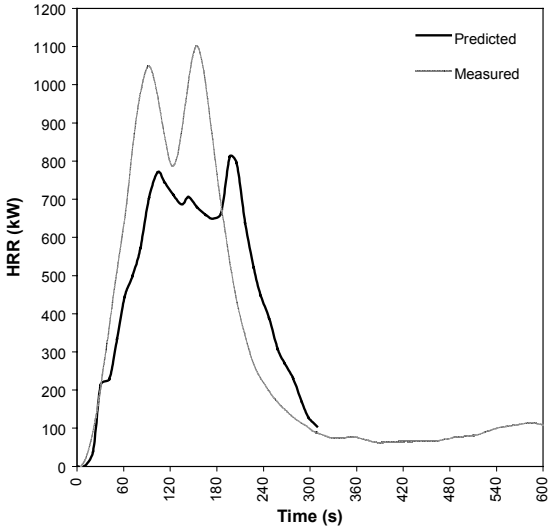

Figure 64: Item 3, A3S1

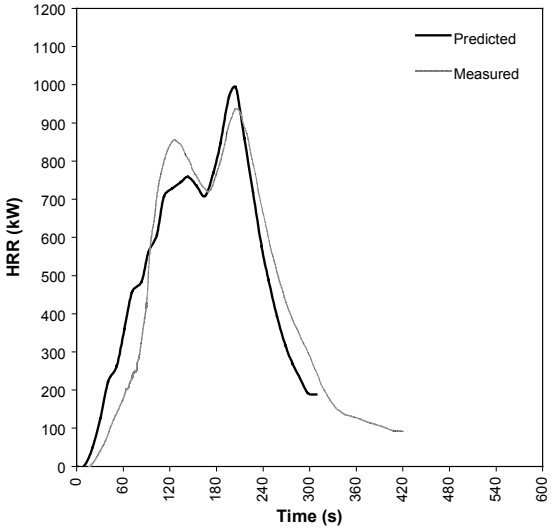

Figure 65: Item 4, A4S1

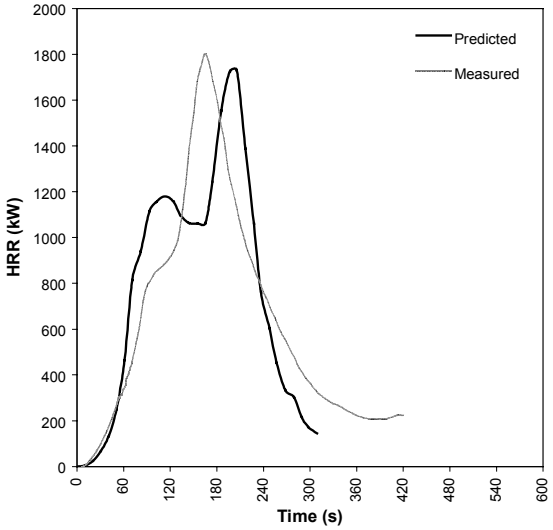

Figure 66: Item 5, A5S1

The following Figures represent the results of measured peak HRR, total heat and time to peak HRR against predicted values.

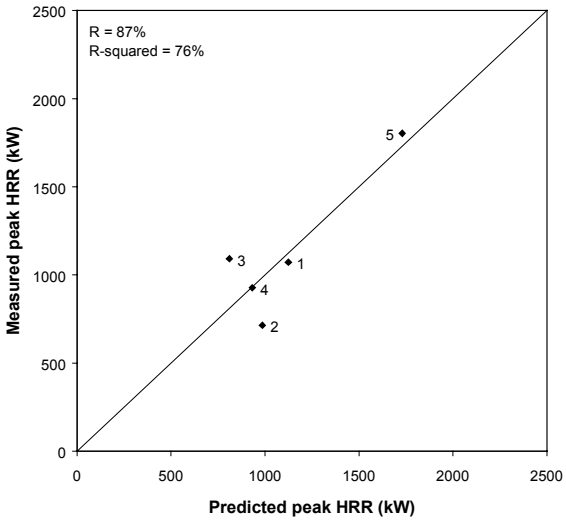

Figure 67: Predicted peak HRR

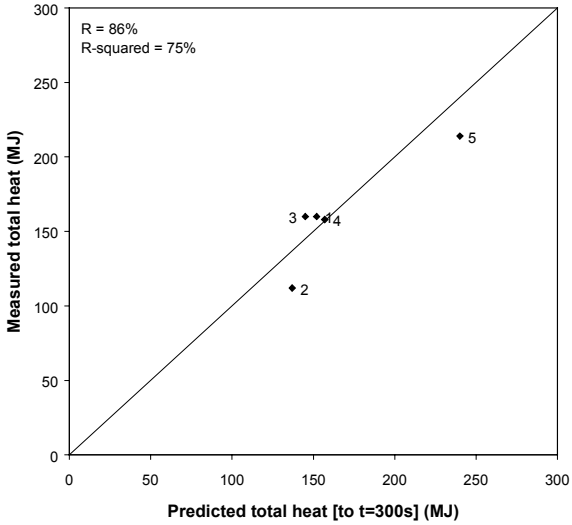

Figure 68: Predicted total heat [t < 300 s]

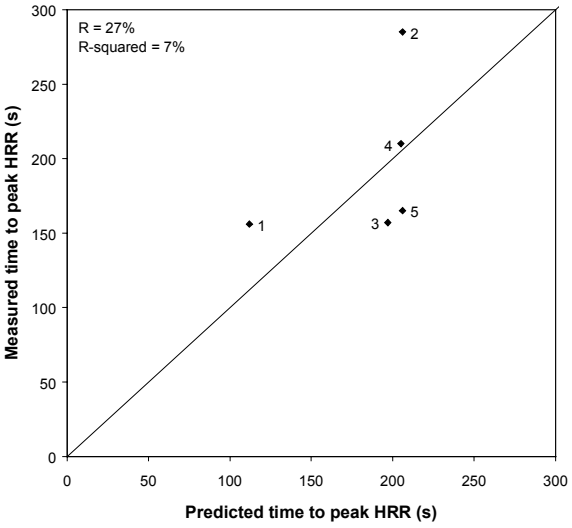

Figure 69: Predicted time to peak HRR

'A' SERIES, 1-5	CORRELATION 'R'	DETERMINATION 'R^2'
Peak HRR (kW)	87%	76%
Total heat [t<300 s] (MJ)	86%	75%
Time to peak (s)	27%	7%

Table 14: Correlation statistics, items 1-5 (A1S1-A5S1) (Model II)

7.6.5 Results of Model II - Items 1 to 8 (A1S1-A5S1, B6S1, C7S1 and D8S1)

Using the same methodology as above, the non-dimensionalised area burning rate history is shown in Figure 70 and the form tabulated in Table 15.

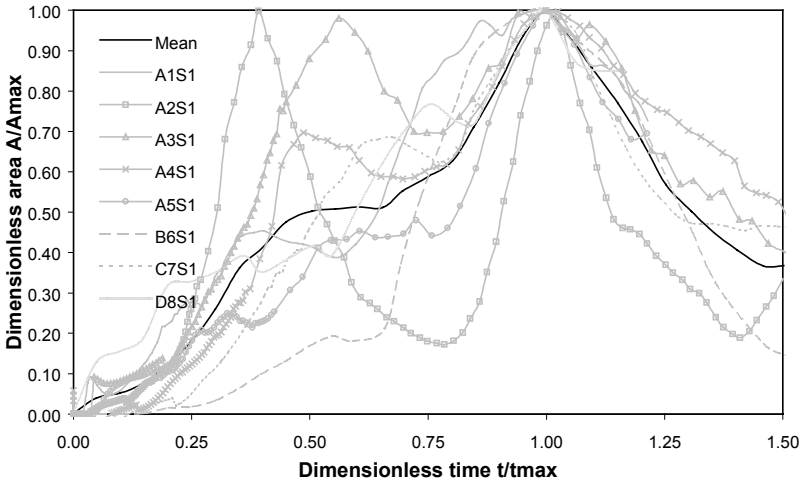

Figure 70: Dimensionless area versus time, items 1-8 (A1S1-A5S1, B6S1, C7S1, D8S1)

$t/t_{\max}$	$a(t/t_{\max})/A_{\max}$
0.00	0.00
0.10	0.05
0.20	0.12
0.30	0.26
0.40	0.41
0.50	0.50
0.60	0.51
0.70	0.55
0.80	0.63
0.90	0.82
1.00	1.00
1.10	0.86
1.20	0.67
1.30	0.50
1.40	0.41
1.50	0.37

Table 15: Dimensionless area versus time, items 1-8 (A1S1-A5S1, B6S1, C7S1, D8S1)

The mean time to peak, $t_{\max}$ from the NZ-CBUF sample set A1S1-A5S1 is 196 s. This compares with the CBUF value of $t_{\max}$ = 250 s.

CBUF uses Equation 254 with a *k* value of 150.2. This relationship is demonstrated in the following figures, the second of which – corresponding to a k value of 191.4 – is adopted for NZ-CBUF items 1 to 8.

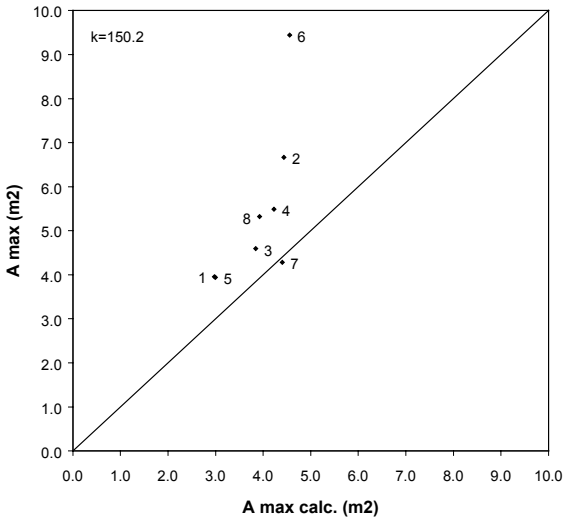

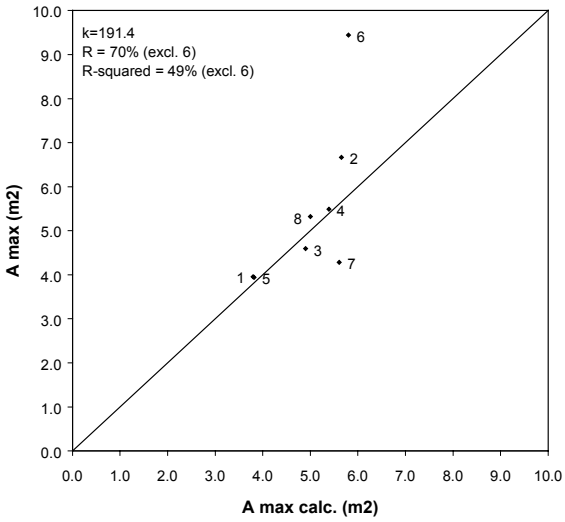

Figure 71: Correlation of A_{max} with k=150.2 **Figure 72:** Correlation of A_{max} with k=191.4

Following are the predicted and measured HRR histories for items 1 to 8 (A1S1-A5S1, B6S1, C7S1, D8S1). Items 1 to 5 also include the previous prediction for comparison.

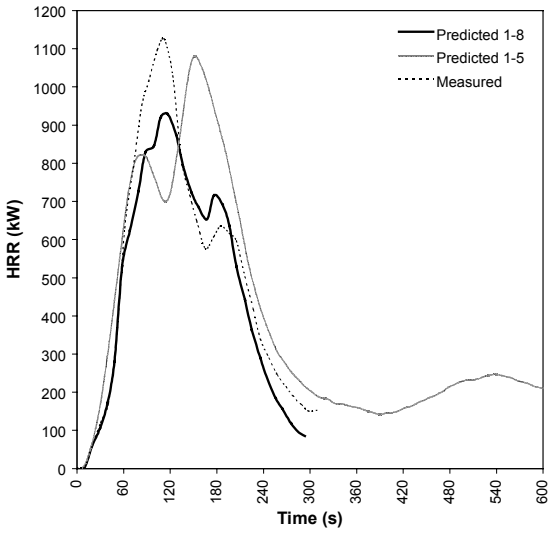

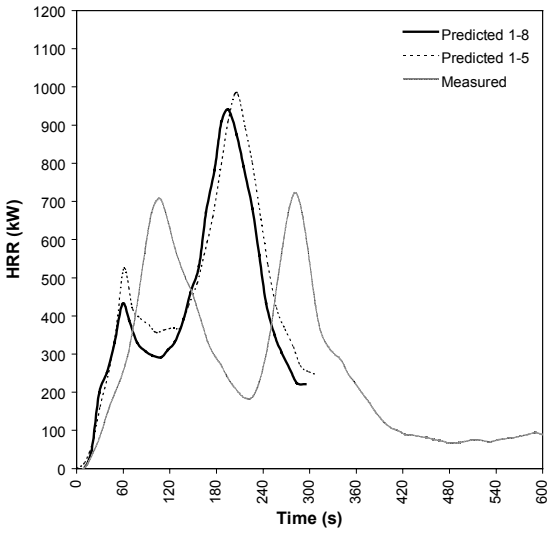

Figure 73: Item 1, A1S1

Figure 74: Item 2, A2S1

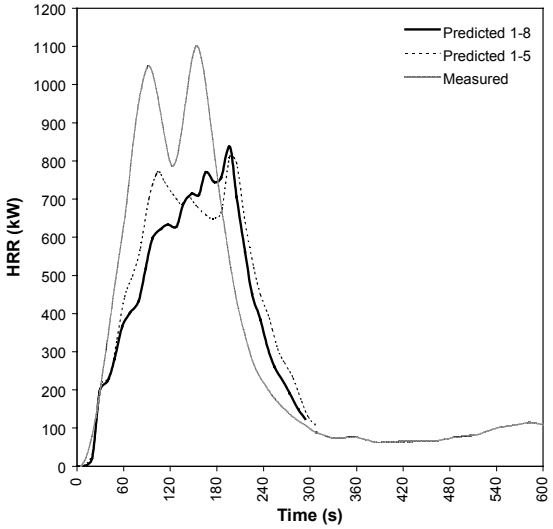

Figure 75: Item 3, A3S1

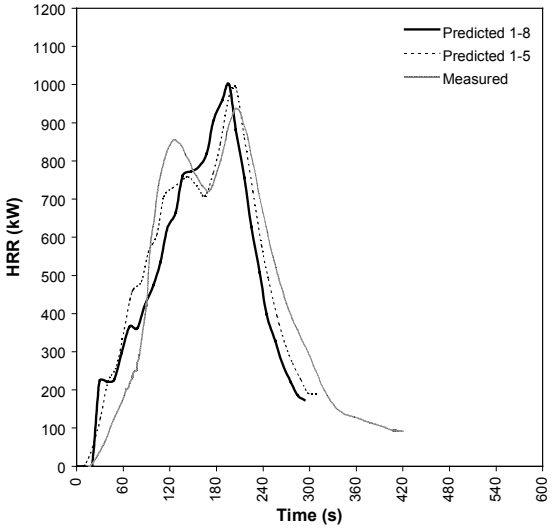

Figure 76: Item 4, A4S1

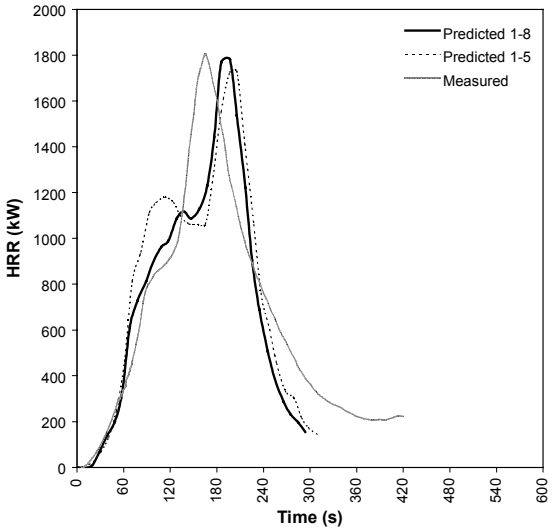

Figure 77: Item 5, A5S1

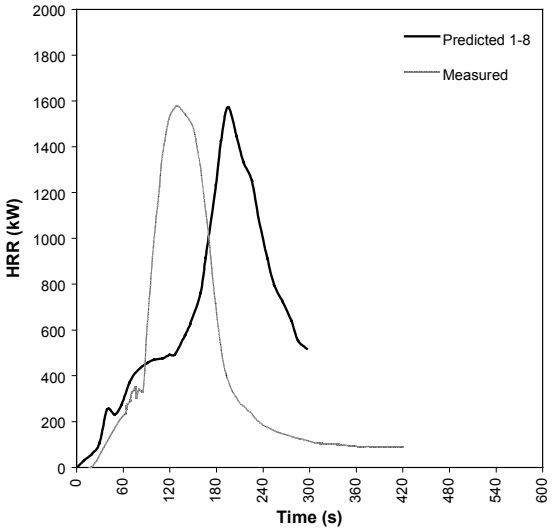

Figure 78: Item 6, B6S1

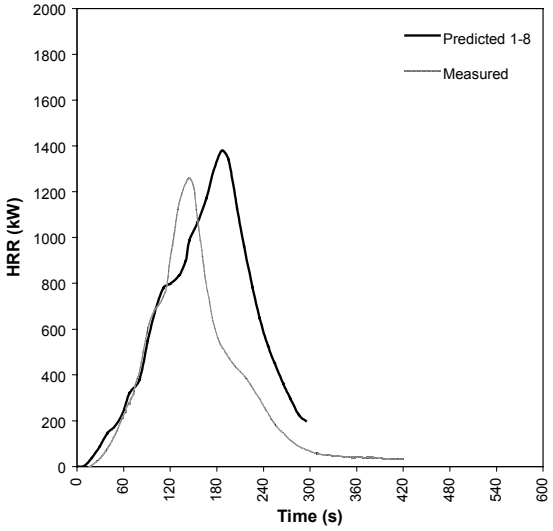

Figure 79: Item 7, C7S1

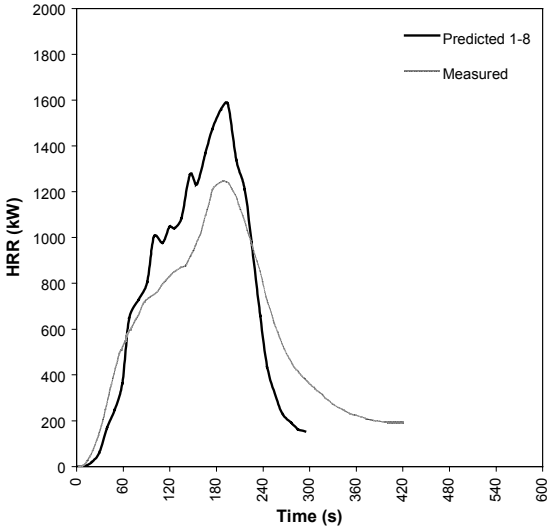

Figure 80: Item 8, D8S1

The following Figures represent the results of measured peak HRR, total heat and time to peak HRR against predicted values.

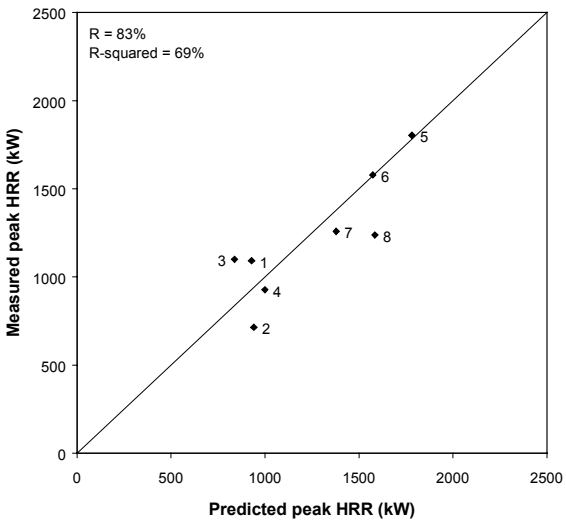

Figure 81: Predicted peak HRR

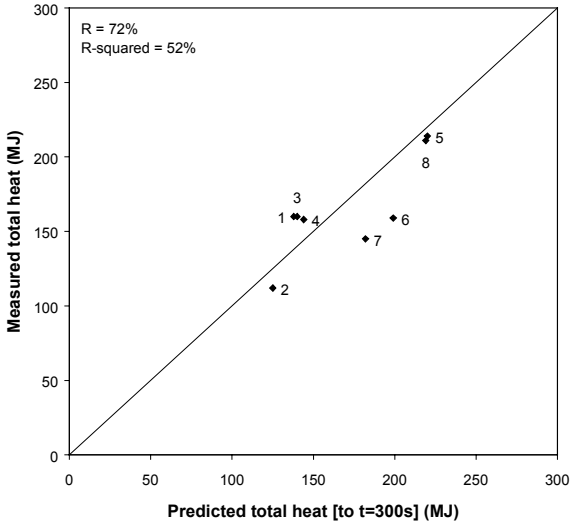

Figure 82: Predicted total heat [t < 300 s]

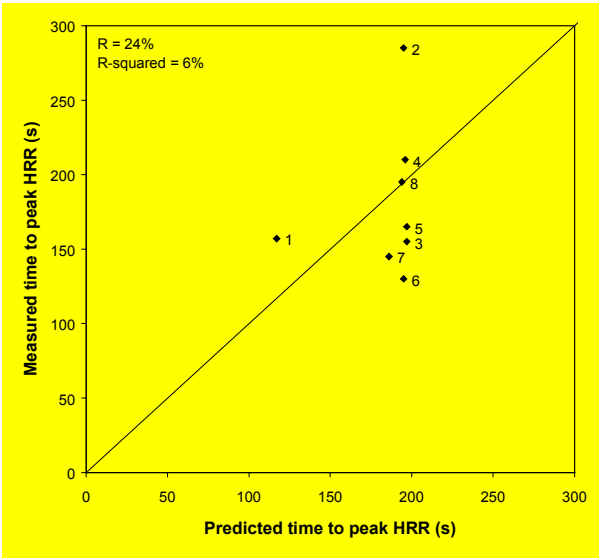

Figure 83: Predicted time to peak HRR

A, B, C, D SERIES'	CORRELATION 'R'		DETERMINATION 'R^2'	
	1-5 only	1-8	1-5 only	1-8
Peak HRR (kW)	87%	83%	76%	69%
Total heat [t<300 s] (MJ)	86%	72%	75%	52%
Time to peak (s)	27%	24%	7%	6%

Table 16: Correlation statistics, items 1-8 (A1S1-A5S1, B6S1, C7S1, D8S1) (Model II)

7.6.6 Results of Model II - Items 9 to 13 (A1S2, A2S2, B6S2, C7S2 and D8S2)

These results are for the two-seat sofas. However, these should be qualitative rather than quantitative as a water knock-down was applied to two items 9 (A1S2) and 11 (B6S2) Using the same methodology as above, the non-dimensionalised area burning rate history is shown in Figure 84 and the form tabulated in Table 17.

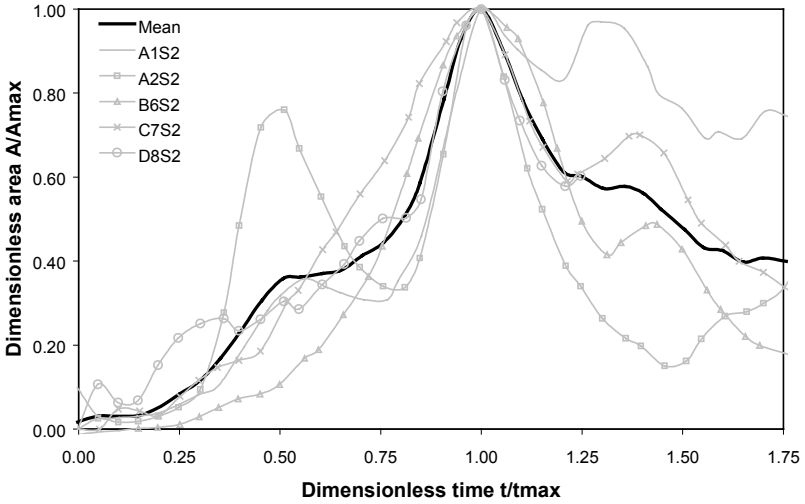

Figure 84: Dimensionless area versus time, items 1-5 (A1S1-A5S1)

t/t_{max}	$a(t/t_{max})/A_{max}$
0.00	0.02
0.10	0.03
0.20	0.05
0.30	0.11
0.40	0.23
0.50	0.36
0.60	0.37
0.70	0.41
0.80	0.51
0.90	0.79
1.00	1.00
1.10	0.78
1.20	0.61
1.30	0.57
1.40	0.56
1.50	0.48

Table 17: Dimensionless area versus time, items 1-5 (A1S1-A5S1)

The mean time to peak, t_{max} from the NZ-CBUF sample set A1S2, A2S2. B6S2, C7S2 and D8S2 is 205 s. This compares with the CBUF value of t_{max} = 250 s.

CBUF uses Equation 254 with a *k* value of 150.2. This relationship is demonstrated in the following figures, the second of which – corresponding to a *k* value of 288.9 – is adopted for NZ-CBUF items 9 to 13. Although the fit is very poor.

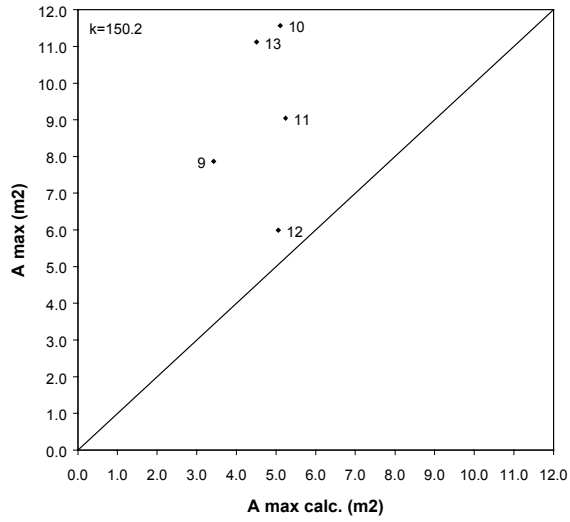

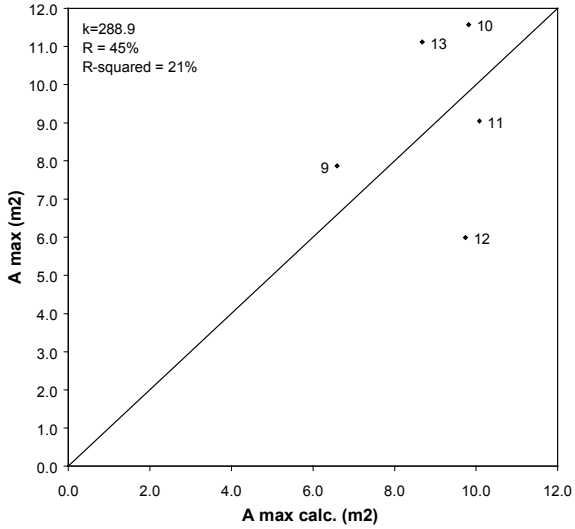

Figure 85: Correlation of A_{max} with k=150.2 **Figure 86:** Correlation of A_{max} with k=288.9

Following are the predicted and measured HRR histories for items 9 to 13 (A1S2, A2S2, B6S2, C7S2, D8S2).

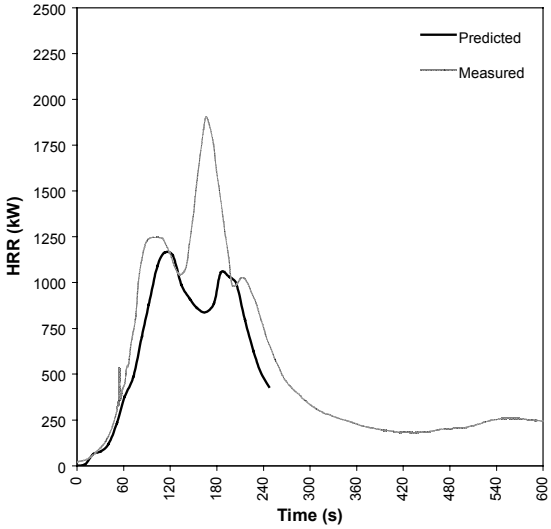

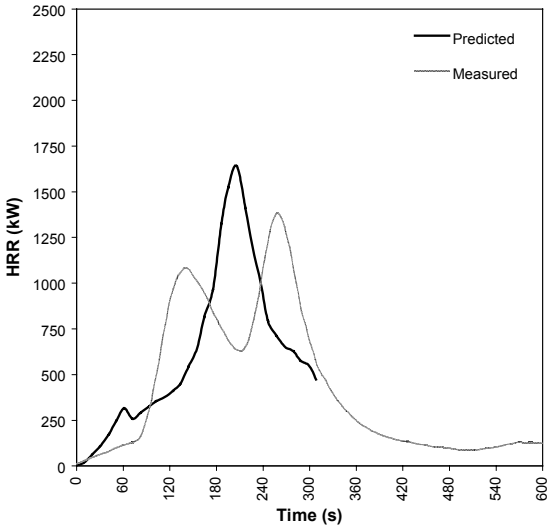

Figure 87: Item 9, A1S2 **Figure 88:** Item 10, A2S2

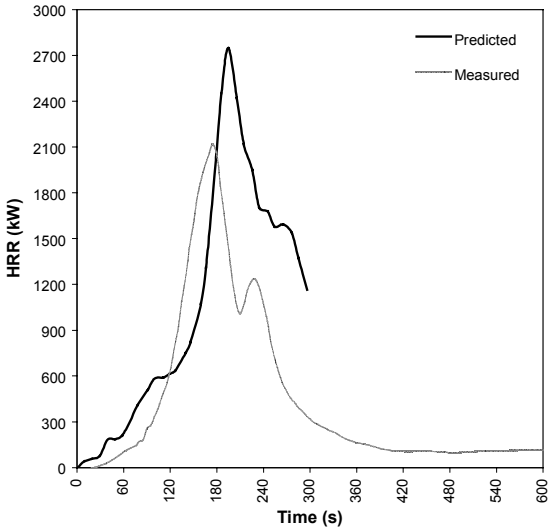

Figure 89: Item 11, B6S2

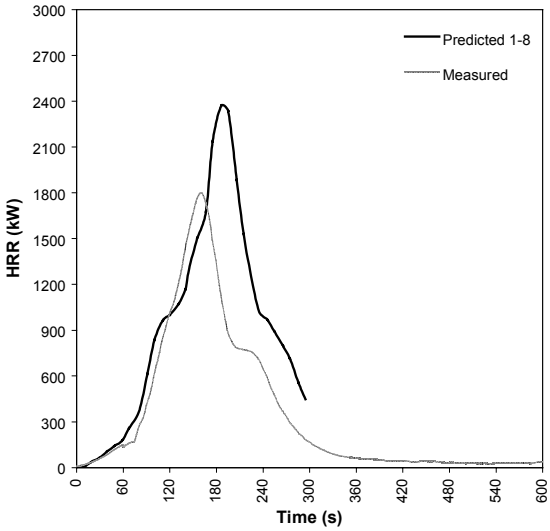

Figure 90: Item 12, C7S2

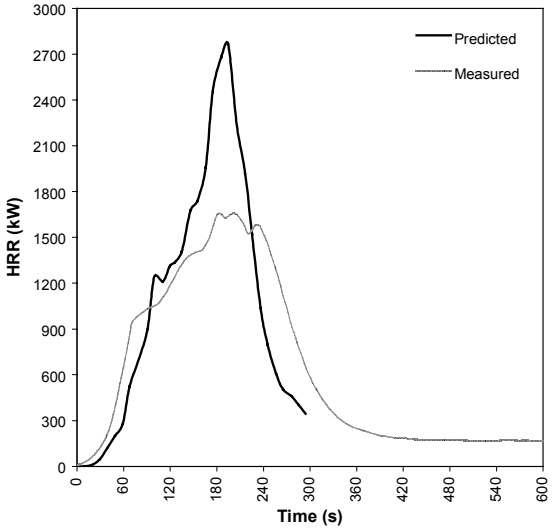

Figure 91: Item 13, D8S2

The following Figures represent the results of measured peak HRR, total heat and time to peak HRR against predicted values.

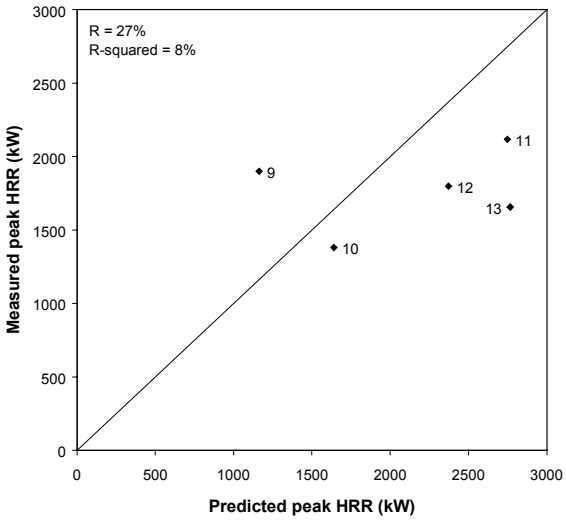

Figure 92: Predicted peak HRR

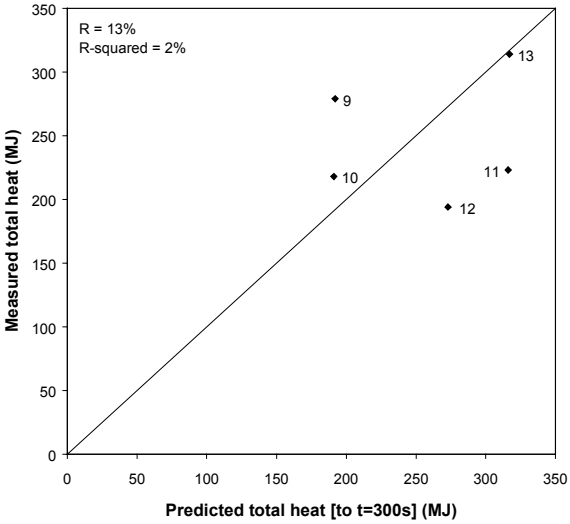

Figure 93: Predicted total heat [t < 300 s]

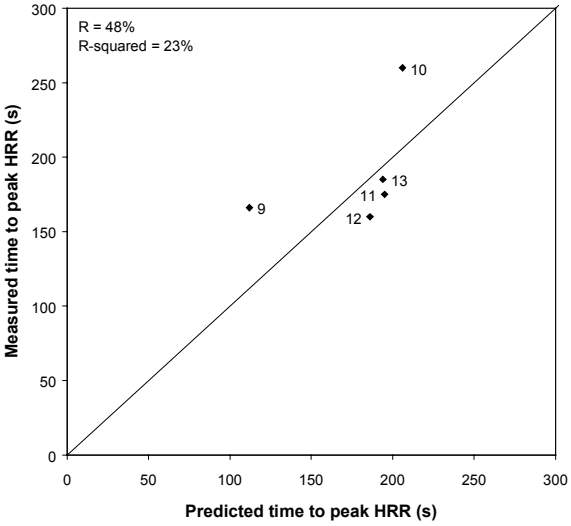

Figure 94: Predicted time to peak HRR

2-SEAT SOFAS	CORRELATION 'R'	DETERMINATION 'R^2'
Peak HRR (kW)	27%	8%
Total heat [t<300 s] (MJ)	13%	2%
Time to peak (s)	48%	23%

Table 18: Correlation statistics, items 9-13 (A1S2, A2S2, B6S2, C7S2, D8S2) (Model II)

7.6.7 Discussion of results of Model II and its applicability to the NZ items

Even more so than Model I, the NZ-CBUF sample size is too small to make formal statistical observations – such as a χ^2-Test – with respect to the goodness of the fit of the data. The correlation coefficient 'and the coefficient of determination 'R^2' are calculated for the sample set. However, these are noted with caution.

Qualitatively, Model II provides a reasonable predictive tool for items 1 to 5 alone and to a lesser degree items 1 to 5 with 6 to 8 included. In either case, it is a better prediction tool than Model I, refer to Table 19 below. Model II is more useful than Model I in that it characterises the HRR history rather than just a few key properties.

There is positive feedback in the Model II results reported. This is because all of the items - for which predictive HRR histories were compared with measured – themselves contributed to the effective area growth function. This positive feedback may provide overly optimistic verification results, especially in small data sets. It is one of the aims of the Models to supersede - or at least minimise – full-scale testing. Future research should include verification of full-scale items not contributing to the effective area growth function.

The notable exception to the 'good' correlation of the history of the single seat chairs – if not reported properties – is item 2 (A2S1). Here however, it could have been observed at the cone calorimeter stage that this was an extraordinary test sample and that it would not fit well with other data.

	CORRELATION 'R'				DETERMINATION 'R^2'			
PROPERTY	Model I 1-13	Model II 1-5	Model II 1-8	Model II 9-13	Model I 1-13	Model II 1-5	Model II 1-8	Model II 9-13
Peak HRR kW	57%	87%	83%	27%	32%	76%	69%	8%
Total heat MJ	87%	86%	72%	13%	76%	75%	52%	2%
Time to peak (s)	75%	27%	24%	48%	57%	7%	6%	23%

Table 19: Correlation statistics (Model I and Model II)

The Model II 9-13 data is to be used with caution as items 9 and 11 had a water knockdown at 180 s as they were overwhelming the extract system.

7.7 Conclusions

7.7.1 Pronounced fabric effect observed

A pronounced fabric affect is demonstrated in both the small-scale samples and full-scale items. During the cone calorimeter tests, the fabric showed a trend to either (i) melt and peel, or (ii) split and remain in place – that is, to become char forming. In first phenomena there is typically a large single peak with both fabric and foam contributing to the energy in a similar manner. The second phenomena is more complex. Here a single sharp first peak is observed followed by a lower slower 'foam' peak. The first peak is believed to occur once the foam block has melted below the charring fabric. The additional flux previously used in thermal decomposition is then available to assist. The charring fabrics are believed to be due to cotton backing.

7.7.2 Comparison of combustion behaviour of NZ furniture to European

Relative to CBUF items overall, the NZ-CBUF armchairs exhibited significantly higher peak HRR for relatively similar total heat. From this we can qualitatively deduce quicker times to peak HRR - unfortunately times to peak HRR are not recorded in CBUF.

Exemplary NZ items do not include combustion modified or high resilience foams or fire resistant fabrics or interliners. In comparison to equivalently composed European items, the peak HRR results were more comparable, although still generally higher.

7.7.3 Model I: Goodness of the fit

Unfortunately, the NZ-CBUF sample size is too small to make formal statistical observations in respect to the goodness of the fit of the data to Model I. Qualitatively, we observe that the CBUF Model I is not a good predictor of the behaviour of the exemplary NZ furniture tested. The lack of a goodness of fit of the data to the model is especially pronounced in the peak HRR. Qualitatively, it is assumed that only a minor proportion of the lack of goodness of fit of the model is due to the instrument and assumption uncertainty – developed in detail in CHAPTER 5: 'Propagation of uncertainty of heat release rate measurement'. This is believed to be outweighed by the uncertainties of the highly empirical nature of Model I which is based on a regression analyses.

7.7.4 Model I: Partial dependence of peak HRR upon correlating variable x_1

If not using the thickness scaling sub-model, then the NZ-CBUF results, which are all in the region of higher peak HRR, tend to deny a partial dependence and tend to suggest applying only regime {2} (that is $\dot{Q}_{peak} = 14.4 \cdot x_1$) for style {1}.

7.7.5 Model I: Derivation of correlating variable x_1

The correlating variable x_1 is strongly coupled to the mass of soft combustibles - and the peak HRR prediction is more or less linearly proportional to x_1. The dependence is demonstrated in Figure 54. Many items are clustered in a relatively narrow vertical band - especially items 1 to 5 where only the mass of the fabric varies - yet the cone and furniture calorimeter HRR histories vary greatly. This qualitatively suggests an over dependence on mass of combustibles in calculating x_1 .

7.7.6 Model I: Scaling and averaging effects

Within NZ-CBUF there are two predictive scenarios, (i) without thickness scaling and using 5s running averaging and (ii) with thickness scaling and using 30s running averaging. In the second case the following differences were observed:

The peak HRR prediction is 'artificially' improved, not surprising given that the 30 s averaging significantly lowers peak 'actual' 5 s peaks. In addition, the higher $\dot{q}''_{300}$, q'' and subsequent x_1 lead increased predicted peaks. Often by changing the regime to $\dot{Q} = x_2$. The total energy prediction is significantly worsened – albeit in a conservative manner as the energy is over-predicted. This is also not surprising given that thickness scaling 'artificially' increases $\Delta h_{c,eff}$. The 30 s running averaging does not effect the prediction of total heat. The time to peak HRR prediction is again significantly and 'artificially' worsened – and again in a conservative manner as the time is under predicted. This is also not a surprising due to the affect of the 30 s averaging slowing the response of the measured result.

7.7.7 Model II: Goodness of the fit

Qualitatively, Model II provides a reasonable predictive tool for items 1 to 5 alone and to a lesser degree items 1 to 5 with 6-8 included. In either case, qualitatively it is a better

prediction tool than Model I. This is an expected result as the 'deconvolution' works backward from the measured full-scale data. See the 'feedback' comments below.

The real test of Model II is to extrapolate it by applying it to bench-scale samples corresponding to the similar style full-scale items. Then to test the full-scale item without including that particular full-scale effective area to the dimensionless function. As described above all predictions in the NZ-CBUF data set actually effect the outcome as all are contributing to the effective area function. Unfortunately, this is necessary due to ourt small data set.

Model II is more useful than Model I in that it characterises the HRR history rather than just a few properties.

7.7.8 Model II: Positive feedback

There is positive feedback in the Model II results. This is because all of the items - for which predictive HRR histories were compared with measured – themselves contributed to the effective area growth function. This positive feedback may provide overly optimistic verification results, especially in small data sets. It is one of the aims of the Models to supersede - or at least minimise – full-scale testing. Future research should include verification of full-scale items not contributing to the effective area growth function.

7.7.9 Strategies for improved furniture design

The objectives of this phase of NZ-CBUF is to verify the applicability of the Models. The data set is too limited in the number of items tested to draw meaningful conclusions of effects of materials and design on fire performance (combustion behaviour). The Final Report discusses in detail the positive effects of various design aspects. We would assume that these strategies apply to NZ furniture and this is an obvious direction for future research.

7.7.10 Future research

The NZ-CBUF data set is of limited size. Therefore, further research is required to expand this data set. Different combinations of common foams and fabrics (statistically sampled) should be tested in the cone calorimeter and furniture calorimeter on a standard frame. In

particular more work should be done with interliners as the European study shows these can have a positive effect.

An expanded data set will allow more statistically meaningful conclusions to be drawn analytically. In particular, regarding the applicability of CBUF Model I and II and in general of combustion behaviour. In addition to statistically considering the NZ-CBUF data in isolation, future research should incorporate it into the CBUF data set, with wider comments made and conclusions drawn. An expanded data set should include full-scale verification of CBUF Model II using items outside of the feedback loop. In addition to future research continuing the verification and refinement of Models I and II, it should begin the task of developing strategies for improved design of NZ furniture.

CHAPTER 8: CONCLUSIONS AND FUTURE RESEARCH

8.1 General conclusions

Loss of life in residential buildings dominates NZ annual fire death statistics. Few items within these buildings have the potential to bring about untenable conditions as swiftly as upholstered furniture.

Prediction of combustion behaviour of upholstered furniture (CBUF) is a powerful and valuable tool in mitigating the consequences of unwanted fires in buildings. Such predictions may also be used by engineering practitioners in selecting 'design' fires. Recently, the European Commission sponsored CBUF programme undertook a large and comprehensive research initiative. Two predictive models for upholstered armchairs and sofa's were developed. A major contribution of this work is the examination of the applicability of these models to a small but exemplary data set of NZ furniture items. It is found that the models do not predict with goodness the combustion behaviour.

On the way to achieving the goal of examining the applicability of the CBUF Models, other contributions are made. The most tangible of these contributions – while not a unique contribution to the body of knowledge – is the design and commissioning of the UC Cone and Furniture Calorimeters. These are of an international standard and the characterisation of these apparatuses is included in this work. This is.

In terms of contributions to the body of knowledge, the theory of contemporary oxygen consumption calorimetry used for HRR measurement, is thoroughly examined and appears in this work. A novel extension and unique contribution is the development of general equations for HRR measurement using a thermochemistry based technique. It is not recommended that this technique is favoured ahead of oxygen consumption. However, the second techniques is an independent way of measuring the reaction-to-fire property of most interest and is therefore of great interest. An application of the use of the thermochemistry technique – as an alternative means of calculation the Cone Calorimeter calibration constant – is demonstrated in the thesis.

This thesis makes a significant contribution in developing methods of calculating experimental uncertainty in HRR measurement. Specifically, the propagation of uncertainty

from random instrument uncertainty and systematic uncertainties introduced by assumptions in the general equations. The work does not include consideration of random uncertainties of the fuel samples nor random and systematic uncertainties associated with human operational error. An example is given demonstrating the use of the uncertainty equations and results for a typical Cone Calorimeter test. The inclusion of such uncertainty information during routine testing is recommended.

The contributions made in this work are of interest and direct relevance to those working in the field of fire safety engineering.

8.2 Part-specific Conclusions

8.2.1 PART A: Calorimetric technique

This work re-derives the equations for calculating the HRR measurement using the conventional oxygen consumption technique. In addition, corresponding equations are derived using the thermochemistry technique.

The thermochemistry technique is fundamentally more sound, but is disadvantaged by relying on some prior knowledge of the fuel. That is, the fuel's heat of formation must be known. The oxygen consumption technique is based on a principal rather than a law, but has the advantage of Huggett's constant holding true to within ±5%.

8.2.2 PART B: Uncertainty analysis of HRR measurement

The types of HRR uncertainty investigated in this dissertation are instrument and assumption orientated. Random uncertainties, associated with the sample and operator errors are not included. The uncertainty of an instrument measurement is investigated in so far as the instrument can be relied upon to be giving a true reading. Assumed physical properties used as constants also have uncertainties associated with them.

An uncertainty analysis of the HRR calculation is not computationally onerous. The partial derivatives are reasonably simple and such a calculation should be incorporated in the cone calorimeter standards and software.

The uncertainty of the calculation is very strongly coupled to any assumed effective heat of combustion term. This uncertainty can be reduced if the composition of the fuel is known. Or to a lesser degree if additional gases are measured such as CO_2, CO and H_2O. The uncertainty of the calculation is very strongly coupled to any assumed combustion expansion at lower HRR values. This uncertainty can be reduced if the composition of the fuel is known, or if additional analysers (CO_2, CO and H_2O) are used to measure the species. If the fuel composition is unknown any uncertainty analysis needs to include due allowance for the combustion expansion as it is significant. The uncertainty of the calculation is very strongly coupled to the oxygen analyser uncertainty if the analyser is allowed to vary up to its proprietary uncertainty (beyond the +/- 100 ppm by volume specified in the standard). This is not surprising, because the measurement range is a relatively small difference with an increasing uncertainty. Such a disproportional uncertainty contribution of the oxygen analyser may not be necessary. Further research is necessary to quantify the reduction in the oxygen component of the overall uncertainty by using a suppressed zero measuring range or otherwise measuring the oxygen difference directly.

The thermochemistry technique used is a valid technique for calculating the calibration constant used in the cone calorimeter. This alternative method is independent of the oxygen concentration and has been shown to have a marginally lower uncertainty compared to the Standard method. Although, the Standard method remains the preferred technique for calculating the calibration constant as it is based on the operating principle of the apparatus and includes an oxygen measurement term. The simplicity of the final equation for the alternative method makes it easy to incorporate into software used on the cone calorimeter and can be used as a means of checking/troubleshooting the system.

8.2.3 PART C: 'Instrumentation and validation of furniture fire modelling'

A pronounced fabric affect is demonstrated in both the small-scale samples and full-scale items. During the cone calorimeter tests, the fabric showed a trend to either (i) melt and peel, or (ii) split and remain in place – that is, to become char forming. In first phenomena there is typically a large single peak with both fabric and foam contributing to the energy in a similar manner. The second phenomena is more complex. A single sharp first peak is observed followed by a lower slower 'foam' peak. The first peak is believed to the rapid combustion of pyrolozates previously decomposed by the radiant source of both the fabric and initial foam. The foam then melts and drops below the surface of the fabric. Once all the readily

combustible fuel is consumed off the charring fabric – for example polypropylene fibre on cotton backing – then the energy transfer from the heater element can focus on the molten foam pool. This drives the second foam peak.

Relative to CBUF items overall, the NZ-CBUF armchairs exhibited significantly higher peak HRR for relatively similar total heat. From this we can qualitatively deduce quicker times to peak HRR - unfortunately times to peak HRR are not recorded in CBUF.

Exemplary NZ items do not include combustion modified or high resilience foams or fire resistant fabrics or interliners. In comparison to equivalently composed European items, the peak HRR results were more comparable, although still generally higher.

Unfortunately, the NZ-CBUF sample size is too small to make formal statistical observations in respect to the goodness of the fit of the data to Model I. Qualitatively, we observe that the CBUF Model I is not a good predictor of the behaviour of the exemplary NZ furniture tested. The lack of a goodness of fit of the data to the model is especially pronounced in the peak HRR. Qualitatively, it is assumed that only a minor proportion of the lack of goodness of fit of the model is due to the instrument and assumption uncertainty – developed in detail in CHAPTER 5: 'Propagation of uncertainty of heat release rate measurement'. This is believed to be outweighed by the uncertainties of the highly empirical nature of Model I which is based on a regression analyses.

If not using the thickness scaling sub-model, then the NZ-CBUF results, which are all in the region of higher peak HRR, tend to deny a partial dependence and tend to suggest applying only regime $\{2\}$ (that is $\dot{Q}_{peak} = 14.4 \cdot x_1$) for style $\{1\}$.

The correlating variable x_1 is strongly coupled to the mass of soft combustibles - and the peak HRR prediction is more or less linearly proportional to x_1. The dependence is demonstrated in Figure 54. Many items are clustered in a relatively narrow vertical band - especially items 1 to 5 where only the mass of the fabric varies - yet the cone and furniture calorimeter HRR histories vary greatly. This qualitatively suggests an over dependence on mass of combustibles in calculating x_1 .

Within NZ-CBUF there are two predictive scenarios, (i) without thickness scaling and using 5s running averaging and (ii) with thickness scaling and using 30s running averaging. In the second case the following differences were observed:

The peak HRR prediction is 'artificially' improved, not surprising given that the 30 s averaging significantly lowers peak 'actual' 5 s peaks. In addition, the higher $\dot{q}''_{300}$, q'' and subsequent x_1 lead increased predicted peaks. Often by changing the regime to $\dot{Q} = x_2$. The total energy prediction is significantly worsened – albeit in a conservative manner as the energy is over-predicted. This is also not surprising given that thickness scaling 'artificially' increases $\Delta h_{c,eff}$. The 30 s running averaging does not effect the prediction of total heat. The time to peak HRR prediction is again significantly and 'artificially' worsened – and again in a conservative manner as the time is under predicted. This is also not a surprising due to the affect of the 30 s averaging slowing the response of the measured result.

Qualitatively, Model II provides a reasonable predictive tool for items 1 to 5 alone and to a lesser degree items 1 to 5 with 6-8 included. In either case, qualitatively it is a better prediction tool than Model I. This is an expected result as the 'deconvolution' works backward from the measured full-scale data. See the 'feedback' comments below.

The real test of Model II is to extrapolate it by applying it to bench-scale samples corresponding to the similar style full-scale items. Then to test the full-scale item without including that particular full-scale effective area to the dimensionless function. As described above all predictions in the NZ-CBUF data set actually effect the outcome as all are contributing to the effective area function. Unfortunately, this is necessary due to the small data set.

Model II is more useful than Model I in that it characterises the HRR history rather than just a few properties.

There is positive feedback in the Model II results. This is because all of the items - for which predictive HRR histories were compared with measured – themselves contributed to the effective area growth function. This positive feedback may provide overly optimistic verification results, especially in small data sets. It is one of the aims of the Models to

supersede - or at least minimise – full-scale testing. Future research should include verification of full-scale items not contributing to the effective area growth function.

The objectives of this phase of NZ-CBUF is to verify the applicability of the Models. The data set is too limited in the number of items tested to draw meaningful conclusions of effects of materials and design on fire performance (combustion behaviour). The CBUF Final Report discusses in detail the positive effects of various design aspects. We would assume that these strategies apply to NZ furniture and this is an obvious direction for future research.

8.3 Future research

8.3.1 PART A: Calorimetric technique

The instrumentation set-up is workable but clumsy. Different instruments have different conditioning and therefore different time lags. Some instruments are slower than others and have slow response times and dubious accuracy. One remedy worth investigation is to consider using a mass spectrometer in place of the species measurements.

The mass spectrometer, while more expensive than any one single-species gas analyser, is less expensive that any two. It has the significant advantage of measuring many species. Including all those of calorimetric interest O_2, CO_2, CO, H_2O as well of those toxic gases commonly measured in the exhaust. The mass spectrometer is more accurate, faster and will measure all species at the same time interval.

It would be encouraging to analytically address the contribution of volume changes in the calorimeter sampling system response time delays. This was found to be significant in the development of the UC Cone Calorimeter. Volume changes along the sampling line – such as the cold-trap, its separation chamber and desiccant holders – each significantly elongated the characteristic response to a plug flow. It was found necessary to reduce these volumes to get the characteristic response times down to an acceptable level. It would be a worthwhile exercise to approach this problem analytically and try and describe the elongation via use of characterising ‘concentration mixing’ differential equations. This would be of value in post-analysis adjusting of response times.

8.3.2 PART B: Uncertainty analysis of HRR measurement

The uncertainty analysis should be expanded twofold. On the one hand, probabilistic distributions could be developed for component uncertainty instead of the rectangular distributions. On the other, measures should be explored to account for the random uncertainties associated with the fuel and random and systematic uncertainties associated with human operation. The most obvious solution is to introduce a factor to the calculated uncertainties. This should be explored in more detail.

Uncertainty equations of HRR measurement via the thermochemistry technique should be developed to complement the oxygen consumption technique uncertainty equations developed in this work. An 'effective heat of formation' term could be developed for the fuel similar to Huggett's constant for oxygen consumed. It is an expected result that the effective heat of formation would have a larger uncertainty that the ±5% often attributed to Huggett's constant. Tewarson[30] reports a value of ±11%. However, given the greater simplicity of the thermochemistry equations and the independence of the oxygen term many useful tools may result. This includes the possibility that for a given variation of heat of formation the thermochemistry technique may yet be more accurate than oxygen consumption. If this were the case, then disposing of the requirement to measure oxygen would be desirable as the paramagnetic oxygen analysers are typically slow to respond, are prone to being inaccurate if not carefully controlled and they require special conditioning of the sample.

8.3.3 PART C: 'Instrumentation and validation of furniture fire modelling'

The NZ-CBUF data set is of limited size. Therefore, further research is required to expand this data set. Different combinations of common foams and fabrics (statistically sampled) should be tested in the cone calorimeter and furniture calorimeter on a standard frame. In particular more work should be done with interliners as the European study shows these can have a positive effect.

An expanded data set will allow more statistically meaningful conclusions to be drawn analytically. In particular, regarding the applicability of CBUF Model I and II and in general of combustion behaviour. In addition to statistically considering the NZ-CBUF data in isolation, future research should incorporate it into the CBUF data set, with wider comments made and conclusions drawn. An expanded data set should include full-scale verification of CBUF Model II using items outside of the feedback loop. In addition to future research

continuing the verification and refinement of Models I and II, it should begin the task of developing strategies for improved design of NZ furniture.

NOTATION

Greek notation

α expansion factor (--)

β stoichiometric expansion factor (--)

δz uncertainty (absolute) associated with variable "z" i.e. $\delta \dot{q}'', \delta \dot{Q}$

ϕ oxygen depletion factor (--)

ρ_e density of exhaust gas ($kg.m^{-3}$)

ρ_{ref} reference density of air ($kg/^{m-3}$)

Notation

A cross sectional area of the duct (m^2)

A_0 flow area of orifice plate (m^2)

C calibration constant ($m^{\cdot}kg^{\cdot}K$)

C_1 mass flow rate constant in the small-scale ($m^{\cdot}kg^{\cdot}K$)

C_2 mass flow rate constant in the full-scale ($m^{\cdot}kg^{\cdot}K$)

C_O calibration constant calculated via O_2 consumption technique ($m^{\cdot}kg^{\cdot}K$)

C_T calibration constant calculated via thermochemistry technique ($m^{\cdot}kg^{\cdot}K$)

C_x mass flow rate constant ($m^{\cdot}kg^{\cdot}K$)

D duct diameter (m)

$f(\mathrm{Re})$ instrument dependent correction as a function of the Reynolds number (--)

g_c gravitational constant, value of 1.0 ($kg^{\cdot}m^{\cdot}N^{-1\cdot}s^{-2}$)

Δh_c net heat of combustion ($kJ^{\cdot}kg^{-1}$)

$\Delta h_{c,eff}$ effective heat of combustion of the bench-scale composite sample ($MJ.kg^{-1}$)

$\left(\Delta H_f^o\right)_i$ enthalpy of formation of species i at 25°C ($kJ^{\cdot}kg^{-1}$)

k_c velocity shape factor (--)

$m_{comb,total}$ mass of the total combustible material of the full-scale item (kg)

m_{soft} mass of the soft combustible material of the full-scale item (kg)

$\dot{m}_e$ mass flow rate of exhaust gases ($kg^{\cdot}s^{-1}$)

$\dot{m}_i^o$ mass flow rate of species i in the incoming air ($kg \cdot s^{-1}$)

$\dot{m}_i$ mass flow rate of species i in the exhaust gases ($kg \cdot s^{-1}$)

M_a molecular weight of ambient incoming air ($g \cdot mol^{-1}$)

M_{CO} molecular weight of carbon monoxide ($g \cdot mol^{-1}$)

M_{CO_2} molecular weight of carbon dioxide ($g \cdot mol^{-1}$)

M_{dry} molecular weight of dry ambient incoming air ($g \cdot mol^{-1}$)

M_e molecular mass of exhaust gases ($kg \cdot mol^{-1}$)

M_{H_2O} molecular weight of H_2O ($g \cdot mol^{-1}$)

M_i molecular mass of species i ($kg \cdot mol^{-1}$)

M_{N_2} molecular weight of nitrogen ($g \cdot mol^{-1}$)

M_{O_2} molecular weight of oxygen ($g \cdot mol^{-1}$)

n number of moles (--)

n_i moles of species i (mol)

n_i^g moles of species i generated (mol)

n_{fuel}^l moles of fuel combusted (mol)

Δp differential pressure (Pa)

P_a atmospheric pressure (Pa)

$P_s(T_a)$ saturation pressure of water vapour at T_a (Pa)

q'' total heat released per unit area of the bench-scale composite sample ($MJ.m^{-2}$)

Q total heat released of the full-scale item (MJ)

$\dot{q}''_{300}$ HRR per unit area (bench-scale) averaged over 300 s from ignition ($kW.m^{-2}$)

$\dot{q}''_{pk}$ peak HRR per unit area of the bench-scale composite sample ($kW.m^{-2}$)

$\dot{q}''_{pk\#2}$ second peak HRR per unit area (bench-scale) ($kW.m^{-2}$)

$\dot{q}''_{trough}$ trough between two peak HRR, per unit area (bench-scale) ($kW.m^{-2}$)

$\dot{Q}$ HRR, measured or predicted, of the full-scale item (kW)

$\dot{Q}_{pk}$ peak HRR, measured or predicted, of the full-scale item (kW)

r_0 stoichiometric oxygen to fuel ratio (--)

RH relative humidity (%)

$style\_fac$ characteristic style factor A or B of the full-scale item (--)

t_{ig} time to ignition of the bench-scale composite sample (s)

t_{pk} time to peak HRR of the full-scale item (s)

$t_{pk\#1}$ time to characteristic 'first' peak of the bench-scale composite sample (s)

t_{UT} time to untenable conditions in a standard room (s)

T_a ambient temperature of incoming air (K)

T_e absolute gas temperature at orifice meter (K)

T_{ref} reference temperature of air (K)

v velocity ($m \cdot s^{-1}$)

$\bar{v}$ average velocity ($m \cdot s^{-1}$)

v_c centreline velocity ($m \cdot s^{-1}$)

$v(y)$ velocity at point y along the duct diameter ($m \cdot s^{-1}$)

$\dot{V}$ volumetric flow rate ($m^3 \cdot s^{-1}$)

x_1 correlating variable in CBUF Model I (--)

x_2 correlating variable in CBUF Model I (--)

x_i^o ambient mole fraction of species i, excluding H_2O (--)

x_i mole fraction of species i (--)

x_i^a measured (by analyser) mole fraction of species i (--)

x_i^g mole fraction of species i generated (--)

x_i^o ambient mole fraction of species i (--)

REFERENCES

1 Thornton, W. "The Relationship of Oxygen to the Heat of Combustion of Organic Compounds" *Philosophical Magazine and Journal of Science* **33** pp196-203 (1917)

2 Huggett, C. "Estimation of Rate of Heat Release by Means of Oxygen Consumption Measurements" *Fire and Materials* **4** pp61-65 (1980)

3 Janssens, M. and Parker, W. "Oxygen Consumption Calorimetry" Chapter 3 in: *Heat Release in Fires* Ed: V. Babrauskas & S. Grayson, Interscience Communications London, pp31-59 (1992)

4 Parker, W. J. "Calculations of the Heat Release Rate by Oxygen Consumption for Various Applications" *NBSIR 81-2427* National Bureau of Standards, Gaithersburg, MD (1982)

5 Janssens, M. L. "Measuring Rate of Heat Release by Oxygen Consumption" *Fire Technology* **27** pp235-249 (1991)

6 ISO5660.1 "Fire tests - Reaction to fire - Part 1: Rate of heat release from building products (cone calorimeter method) " *ISO5660-1:1993 (E).* International Standards Organisation, Geneva (1993)

7 NT FIRE 032. "Upholstered furniture: Burning behaviour – Full-scale test" Second Edition (1991)

8 Chang, R. "Thermochemistry" Chapter 6 in: *Chemistry (Fourth Edition)*, McGraw-Hill (1991)

9 Drysdale, D. D. "Thermochemistry" Section 1 Chapter 5 *The SFPE Handbook of Fire Protection Engineering (Second Edition)* Society of Fire Protection Engineers. Quincy, MA. (1995)

10 Holman, J. P. "Experimental Methods for Engineers" McGraw-Hill Book Company, USA. (1978)

11 McCaffrey, B. J. and Heskestad, G. "A Robust Bidirectional Low-velocity Probe for Flame and Fire Application" Brief Communications. *Combustion and Flame* **26** pp125-127 (1976)

12 Ross, D. and Robertson, J. "A Superposition Analysis of the Turbulent Boundary Layer in Adverse Pressure Gradient" *Journal of Applied Mechanics* **18** pp95-100 (1951)

13 Ower, E. and Pankhurst, R. "The Measurement of Air Flow" 5th Edition. Pergamon Press (1977)

14 Babrauskas, V. and Peacock, R. D. "Heat Release Rate: The Single Most Important Variable in Fire Hazard" *Fire Safety Journal* **18** pp255-272 (1992)

15 Janssens, M. L. "Calorimetry*"* Section 3 Chapter 2 *The SFPE Handbook of Fire Protection Engineering (Second Edition)* Society of Fire Protection Engineers. Quincy, MA. (1995)

16 ASTM 1354-90 "Standard Test Method for Heat and Visible Smoke Release Rates for Materials and Products using an Oxygen Consumption Calorimeter" *Annual Book of ASTM Standards ASTM 1354-90 (1995)* American Society for Testing Materials, Philadelphia (1995)

17 ISO9705 "Fire Tests - Full-scale Room Test for Surface Products" *ISO9705:1993 (E)* International Standards Organisation, Geneva (1993)

18 Ku, H. H. "Uncertainty and Accuracy in Physical Measurements" *NIST Special Publication 805* National Institute of Standards and Technology, Gaithersburg, MD (1990)

19 Baird, D. C. "Experimentation: An Introduction to Measurement Theory and Experiment Design" Prentice-Hall, Englewood Cliffs, New Jersey (1962)

20 Yeager, R. W. "Uncertainty Analysis of Energy Release Rate Measurement for Room Fires*"* *Journal of Fire Sciences* **4** pp276-296 (1986)

21 Babrauskas, V. "Development of the Cone Calorimeter – A Bench-scale Heat Release Rate Apparatus based on Oxygen Consumption" *Fire and Materials* **8**(2), pp81-95 (1984)

22 Babrauskas, V. "Development of the Cone Calorimeter – A Bench-scale Heat Release Rate Apparatus based on Oxygen Consumption" *NBSIR 82-2611* National Institute of Standards and Technology, Gaithersburg, MD (1982)

23 Hayward, A. T. J. *Flowmeters* The Macmillan Press Ltd, London, UK (1979)

24 Babrauskas, V. "The Cone Calorimeter" Section 3 Chapter 3 *The SFPE Handbook of Fire Protection Engineering (Second Edition)* Society of Fire Protection Engineers. Quincy, MA. (1995)

25 Enright, P. A. and Fleischmann, C. M. "Uncertainty of Heat Release Rate Calculation of the ISO5660-1 Cone Calorimeter Standard Test Method" *Fire Technology* **35**(2), pp153-169 (1999)

26 Sundstrom, B. (ed.) "Fire Safety of Upholstered Furniture – The final report on the CBUF research programme. Appendix A7 Furniture Calorimeter test protocol" *Report*

EUR 16477 EN Directorate-General Science (Measurements and Testing). European Commission. Distributed by Interscience Communication Ltd, London (1995)

27 ISO 5660.1 (DRAFT) "Fire tests - Reaction to fire - Part 1: Rate of heat release from building products (cone calorimeter method) " *ISO 5660-1 (DRAFT).* International Standards Organisation, Geneva. (1997)

28 Babrauskas, V. and Thureson, P. "Short Communication: Drying Agents' Effects on CO_2 Readings" *Fire and Materials* **18** pp261-262 (1994)

29 TB 133. "Technical Bulletin 133: Flammability test procedure for seating furniture for use in public occupancies" California, Department of Consumer Affairs (1992)

30 Tewarson, A. "Generation of heat and chemical compounds on fires" Section 3 Chapter 4 in: *The SFPE Handbook of Fire Protection Engineering (Second Edition)* Ed: J. DiNenno, Society of Fire Protection Engineers. Quincy, MA. (1995)

31 Verdin, A. "Gas analysis instrumentation" Macmillan Press, London, UK (1973)

32 Croce, P. A. "A method for improved measurement of gas concentration histories in rapidly developing fires" *Combustion Science and Technology* **14** pp221-228 (1976)

33 Babrauskas, V., and Krasny J. F., "Fire Behaviour of Upholstered Furniture" *NBS Monograph 173* US National Bureau of Standards, Gaithersburg, (1985)

34 Babrauskas, V., Baroudi, D., Myllymaki, J. and Kokkala, M. "The cone calorimeter used for predictions of the full-scale burning behaviour of upholstered furniture*" Fire and Materials*, **21**, pp95-105, (1997)

35 Wickstrom, U. and Goransson, U., "Full-scale/Bench-scale Correlation's of Wall and ceiling Linings" Chapter 13 in: *Heat Release in Fires* Ed: V. Babrauskas & S. Grayson, Interscience Communications London, pp461-477, (1992)

36 Myllymaki, J. and Baroudi, D., "Prediction of Heat Release Rate of Upholstered Furniture using Integral Formulation" Proceedings Interflam 1996, pp27-35, (1996)

APPENDIX A – FULL-SCALE FIRE TEST DATA

Item 1: A1S1

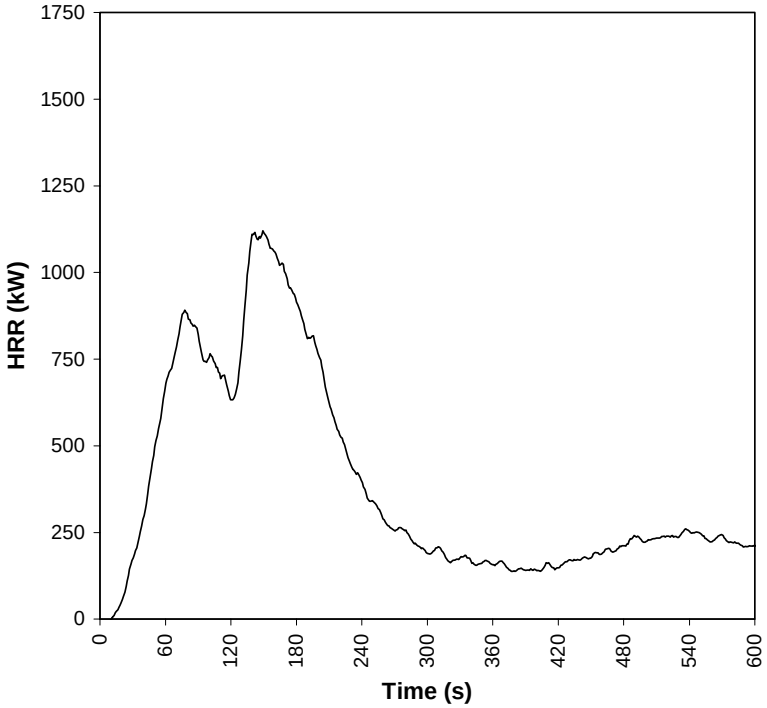

Figure I: Full-scale HRR history for item A1S1. Time zero is ignition.

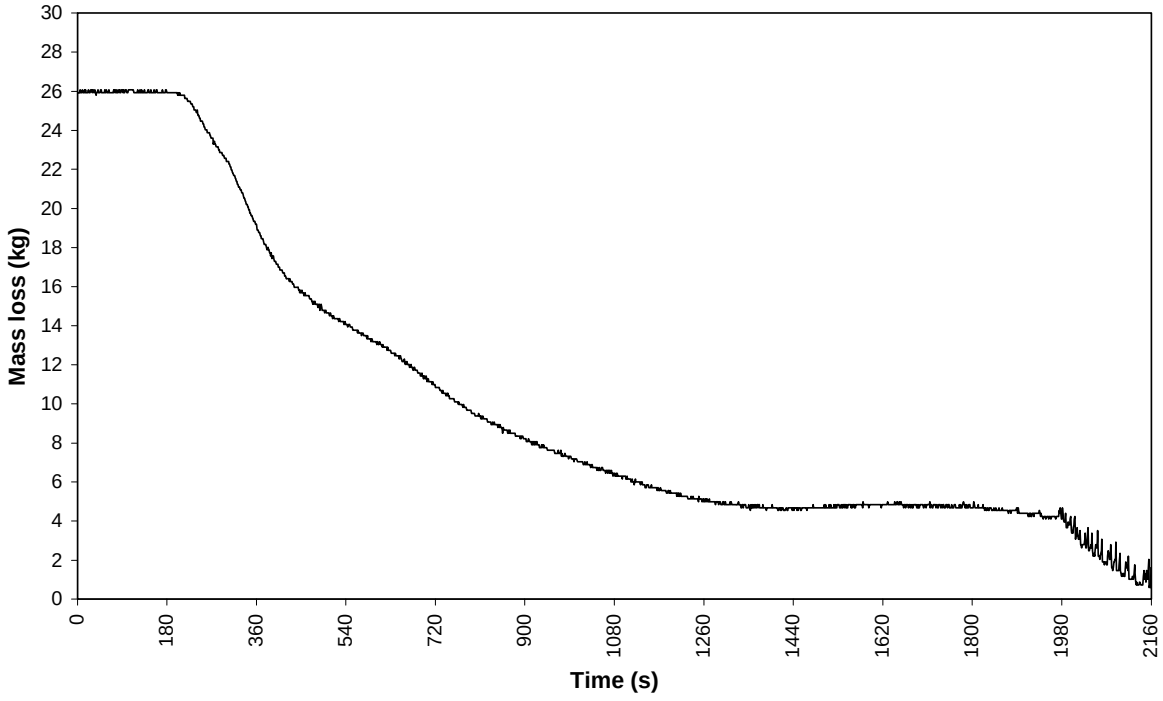

Figure II: Mass loss rate for item A1S1. Time zero is baseline. Ignition is 180s.

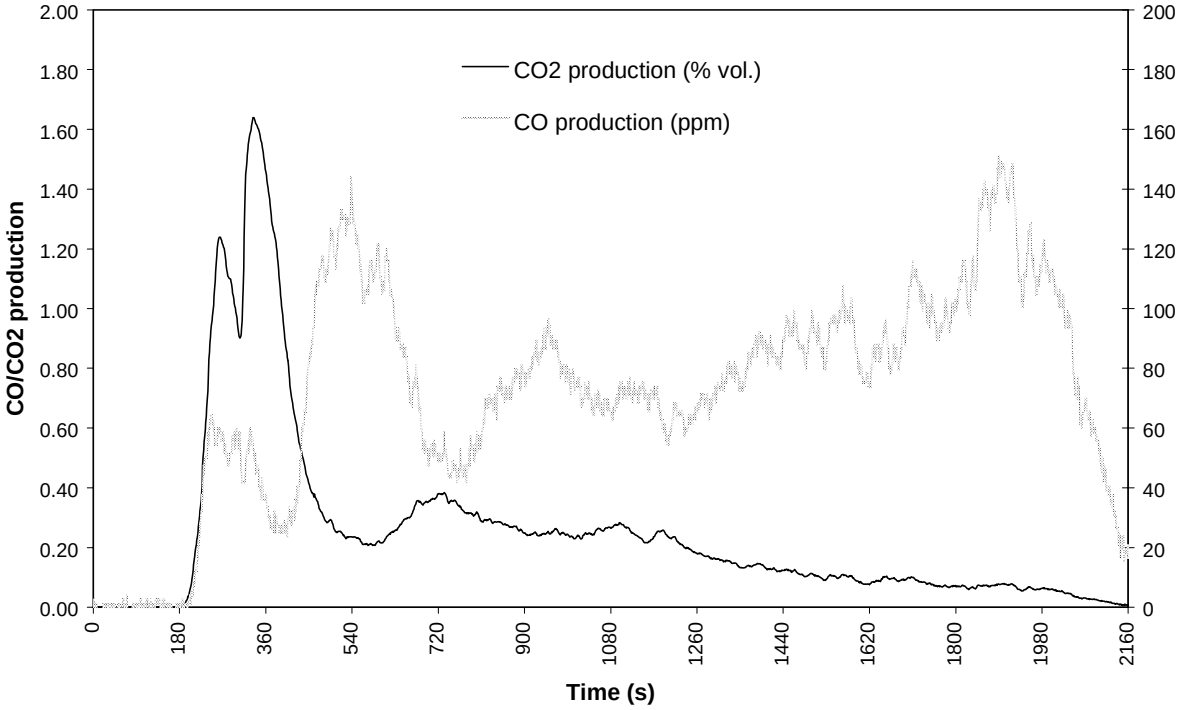

Figure III: CO_2 and CO production for item A1S1. Time zero is baseline. Ignition is 180s.

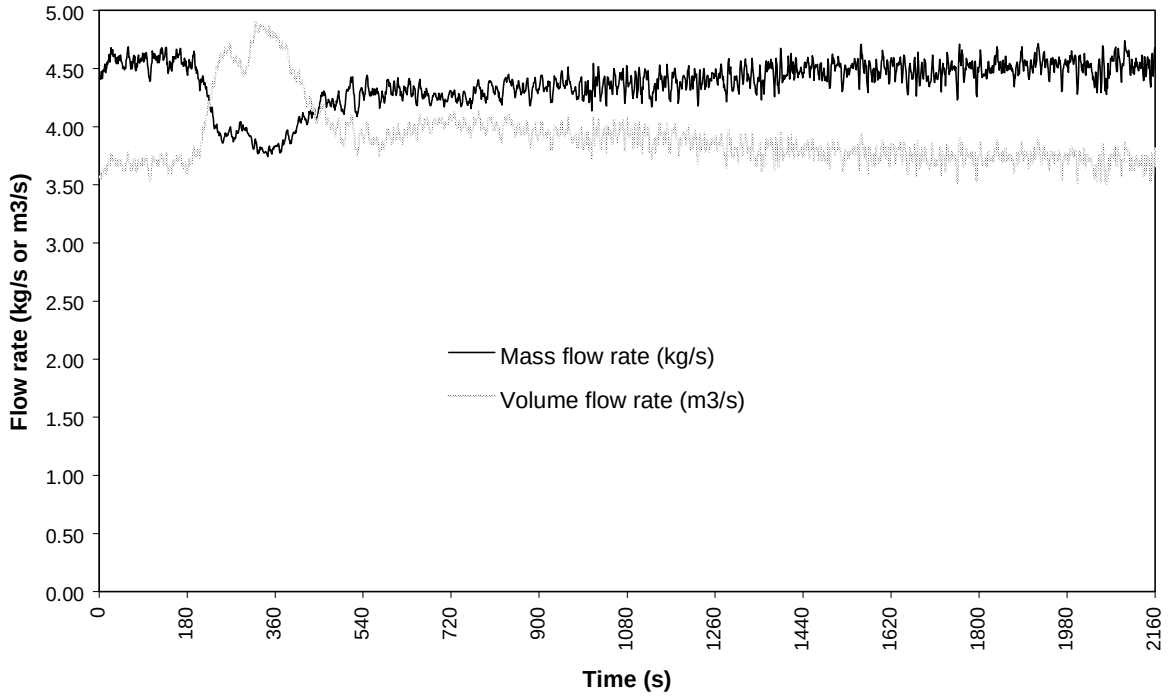

Figure IV: Mass flow rate and volume flow rate for item A1S1. Time zero is baseline. Ignition is 180s.

Item 2: A2S1

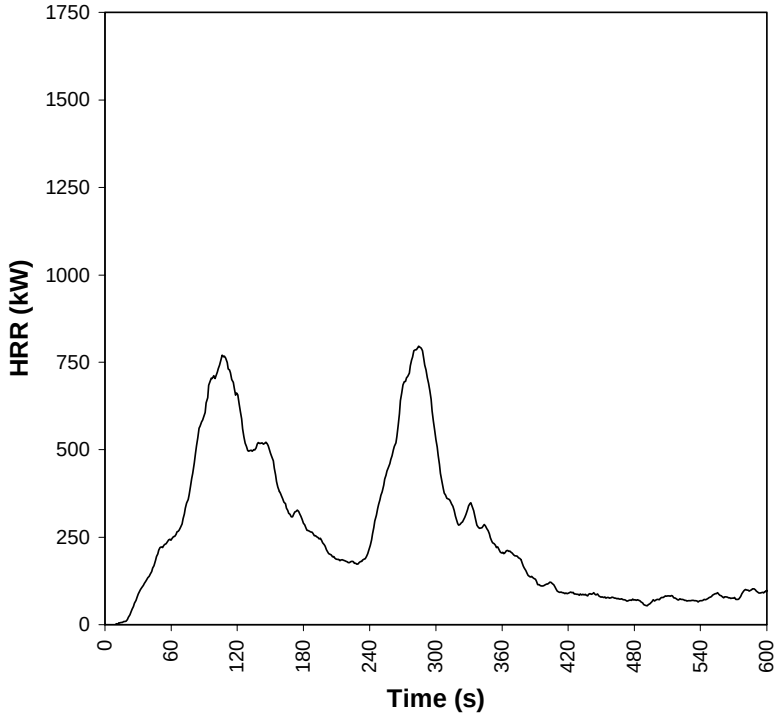

Figure V: Full-scale HRR history for item A2S1. Time zero is ignition.

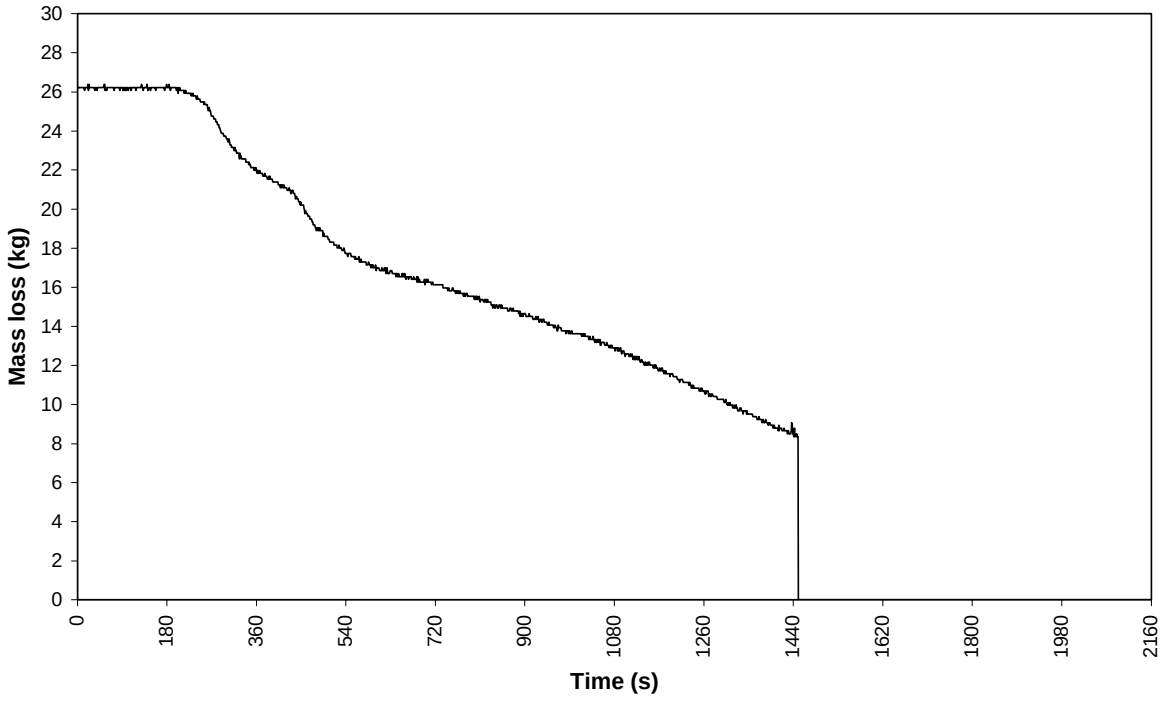

Figure VI: Mass loss rate for item A2S1. Time zero is baseline. Ignition is 180s.

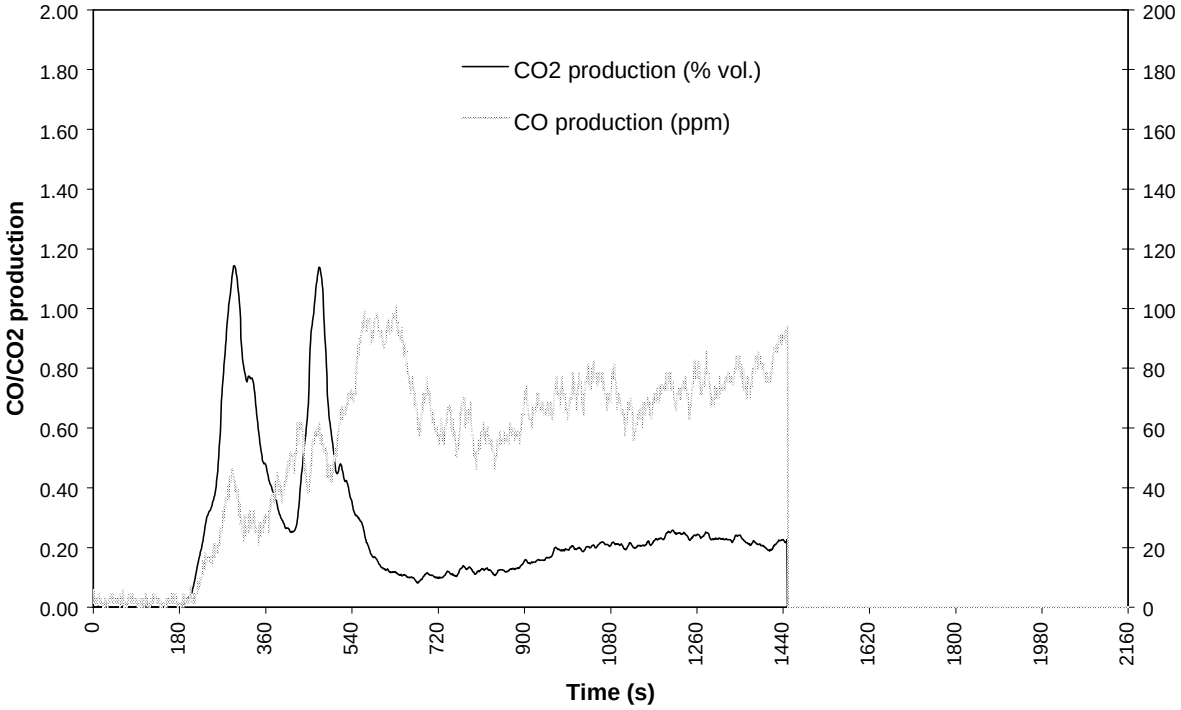

Figure VII: CO_2 and CO production for item A2S1. Time zero is baseline. Ignition is 180s.

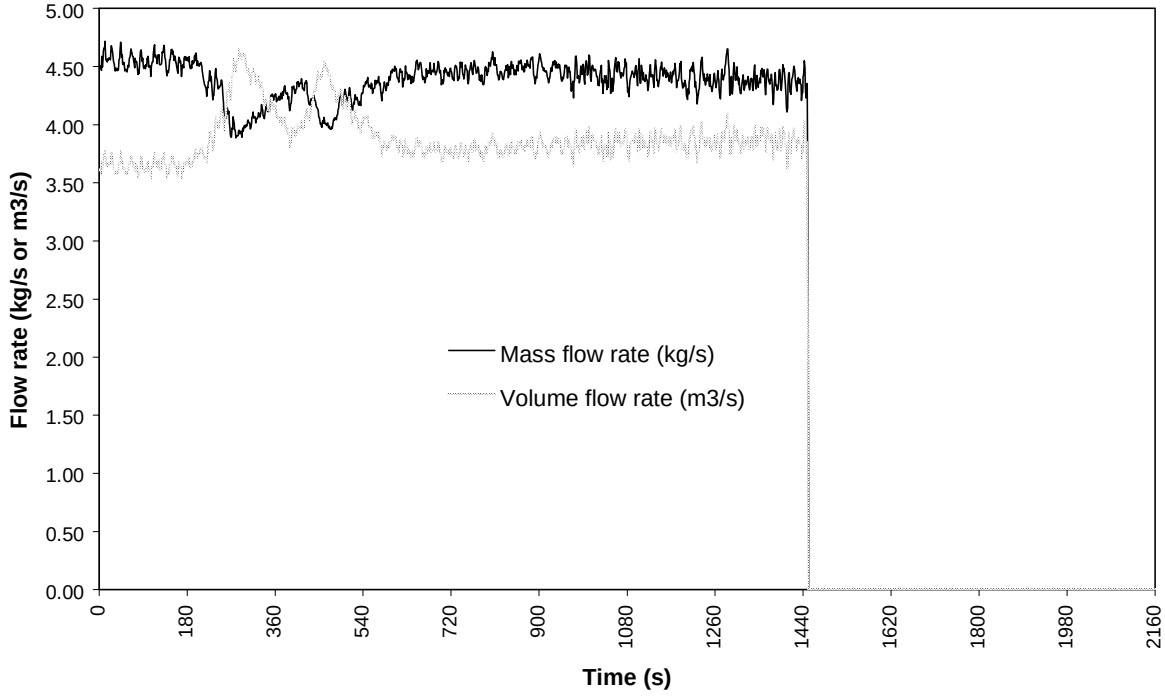

Figure VIII: Mass flow rate and volume flow rate for item A2S1. Time zero is baseline. Ignition is 180s.

Item 3: A3S1

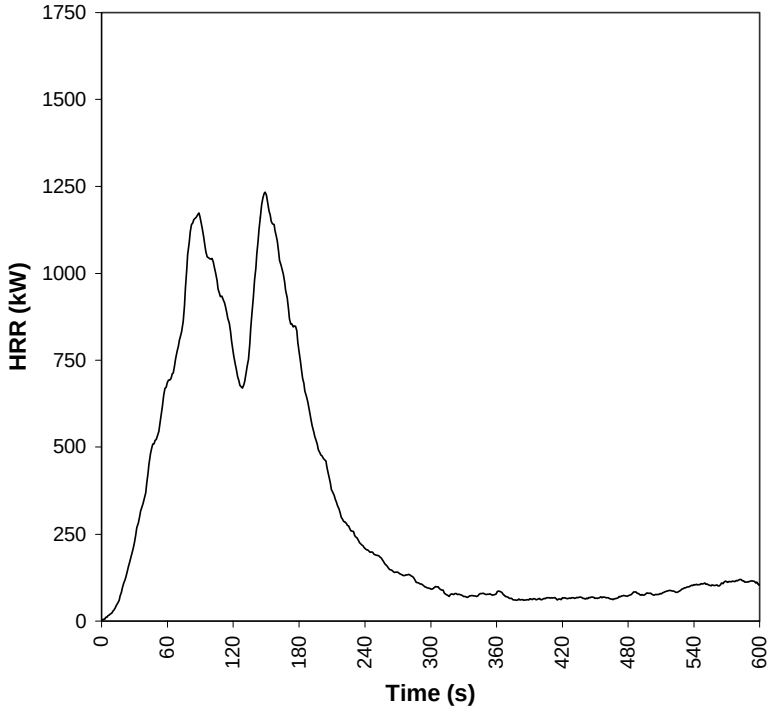

Figure IX: Full-scale HRR history for item A3S1. Time zero is ignition.

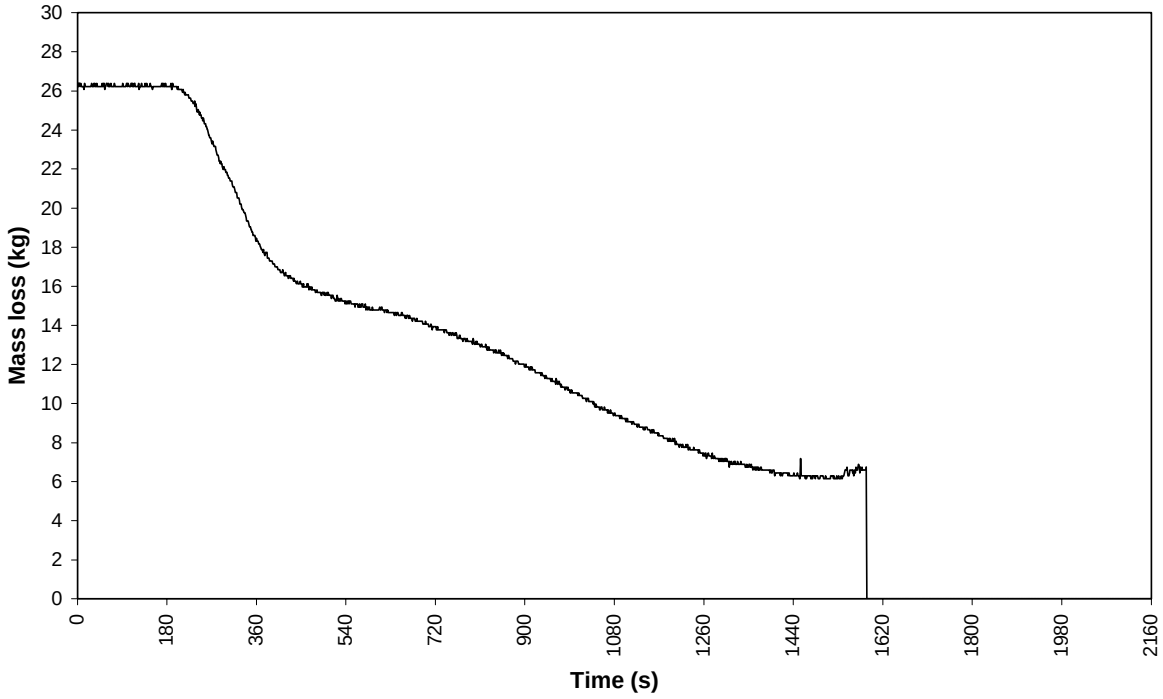

Figure X: Mass loss rate for item A3S1. Time zero is baseline. Ignition is 180s.

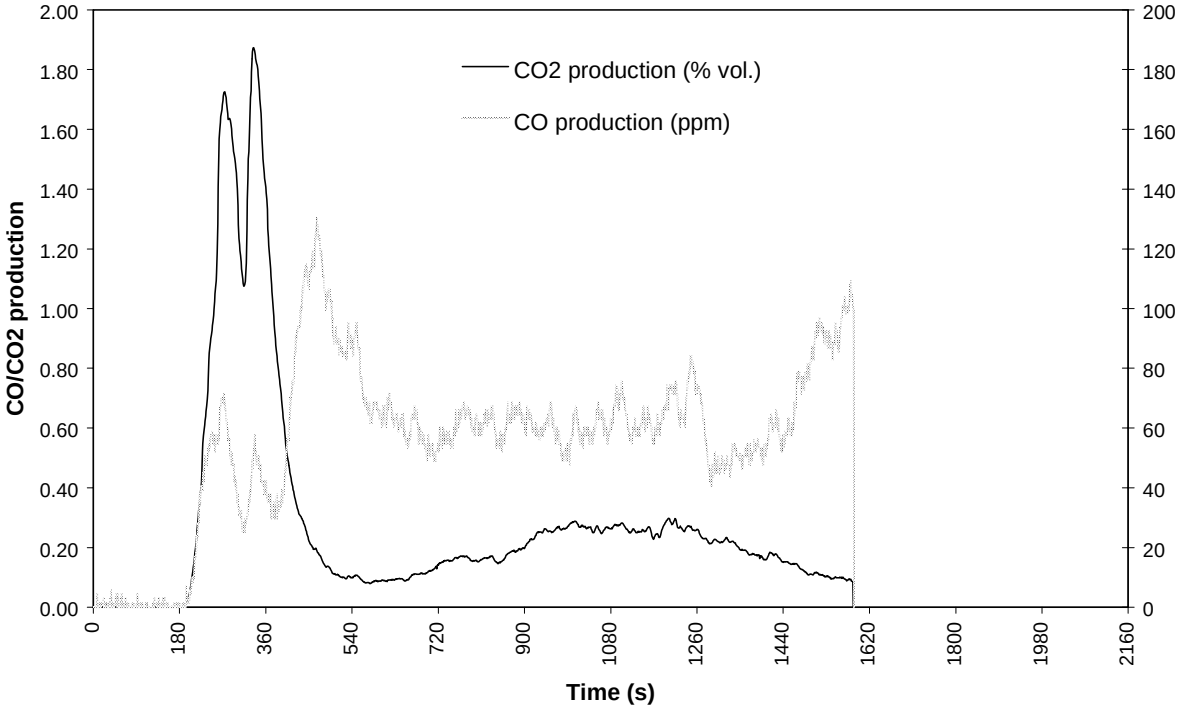

Figure XI: CO_2 and CO production for item A3S1. Time zero is baseline. Ignition is 180s.

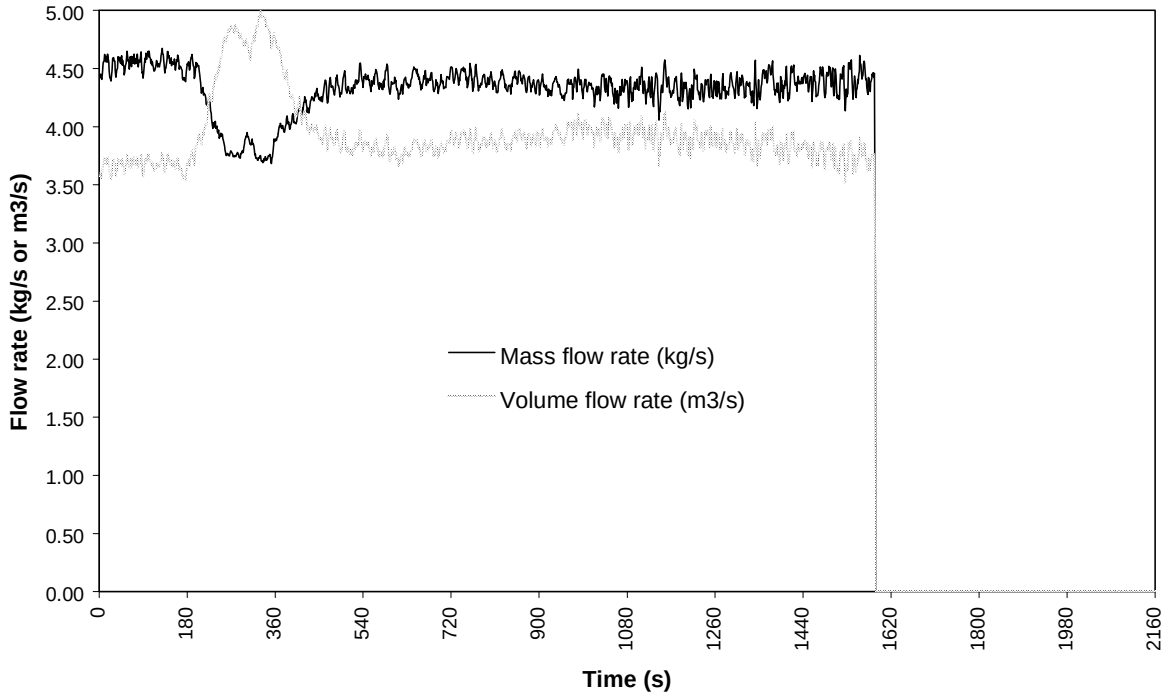

Figure XII: Mass flow rate and volume flow rate for item A3S1. Time zero is baseline. Ignition is 180s.

Item 4: A4S1

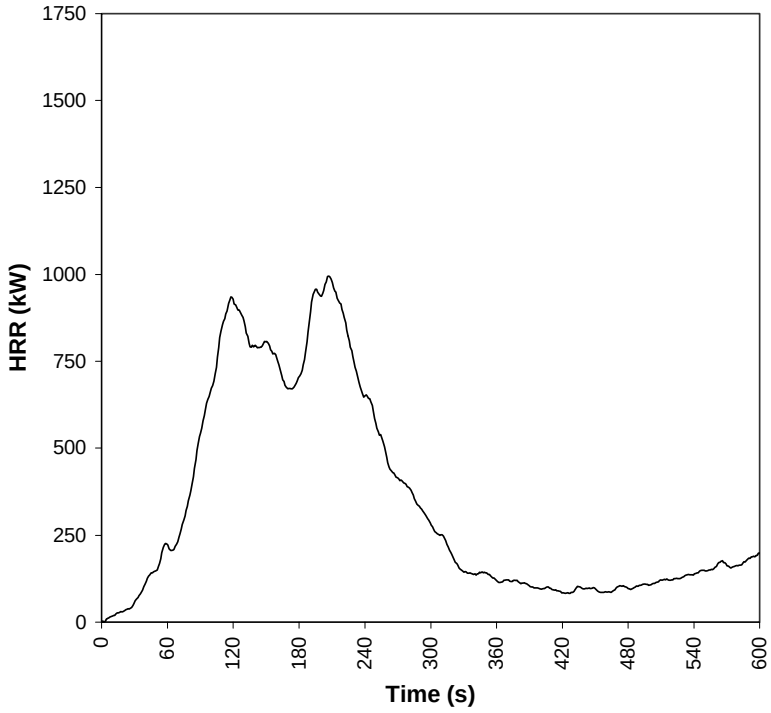

Figure XIII: Full-scale HRR history for item A4S. Time zero is ignition.

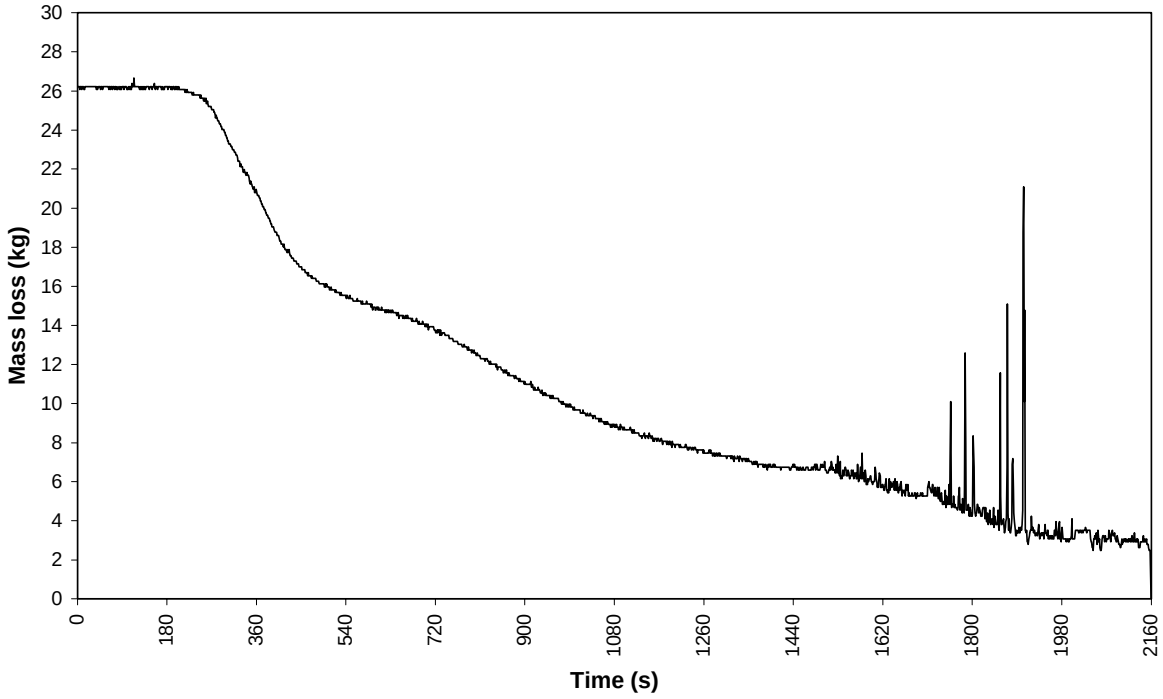

Figure XIV: Mass loss rate for item A4S1. Time zero is baseline. Ignition is 180s.

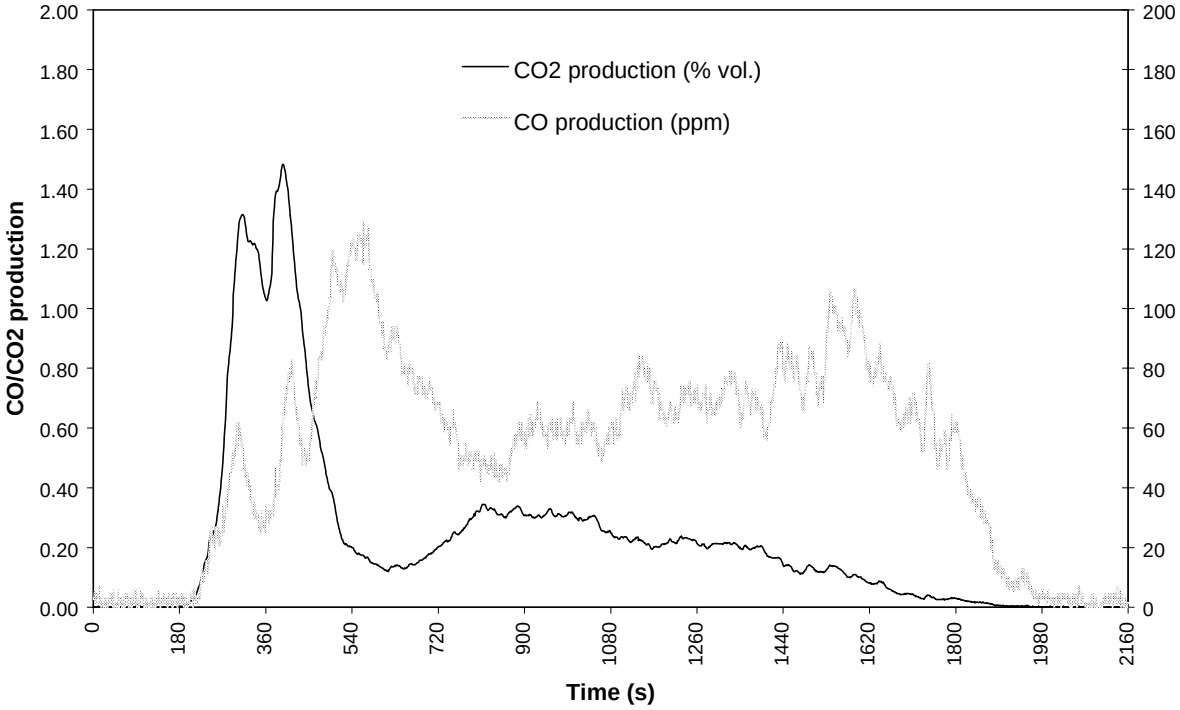

Figure XV: CO_2 and CO production for item A4S1. Time zero is baseline. Ignition is 180s.

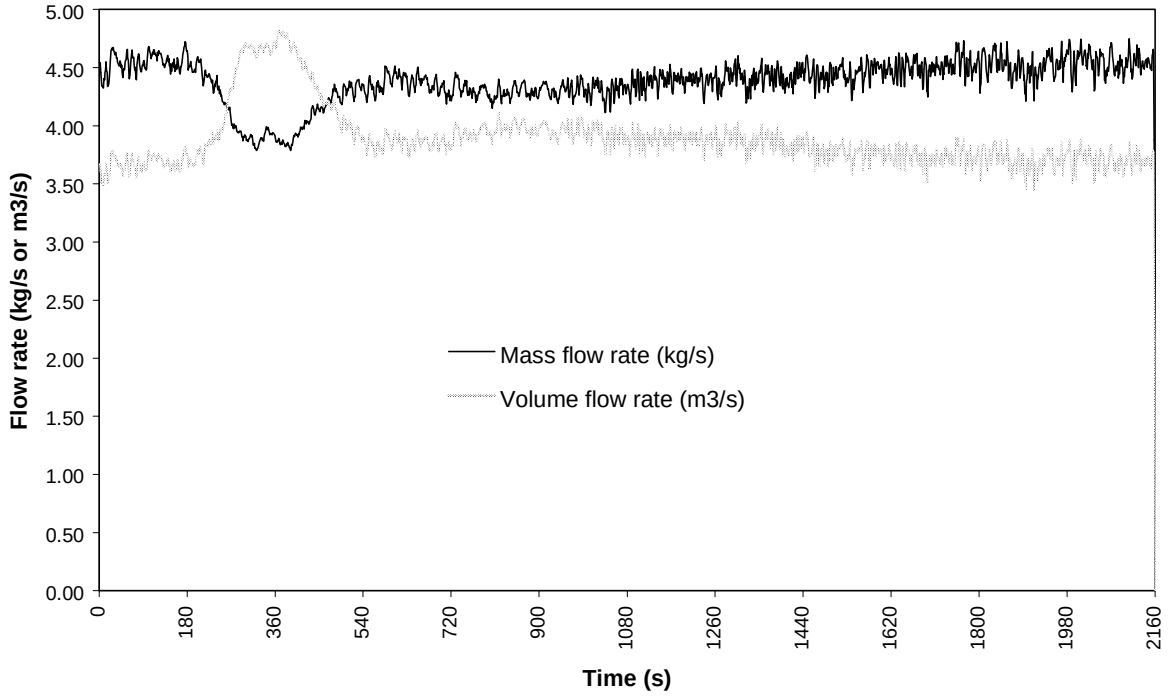

Figure XVI: Mass flow rate and volume flow rate for item A4S1. Time zero is baseline. Ignition is 180s.

Item 5: A5S1

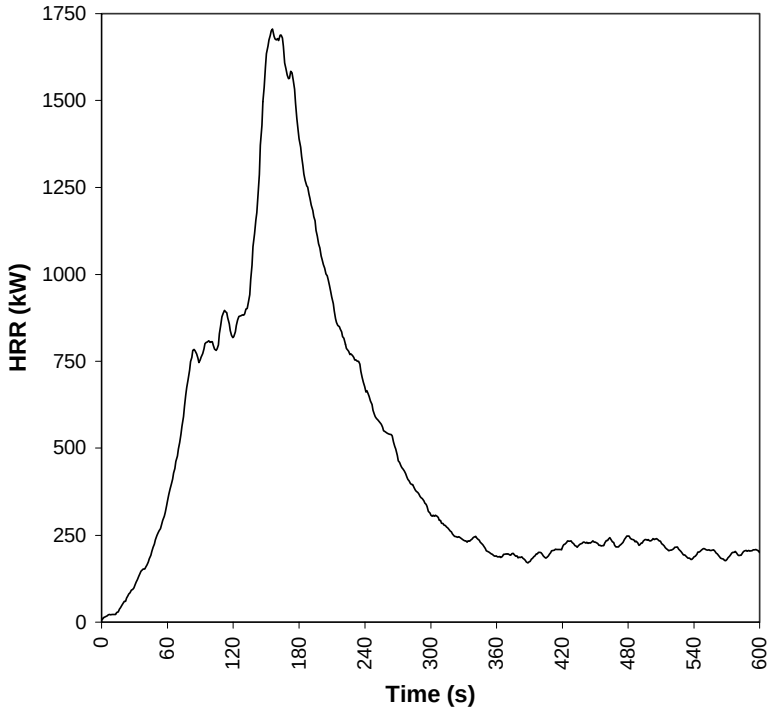

Figure XVII: Full-scale HRR history for item A5S. Time zero is ignition.

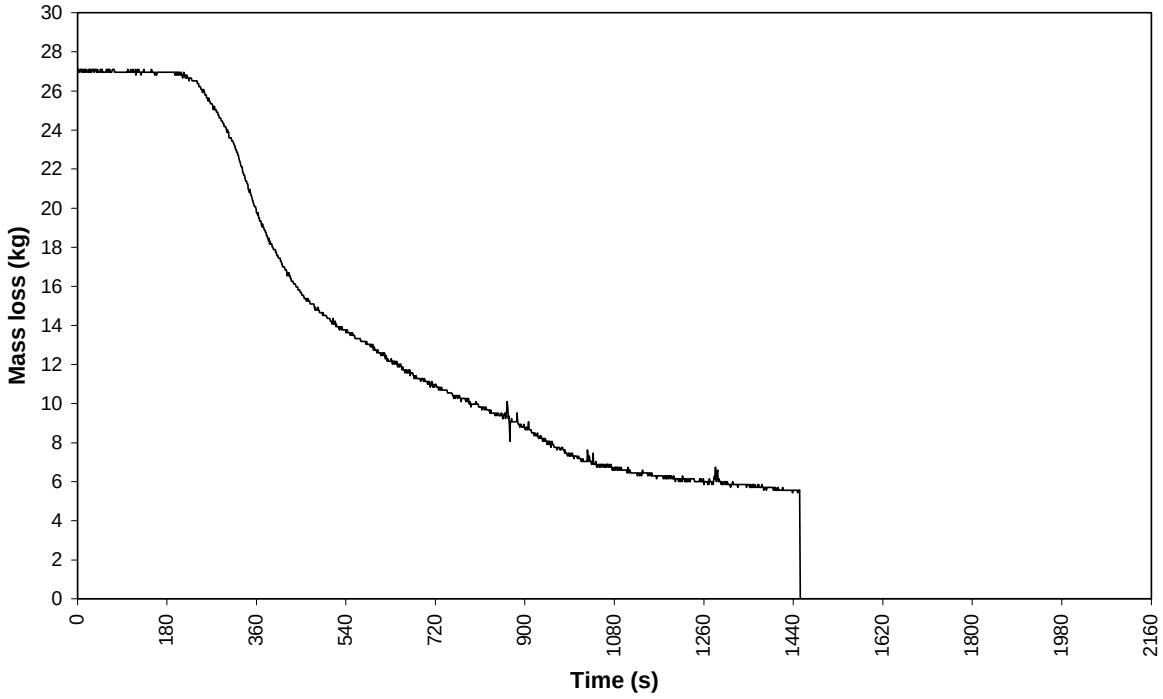

Figure XVIII: Mass loss rate for item A5S1. Time zero is baseline. Ignition is 180s.

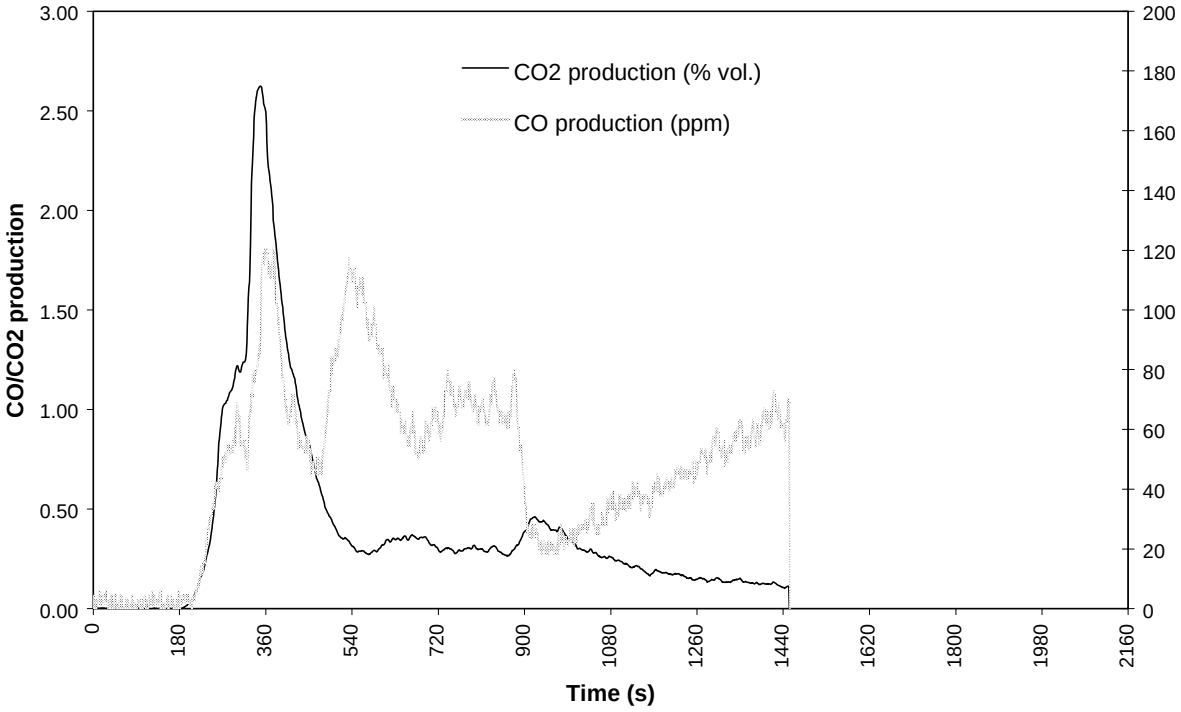

Figure XIX: CO_2 and CO production for item A5S1. Time zero is baseline. Ignition is 180s.

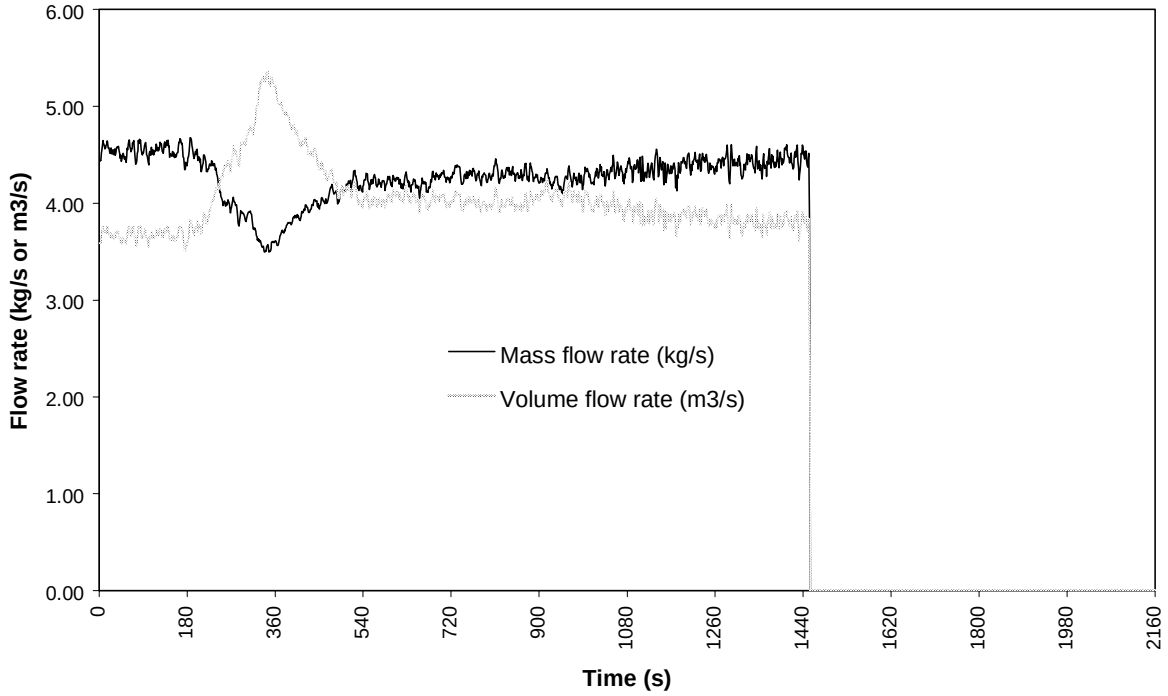

Figure XX: Mass flow rate and volume flow rate for item A5S1. Time zero is baseline. Ignition is 180s.

Item 6: B6S1

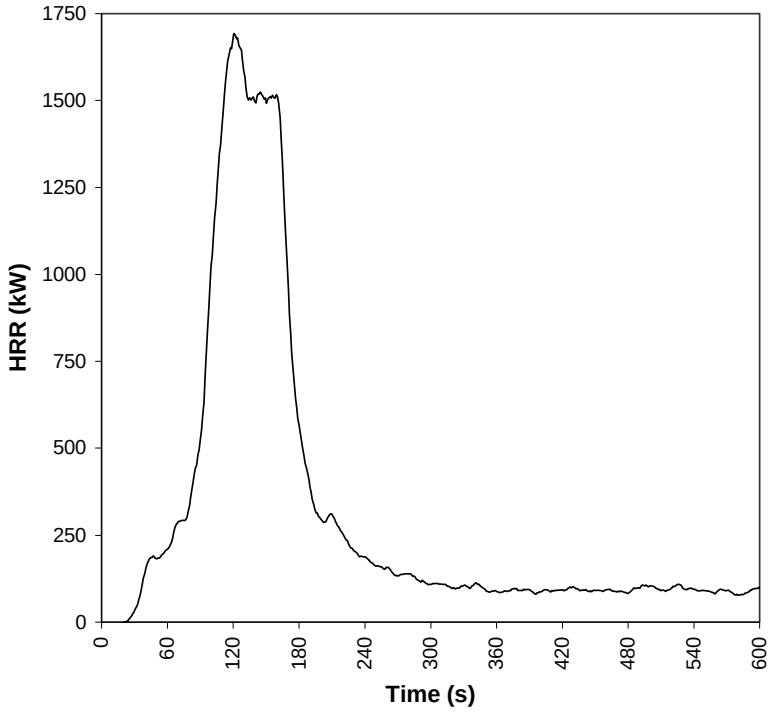

Figure XXI: Full-scale HRR history for item B6S1. Time zero is ignition.

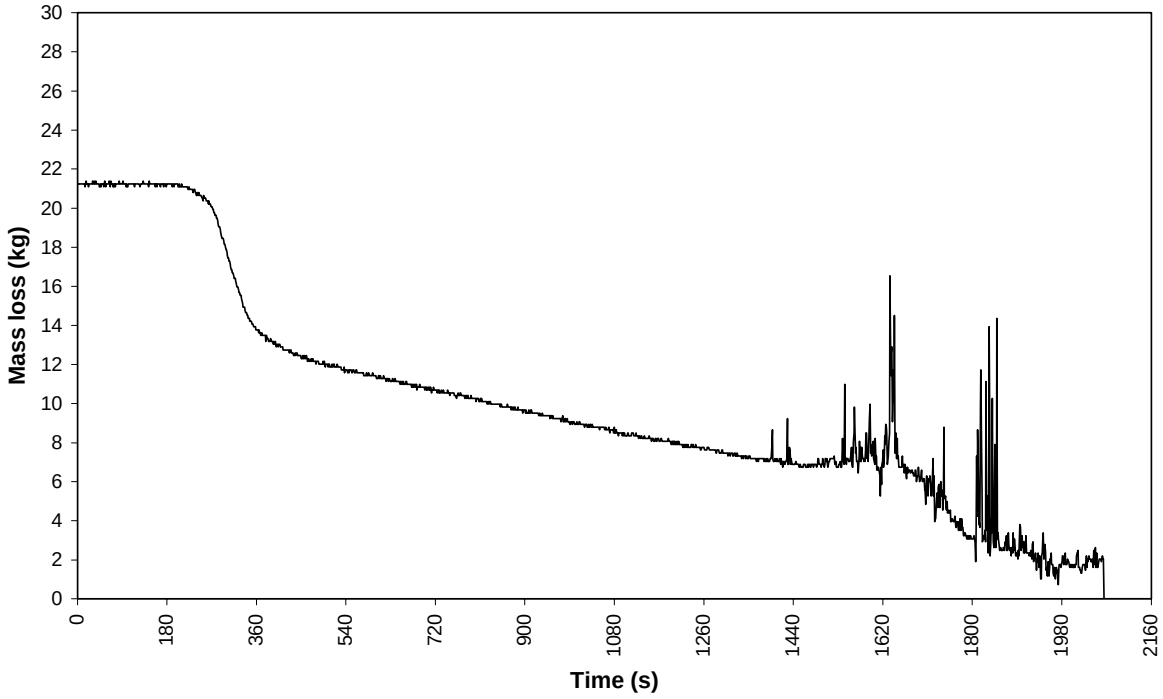

Figure XXII: Mass loss rate for item B6S1. Time zero is baseline. Ignition is 180s.

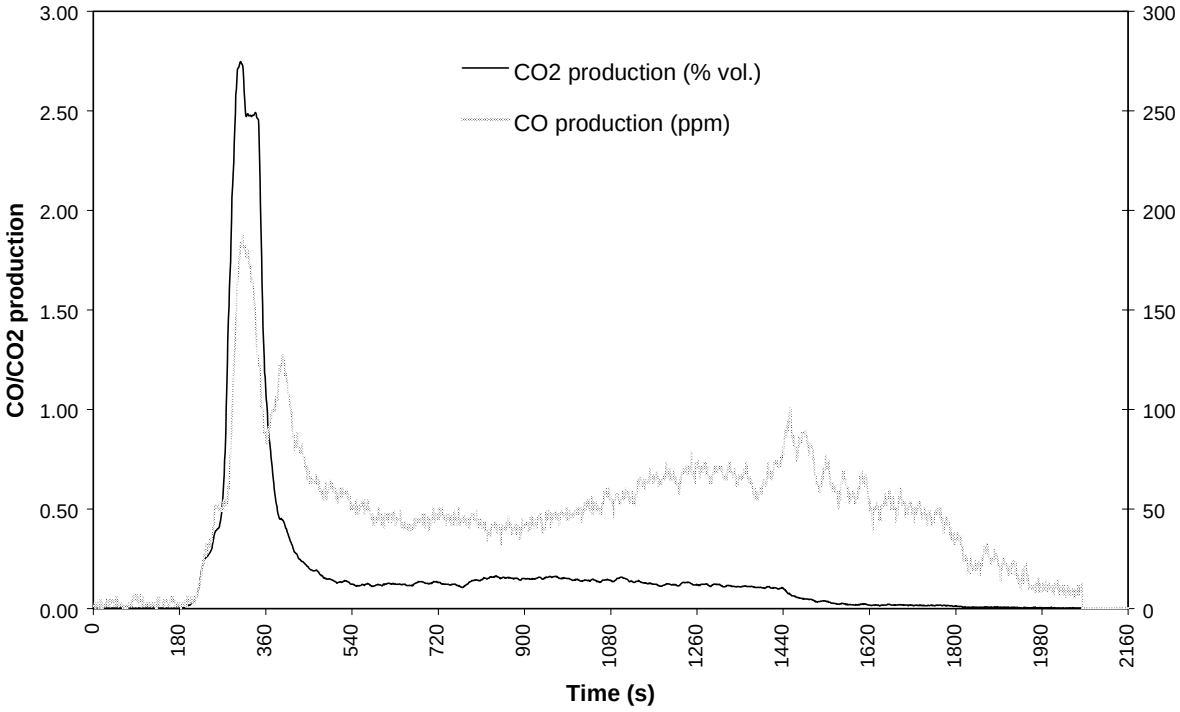

Figure XXIII: CO_2 and CO production for item B6S1. Time zero is baseline. Ignition is 180s.

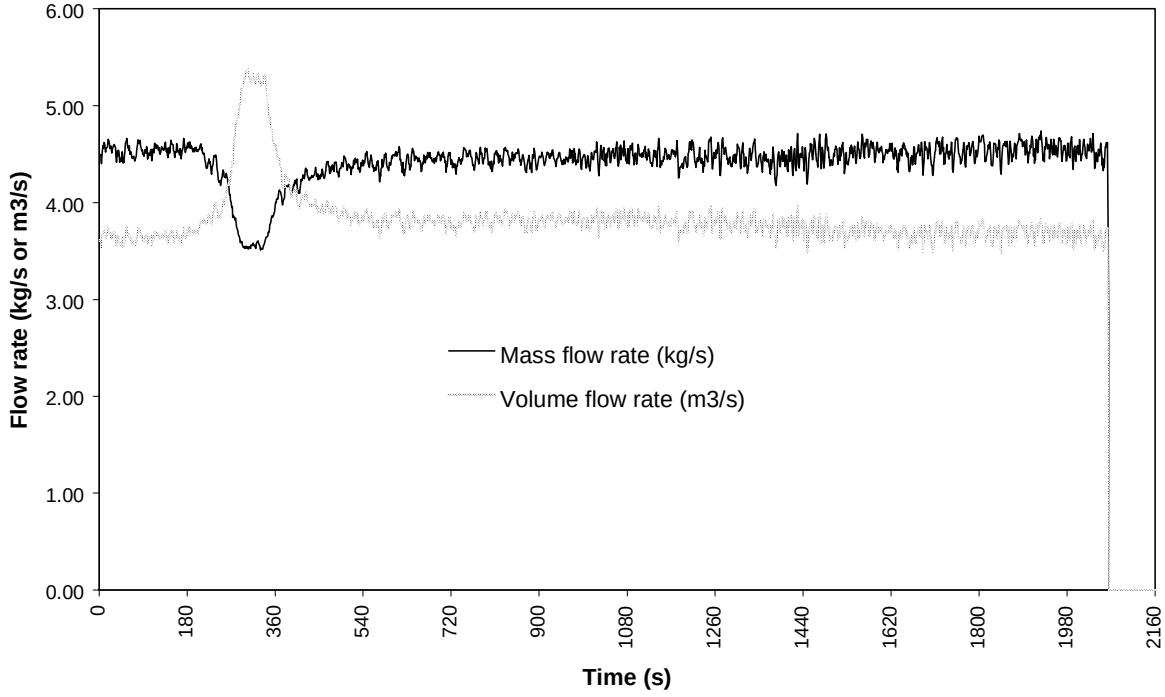

Figure XXIV: Mass flow rate and volume flow rate for item B6S1. Time zero is baseline. Ignition is 180s.

Item 7: C7S1

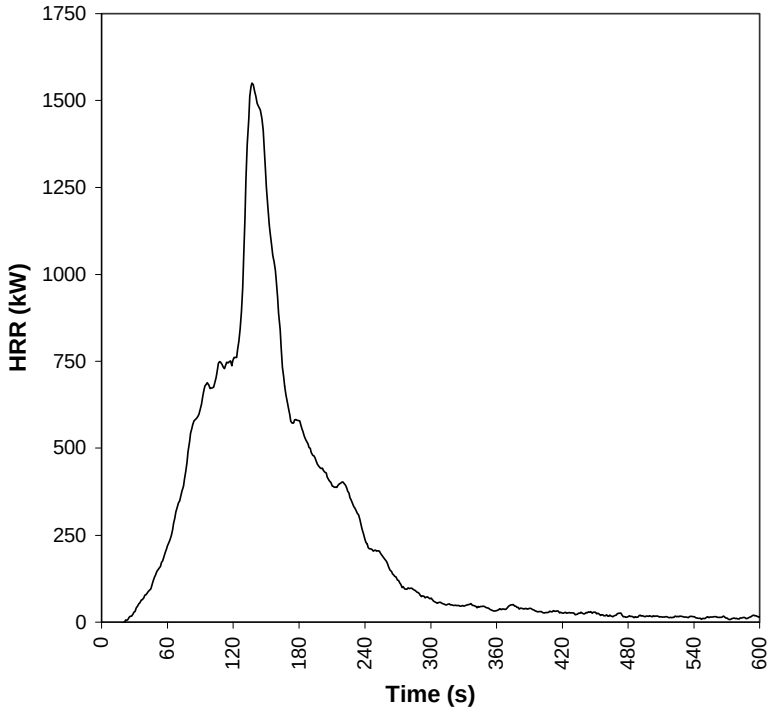

Figure XXV: Full-scale HRR history for item C7S1. Time zero is ignition.

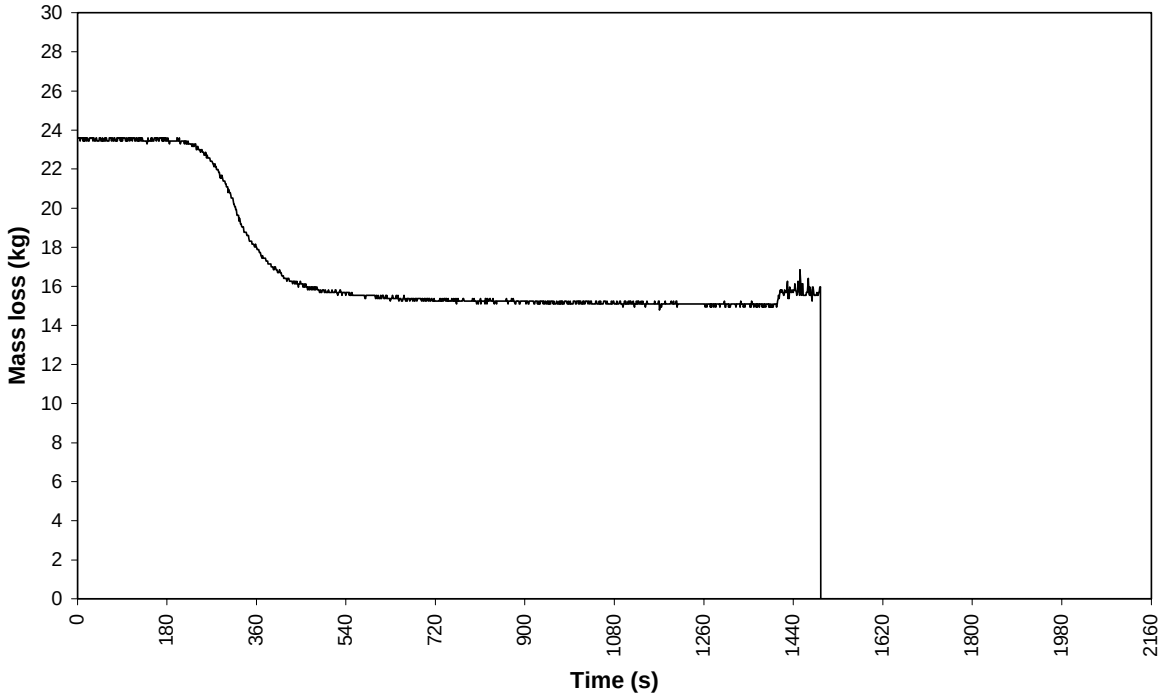

Figure XXVI: Mass loss rate for item C7S1. Time zero is baseline. Ignition is 180s.

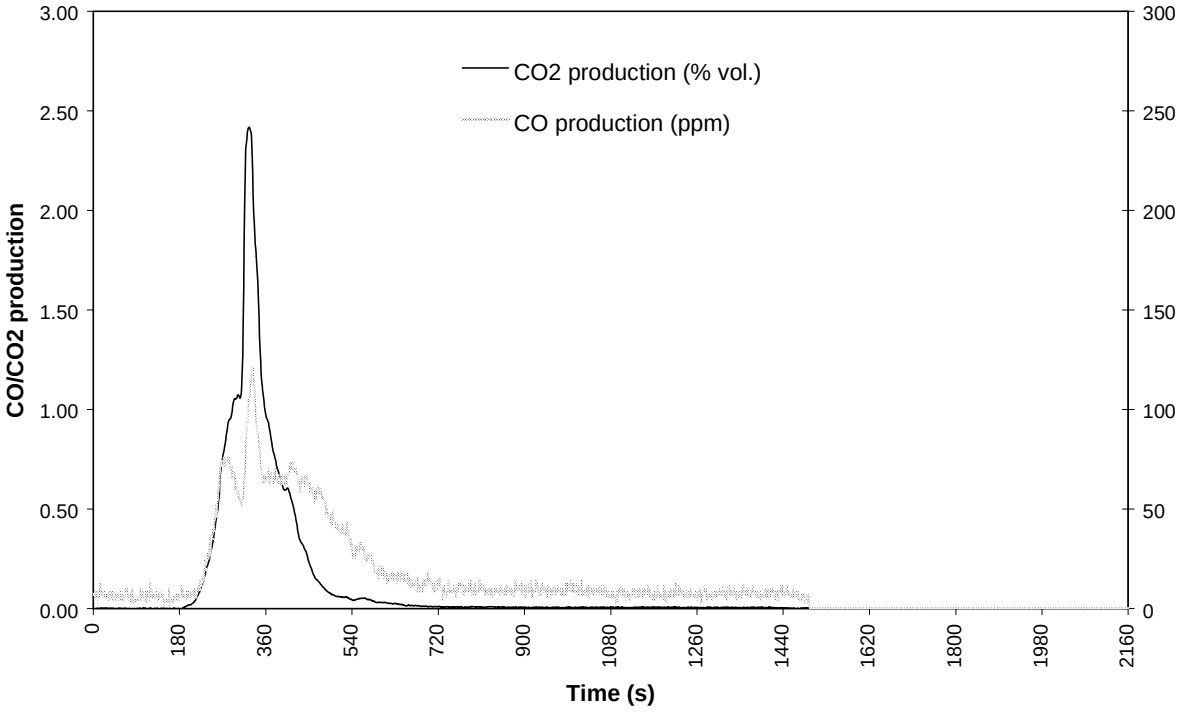

Figure XXVII: CO_2 and CO production for item C7S1. Time zero is baseline. Ignition is 180s.

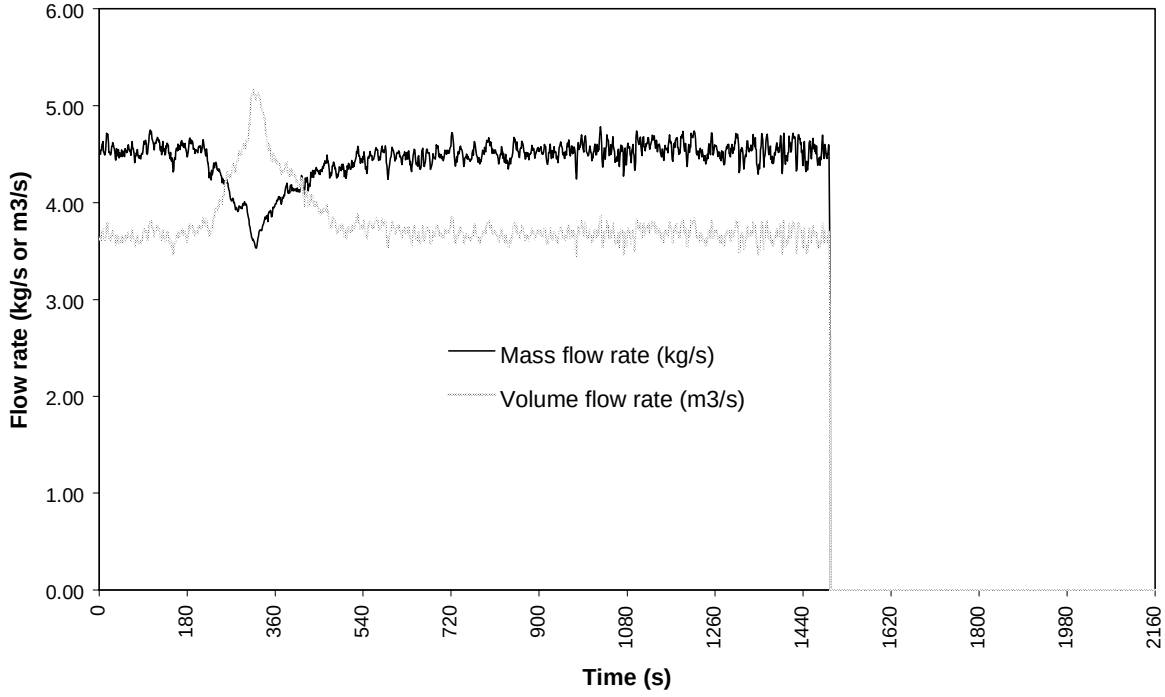

Figure XXVIII: Mass flow rate and volume flow rate for item C7S1. Time zero is baseline. Ignition is 180s.

Item 8: D8S1

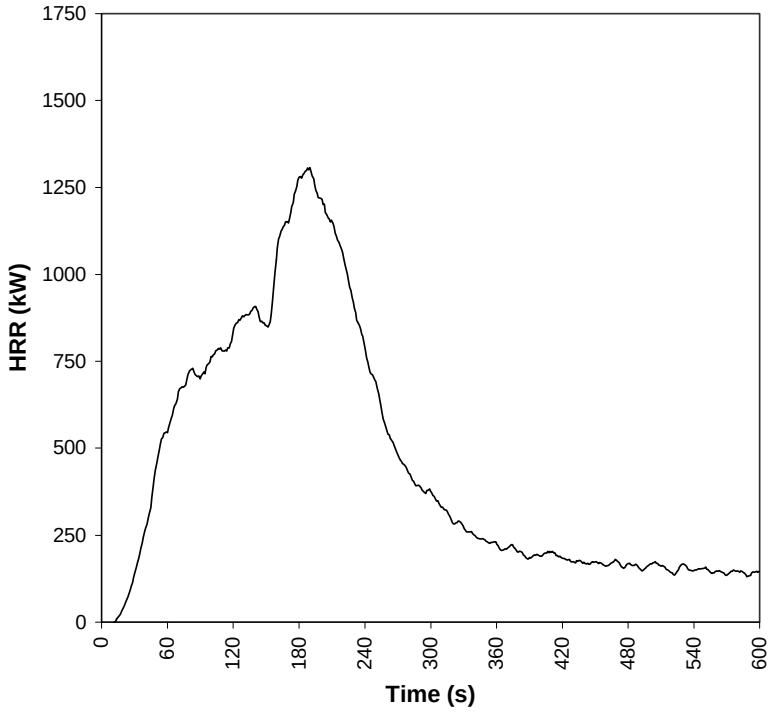

Figure XXIX: Full-scale HRR history for item D8S1. Time zero is ignition.

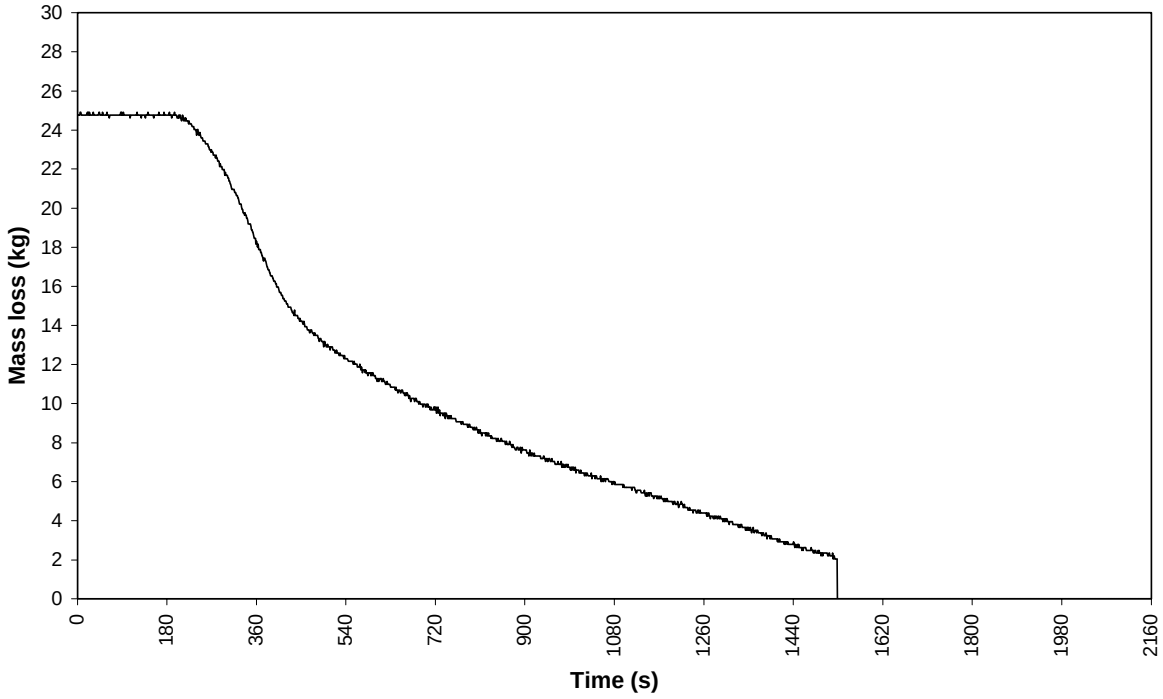

Figure XXX: Mass loss rate for item D8S1. Time zero is baseline. Ignition is 180s.

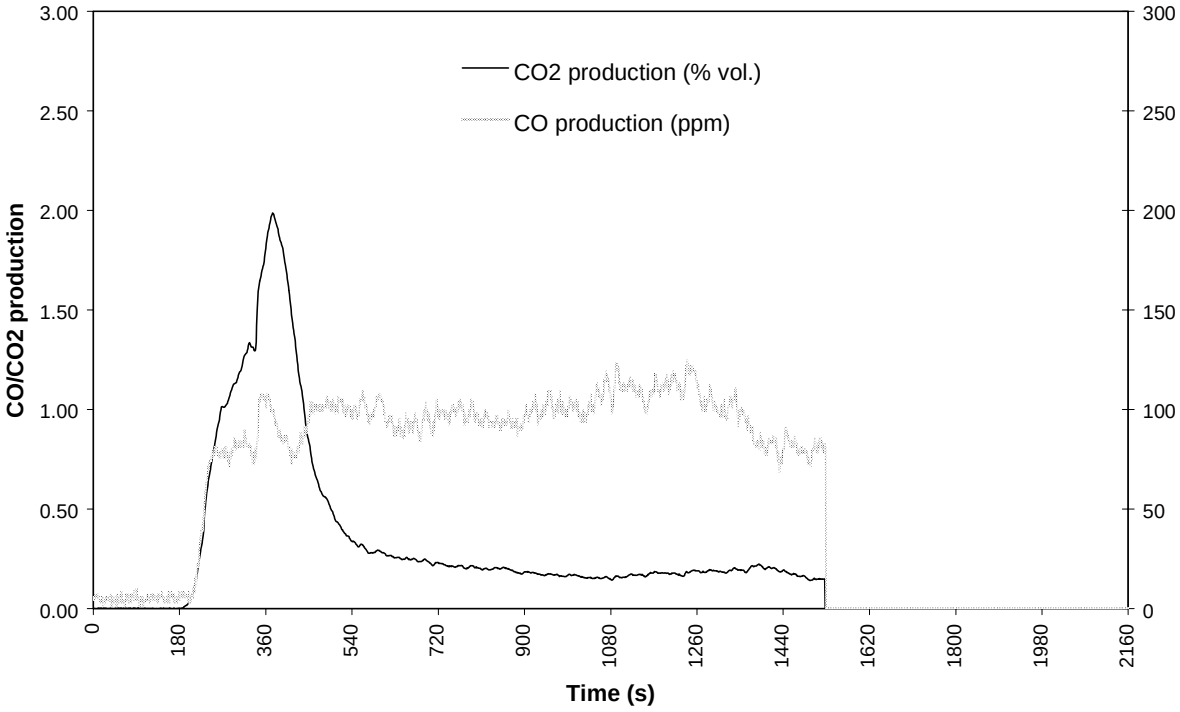

Figure XXXI: CO_2 and CO production for item D8S1. Time zero is baseline. Ignition is 180s.

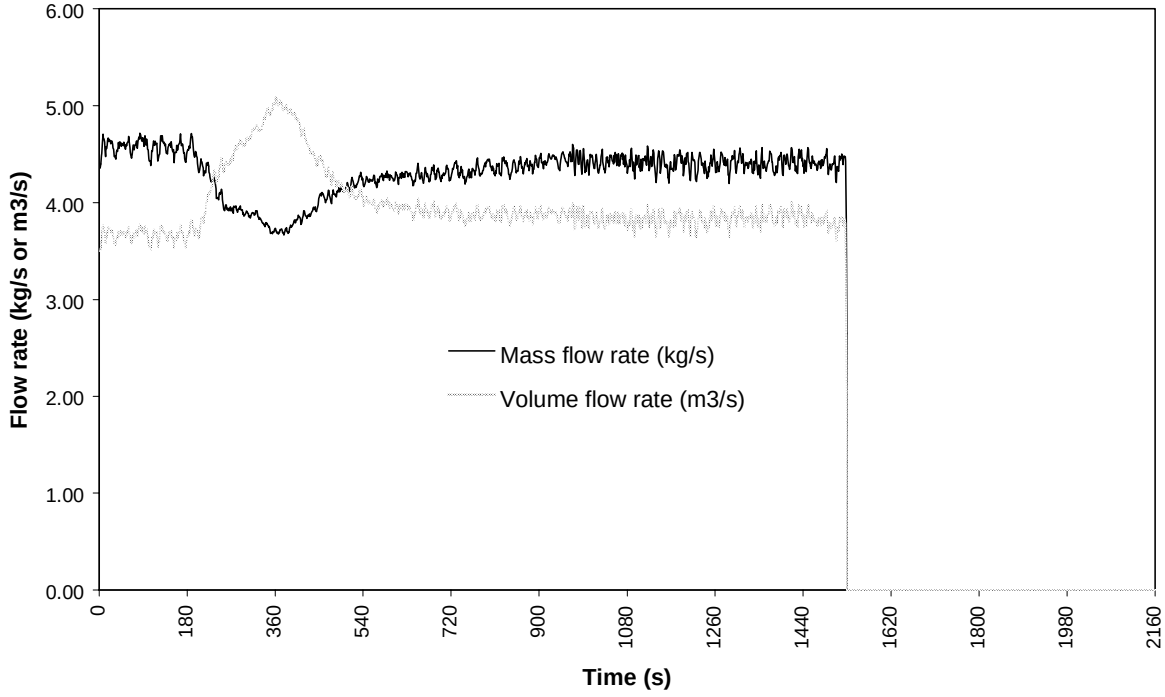

Figure XXXII: Mass flow rate and volume flow rate for item D8S1. Time zero is baseline. Ignition is 180s.

Item 9: A1S2

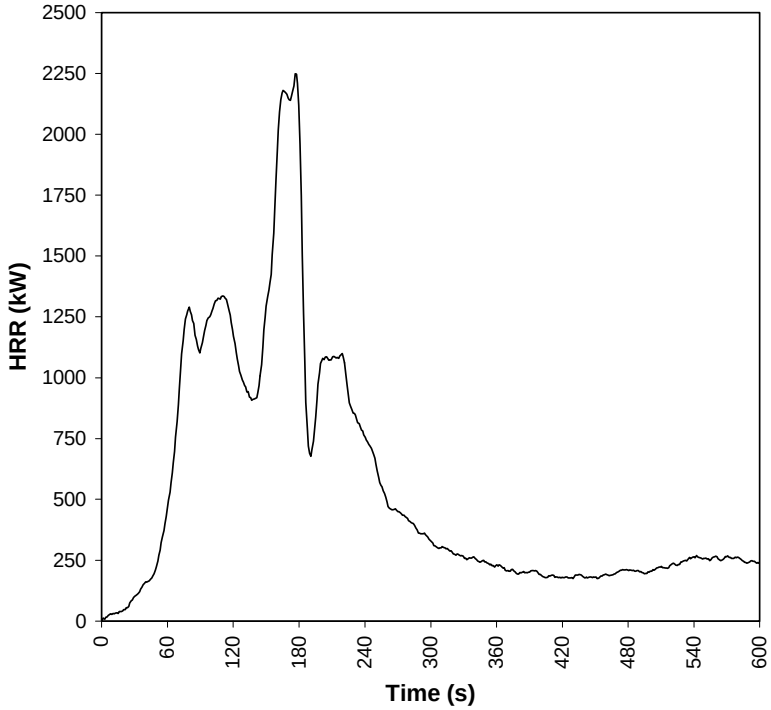

Figure XXXIII: Full-scale HRR history for item A1S2. Time zero is ignition. Note water applied at 180s from ignition.

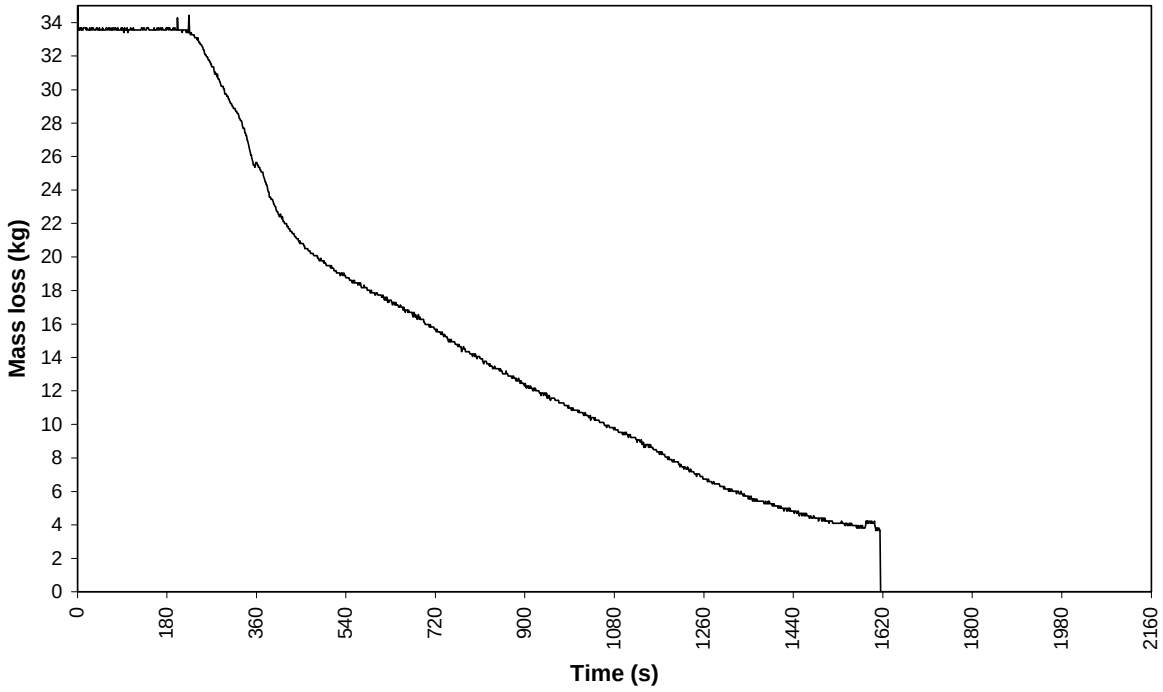

Figure XXXIV: Mass loss rate for item A1S2. Time zero is baseline. Ignition is 180s.

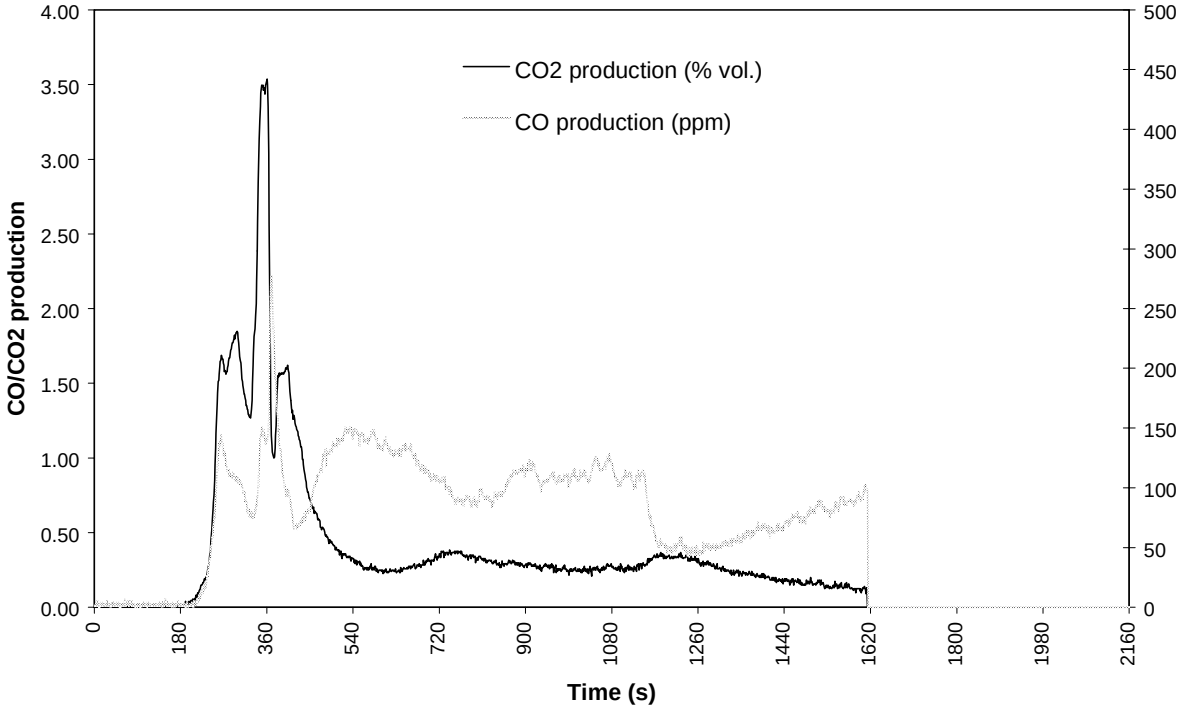

Figure XXXV: CO_2 and CO production for item A1S2. Time zero is baseline. Ignition is 180s.

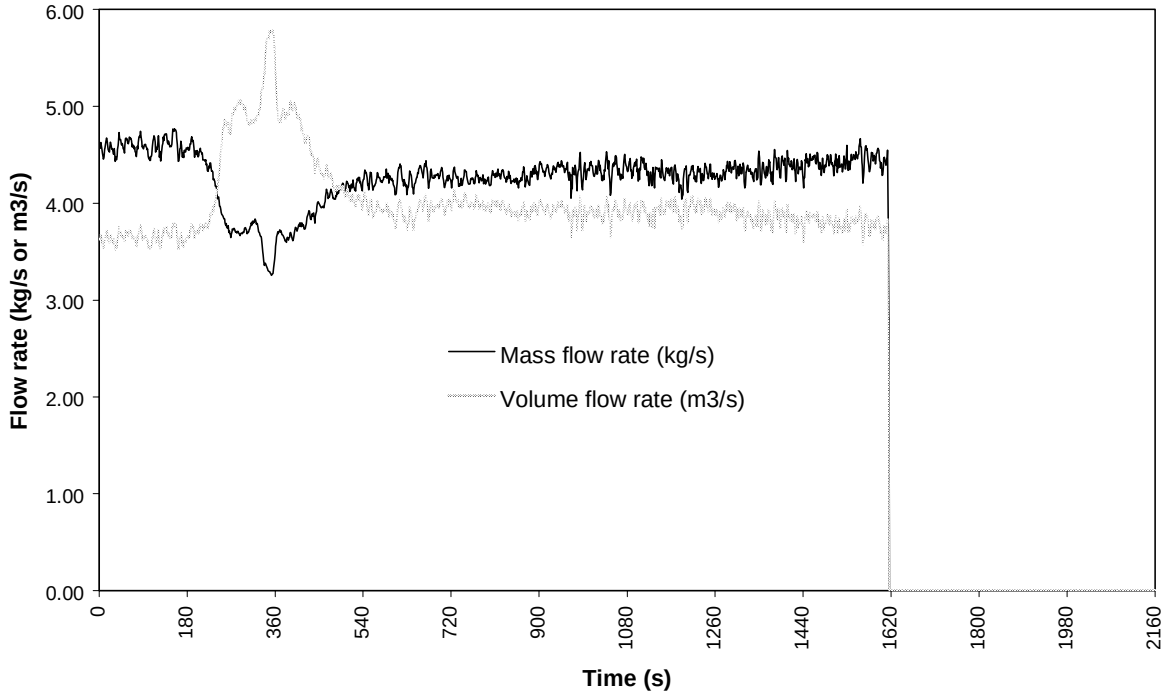

Figure XXXVI: Mass flow rate and volume flow rate for item A1S2. Time zero is baseline. Ignition is 180s.

Item 10: A2S2

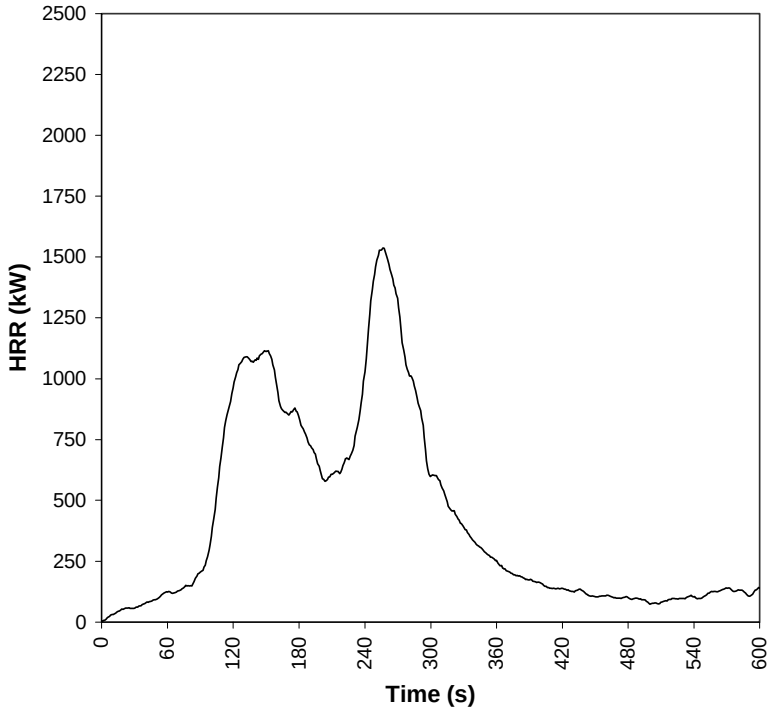

Figure XXXVII: Full-scale HRR history for item A2S2. Time zero is ignition.

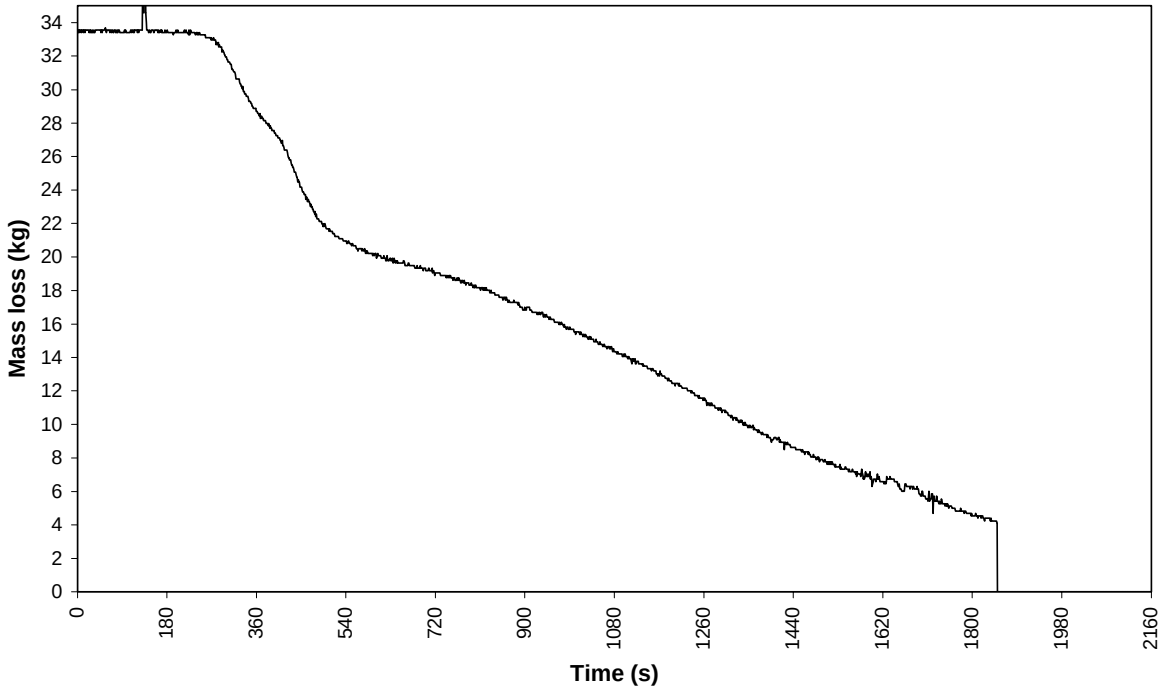

Figure XXXVIII: Mass loss rate for item A2S2. Time zero is baseline. Ignition is 180s.

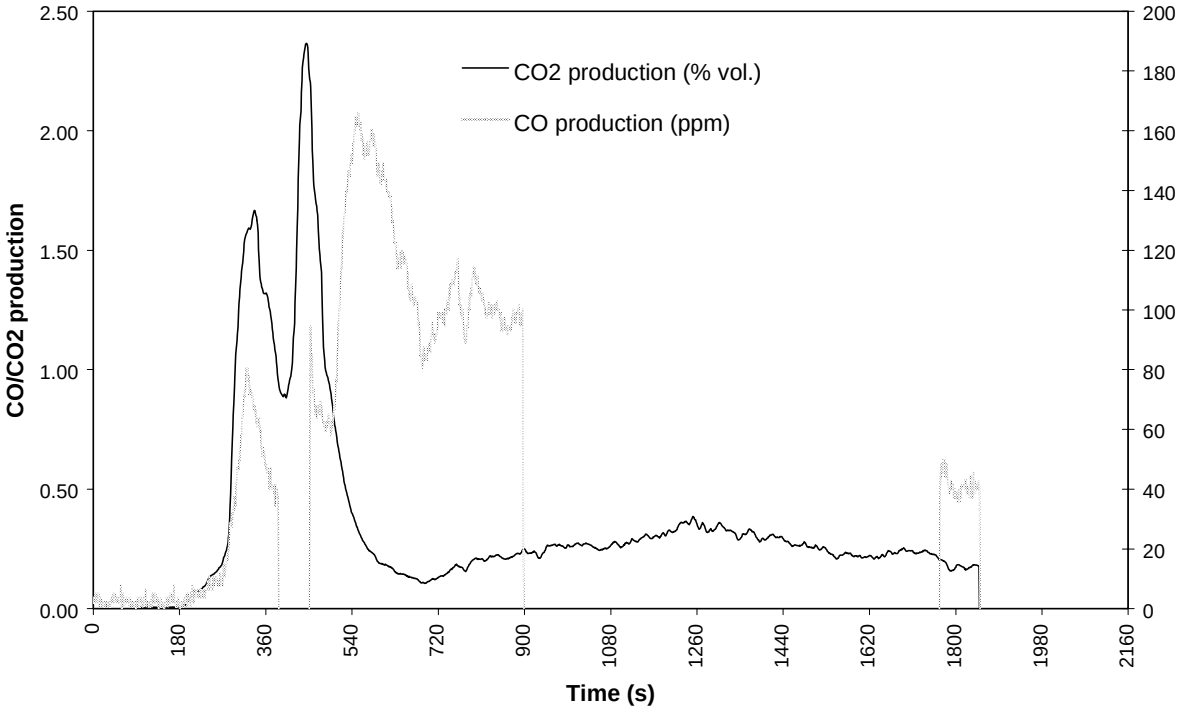

Figure XXXIX: CO_2 and CO production for item A2S2. Time zero is baseline. Ignition is 180s.

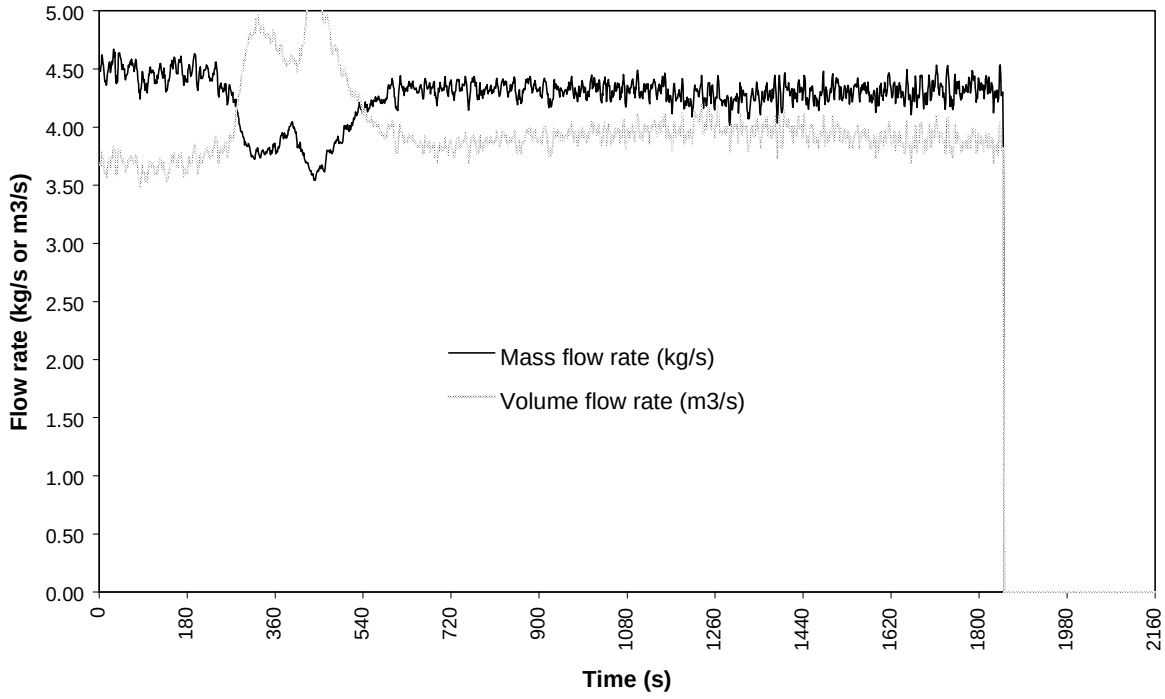

Figure XL: Mass flow rate and volume flow rate for item A2S2. Time zero is baseline. Ignition is 180s.

Item 11: B6S2

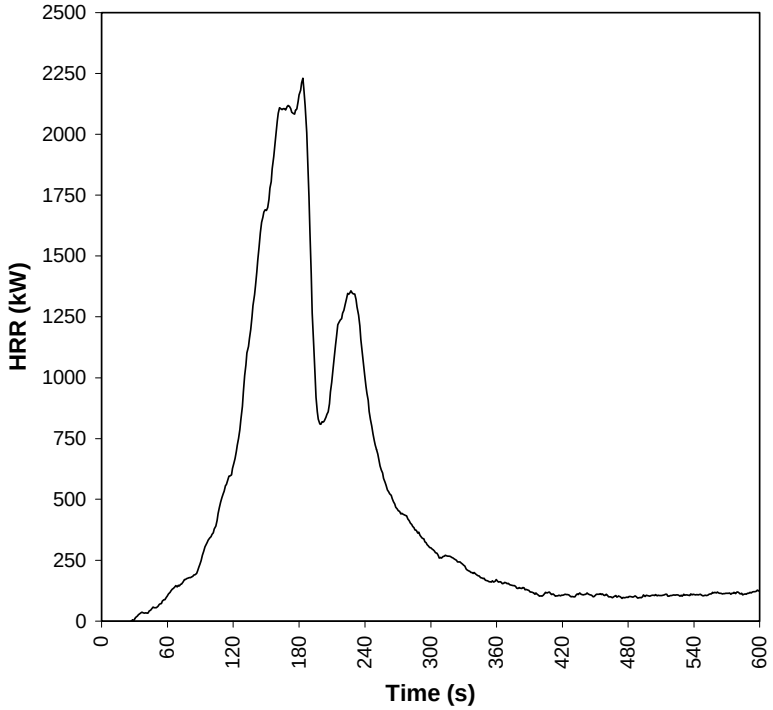

Figure XLI: Full-scale HRR history for item B6S2. Time zero is ignition. Note water applied at 180s from ignition.

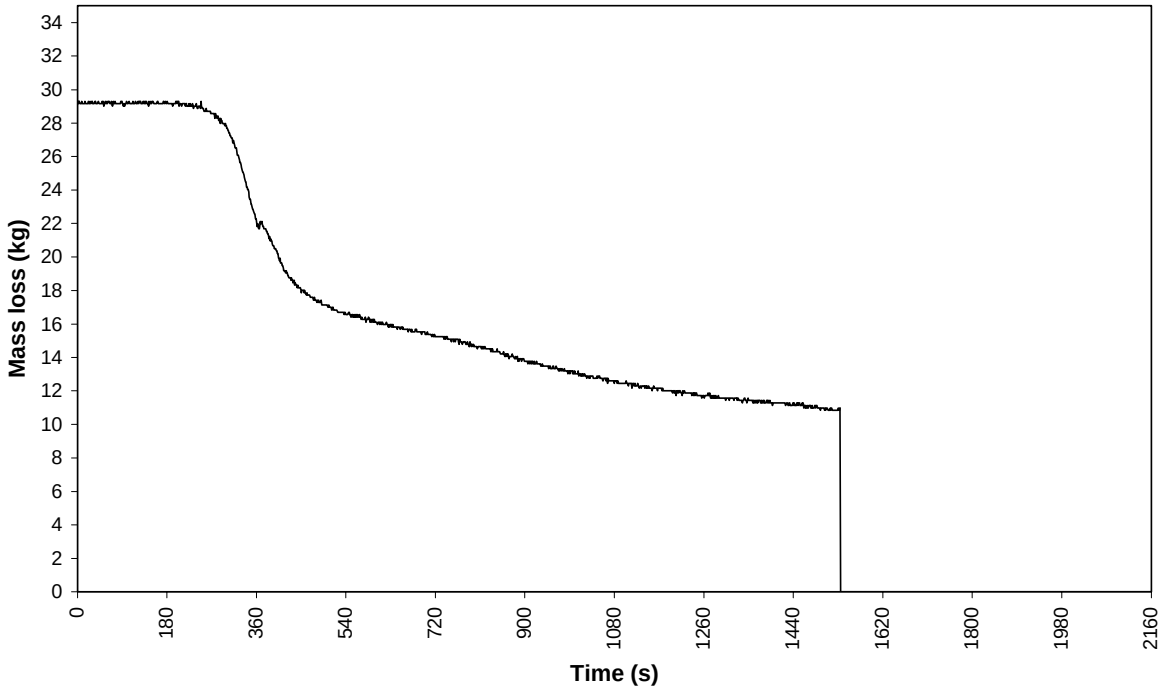

Figure XLII: Mass loss rate for item B6S2. Time zero is baseline. Ignition is 180s.

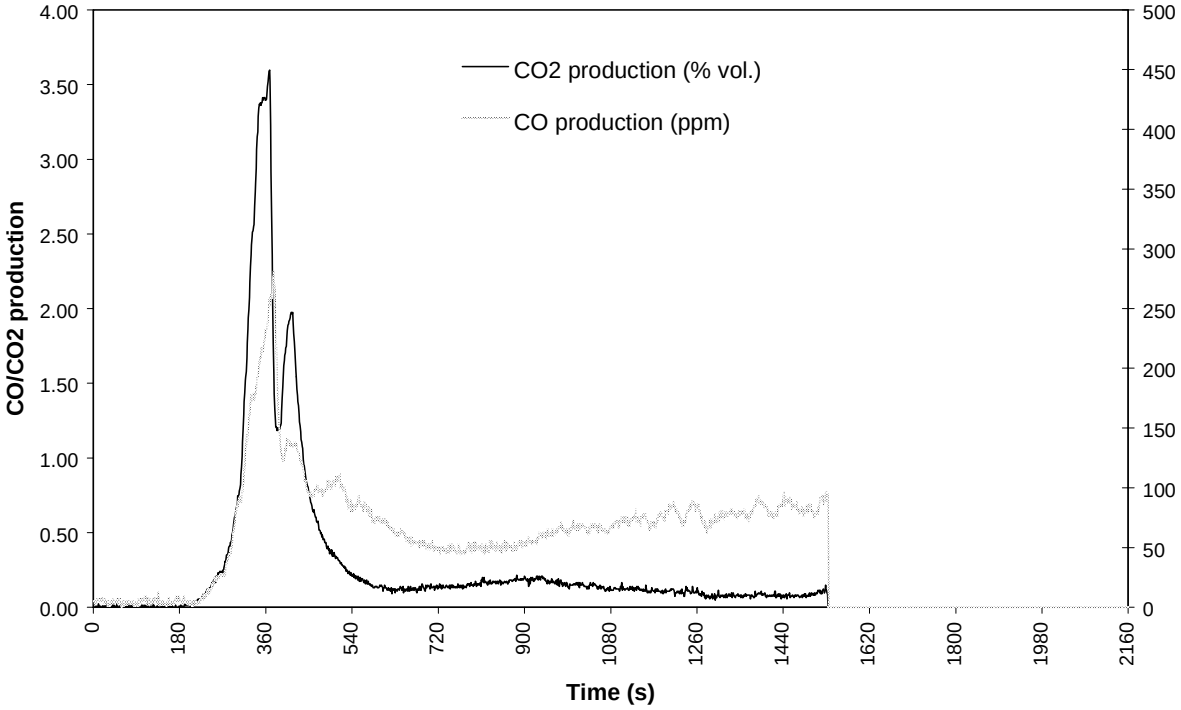

Figure XLIII: CO_2 and CO production for item B6S2. Time zero is baseline. Ignition is 180s.

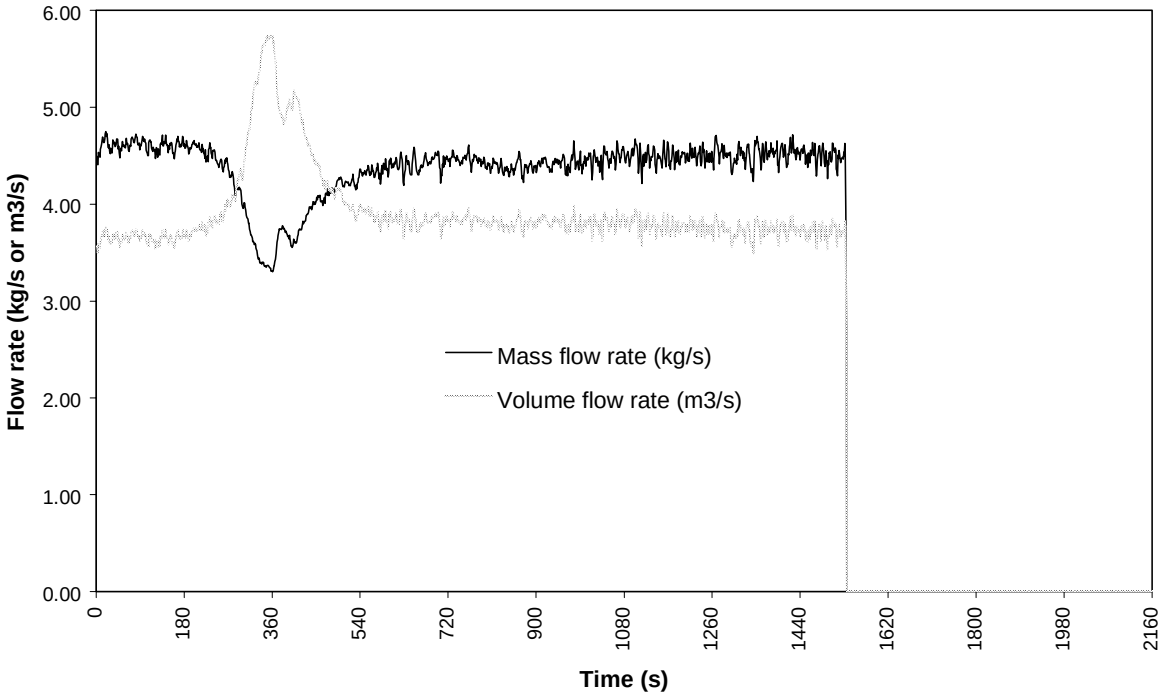

Figure XLIV: Mass flow rate and volume flow rate for item B6S2. Time zero is baseline. Ignition is 180s.

Item 12: C7S2

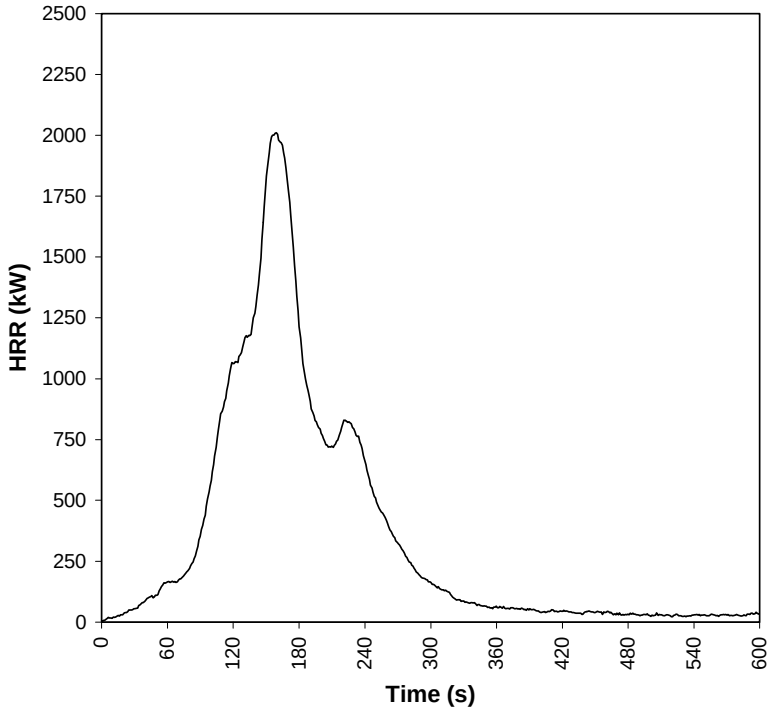

Figure XLV: Full-scale HRR history for item C7S2. Time zero is ignition.

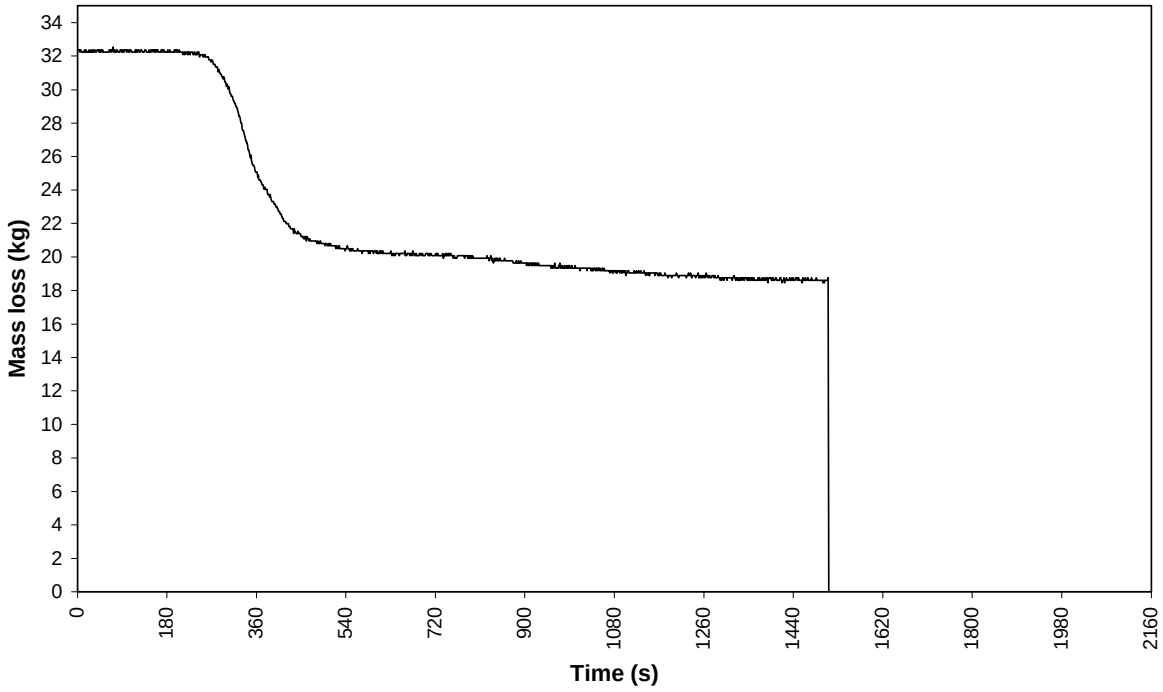

Figure XLVI: Mass loss rate for item C7S2. Time zero is baseline. Ignition is 180s.

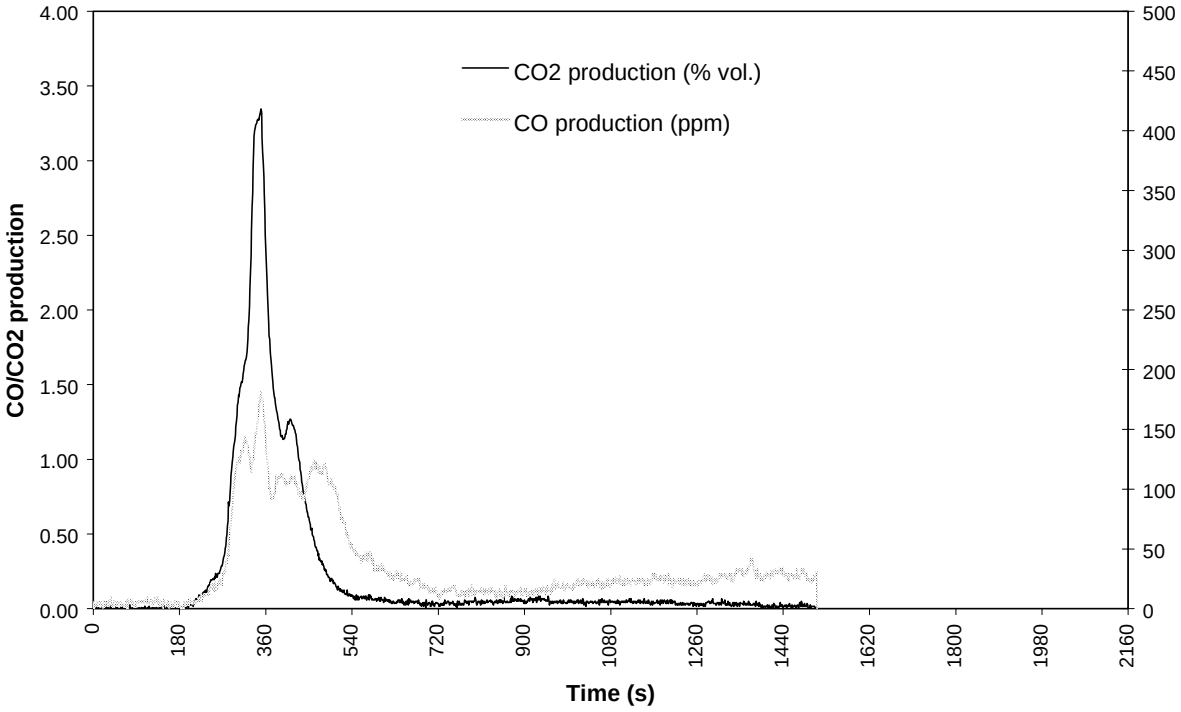

Figure XLVII: CO_2 and CO production for item C7S2. Time zero is baseline. Ignition is 180s.

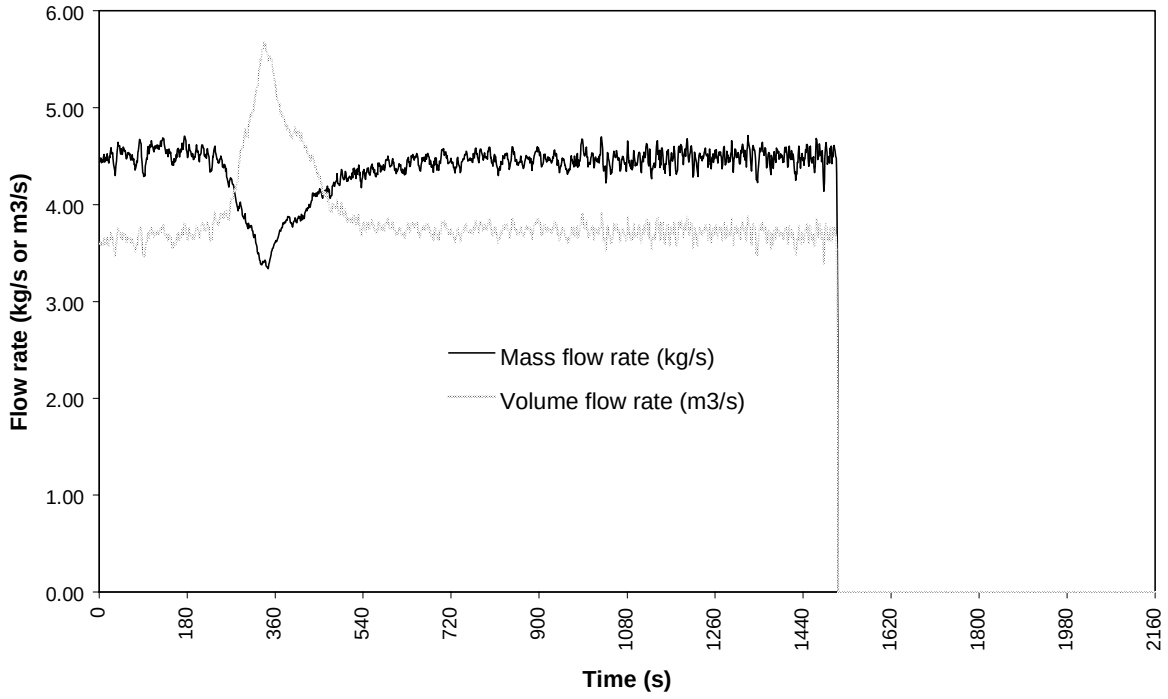

Figure XLVIII: Mass flow rate and volume flow rate for item C7S2. Time zero is baseline. Ignition is 180s.

Item 13: D8S2

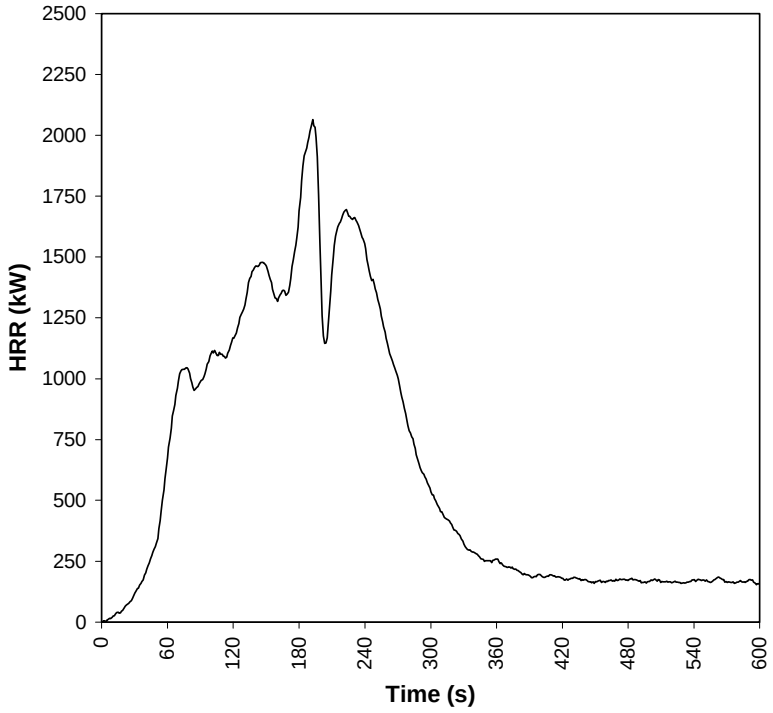

Figure XLIX: Full-scale HRR history for item D8S2. Time zero is ignition.

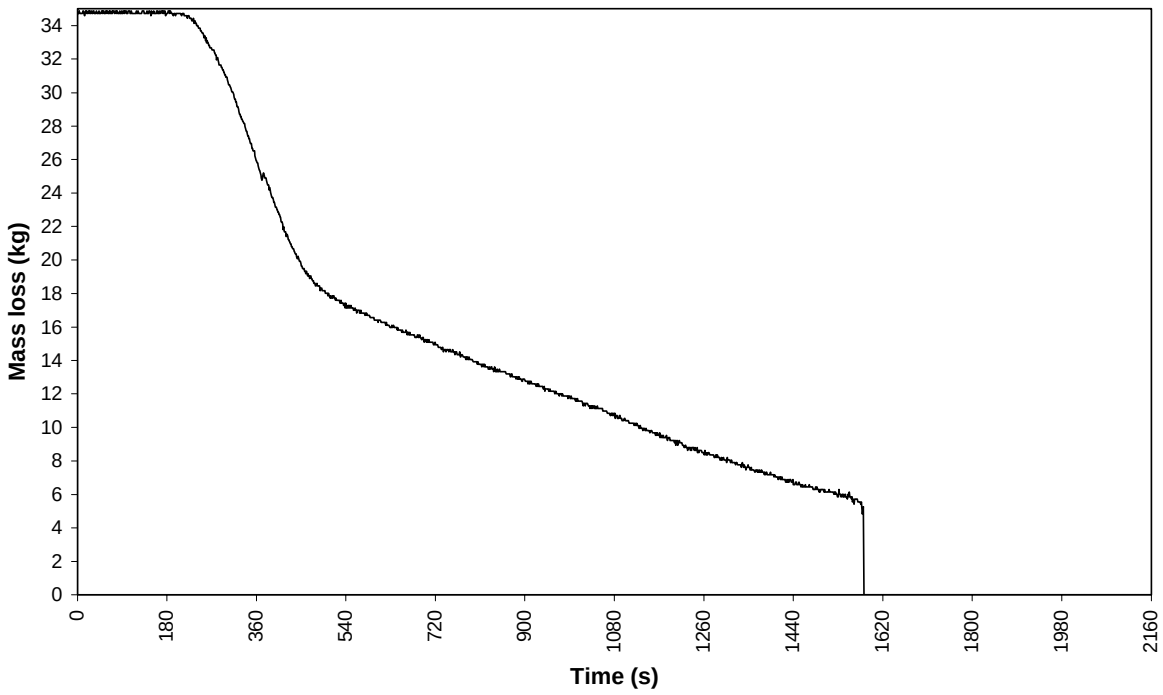

Figure L: Mass loss rate for item D8S2. Time zero is baseline. Ignition is 180s.

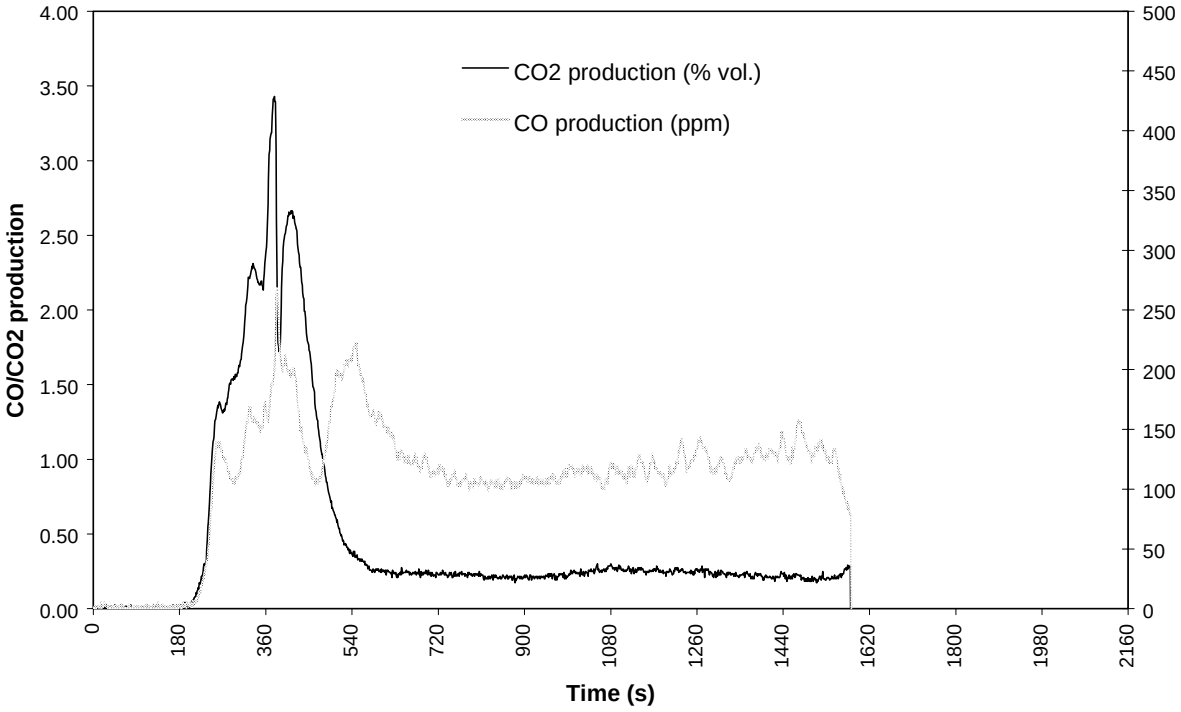

Figure LI: CO_2 and CO production for item D8S2. Time zero is baseline. Ignition is 180s.

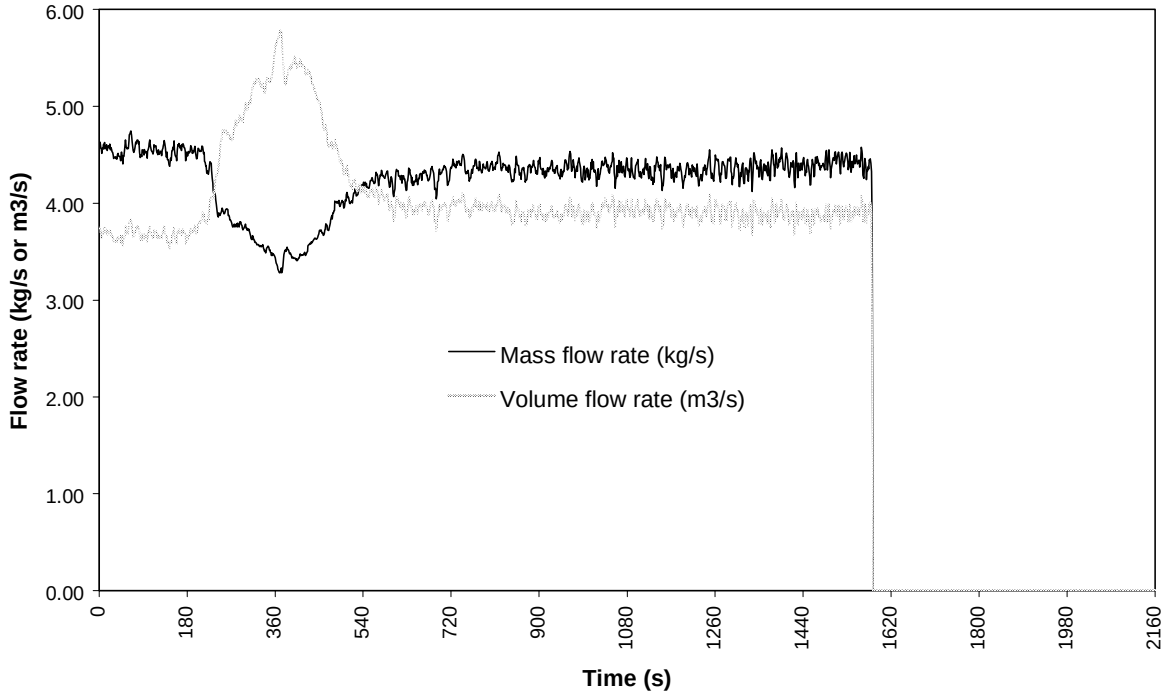

Figure LII: Mass flow rate and volume flow rate for item D8S2. Time zero is baseline. Ignition is 180s.